



UNIVERSITÄT ZU LÜBECK

Aus dem Institut für Chemie  
der Universität zu Lübeck  
Direktor: Prof. Dr. rer. nat. Thomas Peters

**Insights into Binding of Attachment Factors  
and Inhibitors to a Human Norovirus  
from NMR and SPR Experiments**

Inauguraldissertation  
zur  
Erlangung der Doktorwürde  
der Universität zu Lübeck

Aus der Sektion Naturwissenschaften

vorgelegt von  
Brigitte Fiege geb. Langpap  
aus Schwerin

Lübeck 2012



- |                      |                             |
|----------------------|-----------------------------|
| 1. Berichterstatter: | Professor Dr. Thomas Peters |
| 2. Berichterstatter: | Professor Dr. Norbert Tautz |

Tag der mündlichen Prüfung: 03.07.2012

Zum Druck genehmigt, Lübeck 06.07.2012





Für meine Familie und meinen Mann Thomas



## Abstract

Noroviruses (NoV) from the family of caliciviruses are an emerging viral threat that after their first detection in 1968 became the major cause of non-bacterial acute gastroenteritis. Epidemic outbreaks in social settings such as hospitals, nursing homes, schools and military impose a huge socio-economic burden worldwide. Transmission of NoV is facilitated by its extremely high contagiousness and pronounced stability towards environmental influences and disinfectants. Symptoms of vomiting and diarrhea typically abate after two to three days which often prevents the build-up of a long-term immunity. Medication or vaccine development has been hampered by the limited availability of cell culture or animal models for human NoV. Broadband vaccination is additionally limited by the high strain diversity and the genetic drift of NoV that lead to escape from the so-called 'herd immunity' in the population and the frequent appearance of new epidemic strains.

An alternative strategy for disease prevention and control is the development of entry-inhibitors directed against the non-enveloped capsid. NoV infection critically depends on attachment to histo-blood group antigens (HBGAs) on the surface of the gastrointestinal mucosa. In this work the binding of synthetic HBGAs to non-infectious so-called virus-like particles (VLPs) of a NoV strain from the currently dominating subgroup GII.4 was investigated. Saturation transfer difference (STD) and nuclear Overhauser enhancement (NOESY) NMR experiments furnished detailed binding models and revealed a strict specificity for fucosylated HBGAs. Amino acids of the capsid protein recognizing the L-fucose moiety were found to be strictly conserved among GII.4 strains from the last three decades. This encouraged the attempt to design entry-inhibitors targeted against the HBGA binding site of a large group of NoV and constitutes the second part of this work. L-fucose and hits from two different library screening approaches served as starting point for the design of divalent and multivalent inhibitors. NMR and surface plasmon resonance (SPR) titration experiments as well as hemagglutination assays were employed to compare the binding strength of HBGAs and prototype inhibitors. An avidity increase by a factor of 100 to 1000 compared to the monovalent interaction was determined for multivalent polyacryl-amide-based inhibitors. Chemical derivatization and optimization of linker lengths will likely lead to further increase of inhibition efficiencies.

In conclusion, the experiments with NMR and other biophysical methods presented in this thesis provide a comprehensive view on the HBGA and inhibitor binding properties of a human NoV strain.



## Zusammenfassung

Noroviren (NoV) aus der Familie der Caliciviren traten erstmals 1968 in den USA auf und haben sich seitdem zur Hauptursache nicht-bakterieller akuter Gastroenteritis entwickelt. NoV Epidemien treten insbesondere in sozialen Einrichtungen wie Krankenhäusern, Altersheimen, Schulen und im militärischen Bereich auf und verursachen weltweit großen sozioökonomischen Schaden. Die Verbreitung von NoV wird begünstigt durch ihre extrem hohe Ansteckungsrate und eine ausgeprägte Stabilität gegenüber Umwelteinflüssen und Desinfektionsmitteln. Symptome wie Erbrechen und Diarrhöe dauern typischerweise zwei bis drei Tage an, sodass häufig keine Langzeitimmunität aufgebaut wird. Die Entwicklung von Therapie- oder Impfstrategien wird erschwert durch die begrenzte Verfügbarkeit von Zellkultur- oder Tiermodellen für humane NoV. Die hohe Variabilität und genetische Drift von NoV-Stämmen stellen eine zusätzliche Limitierung für Impfungen mit breiter Wirksamkeit dar. Sie führen auch zum Durchbrechen der sogenannten „Herden-Immunität“ und dem Auftreten neuer epidemischer Virusstämme in regelmäßigen Abständen.

Eine alternative Strategie zur Prävention und Eindämmung von NoV-Epidemien ist die Entwicklung von „Entry-Inhibitoren“, die gegen das unbehüllte NoV-Kapsid gerichtet sind. Für die Infektion ist die Erkennung von Histo-Blutgruppenantigenen (HBGAs) auf der Oberfläche der Darmmucosa erforderlich. In dieser Arbeit wird die Bindung von synthetischen HBGAs an nichtinfektiöse virusähnliche Partikel (VLPs) eines NoV-Stamms aus der derzeit vorherrschenden Untergruppe GII.4 untersucht. Sättigungs-Transfer-Differenz- (STD-) und Kern-Overhauser-Effekt- (NOESY-)NMR-Experimente lieferten detaillierte Bindungsmodelle und ergaben eine hohe Spezifität für fucosylierte HBGAs. Die Aminosäuren in der L-Fucose-Bindungstasche des Kapsidproteins sind unter GII.4-Stämmen aus über drei Jahrzehnte hochkonserviert. Dies eröffnete die Möglichkeit zum Design von Entry-Inhibitoren gegen die HBGA-Bindungstasche dieser großen Gruppe von NoV, welches den zweiten Teil dieser Arbeit darstellt. L-Fucose und Verbindungen aus zwei verschiedenen Bibliotheks-Screeningverfahren dienten als Ausgangspunkt für die Entwicklung divalenter und multivalenter Inhibitoren. Titrationsexperimente mit NMR und Oberflächen-Plasmonen-Resonanz-Spektroskopie (SPR) sowie Hämagglutinationsversuche dienten zur Bestimmung der Bindungsstärke von HBGAs und Prototyp-inhibitoren. Eine Erhöhung der Bindungsstärke um zwei bis drei Größenordnungen im Vergleich zur monomeren Bindung wurde für multivalente Polyacrylamid-basierte

Inhibitoren ermittelt. Eine Optimierung der Linkerlänge sowie chemische Derivatisierung werden in Zukunft zu einer weiteren Verbesserung der Wirkstoffeffizienz führen.

Zusammenfassend liefern die in dieser Arbeit vorgestellten NMR- und SPR-Experimente ein umfassendes Bild der HBGA- und Inhibitorbindung an einen humanen Norovirus.

## Content

<b>Abstract .....</b>	<b>I</b>
<b>Zusammenfassung .....</b>	<b>III</b>
<b>Content .....</b>	<b>V</b>
<b>Abbreviations .....</b>	<b>IX</b>
<b>List of Figures .....</b>	<b>XI</b>
<b>List of Tables .....</b>	<b>XIV</b>
<b>1 Introduction .....</b>	<b>1</b>
1.1 Caliciviruses .....	1
1.2 Norovirus Epidemiology .....	2
1.3 Genomic Organization and Variability of Noroviruses .....	4
1.4 Host Attachment Factors: Histo-Blood Group Antigens .....	7
1.5 Characterization of Norovirus Attachment Factors .....	11
1.6 Attachment Factors of other Caliciviruses .....	13
1.7 Structure of the Norovirus Capsid .....	16
1.8 Structural Details on HBGA Recognition by Noroviruses .....	17
1.9 Vaccine and Inhibitor Design against Human Norovirus VLPs .....	20
1.10 Entry-Inhibitor Design against Ast6139 VLPs .....	22
1.11 Biophysical Characterization of Norovirus Binding to HBGAs .....	24
1.11.1 NMR Spectroscopy .....	24
1.11.2 Surface Plasmon Resonance Spectroscopy .....	29
1.11.3 Hemagglutination Assays .....	32
<b>2 Objectives .....</b>	<b>35</b>
<b>3 Material and Methods .....</b>	<b>37</b>
3.1 Expression of Norovirus VLPs .....	37
3.1.1 Cloning of Single Site Mutants .....	38
3.2 Molecules Studied for Binding to Norovirus VLPs .....	40
3.2.1 Carbohydrates .....	40
3.2.2 Synthetic Inhibitors Based on HBGA Fragments .....	43

3.3	NMR Spectroscopy.....	47
3.3.1	Assignment Experiments.....	47
3.3.2	STD NMR Spectroscopy.....	47
	Binding Epitopes from Group Epitope Mapping.....	47
	Direct STD Titration Experiments.....	49
	Competitive STD Titration Experiments.....	50
3.3.3	Transferred NOESY Experiments.....	53
3.3.4	ROESY Experiments.....	53
3.3.5	Stability Measurements of Carbamates.....	54
3.4	Surface Plasmon Resonance.....	55
3.4.1	Direct Immobilization of Norovirus VLPs.....	55
3.4.2	Competitive Assay for Estimation of IC <sub>50</sub> Values.....	57
	Competitive Assay using PAA Sugar Conjugates.....	57
	Competitive Assay using BSA Sugar Conjugates.....	58
3.5	Hemagglutination Assay.....	60
3.6	Molecule Visualization.....	60
<b>4</b>	<b>Results .....</b>	<b>61</b>
4.1	Expression of Wildtype and Mutant Norovirus VLPs.....	61
4.2	STD NMR Experiments with HBGA Fragments.....	61
4.2.1	HBGA Binding Specificity from STD NMR.....	61
4.2.2	Binding Epitopes from Group Epitope Mapping.....	64
4.2.3	Comparative STD NMR studies of Bovine NoV.....	69
4.2.4	STD NMR Experiments with Mutant NoV VLPs.....	72
4.3	TrNOESY Experiments of sLe <sup>x</sup> .....	73
4.4	Docking Studies and MD Simulations of HBGAs.....	79
4.5	STD NMR Experiments with Inhibitors based on L-Fuc.....	82
4.5.1	Compounds with Fragments from NMR Screening.....	82
4.5.2	Hits from Virtual Library Screening.....	84
4.5.3	STD Titration of Virtual Screening Hit 42.....	85



4.6	Competitive STD Titration Experiments .....	87
4.6.1	Experiments with HBGAs and Divalent Inhibitors .....	87
4.6.2	Experiments with Polymeric Inhibitors .....	91
4.7	Direct SPR Binding Assays with Immobilized VLPs.....	95
4.7.1	Binding Studies with HBGA Fragments .....	96
4.7.2	Investigation of pH and Buffer Dependence .....	104
4.7.3	Experiments with Hits from Virtual Library Screening .....	105
4.7.4	Experiments with Polymeric Inhibitors .....	108
4.8	Competitive SPR Experiments .....	115
4.8.1	Measurements on PAA Sugar Conjugates .....	115
4.8.2	Measurements on BSA Sugar Conjugates .....	119
4.9	Hemagglutination Assays .....	123
<b>5</b>	<b>Discussion .....</b>	<b>127</b>
5.1	General Considerations for Studying NoV-HBGA Interaction .....	127
5.2	Optimization of Experimental Parameters for STD NMR.....	128
5.3	HBGA Binding Patterns Vary with the Chosen Methods .....	130
5.4	NMR Furnished Binding Epitopes for HBGAs .....	132
5.5	Comparison of STD Binding Epitopes with Docking Models .....	134
5.6	HBGA Specificities of other Caliciviruses .....	137
5.7	Bioactive Conformation of sLe <sup>x</sup> from trNOESY Experiments.....	139
5.8	Affinity Data for HBGAs from STD NMR experiments.....	142
5.9	Binding Mode and Affinity of HBGAs from SPR Measurements .....	144
5.10	Lead Compounds for Entry-Inhibitor Design .....	147
5.11	Titration Experiments with Polymeric Inhibitors .....	149
<b>6</b>	<b>Summary and Outlook.....</b>	<b>153</b>
<b>7</b>	<b>Appendix .....</b>	<b>157</b>
7.1	List of Chemicals .....	157
7.2	List of Equipment .....	158
7.3	List of used Software .....	158

---

7.4	Sequence Alignments of Norovirus Capsid Proteins.....	159
7.5	LigPlot Analysis of Norovirus-HBGA Complexes .....	162
7.6	NMR Experiments .....	164
7.6.1	STD Titration of $\alpha$ -L-Fuc-(1, <i>O</i> )-CH <sub>3</sub> .....	164
7.6.2	K <sub>D</sub> of HBGAs from Competitive STD Titrations.....	165
7.6.3	TrREOSY Experiment of sLe <sup>x</sup> .....	169
7.6.4	TrNOEs Simulated for Simple Two-Spin Systems .....	169
7.6.5	STD Titration of Virtual Screening Hit 42 .....	170
7.6.6	Assignment of HBGA Fragments.....	171
7.6.7	Used Pulse Programs and Parameters .....	183
	STD NMR Experiments .....	183
	NOESY and ROESY Experiments.....	188
	Assignment Experiments .....	188
7.7	Sensorgrams from SPR Experiments.....	197
7.7.1	Measurements with HBGAs .....	197
7.7.2	Measurements with Hits from Virtual Library Screening .....	203
7.7.3	Measurements with Polymeric Inhibitors .....	206
7.7.4	SPR Assays with Immobilized PAA Sugar Conjugates .....	210
<b>8</b>	<b>Literature .....</b>	<b>214</b>
	<b>Acknowledgment .....</b>	<b>237</b>
	<b>Curriculum Vitae .....</b>	<b>239</b>

## Abbreviations

Ast6139:	human norovirus strain Ast6139/01/Sp
bp:	base pair
COSY:	Correlation Spectroscopy
cssf:	chemical shift selective filter
Da:	Dalton, unit of the molecular weight, 1 Da = 1 g/mol
EC <sub>50</sub> :	effective concentration of a drug (agonist) causing half of the maximum response in a biological system, measure for the potency of a drug
Fc:	flow cell on an SPR sensor chip
Fuc:	fucopyranose
Gal:	galactopyranose
GalNAc:	<i>N</i> -acetylgalactosamine (pyranose)
Glc:	glucopyranose
GlcNAc:	<i>N</i> -acetylglucosamine (pyranose)
K <sub>A</sub> :	equilibrium association constant [M]
K <sub>D</sub> :	equilibrium dissociation constant [M <sup>-1</sup> ]
k <sub>off</sub> :	dissociation rate constant [s <sup>-1</sup> ]
k <sub>on</sub> :	association rate constant [M <sup>-1</sup> *s <sup>-1</sup> ]
HBGA:	histo-blood group antigen
HSQC:	Heteronuclear Single Quantum Coherence
HTS:	High Throughput Screening
IC <sub>50</sub> :	concentration of an inhibitory compound causing half of the maximum inhibition, measure for the inhibitory efficiency of a compound
ILOE:	Interligand Overhauser enhancement
LacNAc:	β-D-Gal-(1,4)-D-GlcNAc (type 2 precursor)
Le <sup>a</sup> :	Lewis <sup>a</sup> trisaccharide, β-D-Gal-(1,3)-[α-L-Fuc-(1,4)]-β-D-GlcNAc
Le <sup>b</sup> :	Lewis <sup>b</sup> tetrasaccharide, α-L-Fuc-(1,2)-β-D-Gal-(1,3)-[α-L-Fuc-(1,4)]-β-D-GlcNAc
Le <sup>x</sup> :	Lewis <sup>x</sup> trisaccharide, β-D-Gal-(1,4)-[α-L-Fuc-(1,3)]-β-D-GlcNAc
Le <sup>y</sup> :	Lewis <sup>y</sup> tetrasaccharide, α-L-Fuc-(1,2)-β-D-Gal-(1,4)-[α-L-Fuc-(1,3)]-β-D-GlcNAc
ManNAc:	<i>N</i> -acetylmannosamine (pyranose)
MD:	molecular dynamics

---

MMC:	Metropolis Monte Carlo (algorithm applied to statistical distributions)
MW:	molecular weight in Dalton or g/mol
NB2:	bovine norovirus strain Bo/Newbury2/1976/UK
Neu5Ac:	<i>N</i> -acetylneuraminic acid
NMR:	Nuclear Magnetic Resonance
NOE:	Nuclear Overhauser Enhancement
NOESY:	Nuclear Overhauser Enhancement Spectroscopy
NoV:	norovirus
ORF:	open reading frame
ppm:	parts per million
RBC:	red blood cell
RF:	radiofrequency used in NMR spectroscopy (ca. 60 – 1000 MHz)
RHDV:	rabbit hemorrhagic disease virus
RKI:	Robert Koch-Institut
ROESY:	Rotational Overhauser Effect Spectroscopy
rpm:	revolutions per minute
RU:	Response Units, 1 RU = 1 pg/mm <sup>2</sup>
sLe <sup>x</sup> :	sialyl-Lewis <sup>x</sup> , $\alpha$ -D-Neu5Ac-(2,3)- $\beta$ -D-Gal-(1,4)-[ $\alpha$ -L-Fuc-(1,3)]- $\beta$ -D-GlcNAc
sLe <sup>a</sup> :	sialyl-Lewis <sup>a</sup> , $\alpha$ -D-Neu5Ac-(2,3)- $\beta$ -D-Gal-(1,3)-[ $\alpha$ -L-Fuc-(1,4)]- $\beta$ -D-GlcNAc
SPR:	Surface Plasmon Resonance
STD:	Saturation Transfer Difference
$T_1$ :	Longitudinal relaxation time
$T_2$ :	Transversal relaxation time
$\tau_m$ :	mixing time in two-dimensional NMR experiments
TOCSY:	Total Correlation Spectroscopy
trNOE:	transferred Nuclear Overhauser Enhancement
TSP:	trimethylsilyl-2,2,3,3-tetradeuteriopropionic acid
VLP:	virus-like particle
VP1:	major capsid protein of caliciviruses (viral protein 1)
WATERGATE:	Water Suppression Through Gradient Tailored Excitation

## List of Figures

Figure 1.1. Structural organisation of the NoV genome and the VP1 protein. ....	5
Figure 1.2. Variable and conserved sites of GII.4 NoV major capsid proteins.....	6
Figure 1.3. Biosynthesis pathways of HBGAs from type 1 precursors.....	9
Figure 1.4. Known HBGA binding patterns of NoV capsids.....	12
Figure 1.5. Structure of the capsid protein of the GI.1 Norwalk virus.....	16
Figure 1.6. Phylogenetic tree and binding pattern of crystallized capsid proteins.....	18
Figure 1.7. Structure of the VA387 P protein in complex with B trisaccharide. ....	19
Figure 1.8. Principles of the STD NMR experiment.....	25
Figure 1.9. Theoretical steady-state NOE enhancement for a two-spin system.....	27
Figure 1.10. Schematic principle of trNOESY experiments with VLPs and HBGAs. ....	28
Figure 1.11. Principles of SPR spectroscopy. ....	30
Figure 1.12. SPR assay formats with NoV VLPs.....	31
Figure 1.13. Principles of hemagglutination by VLPs. ....	32
Figure 3.1. Structures of ABH and Lewis antigens containing an L-Fuc moiety. ....	41
Figure 3.2. Structures of HBGAs without an L-Fuc moiety. ....	42
Figure 3.3. Structures of inhibitors with L-Fuc and/ or fragment 160. ....	43
Figure 3.4. Polymeric PAA-based inhibitors with L-Fuc and/or fragment 160.....	44
Figure 3.5. Polymeric inhibitors containing L-Fuc and ‘adjacent site’ fragments.....	45
Figure 3.6. Structures of inhibitors obtained from virtual library screening.....	46
Figure 4.1. STD experiments and binding epitopes of A trisaccharide and sLe <sup>x</sup> .....	63
Figure 4.2. Binding epitopes of HBGAs in presence of Ast6139 VLPs. ....	65
Figure 4.3. The stereochemistry of L-Fuc and L-Gal.....	66
Figure 4.4. Binding pocket of GII.4 NoV capsids with B trisaccharide.....	66
Figure 4.5. Differences in the STD effect of <i>N</i> -acetyl groups of Le <sup>x</sup> and Le <sup>a</sup> .....	67
Figure 4.6. Structure and binding epitope of Le <sup>y</sup> . ....	68
Figure 4.7. STD experiment of xenoantigen with NB2 VLPs. ....	70
Figure 4.8. STD titration of xenoantigen in presence of NB2 VLPs. ....	71
Figure 4.9. Binding epitopes for wildtype and mutant Ast6139 VLPs. ....	72
Figure 4.10. Stereochemical presentation of sLe <sup>x</sup> major solution conformations.....	74
Figure 4.11. NOESY spectra of free sLe <sup>x</sup> . ....	75
Figure 4.12. TrNOESY spectrum of sLe <sup>x</sup> in presence of Ast6139 VLPs. ....	76
Figure 4.13. Build-up curves of selected sLe <sup>x</sup> trNOE cross peaks.....	78
Figure 4.14. Schematic presentation of informative trNOEs of sLe <sup>x</sup> .....	78

Figure 4.15. Docking poses of selected HBGA in the VA387 binding pocket.....	79
Figure 4.16. Bound conformations of sLe <sup>x</sup> from MD simulation. ....	81
Figure 4.17. Binding epitope of heterodivalent inhibitor <b>31</b> .....	83
Figure 4.18. STD binding epitopes of hits from virtual screening.....	84
Figure 4.19. STD titration of virtual screening compound <b>42</b> . ....	85
Figure 4.20. Competitive STD titration of A trisaccharide with $\alpha$ -L-Fuc-(1, <i>O</i> )-CH <sub>3</sub> . ....	88
Figure 4.21. Competitive STD titration of divalent inhibitors with $\alpha$ -L-Fuc-(1, <i>O</i> )-CH <sub>3</sub> . ..	89
Figure 4.22. STD competition experiments with polymeric inhibitors.....	91
Figure 4.23. Competitive STD titration of BSA sugar conjugate. ....	93
Figure 4.24. SPR experiments with L-Fuc at different coverage rates of VLPs.....	96
Figure 4.25. SPR experiments with HBGAs showing negative response differences.....	97
Figure 4.26. Injections of H-disaccharide and B trisaccharide. ....	98
Figure 4.27. SPR experiments with monosaccharides yielding binding curves. ....	99
Figure 4.28. SPR experiments with fucosylated compounds.....	101
Figure 4.29. SPR experiment of H-disaccharide with immobilized VLPs. ....	103
Figure 4.30. Binding of H-disaccharide as a function of pH and buffer.....	104
Figure 4.31. SPR experiment with virtual screening hit <b>42</b> . ....	106
Figure 4.32. SPR experiment with virtual screening hits <b>43</b> and <b>44</b> .....	107
Figure 4.33. SPR experiments with the polyacrylamide backbone <b>34</b> .....	108
Figure 4.34. SPR experiments with polymeric compound <b>35</b> with L-Fuc.....	109
Figure 4.35. SPR experiments with polymeric compound <b>36</b> with fragment 160. ....	110
Figure 4.36. SPR experiments with other polymeric compounds.....	111
Figure 4.37. SPR response for polymeric compound as a function of VLP coverage.....	113
Figure 4.38. Binding of polymeric compound to VLPs and GTB. ....	114
Figure 4.39. Concentration-dependent VLP binding to PAA-fucose. ....	115
Figure 4.40. Competitive SPR experiments with polymers <b>35</b> and <b>37</b> on PAA-Fuc.....	116
Figure 4.41. Competitive SPR experiments with other polymers on PAA-Fuc. ....	117
Figure 4.42. Responses of VLP injection on BSA sugar conjugates. ....	119
Figure 4.43. pH profile of VLP binding to BSA sugar conjugates. ....	120
Figure 4.44. Competitive SPR experiments with VLPs with L-Fuc.....	121
Figure 4.45. Determination of titer of hemagglutination of VLP samples. ....	123
Figure 4.46. Hemagglutination assay with polymers and Ast6139 VLPs. ....	124
Figure 4.47. Hemagglutination assay with polymers and RHDV VLPs.....	125
Figure 5.1: Schematic presentation of HBGA antigen.....	128
Figure 5.2. Docking models of Le <sup>x</sup> and Le <sup>a</sup> . ....	135

Figure 5.3. Binding epitopes of H trisaccharide type 2 with Ast6139 and RHDV. ....	138
Figure 5.4. Minimal structural recognition motifs of three caliciviruses. ....	139
Figure 5.5. Predominant bound conformation of sLe <sup>x</sup> from MD simulation. ....	141
Figure 5.6. Ranking of HBGA binding strengths from STD NMR. ....	143
Figure 5.7. Basis of high affinity binding of virtual screening hit <b>42</b> . ....	149
Figure 7.1. Sequence alignment of NoV GII.4 strains from 32 years. ....	160
Figure 7.2. Sequence alignment of closely related NoV GII.4 strains. ....	161
Figure 7.3. HBGA binding pocket of GII NoV from protein crystallization. ....	162
Figure 7.4. Interaction sites of Lewis antigens with a GII.9 NoV. ....	163
Figure 7.5. STD titration of $\alpha$ -L-Fuc-(1, <i>O</i> )-CH <sub>3</sub> ( <b>2</b> ). ....	165
Figure 7.6. trROESY spectrum of sLe <sup>x</sup> in presence of VLPs. ....	169
Figure 7.7. Dependence of trNOE intensity on K <sub>D</sub> and k <sub>on</sub> . ....	169
Figure 7.8. Chemical shift changes during titration of <b>42</b> . ....	170
Figure 7.9. Sensorgrams of L-Fuc ( <b>1</b> ) injections on sensor chip C. ....	197
Figure 7.10. Sensorgrams of H type 6 ( <b>8a</b> ) injections on sensor chip C. ....	197
Figure 7.11. Sensorgrams of compound <b>30</b> injections on sensor chip C. ....	198
Figure 7.12. Sensorgrams of compound <b>31</b> injections on sensor chip C. ....	199
Figure 7.13. Measurement of H-disaccharide <b>3b</b> on sensor chip A in triplicate. ....	200
Figure 7.14. Measurement of H-disaccharide <b>3b</b> on sensor chip A in duplicate. ....	201
Figure 7.15. Measurement of H-disaccharide <b>3b</b> on sensor chip B in duplicate. ....	202
Figure 7.16. Measurement of virtual screening hit <b>42</b> on sensor chip C. ....	203
Figure 7.17. Measurement of virtual screening compound <b>43</b> on sensor chip C. ....	204
Figure 7.18. Measurement of virtual screening hit <b>44</b> on sensor chip C. ....	205
Figure 7.19. Measurement of polymeric compound <b>36</b> . ....	206
Figure 7.20. Measurement of polymeric compound <b>38</b> . ....	207
Figure 7.21. Measurement of polymeric compound <b>39</b> . ....	207
Figure 7.22. Measurement of polymeric compound <b>40</b> . ....	208
Figure 7.23. Measurement of polymeric compound <b>41</b> . ....	208
Figure 7.24. Measurement of polymeric compound <b>46</b> . ....	209
Figure 7.25. Measurement of polymeric compound <b>47</b> . ....	209
Figure 7.26. Dependence of VLP binding to PAA sugars on the flow rate. ....	210
Figure 7.27. Concentration dependent binding of VLPs to PAA sugars. ....	211
Figure 7.28. Inhibition curves for polymeric compounds on different PAA sugars. ....	212

## List of Tables

Table 1.1. Disease and species range of caliciviruses.....	2
Table 1.2. HBGA structures present in humans.....	8
Table 1.3. Known attachment factors of human and animal caliciviruses.....	15
Table 1.4. Crystal structures of NoV capsid proteins in complex with HBGAs.....	17
Table 3.1. Primers used for site-directed mutagenesis of VP1..	38
Table 4.1. HBGA binding specificity of Ast6139 VLPs determined by STD NMR.....	62
Table 4.2. HBGA specificity of bovine NoV NB2 determined by STD NMR.....	69
Table 4.3. Results of STD titration of xenoantigen with NB2.....	71
Table 4.4. Major solution conformational families of sLe <sup>x</sup> ..	73
Table 4.5. Analysis of selected sLe <sup>x</sup> trNOE build-up curves.....	77
Table 4.6. K <sub>D</sub> values from STD titration of compound <b>42</b> .....	86
Table 4.7. IC <sub>50</sub> values from competitive STD titration of HBGAs.....	90
Table 4.8. IC <sub>50</sub> values of polymeric inhibitors from competitive STD titrations.....	92
Table 4.9. IC <sub>50</sub> values from competitive STD titration of BSA-H type 2 conjugate..	93
Table 4.10. Results from SPR measurements with HBGAs and divalent inhibitors. ....	102
Table 4.11. Results from SPR measurement of virtual screening hit <b>42</b> . ....	106
Table 4.12. Results from SPR measurement of other virtual screening hits.....	108
Table 4.13. Results from SPR measurement of polymeric inhibitors.....	112
Table 4.14. Competitive SPR measurements with polymers on PAA-fucose. ....	118
Table 4.15. Competitive SPR measurements on BSA-H2 conjugate. ....	121
Table 4.16. Results of hemagglutination assays with VLPs and polymeric inhibitors.....	125
Table 5.1. K <sub>D</sub> and IC <sub>50</sub> values of polymers from different assay formats.....	150
Table 7.1. Results from curve fitting of $\alpha$ -L-Fuc-(1,O)-CH <sub>3</sub> titration curves.....	165
Table 7.2. Calculation of K <sub>D</sub> values of HBGAs from IC <sub>50</sub> values.....	166
Table 7.3. Sample composition and experimental parameters for STD NMR. ....	187
Table 7.4. Sample composition and parameters for NOESY and ROESY NMR.....	188
Table 7.5. Experimental parameters for assignment experiments. ....	196
Table 7.6. Results from SPR measurements of <b>43</b> and <b>44</b> on sensor chip C. ....	205
Table 7.7. Competitive measurements with polymeric compounds on PAA sugars..	213



## 1 Introduction

### 1.1 Caliciviruses

Noroviruses (NoV) are non-enveloped (+)-single stranded RNA viruses from the family *Caliciviridae*. They cause acute gastrointestinal infections in humans and animals and are well-known as ‘gastric flu’ or ‘winter vomiting disease’. In general, caliciviruses infect a broad range of hosts causing a variety of diseases (Green *et al.*, 2001; Thiel & Konig, 1999) (Table 1.1). Caliciviruses are grouped into five genera, namely Lagovirus, Vesivirus, Sapovirus, Norovirus and Nebovirus (International Committee on Taxonomy of Viruses, <http://ictvonline.org/>). Lagovirus comprises the European brown hare syndrome virus and the rabbit hemorrhagic disease virus (RHDV). RHDV leads to devastating hemorrhagic disease and liver damage in rabbits leading to death in a period as short as 48 hours. Since its first occurrence in 1984 in China (Liu *et al.*, 1984; Parra & Prieto, 1990) it caused epidemic outbreaks on all continents killing 90% of wild rabbit populations. It is therefore regarded as an emerging virus that was found to have originated from an avirulent ancestor by mutation (Kerr *et al.*, 2009; Moss *et al.*, 2002). Vesiviruses cause vesicular lesions and abortion in sea mammals and swine (Neill *et al.*, 1995), respiratory infections in cats (Geissler *et al.*, 1997) and were also found in a broad range of other animals (Neill *et al.*, 1998). Sapoviruses are responsible for sporadic gastroenteritis in humans and were detected in diarrheic pigs and minks (Guo *et al.*, 2001; Reuter *et al.*, 2010). Norovirus is by far the largest and best-studied genus that causes gastroenteritis in humans, cows, pigs and mice. It is divided into 5 genogroups GI to GV of which GI, GII and GIV cause infections in humans. GIII and GV comprise bovine and murine noroviruses, respectively, while porcine NoV strains belong to genogroup GII (Scipioni *et al.*, 2008; Zheng *et al.*, 2006). Nebovirus comprises only one species, Newbury-1 virus, and similar to bovine NoV causes gastroenteritis in cows (Oliver *et al.*, 2006). A sixth genus named Recovirus (rhesus enteric calicivirus) has been proposed (Farkas *et al.*, 2010; Farkas *et al.*, 2008).

Crossing of species barriers has been observed for animal caliciviruses (Bank-Wolf *et al.*, 2010; Koopmans, 2008; Smith *et al.*, 1998; Thiel & Konig, 1999). Shared attachment factor specificities can facilitate such inter-species transmissions although other host cell factors may prevent reproductive infections. Zoonotic infections in humans especially with the closely related porcine GII NoV seem possible but have not been reliably reported (Scipioni *et al.*, 2008).

Table 1.1. Disease and species range of caliciviruses.

Genus	Species	Virus	Disease symptoms
Lagovirus	hares	European brown hare syndrome virus (EBHSV)	hemorrhagic disease, necrotic hepatitis
	rabbits	Rabbit hemorrhagic disease virus (RHDV)	hemorrhagic disease, necrotic hepatitis, organ failure
Vesivirus	sea mammals	San Miguel Sea Lion virus (SMSV)	vesicular lesions, abortion
	swine	Vesicular exanthema of swine virus (VESV)	vesicular lesions
	cats	Feline calicivirus (FCV)	respiratory symptoms, conjunctivitis, oral ulceration; severe systemic disease
Sapovirus	humans, swine, mink	Sapporo and Sapporo-like viruses	acute gastroenteritis, diarrhea
Norovirus	humans, cows, swine, mice	Norwalk and Norwalk-like viruses	acute gastroenteritis, vomiting, diarrhea
Nebovirus	cows	Newbury-1	gastroenteritis
Recovirus	rhesus macaques	Tulane virus	unknown pathogenicity

## 1.2 Norovirus Epidemiology

NoV was first detected as infectious agent in an epidemic outbreak of gastroenteritis 1968 in Norwalk, Ohio (Kapikian *et al.*, 1972). Since then NoV became the major cause of acute non-bacterial gastroenteritis in humans certainly rendering them as emerging infectious disease (Patel *et al.*, 2008; Siebenga *et al.*, 2009). NoV infections have caught up with rotavirus infections that are still the major cause of severe gastroenteritis in children <5 years (Jiang *et al.*, 2010). NoV infection is diagnosed utilizing the so-called ‘Kaplan criteria’: 1) mean illness duration of 12 to 60 h, 2) an incubation period of 24 to 48 h, 3) more than 50% of infected people displaying symptoms of vomiting, and 4) the absence of a bacterial agent. All four criteria are a safe hint towards NoV infections although a significant portion does not meet each of the four criteria. Symptoms are rapid onset of watery diarrhea and vomiting, nausea, abdominal cramps, headaches, myalgia and fatigue (according to Robert Koch-Institute (RKI), Berlin). NoV infections are usually self-limiting with symptoms typically lasting for 12 h to three days. However patients can shed infectious virus particles for several days to weeks after recovery (Siebenga *et al.*, 2008; Tu *et al.*, 2008). Moreover, chronic NoV infections are frequently observed in immuno-compromised long-term hospitalized patients that display prolonged virus shedding for

month or even years (Beersma *et al.*, 2009; Saif *et al.*, 2011; Sukhrie *et al.*, 2010; Wingfield *et al.*, 2010). Together with shedding from asymptomatic infections this may be the basis for maintaining a basal level of NoV infection in the human population.

Strains from genogroups GI and GII cause the overwhelming majority of NoV infections in humans with 270 million reported and innumerable unreported cases worldwide each year (Donaldson *et al.*, 2008). In Germany 100.000 to 150.000 cases were reported annually by the RKI in the past five years constituting a nearly doubling of cases since the early 2000s. This may only in part be related to increased public awareness and hence higher diagnosis rates (Lopman *et al.*, 2004; Siebenga *et al.*, 2010). Since NoV are highly contagious, epidemic outbreaks are likely to occur in social settings such as nursing homes, hospitals, childcare centers, schools, restaurants, prisons, military and cruise ships (Fankhauser *et al.*, 2002; Lindesmith *et al.*, 2008; Matthews *et al.*, 2012). In addition to the enormous socio-economic losses (Johnston *et al.*, 2007) NoV can become a life-threatening disease in children, elderly and immunocompromised patients causing one million hospitalizations and 200,000 deaths in young children per year (Patel *et al.*, 2008). An increased incidence in the winter season initially led to the label ‘winter vomiting disease’ and ‘gastric flu’ with reference to influenza viruses that display a similar seasonality (Greer *et al.*, 2009; Lopman *et al.*, 2004; Lopman *et al.*, 2008; Mounts *et al.*, 2000).

NoV outbreaks are facilitated by an extremely high infection rate on the fecal-oral route via contaminated water and food, contaminated surfaces and direct person-to-person contact. An infectious dose of 10 to 100 virus particles was reported (Atmar & Estes, 2006). A more recent study even yielded an average infection probability of 0.5 per single NoV particle (Teunis *et al.*, 2008). Additionally, NoV display a high environmental stability and resistance towards many disinfectants which is directly linked to the high capsid stability (Ausar *et al.*, 2006; Cuellar *et al.*, 2010; D'Souza *et al.*, 2006; Duizer *et al.*, 2004a; Feng *et al.*, 2011). NoV are therefore classified as category B biodefense agents.

Due to the rapid clearance of the infection usually no long-termed immunity against NoV is established. Moreover, antibodies induced often lack cross-reactivity with other highly diverse NoV strains (see section 1.3). Immunity against one strain may not protect against infection with another strain. However, the high NoV prevalence and hence widespread short-term immunity in the human population is proposed to create a so-called ‘herd-immunity’ (Lindesmith *et al.*, 2008; Siebenga *et al.*, 2007). The resulting negative selection by the host immune response force NoV to undergo antigenic drift (Bull *et al.*, 2010; Donaldson *et al.*, 2008; Lindesmith *et al.*, 2011; Siebenga *et al.*, 2007). A linear,

epochal evolution of antigenic sites of the NoV capsid causes the appearance of new epidemic variants every two to three years (Shanker *et al.*, 2011; Siebenga *et al.*, 2007). In seasons of particularly high NoV incidence rates strains from the subcluster (genotype) GII.4 were shown to dominate while in other seasons a broader range of both GI and GII strains are detected (Koopmans, 2008; Kroneman *et al.*, 2008). This indicates differences in the infectiousness and/or pathogenicity of different genoclusters.

No medication is yet available for NoV infections. Treatment of hospitalized patients is limited to water and electrolyte replenishment and nutritional support. Clearance of chronic NoV infections in immunocompromised patients usually requires recovery of the immune system (Saif *et al.*, 2011). Vaccination strategies for NoV disease have been developed but the fast antigenic drift of NoV creates certain limitations (see section 1.9). The limited availability of cell culture and animal model systems for human NoV hampered the development of medical treatments and vaccines (Duizer *et al.*, 2004b; Lay *et al.*, 2010). The development and testing of so-called entry-inhibitors directed against initial host cell attachment during NoV infection is the central issue of this work.

### 1.3 Genomic Organization and Variability of Noroviruses

NoV are non-enveloped icosahedral viruses containing a 7.5 to 7.7 kB positive-sense single-stranded RNA genome. Early studies revealed the presence of three open reading frames (ORFs) in the NoV genome (Xi *et al.*, 1990) (Figure 1.1). ORF1 encodes nonstructural proteins, including a nucleotide triphosphatase (NTPase), the VPg protein that is covalently linked to the 5' end of the genomic RNA, a 3C-like cysteine protease (Pro) and an RNA-dependent RNA polymerase (Pol). It is expressed as a ~200 kDa polyprotein and further processed by the viral protease. ORF2 encodes the 60 kDa major capsid protein VP1 of which 180 copies form the capsid. ORF3 encodes for a smaller 22 kDa structural protein that is present in a lower copy number per virus particle. It may play a role in enhancing VP1 expression and stability (Bertolotti-Ciarlet *et al.*, 2003). Both structural proteins are expressed from a 2.3 to 2.5 kB subgenomic RNA that is transcribed from the genomic RNA by the non-structural proteins (Asanaka *et al.*, 2005; Bertolotti-Ciarlet *et al.*, 2003).

The major capsid protein VP1 is divided into an N-terminal shell (S) domain responsible for spherical particle formation and a protruding (P) domain. The outmost P2 domain is an

insert of the P1 domain. It contains antigenic epitopes and binding sites to host attachment factors that have been identified as histo-blood group antigens (HBGAs) on the surface of the gastrointestinal epithelium (Hutson *et al.*, 2003; Marionneau *et al.*, 2002) (see sections 1.4 and 1.5).

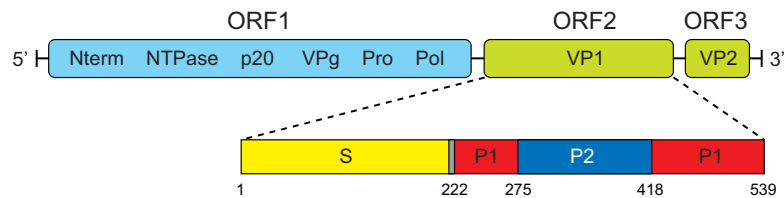


Figure 1.1. Structural organisation of the NoV genome and the VP1 protein. Top panel: NoV genome with three ORFs encoding for non-structural proteins (blue) and the major and minor capsid proteins (green). Bottom panel: domain organization of the major capsid protein VP1 that can be divided into a shell (S) and a protruding (P) domain separated by a small hinge; residue numbers indicate domain boundaries for the GII.4 strain Ast6139 used in this study.

The major capsid protein is under high pressure to evade the host immune system resulting in a fast mutation rate especially in the P2 domain (Bok *et al.*, 2009a; Bull *et al.*, 2010; Nilsson *et al.*, 2003; Rohayem *et al.*, 2005). The resulting antigenic drift creates a large sequence diversity (Lindesmith *et al.*, 2011) that probably contributes to rapid worldwide distribution of NoV and that leads to many new epidemic variants (Lindesmith *et al.*, 2008; Siebenga *et al.*, 2007). A high mutation rate seems to be a common feature of emerging viruses that are most often single-stranded RNA viruses of either positive sense (e.g. SARS coronavirus, Chikungunya virus and West Nile virus) or negative sense (e.g. Ebola virus and reassorted influenza viruses).

NoV are clustered into five genogroups GI to GV and at least 29 genotypes based on phylogenetic analysis of the major capsid protein VP1 (Zheng *et al.*, 2006). Recently NoV with recombinant genomes of different genogroups have been characterized as well (Motomura *et al.*, 2010; Rohayem *et al.*, 2005). The sequence variation within a genogroup is 20% to 40% while different genogroups differ by 40% to 60% (Bok *et al.*, 2009a; Zheng *et al.*, 2006). The best-studied NoV group is the currently dominating GII.4 genotype. Analysis of the full length capsid protein sequences of 185 GII.4 strains from a period of 34 years (1974 – 2008) revealed a mutation rate of  $4.3 \times 10^{-3}$  nucleotide substitutions per site per year (Bok *et al.*, 2009a) which is close to the average evolution rate of RNA viruses of about  $1 \times 10^{-3}$  (Duffy *et al.*, 2008). One half of the 13.5% variable sites of VP1 were located in the P2 domain that constitutes only one fourth of the protein length (Figure 1.2).

Despite the high sequence diversity, a strict conservation of residues directly involved in HBGA recognition was found by multiple sequence alignment of GII.4 strains from the past three decades (Bok *et al.*, 2009a; Lindesmith *et al.*, 2008). The HBGA binding site was identified previously by co-crystallization of the GII.4 strain VA387 in complex with A and B antigens (Cao *et al.*, 2007) (see section 1.8). It is proposed that NoV infection strictly requires binding to HBGAs and the respective residues are therefore under high selective pressure. Nevertheless, mutation of residues close to this binding site can modify the attachment factor specificity. The invasion of new host populations by altered attachment factor specificities is thought to be one of the driving forces that lead to the emergence of new epidemic NoV strains every two to three years (Donaldson *et al.*, 2008; Lindesmith *et al.*, 2008). The high variability of surface exposed residues also reflects antigenic epitope variation. Escape from herd immunity by antigenic drift is even proposed to be the main evolutionary pressure to NoV (Lindesmith *et al.*, 2011; Siebenga *et al.*, 2007).

The informative and conserved sites of the major capsid protein of representative GII.4 strains are depicted in Figure 1.2 (see Figure 7.1 in the appendix for a full sequence alignment). The GII.4 strain Ast6139 studied in this work is included for comparison.

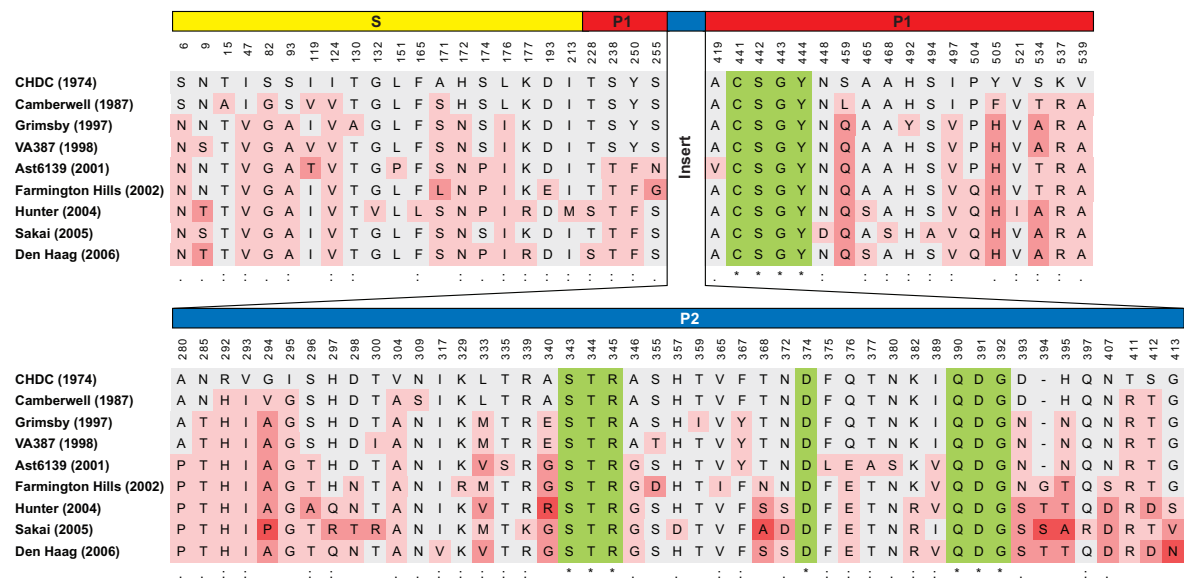


Figure 1.2. Variable and conserved sites of GII.4 NoV major capsid proteins. Multiple sequence alignment of prototype strains of main clusters from 32 years as well as strains VA387 (Grimsby cluster) and Ast6139 (Farmington Hills cluster) was created with ClustalW (Larkin *et al.*, 2007). Red coloring indicates accumulation of mutations at variables sites; green color marks conserved sites in the HBGA binding pocket. Modified from (Bok *et al.*, 2009a).

Each strain except VA387 and Ast6139 represents an identically named GII.4 cluster: CHDC (1974–1977), Camberwell (1987–1994), Grimsby (1995–2001), Farmington Hills (2002–2004), Hunter (2002–2006), Sakai (2004–2007) and Den Haag (2006–2007) (Bok *et al.*, 2009a). Post-2002 strains are characterized by a single amino acid insertion at position 395, most often a threonine. This insertion is reported to cause enhanced HBGA binding affinity and hence undergoes positive selection (de Rougemont *et al.*, 2011; Siebenga *et al.*, 2010).

The strain Ast6139 investigated in this work most closely belongs to the Farmington Hills cluster although it lacks the T395 insertion. The GII.4 strain VA387 from the Grimsby cluster has 95% sequence identity with Ast6139. Therefore the experimental results for Ast6139 will be compared to previously published data of VA387 attachment factor binding (Cao *et al.*, 2007; Huang *et al.*, 2005).

#### **1.4 Host Attachment Factors: Histo-Blood Group Antigens**

Human NoV were discovered to exploit so-called histo-blood group antigens (HBGAs) as attachment factors (Harrington *et al.*, 2002; Hutson *et al.*, 2002; Lindesmith *et al.*, 2003).

HBGAs are the carbohydrate entities of glycoproteins and glycolipids on the surface of many cell and tissues types (Marionneau *et al.*, 2001; Milland & Sandrin, 2006; Stanley & Cummings, 2009). They form the ca. 100 nm wide glycocalyx that plays a role in protection against physical and chemical damage, in cell-cell adhesion and communication, embryogenesis and identification of ‘self’ and ‘non-self’ by the immune system (Reitsma *et al.*, 2007). HBGA are present in mucosal epithelia of the gastrointestinal, respiratory and genitourinary tracts. On red blood cells and vascular endothelia they determine the blood group of an individual. The formation of antibodies against ‘foreign’ HBGA not present in an individual is the reason for immunologic shock syndromes after erroneous blood transfusions as well as graft rejection after organ transplantations (Milland & Sandrin, 2006). HBGA are also present as free oligosaccharides in body fluids such as saliva and milk where they may function as decoy receptors for pathogens (Le Pendu, 2004). Epidemiologic and *in vitro* data indicated a blocking effect of mother milk against a range of pathogens including caliciviruses offering protection of breast-fed infants (Jiang *et al.*, 2004; Morrow *et al.*, 2005; Ruvoen-Clouet *et al.*, 2006).

HBGAs can be generally divided into ABH and Lewis-type antigens (Stanley & Cummings, 2009) that are synthesized from six different precursor types (Marionneau *et al.*, 2001; Meloncelli & Lowary, 2009) (Table 1.2). Their biosynthesis is accomplished by a range of glycosyltransferases that are specific for the type of the donor and acceptor sugar as well as for the created linkage. The major pathways for the biosynthesis of HBGAs in humans are illustrated in Figure 1.3. Genetic polymorphism and variable expression patterns of glycosyltransferases create unique glycosylation patterns in different tissues, individuals and species. Especially the interaction with pathogens that exploit host carbohydrates as attachment factors and receptors is thought to be the evolutionary selection force for the diversification of HBGAs (Gagneux & Varki, 1999).

Table 1.2. HBGA structures present in humans. ‘R’ indicates the position of backbone elongations.

HBGA	Structure	Symbol <sup>[a]</sup>
<b>backbone precursor</b>		
type 1 precursor	D-Gal- $\beta$ (1,3)- $\beta$ -D-GlcNAc-R	
type 2 precursor	D-Gal- $\beta$ (1,4)- $\beta$ -D-GlcNAc-R	
type 3 precursor	D-Gal- $\beta$ (1,3)- $\alpha$ -D-GalNAc-R	
type 4 precursor	D-Gal- $\beta$ (1,3)- $\beta$ -D-GalNAc-R	
type 5 precursor	D-Gal- $\beta$ (1,3)- $\beta$ -D-Gal-R	
type 6 precursor	D-Gal- $\beta$ (1,4)- $\beta$ -D-Glc-R	
<b>ABH antigens</b>		
H-disaccharide	L-Fuc- $\alpha$ (1,2)- $\beta$ -D-Gal-R	
A antigen	D-GalNAc- $\alpha$ (1,3)-[L-Fuc- $\alpha$ (1,2)]- $\beta$ -D-Gal-R	
B antigen	D-Gal- $\alpha$ (1,3)-[L-Fuc- $\alpha$ (1,2)]- $\beta$ -D-Gal-R	
<b>Lewis antigens</b>		
Lewis <sup>x</sup> (Le <sup>x</sup> )	D-Gal- $\beta$ (1,4)-[L-Fuc- $\alpha$ (1,3)]- $\beta$ -D-GlcNAc-R	
Lewis <sup>a</sup> (Le <sup>a</sup> )	D-Gal- $\beta$ (1,3)-[L-Fuc- $\alpha$ (1,4)]- $\beta$ -D-GlcNAc-R	
Lewis <sup>y</sup> (Le <sup>y</sup> )	L-Fuc- $\alpha$ (1,2)-D-Gal- $\beta$ (1,4)-[L-Fuc- $\alpha$ (1,3)]- $\beta$ -D-GlcNAc-R	
Lewis <sup>b</sup> (Le <sup>b</sup> )	L-Fuc- $\alpha$ (1,2)-D-Gal- $\beta$ (1,3)-[L-Fuc- $\alpha$ (1,4)]- $\beta$ -D-GlcNAc-R	
sialyl-Lewis <sup>x</sup> (sLe <sup>x</sup> )	D-Neu5Ac- $\alpha$ (2,3)-D-Gal- $\beta$ (1,4)-[L-Fuc- $\alpha$ (1,3)]- $\beta$ -D-GlcNAc-R	
sialyl-Lewis <sup>a</sup> (sLe <sup>a</sup> )	D-Neu5Ac- $\alpha$ (2,3)-D-Gal- $\beta$ (1,3)-[L-Fuc- $\alpha$ (1,4)]- $\beta$ -D-GlcNAc-R	

[a] Symbols according to the CFG nomenclature (<http://www.functionalglycomics.org/>)



The H-disaccharide is synthesized from one of the precursor disaccharides by attachment of an L-Fuc residue in  $\alpha 1,2$ -linkage to the  $\beta$ -Gal. This step is catalyzed by one of two  $\alpha 1,2$ -fucosyltransferases (FUT) that have different acceptor specificities and are expressed in different tissue types (Mollicone *et al.*, 1995). FUT1 is expressed in erythrocyte precursors and vascular endothelium. Deletion or mutation of the FUT1 locus creates the very rare ‘Bombay’ phenotype that lacks ABH antigens on erythrocytes and is not compatible for blood transfusions from any A, B or O blood group donor. A second  $\alpha 1,2$ -fucosyltransferase FUT2 is expressed in epithelial tissue. Since the synthesized carbohydrates are also excreted from these tissues, the FUT2 locus is named ‘Se’. Individuals with a functional FUT2 are called secretor-positives or secretors. The biosynthesis and presentation of ABH antigens on glycoproteins (mucins) and glycolipids in the mucosal epithelium of the gastrointestinal tract is the basis for the infection with secretor-specific NoV strains. Non-secretors (*se*) with deletions or mutations in the FUT2 gene do not present or excrete ABH antigens in their gastrointestinal tract and are resistant to most NoV strains (see section 1.5). Ca. 20% of the European and North American populations have this phenotype (Marionneau *et al.*, 2001). FUT2 uses mainly type 1 and 3 precursor structures as acceptor sugars while FUT1 displays specificity for type 2 precursors. In the gastrointestinal mucosa ABH antigens of type 1 and type 3 will therefore prevail.

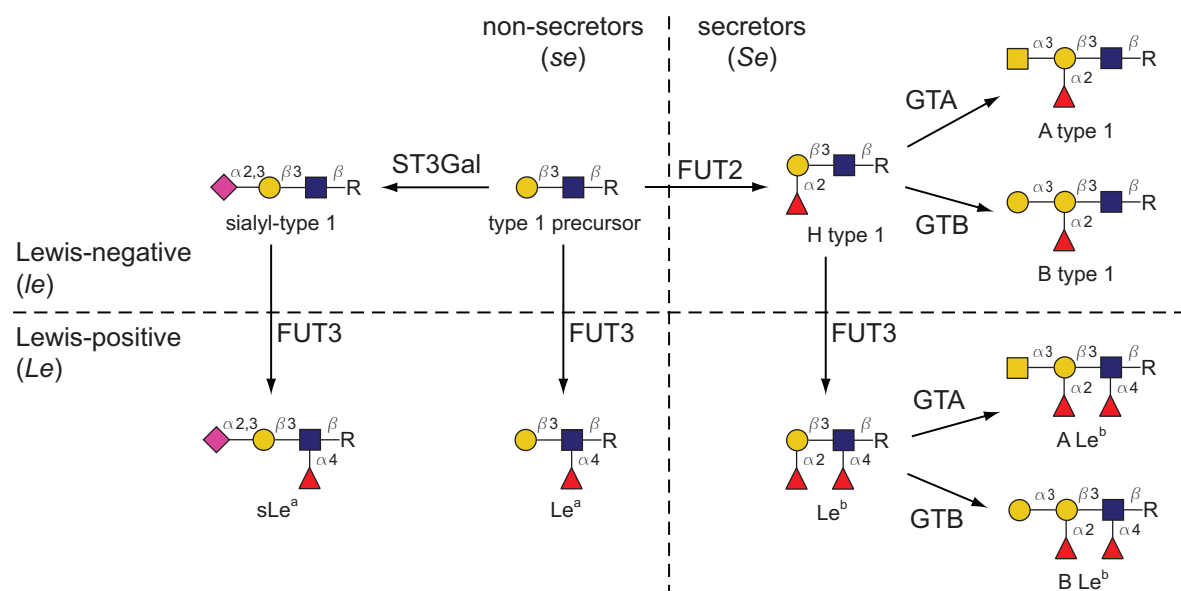


Figure 1.3. Biosynthesis pathways of HBGAs from type 1 precursors. In secretor-positive individuals, FUT2 synthesizes H antigen type 1 from type 1 precursor. It can be further modified by GTA or GTB to yield A or B antigens, respectively. FUT3 can attach  $\alpha 1,4$ -Fuc to the GlcNAc of type 1 precursor or H antigen type 1. Concerted action of  $\alpha 2,3$ -sialyltransferase (ST3Gal) and FUT3 yields  $sLe^a$ .

H antigen can serve as precursor for the attachment of a GalNAc or Gal residue in  $\alpha(1,3)$ -linkage to the  $\beta$ -Gal yielding A and B antigens, respectively. These steps are catalyzed by  $\alpha 1,3$ -N-acetylgalactosaminyltransferase (GTA) and  $\alpha 1,3$ -galactosyltransferase (GTB), respectively. Genetic polymorphisms of both enzymes and their expression on erythrocytes account for the distinct distribution of ABO blood groups in human populations.

The second class of HBGAs are Lewis antigens. They are characterized by  $\alpha 1,3$ - or  $\alpha 1,4$ -linked Fuc on the GlcNAc of type 2 and type 1 structures, respectively.  $Le^a$  comprises  $\alpha 1,4$ -linked Fuc and is synthesized from the type 1 precursor by the  $\alpha 1,3/\alpha 1,4$ -fucosyltransferase FUT3 (locus *Le*) (Marionneau *et al.*, 2001). FUT5 can also catalyze this step, but it has a marked preference for type 2 structures. Individuals without a functional FUT3 therefore *de facto* have a 'Lewis-negative' phenotype. Difucosylated  $Le^b$  is synthesized by the concerted action of FUT3 and FUT2 (Figure 1.3). Both enzymes have similar tissue expression patterns so that secretor- and Lewis-positive individuals mainly present  $Le^b$  antigens in their gastrointestinal mucosa, while Lewis-positive non-secretors have only  $Le^a$ . Secretor- and Lewis-negative individuals display only the type 1 precursor.

$Le^x$  contains  $\alpha 1,3$ -linked Fuc and is synthesized from the type 2 precursor by at least five different  $\alpha 1,3$ -fucosyltransferases (Marionneau *et al.*, 2001). Similar to  $Le^a$ , the additional attachment of  $\alpha 1,2$ -Fuc to the  $\beta$ -Gal by FUT1 yields difucosylated  $Le^y$ . The requirement of type 2 precursor structures and FUT1 activity limits the expression of  $Le^y$  to erythrocytes and vascular endothelium.

Addition of sialic acid in  $\alpha 2,3$ -linkage to the  $\beta$ -Gal of type 1 or 2 precursors is catalyzed by different  $\alpha 2,3$ -sialyltransferases (ST3Gal) (Marionneau *et al.*, 2001). The following action of FUT3 yields sialyl- $Le^x$  ( $sLe^x$ ) and sialyl- $Le^a$  ( $sLe^a$ ) (Figure 1.3). Lewis blood group antigens play an important role in selectin-mediated endothelial adhesion –the so-called 'rolling'– of lymphocytes (Schauer, 2009). Lewis and especially sialyl-Lewis antigens have been identified as cancer-associated antigens that mediated tumor metastasis due to exploitation of the same selectin pathways (Heimburg-Molinaro *et al.*, 2011).

## 1.5 Characterization of Norovirus Attachment Factors

The characterization of attachment factors or cell receptors for viruses is usually achieved with infectious virus particles in cell or tissue cultures and animal models. Routine cell culture assays for human NoV are not available yet (Duizer *et al.*, 2004b; Lay *et al.*, 2010). Only very recently a complex 3-dimensional cell culture model of the human small and large intestine was established for infectivity assays with human NoV (Straub *et al.*, 2011; Straub *et al.*, 2007). It will provide crucial information on host cell attachment and entry, pathogenesis and immune response upon NoV infections in humans in the future.

Animal models for *in vivo* studies of human NoV are very limited. Recently, a study was published in which gnotobiotic calves and pigs were infected with human NoV (Cheetham *et al.*, 2006; Souza *et al.*, 2008). Despite similar symptoms, the pathogenesis and host immune response of the caused diseases may differ from that in humans.

Valuable information on the disease pathogenesis in humans was obtained by challenging volunteers with human NoV. Thereby ABH antigens present on the gastrointestinal epithelium were identified as host cell attachment factors for NoV (Harrington *et al.*, 2002; Hutson *et al.*, 2002; Parrino *et al.*, 1977). A high increase of the infection risk for volunteers with a positive secretor status implicated the FUT2 locus as a genetic risk factor for infectivity (Hutson *et al.*, 2005; Larsson *et al.*, 2006; Le Pendu *et al.*, 2006; Thorven *et al.*, 2005) although some NoV strains can infect also secretor-negative individuals (Carlsson *et al.*, 2009; Lindesmith *et al.*, 2005; Nordgren *et al.*, 2010).

The ability to recombinantly express the major capsid protein *in vitro* had large impact on the field and enabled more detailed studies of HBGA binding to NoV. Cloning of the full length VP1 gene into recombinant baculoviruses allowed its expression in insect cell culture (Hale *et al.*, 1999; Jiang *et al.*, 1992; Jiang *et al.*, 2002; Lew *et al.*, 1994). Expressed VP1 self-assembles into so-called virus-like particles (VLPs) that have very similar morphologic and antigenic properties compared to the native virions (Green *et al.*, 1993; Hale *et al.*, 1998; Jiang *et al.*, 1992). Availability of non-infectious VLPs facilitated studies of structural, biophysical and immunological properties and of host attachment factor binding to NoV. VLPs were used in ELISA-based binding assays with captured saliva samples and synthetic oligosaccharides (Huang *et al.*, 2005; Hutson *et al.*, 2005; Marionneau *et al.*, 2005; Tan & Jiang, 2005a). Eight HBGA binding patterns were described for VLPs of different NoV strains (Tan & Jiang, 2005a) (Figure 1.4). Most NoV strains including the dominating epidemic GII.4 strains (e.g. VA387) show secretor-

dependent binding. The prototype Norwalk virus from genogroup GI.1 binds to saliva of O or A blood group but not to B type saliva or B trisaccharide. The resulting reduced risk of infection for blood group B volunteers contributed to the discovery of HBGAs as attachment factors for NoV (Hutson *et al.*, 2002). Only very few strains showed a Lewis-dependent binding. The strains Boxer (GI.8) and VA207 (GII.9) bound to Lewis as well as H antigens and therefore recognized both non-secretor- and secretor-type saliva. The GII.21 strain OIF ('Operation Iraqi Freedom') only bound to Lewis oligosaccharides and exhibited exclusive binding to non-secretor-type saliva. Some strains did not bind to any of the tested saliva or carbohydrates indicating yet another attachment factor(s).

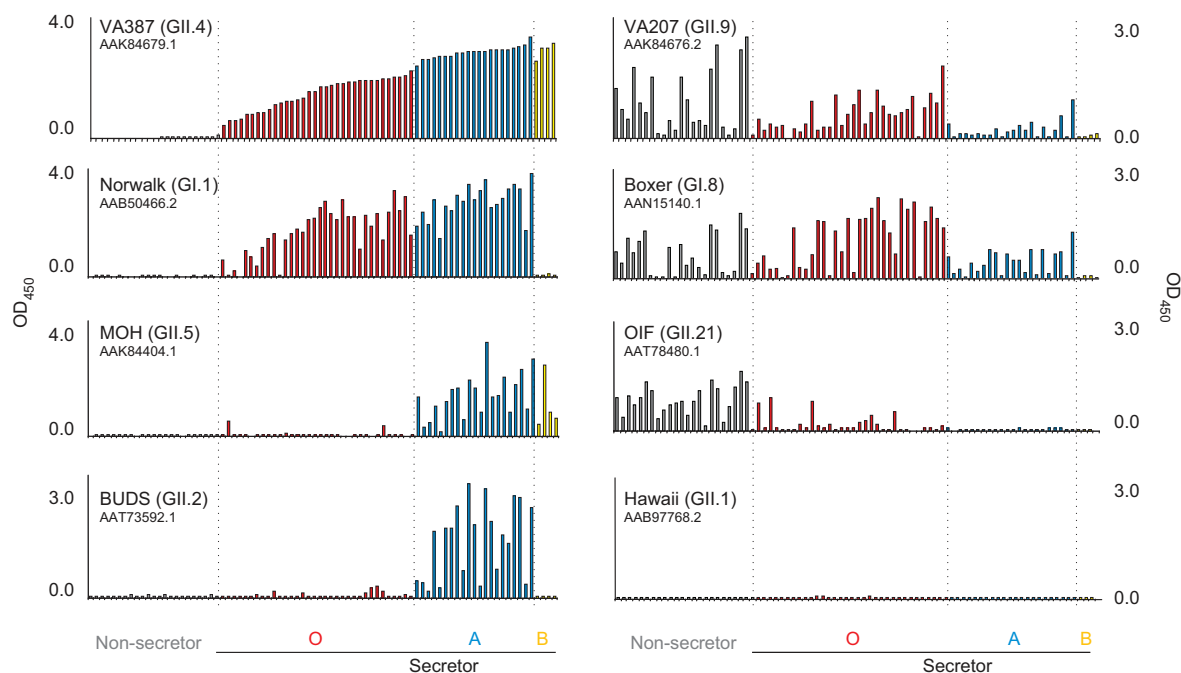


Figure 1.4. Known HBGA binding patterns of NoV capsids. Results from ELISA-based binding assays using saliva of secretor and non-secretor type individuals show eight unique binding patterns each represented by one NoV strain (given with genotype and GenBank accession number). Previously unclassified NoV isolates have been assigned with an automated genotyping tool (<http://www.rivm.nl/mpf/norovirus/typingtool/>) (Kroneman *et al.*, 2011). The currently dominating GII.4 strains (e.g. VA387) show secretor-dependent binding. The figure was adapted from (Tan & Jiang, 2005a).

Divergent HBGA binding patterns were observed in assays with saliva and monovalent oligosaccharides compared to those with polyvalent neoglycoproteins (de Rougemont *et al.*, 2011; Rydell *et al.*, 2009). The two strains Dijon (epidemic GII.4 strain) and Chron1 (GII.3 from a chronically infected patient) for example showed strong secretor-dependent binding to saliva but nevertheless bound to non-secretor-type sLe<sup>x</sup> neoglycoprotein (Rydell *et al.*, 2009). This may likely be due to increased avidity of polyvalent neoglycoproteins

and the inability of ELISA assays to detect weak binding. The role that such a binding plays for infectivity is yet to be defined.

Surface plasmon resonance (SPR) spectroscopy was likewise employed to investigate the HBGA binding specificity of NoV VLPs on a qualitative and semi-quantitative level. SPR experiments with immobilized monovalent oligosaccharides suggested that GII.4 strains bind tighter to ABH antigens with type 1 backbone structures (Shirato *et al.*, 2008). An SPR study with immobilized polyvalent HBGA neoglycoconjugates demonstrated stronger binding of the epidemic GII.4 strain Den Haag from 2006 to A and B antigens compared to older strains (de Rougemont *et al.*, 2011). The reported positive selection of the insertion T395 in post-2002 variants including Den Haag may be explained by this increased affinity (Siebenga *et al.*, 2010).

Truncated P domains of VP1 can also be expressed in *E.coli* culture. Depending on the expression construct the expressed P protein forms dimers (Tan *et al.*, 2004a) or so-called P particles (Tan & Jiang, 2005b). Both forms can interchange and the P particles have been shown to be stabilized by disulfide bond formation between cysteine rich peptides attached at the C-terminus. P particles are build from 12 identical P dimers (T=1 symmetry) resulting in a molecular weight of ~830 kDa and a diameter of ~5 nm. P dimers and P particles were found to have similar antigenicity and HBGA binding patterns compared to VLPs (Tan *et al.*, 2008a; Tan & Jiang, 2005b; Tan *et al.*, 2004b). Nevertheless differences were observed in the HBGA binding affinity and possibly in the immunogenic properties compared to VLPs (Tamminen *et al.*, 2012).

The stability of VLPs and P particles towards pH and environmental influences has been described (Ausar *et al.*, 2006; Bereszcak *et al.*, 2012). Both forms are stable over a wide range of pH values from ca. pH 3 to 7. Above pH 8 conformational changes and irreversible decomposition of the particles was observed. The pH stability profile may reflect the necessity for NoV to pass the acidic gut to reach the intestinal mucosa.

## 1.6 Attachment Factors of other Caliciviruses

For animal caliciviruses several disease models are available. The bovine NoV strain 'Jena' (GIIL.1) was used to infect newborn gnotobiotic calves that developed severe watery diarrhea (Otto *et al.*, 2011). Histopathologic analysis revealed intestinal lesions and villus atrophy. Similar tissue- and cytopathic effects are likely to occur in NoV infections in

humans. *In vitro* experiments with bovine gut tissue sections and VLPs of bovine NoV GIII.2 strain 'Newbury 2' identified the Galili epitope  $\alpha$ -D-Gal-(1,3)-D-Gal as an attachment factor (Zakhour *et al.*, 2009). It can be found in all mammals except in apes and humans due to inactivation of the  $\alpha$ 1,3-galactosyltransferase gene. Therefore, it is also referred to as xenoantigen (from greek 'xenos' for 'foreign'). Antibodies against bovine GIII.2 NoV were found in veterinarians (Widdowson *et al.*, 2005). This may however be a result of cross-reactive antigenic epitopes of bovine and human NoV rather than zoonotic infections that seem unlikely considering the absence of the Galili epitope in humans.

For murine NoV from genogroup GV cell culture and animal models are well established (Radford *et al.*, 2004; Wobus *et al.*, 2004; Wobus *et al.*, 2006). They replicate in murine dendritic cells and macrophages allowing insight into viral replication, the role of viral and host factors and cellular immune responses (Bok *et al.*, 2009b; Changotra *et al.*, 2009). Infection of laboratory mice with murine NoV provides additional information on the pathogenesis and the efficiency of candidate vaccines *in vivo* (Bailey *et al.*, 2008; Lobue *et al.*, 2009; McFadden *et al.*, 2011; Mumphrey *et al.*, 2007; Strong *et al.*, 2012). Thereby, sialic acids on gangliosides were identified as primary attachment factors for murine NoV (Taube *et al.*, 2009). Sialic acids are also present in the human intestine. But the strong secretor (FUT2) dependency of most human NoV excludes a critical role of sialylated gangliosides in human NoV infections (Kindberg *et al.*, 2007; Le Pendu *et al.*, 2006). Moreover human NoV do not replicate in macrophages or dendritic cells implicating a different host entry site (Lay *et al.*, 2010).

For the Lagovirus RHDV cell culture and animal models showed binding to H type 2 antigens on rabbit epithelial cells and dependence on  $\alpha$ 1,2-fucosyltransferase activity (Guillon *et al.*, 2009; Ruvoen-Clouet *et al.*, 2000). Recognition of B and H type 2 antigen but not type 1 antigens was observed at atomic detail by saturation transfer difference (STD) NMR spectroscopy (Rademacher *et al.*, 2008).

Feline calicivirus (FCV), a member of the Vesivirus genus, can also be propagated in cell culture (Abente *et al.*, 2010; Stuart & Brown, 2007). Beside the use of  $\alpha$ 2,6-linked sialic acid as attachment factor the cellular receptor junctional adhesion molecule 1 (JAM-1) played a functional role in FCV infection (Bhella *et al.*, 2008; Makino *et al.*, 2006). FCV is the only calicivirus for which an additional protein receptor has been identified. The existence of such a receptor for other caliciviruses, facilitating cell entry after initial attachment factor recognition, can be hypothesized.

The known attachment factor specificities of caliciviruses are summarized in Table 1.3.

Table 1.3. Known attachment factors of human and animal caliciviruses.

Genus	Species	Virus	Attachment factor(s)	Citation
Lagovirus	rabbits	RHDV	HBGAs (B, type 2 structures)	(Marionneau <i>et al.</i> , 2002; Rademacher <i>et al.</i> , 2008)
Vesivirus	cats	FCV	sialic acids ( $\alpha$ 2,6-linked)	(Stuart & Brown, 2007)
	sea lions, swine	SMSV, VESV	?	–
Sapovirus	humans, swine, mink	Sapporo-like viruses	?	–
Norovirus	humans (swine ?)	GI, GII	HBGAs (ABH and Lewis antigens), others?	(Le Pendu <i>et al.</i> , 2006; Tan & Jiang, 2005a)
	bovine	GIII	HBGAs (xenoantigen)	(Zakhour <i>et al.</i> , 2009)
	humans	GIV	?	–
	mice	GV	sialic acids on gangliosides	(Taube <i>et al.</i> , 2009)
Nebovirus	cows	Newbury-1	?	–
Recovirus	rhesus macaques	Tulane virus	HBGAs	(Farkas <i>et al.</i> , 2010)

The shared attachment factor specificity of a range of calicivirus raises the question of the probability of zoonotic infections in humans. In particular, this applies for porcine NoV that are within the same genogroup GII as human NoV. No symptomatic infection of this kind has been described so far (Scipioni *et al.*, 2008). Antibodies against porcine NoV found in humans and *vice versa* may reflect cross-reactive antigenic epitopes of porcine and human NoV rather than reproductive infection. Nevertheless, simultaneous presence of animal and human NoV in the same host opens the possibility for recombination and emergence of new chimeric strains with altered pathogenesis and virulence. A co-ingestion of different caliciviruses can occur for example in seafood-born NoV infections since oysters and shellfish enrich caliciviruses by expression of carbohydrates similar to HBGAs in their digestive tracts (Le Guyader *et al.*, 2006; Maalouf *et al.*, 2010).

## 1.7 Structure of the Norovirus Capsid

The general architecture of calicivirus capsids was elucidated with cryo-electron microscopy and three-dimensional reconstruction techniques of VLPs (Katpally *et al.*, 2010; Prasad *et al.*, 1994; Thouvenin *et al.*, 1997). These investigations indicated a  $T = 3$  icosahedral symmetry i.e. 180 copies of the major capsid protein VP1 are assembled in three quasi-equivalent conformations A, B and C. A/B dimers are arranged around the fivefold axis while C/C dimers are located along the twofold axis (cf. Figure 1.7 a)). The dimers are stabilized by  $\sim 2000$  Å contact areas. VP1 can be generally divided into a shell (S) and an archlike protruding (P) domain. The low resolution of the structures did not allow for a detailed investigation of the protein conformation. However, this became possible with the first X-ray crystal structure of whole intact NoV VLPs, namely from the prototype Norwalk virus (Prasad *et al.*, 1999). The phase problem was solved by phase extension using the previously published data from cryo-electron microscopy. A relatively high resolution of 3.4 Å reveals details on the VP1 conformation (Figure 1.5).

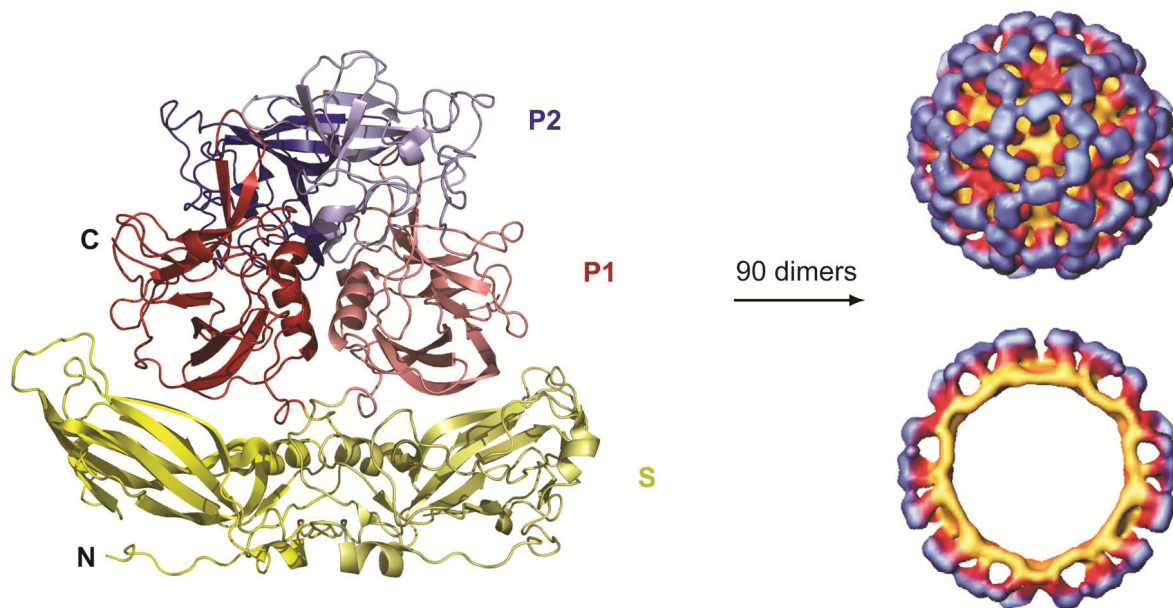


Figure 1.5. Structure of the capsid protein of the GI.1 Norwalk virus. (Left) VP1 forms dimers (monomers indicated by strong and pale coloring, respectively) with interaction sites in the S (yellow), P1 (red) and P2 (blue) domains; N and C terminus are indicated (pdb code 1ihm) (Prasad *et al.*, 1999). (Right) 90 dimers assemble into a full capsid shown in overall view (top) and as cross section (bottom); modified from (Hutson *et al.*, 2004).

The S domain forms the inner shell and consists of the first 225 N-terminal residues of VP1. It contains an 8-stranded antiparallel  $\beta$ -sandwich that is also found in other viral structural proteins. Connected via a flexible hinge follows the P domain that possesses a



fold different from any other known viral protein. It is further divided into the P1 domain consisting of residues 226 to 278 and 406 to 520, and the P2 domain being an insertion of P1 from residues 279 to 405. The P2 domain at the outmost surface of the capsid contains the recognition sites for attachment factors as well as antigenic epitopes.

A second crystal structure of whole VLPs was obtained for the Vesivirus San Miguel sea lion virus (Chen *et al.*, 2006). It revealed a similar overall architecture compared to Norwalk virus. Pronounced differences at the secondary structure level especially in the P domain may be related to the different host specificity and pathogenicity.

### 1.8 Structural Details on HBGA Recognition by Noroviruses

Protein crystal structures of NoV in complex with HBGA fragments have been obtained only for P dimers, the truncated versions of VP1 containing only the P domain (Tan *et al.*, 2004a). HBGAs were either co-crystallized or soaked into pre-crystallized protein. For both methods crystals of whole VLPs seem to be too loose. So far, crystal structures for one GI strain and four GII strains were published (see Table 1.4 for a compilation and Figure 1.6 for phylogenetic analysis and HBGA binding specificities). In most cases the phases of the structures were obtained by the molecular replacement method using the solved crystal structure of Norwalk VLPs (Prasad *et al.*, 1999).

*Table 1.4. Crystal structures of NoV capsid proteins in complex with HBGAs. The only structure of intact VLPs was published for Norwalk virus (Prasad et al., 1999). All co-crystal structures with HBGAs were accomplished with P dimers.*

Strain (genogroup)	GenBank accession No.	HBGAs co-crystallized	Comments	Citation
		–	whole intact VLPs	(Prasad <i>et al.</i> , 1999)
Norwalk (GI.1)	AAB50466.2	A trisaccharide, H type 1 pentasaccharide A trisaccharide		(Choi <i>et al.</i> , 2008) (Bu <i>et al.</i> , 2008)
VA387 (GII.4)	AAK84679	A trisaccharide, B trisac- charide		(Cao <i>et al.</i> , 2007)
VA207 (GII.9)	AAK84676.2	Le <sup>y</sup> , sLe <sup>x</sup>	Lewis binder	(Chen <i>et al.</i> , 2011)
Vietnam026 (GII.10)	AAT12445.1	H-disaccharide, A, B and H type 2 trisaccharides, Le <sup>y</sup> , Le <sup>b</sup> (disordered: Le <sup>x</sup> , Le <sup>a</sup> )	$\alpha(1,2)$ Fuc recognized in the binding pocket in all cases	(Hansman <i>et al.</i> , 2011)
Hiro (GII.12)	BAD20208.1	B trisaccharide		(Hansman <i>et al.</i> , 2011)

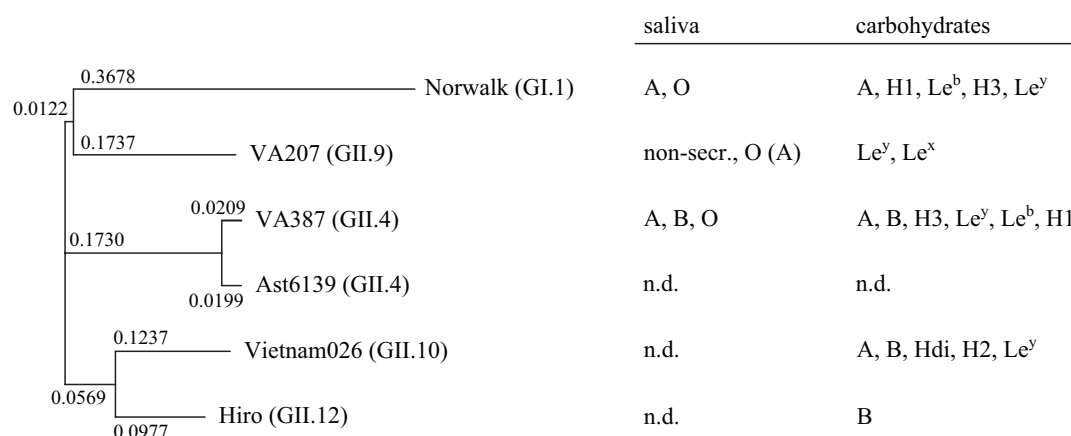


Figure 1.6. Phylogenetic tree and binding pattern of crystallized capsid proteins. Sequence alignment of full length major capsid proteins was done with ClustalW. The strain Ast6139 investigated in this work has not been crystallized but is included for comparison. Binding specificities were determined by ELISA-based binding assays (Tan & Jiang, 2005a) or by protein co-crystallization in case of strains Vietnam026 and Hiro (Hansman *et al.*, 2011).

The first HBGA-complexed structure of a NoV was reported for the GII.4 strain VA387 from the ABH binding group (Cao *et al.*, 2007). Its P domain (residues 214 to 539) was co-crystallized with A and B antigen trisaccharide. Some of the residues that were disordered in the unliganded protein crystal became structured in the presence of carbohydrate ligands. The HBGA binding site was located at the outmost part of the P2 domain at the P dimer interface and involved residues of both monomers (Figure 1.7). In particular, residues S343, T344, R345, D374, S441', G442' and Y443' were predicted to make hydrogen bonds or hydrophobic contacts (Y443' with the Fuc residue (apostrophe indicates 'the other' monomer)). Mutation of these residues led to strong reduction or abolition of HBGA binding (de Rougemont *et al.*, 2011).

Based on mutagenesis studies five critical subsites were identified within close proximity of the binding pocket (Tan *et al.*, 2008b; Tan *et al.*, 2009) (Figure 1.7 c)). Although not all of the residues are involved in direct contacts with HBGAs in the crystal structures mutation of some residues can alter the HBGA binding profile or completely abolish binding upon mutation (Tan *et al.*, 2008b). For example, mutation of residues K348', Q331' and I389' (violet color in Figure 1.7 c)) does not impair binding of B trisaccharide but completely abolishes binding of A trisaccharide to VA387 P protein. Obviously these residues are required for correct accommodation of the acetamide group of A antigen that points into the direction of this subsite and is the only difference to the B antigen.

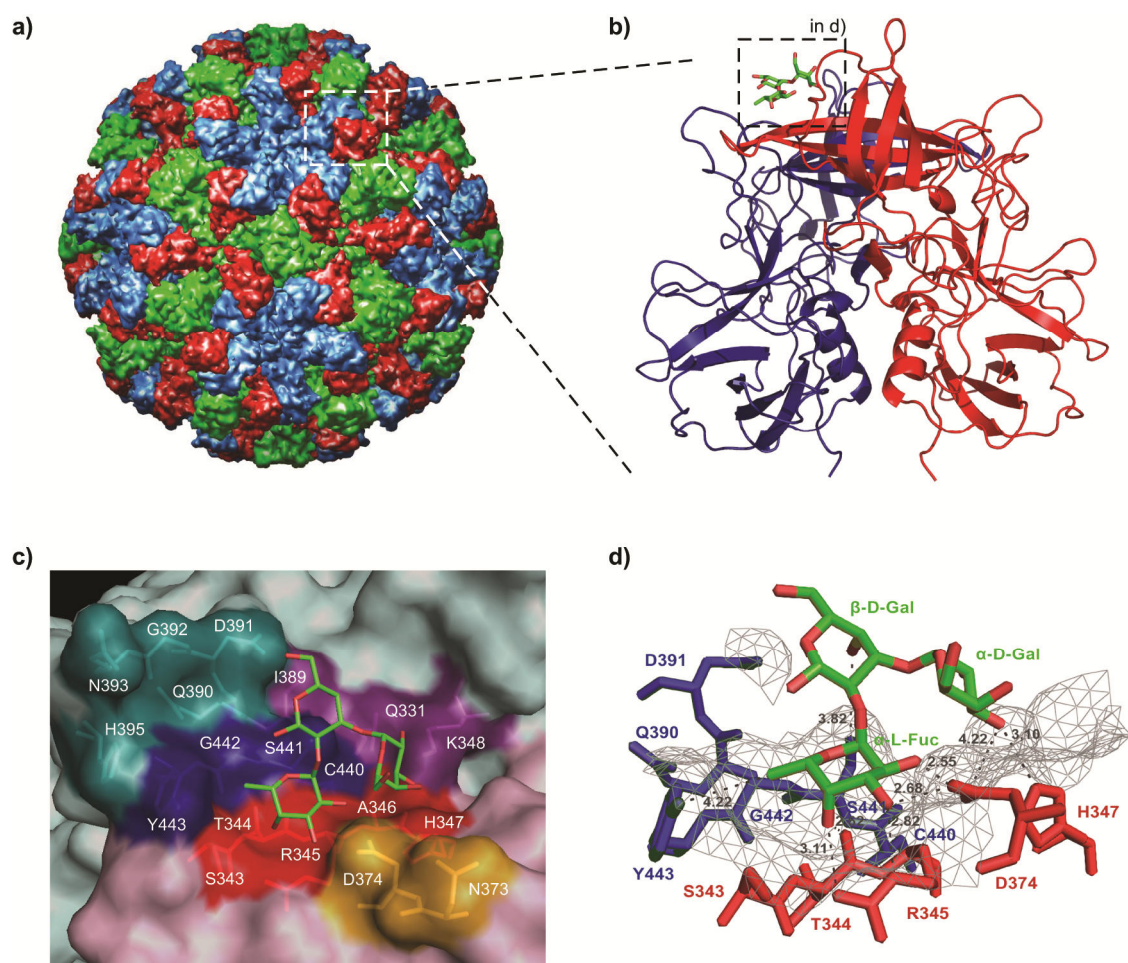


Figure 1.7. Structure of the VA387 P protein in complex with B trisaccharide. a) General architecture of NoV VLPs comprising A/B dimers (red and blue) and C/C dimers (green) (pdb code 1ihm) (Prasad *et al.*, 1999). b)-d) P dimer of VA387 in complex with B trisaccharide (pdb code 2obt) (Cao *et al.*, 2007); b) complete view of a dimer complexed with one B trisaccharide molecule; c) HBGA binding pocket at the dimer interface (monomers colored in pink and pale blue, respectively); the five subsites are colored in red and orange (pink monomer) and blue, dark cyan and violet (pale blue monomer); d) hydrogen bond network involving residues of both monomers (colors analogue to b)).

Structural details on HBGA recognition by the VA387 capsid protein also came from molecular docking and molecular dynamics (MD) simulations (Koppisetty *et al.*, 2010). Binding models of HBGAs up to pentasaccharides (ALe<sup>b</sup>, BLe<sup>b</sup>) were obtained and reproduced the co-crystal structures reasonably well.

In two complementary studies, P dimers of Norwalk virus (GI.1) were co-crystallized with A trisaccharide (Bu *et al.*, 2008; Choi *et al.*, 2008). Norwalk virus binds to ABH antigens but has a limited specificity for A and H but not for B antigens. The data revealed strong interactions not only with the Fuc but also with the  $\alpha$ -GalNAc of A antigen which might explain the absence of binding to B antigen. Comparison with the co-crystal structures of the GII.4 strain VA387 (Cao *et al.*, 2007) demonstrated different HBGA binding site

locations in the P2 domain with completely distinct sets of interacting residues. Such divergent binding modes for shared ligand specificities are indicative for convergent evolution of the capsid proteins of NoV genogroup I and II strains (Tan *et al.*, 2009).

Two rare NoV strains from genogroups GII.10 and GII.12 were co-crystallized with several ABH antigens (Hansman *et al.*, 2011) (cf. Table 1.4). In all cases the secretor-type fucose was recognized in a binding pocket similar to the GII.4 strain VA387 with several conserved residues (see Figure 7.3 in the appendix).

The GII.9 strain VA207 is the only crystallized Lewis binder for which co-crystals with Le<sup>y</sup> and sLe<sup>x</sup> were obtained (Chen *et al.*, 2011). The non-secretor type Fuc was placed in a binding pocket that shares several conserved residues with VA387 (see Figure 7.4 in the appendix). This suggests a common binding site for NoV from the ABH and Lewis binding groups instead of two distinct binding pockets as suggested previously (Huang *et al.*, 2005; Tan & Jiang, 2005a).

## 1.9 Vaccine and Inhibitor Design against Human Norovirus VLPs

Vaccination has proven to be the best strategy in combating virus infections and epidemics in the human history (Graham & Crowe, 2007). A worldwide vaccination program against smallpox has led to eradication of this devastating disease in the 1970s (WHO report, 1980). The availability of attenuated or ‘dead’ vaccines significantly reduced the impact of viral pathogens such as influenza, polio, hepatitis A and B, measles, rubella, mumps, typhoid, tuberculosis, tetanus and diphtheria. The first ‘anti-cancer vaccination’ became available by the recent development of a vaccine against certain papillomaviruses that cause cervix carcinoma and related cancers (Kahn, 2009). Attenuated live vaccines against rotaviruses, the major cause of severe gastroenteritis in children <5 years, has been successfully introduced (Jiang *et al.*, 2010).

Vaccination strategies against NoV have been developed based on VLPs expressed in insect cells or P particles expressed in *E.coli* eventually in combination with an adjuvant (Atmar *et al.*, 2011; Estes *et al.*, 2000; Herbst-Kralovetz *et al.*, 2010). In a comparative study reduced effectivity for immunizing mice was reported for P particles with a His-tag expressed in *E. coli* compared to whole VLPs (Tamminen *et al.*, 2012). However the quality and hence immunogenicity of P particles may vary with the expression construct.

Dual vaccines providing protection against NoV and rotaviruses (Blazevic *et al.*, 2011) or influenza virus (Xia *et al.*, 2011) applying chimeric constructs were proposed.

In a recent study vaccination of healthy humans with NoV VLPs induced a specific serum antibody response in two thirds of the participants and reduced the infection rate upon challenge with a homologous virus by 50% (Atmar *et al.*, 2011). The results indicated that vaccination did not provide full protection likely due to limited virus neutralization by the antibodies. Moreover, antibodies raised against one NoV strain often do not provide protection against other strains even of the same genotype imposing another substantial obstacle on vaccination strategies. The reason for this may be the high mutation rate of antigenic epitopes on the NoV capsid that is a result of the selection forces of the host and herd immunity. In contrast, vaccination of rabbits against the rabbit calicivirus RHDV has been successfully applied over years (Barcena *et al.*, 2000; Boga *et al.*, 1997; Marin *et al.*, 1995). A significant emergence of escape mutants has not been observed pointing to a reduced antigenic drift of RHDV compared to human NoV. In a recent study, mouse monoclonal antibodies with cross-reactivity towards human NoV strains from 1987 and 2006 were raised from dimeric VLPs (Lindesmith *et al.*, 2012). Nevertheless vaccination strategies providing protection against a broad range of currently circulating NoV strains are still far from clinical application.

Alternative strategies for the control of NoV infections aim for inhibitor design e.g. against the capsid or the viral polymerase. Inhibitors directed against the capsid would interfere with the first critical step during infection, i.e. the attachment and concomitant entry into host cells. In a first study concerned with such entry-inhibitor design, a HTS screening approach was applied with NoV VLPs (Feng & Jiang, 2007). “The Diversity Screening Set”-library (Timtec Inc, Newark, Delaware) containing 5000 compounds with molecular weights from 200 to 850 Da was tested for inhibition of three GII strains (VA387, MOH and VA207) and one GI strain (Norwalk) employing ELISA-based binding assays with saliva and synthetic oligosaccharides. 14 compounds displayed effective doses ( $EC_{50}$ ) below 15  $\mu$ M with the highest effectivity of 2.2  $\mu$ M. All these compounds contained six-membered aromatic rings including benzene and pyridine. Some additionally contained five-membered aromatic rings such as furan, thiophene, thiazole or pyrazole. In a very recent publication cyclic and acyclic sulfamide and piperazine derivatives were identified as potent inhibitors of NoV in screening studies with cell-based replicon systems (Dou *et al.*, 2012a; Dou *et al.*, 2012b; Dou *et al.*, 2012c).  $EC_{50}$  values were in the low  $\mu$ M range.

With crystallography and STD NMR titrations citrate was identified as potential inhibitor of VLPs from the GII.10 strain Vietnam026 (Hansman *et al.*, 2012). Together with a water molecule the citrate mimicked a Fuc moiety. Certain natural fruit extracts reduce the infectivity of feline calicivirus and murine NoV (Horn & D'Souza, 2011). Although the responsible inhibitory molecules have not been identified, citrate contained in natural fruits is a potential candidate for the observed inhibitory effects. Other natural substances with NoV inhibiting activity were identified by a screening of Chinese medical herbs (Zhang *et al.*, 2012). Tannic acid was found to be a strong inhibitor of NoV P protein binding to A and B saliva with an IC<sub>50</sub> value of 0.1  $\mu$ M. Verification of *in vivo* efficacy of potential inhibitors by cell culture or animal models is still needed.

### 1.10 Entry-Inhibitor Design against Ast6139 VLPs

The inhibitors studied in this work for binding and inhibitory efficiency towards NoV strain Ast6139 were obtained by two different screening strategies. The first approach follows the concept of fragment-based drug design (Carr *et al.*, 2005; Hajduk & Greer, 2007; Perspicace *et al.*, 2009) in particular using NMR (Campos-Olivas, 2011; Dalvit, 2008; Dalvit, 2009; Huth *et al.*, 2005; Pellecchia *et al.*, 2004). The Maybridge Ro5 Fragment Library (Thermo Fisher Scientific Inc.) was screened against Ast6139 VLPs employing STD and spin-lock filtered NMR experiments for hit identification (Rademacher, 2008; Rademacher *et al.*, 2011). It will be abbreviated by 'Maybridge library' throughout this work. Only 430 of the 500 small organic compounds with molecular weights between 94 and 291 Da were included in the final testing due to limited solubility of the other compounds. An initial hit rate of 61% was reduced to 12% specific hits by competition experiments with  $\alpha$ -L-Fuc-(1,*O*)-CH<sub>3</sub>, B and H type 1 trisaccharides. 26 hits were classified as 'high efficient binders'. Furthermore, four fragments (151, 191, 231 and 473) were identified as 'adjacent' or 'second site binder' based on the observation of inter-ligand NOEs (ILOEs) to  $\alpha$ -L-Fuc-(1,*O*)-CH<sub>3</sub> in presence of Ast6139 VLPs (London, 1999). Prototype inhibitors were synthesized from both competitive and adjacent site hits and were investigated in this and a previous work (Rademacher *et al.*, 2011).

The second approach employs virtual screening that is becoming increasingly popular due to the ability to sample a larger fraction of the chemical space compared to conventional HTS screening (Irwin, 2008; Koppen, 2009; Rester, 2008; Sun, 2008; Swann *et al.*, 2011).

A virtual library of fucosylated compounds that are easy to synthesize using Ugi reactions was screened *in silico* by molecular docking to the HBGA site of the closely related GII.4 strain VA387 (unpublished data, Pavel I. Kitov, University of Alberta, Edmonton). The four hits with the highest predicted free energy of the docking structure were synthesized and subjected to binding and competition studies in this thesis.

The design and synthesis of prototype entry-inhibitors against the NoV capsid made use of the concept of multivalency (Chabre & Roy, 2010; Kitov & Bundle, 2003). For target molecules with multiple binding sites the use of multivalent instead of monovalent ligands leads to strong enhancement of the avidity and potential improvement of the biological activity. The so-called ‘glycosidic cluster effect’ has been described for lectin-carbohydrate interactions (Dam & Brewer, 2009; Dam *et al.*, 2009; Munoz *et al.*, 2009) and ligand-induced oligomerisation of serum amyloid P protein (Ho *et al.*, 2005). An increased affinity can be either explained by reduction of the apparent  $k_{\text{off}}$  rate from rebinding effects, or by ‘true’ affinity increase from simultaneous binding of several functional groups to receptor binding pockets (Dam & Brewer, 2009). In case of glycosidases comprising only a single binding pocket an observed affinity increase for multivalent inhibitors was likely due to re-binding effects (Decroocq *et al.*, 2011). The to date best application of ‘true’ multivalency effects is the design of multivalent inhibitors against the Shiga toxin AB<sub>5</sub> that is expressed by pathogenic *E.coli* strains (Kitov *et al.*, 2008a; Kitov *et al.*, 2008b; Kitov *et al.*, 2011; Kitov *et al.*, 2000). A decameric inhibitor carrying the P<sup>k</sup> trisaccharide ligand of Shiga toxin, the so-called STARFISH ligand, was able to simultaneously bind to the five B subunits arranged in a pentagon-like shape resulting in highly increased affinities (Kitov *et al.*, 2000).

In case of NoV capsids the presence of 180 binding sites on one capsid opens up many strategies for the design of multivalent entry-inhibitors utilizing hits from compound library screenings as well as HBGA fragments. The structures of the first prototype inhibitors are described in the Materials and Methods.

## 1.11 Biophysical Characterization of Norovirus Binding to HBGAs

### 1.11.1 NMR Spectroscopy

Nuclear magnetic resonance (NMR) spectroscopy is a versatile biophysical method to study the structure and interaction of molecules. It is based on the magnetic properties, the spin, of NMR-active nuclei such as  $^1\text{H}$ ,  $^{13}\text{C}$  and  $^{15}\text{N}$ . For a comprehensive introduction into the quantum mechanical backgrounds of NMR the reader is referred to the literature (Berger & Braun, 2004; Claridge, 2000; Keeler, 2005). A variety of NMR experiments with a broad range of accessible information allows analysis of ligand receptor interactions based on the observation of either the ligand or the receptor molecule signals (Dalvit, 2008; Fielding, 2007; Peters, 2007). In case of the interaction of NoV VLPs with HBGAs, protein-observed NMR experiments are not applicable. Due to their large molecular weight VLPs undergo very efficient transverse ( $T_2$ ) relaxation i.e. fast loss of the NMR signal. This makes them literally invisible for NMR spectroscopy unless laborious and highly demanding isotopic labeling strategies are applied. Therefore ligand observed NMR experiments are the method of choice for investigation of ligand binding to NoV VLPs.

*STD NMR experiments.* One NMR method was especially useful in the course of this work: saturation transfer difference (STD) NMR spectroscopy is utilized to identify and characterize the binding of small molecules like peptides, carbohydrates and drug candidates to a large macromolecule (Mayer & Meyer, 1999; Meyer & Peters, 2003). The macromolecule is saturated by a cascade of selective low-power radiofrequency (RF) pulses without directly affecting the ligand. Saturation is quickly spread across the macromolecule via spin diffusion. If a small molecule binds to the macromolecule, saturation is transferred via the nuclear Overhauser effect (NOE) during the lifetime of the complex in a distance dependent manner (Figure 1.8). A reference ‘off-resonance’ experiment is recorded in which the frequency of the saturation pulse is set far away from the resonances of both macromolecule and ligand. Subtraction of the on-resonance spectrum from the reference spectrum provides the difference (STD) spectrum. It shows only signals of ligand protons that have received saturation upon binding to the macromolecule (Figure 1.8). This way, binders of a certain target molecule can be easily identified even from a large compound library. The size of the library is only limited by the necessity to unambiguously assign the resonances of the binders in the spectrum (Mayer & Meyer, 1999).



As a consequence from the distance dependency of the NOE effect, analysis of the STD signal intensities furnishes the binding epitope of a ligand (Mayer & Meyer, 2001). This so-called group epitope mapping yields valuable information on important pharmacophoric groups of the ligand and provides a negative imprint of the receptor binding site.

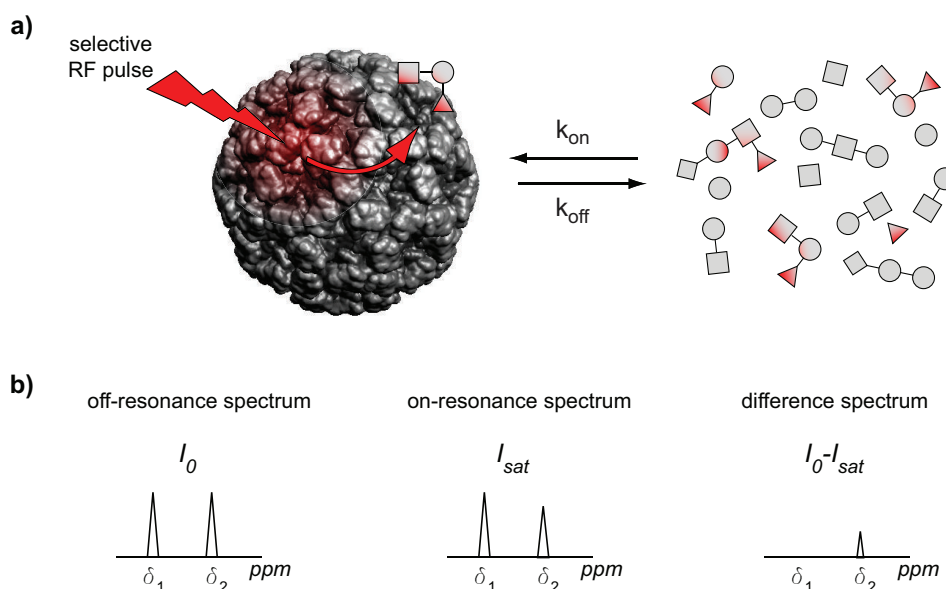


Figure 1.8. Principles of the STD NMR experiment. a) Schematic presentation of the on-resonance experiment. The macromolecule (e.g. VLP) is selectively saturated by a low-power RF pulse; the saturation is spread throughout the molecule via spin-diffusion and transferred to bound ligands via cross-relaxation; partially saturated ligands dissociate and accumulate in solution where they are detected. b) Schematic presentation of 1D- $^1\text{H}$  spectra with each a resonance of a binding ( $\delta_2$ ) and a non-binding ligand ( $\delta_1$ ). The off-resonance experiment corresponds to a normal 1D spectrum; in the on-resonance spectrum the signal intensity of the binding ligand is reduced, while the non-binding ligand is unaffected; the difference spectrum shows selectively the signal of the binding ligand.

In this work, STD NMR spectroscopy is employed to obtain binding epitopes of HBGAs and inhibitors bound to VLPs of the NoV strain Ast6139. It was shown in multiple studies that STD NMR is applicable to very large molecular complexes like viruses (Benie *et al.*, 2003), VLPs (Haselhorst *et al.*, 2011; Haselhorst *et al.*, 2008; Rademacher *et al.*, 2011; Rademacher *et al.*, 2008; Zakhour *et al.*, 2009) or even whole cells (Claasen *et al.*, 2005). In particular, STD NMR furnished binding epitopes of HBGAs bound to VLPs of the rabbit calicivirus RHDV (Rademacher *et al.*, 2008). The huge molecular weight of VLPs (~10.8 MDa) even proved to be beneficial for STD NMR (Rademacher & Peters, 2008). A very fast cross-relaxation rate allows efficient saturation transfer to bound molecules. The extreme line broadening of the VLP resonances due to fast  $T_2$  relaxation abolishes the necessity to use a spin-lock filter for protein signal suppression that could affect ligand

signals. Furthermore, the on-resonance frequency for irradiation of VLPs can be set far away from the ligand signals reducing the risk of direct ligand irradiation.

The affinity of an interaction cannot be deduced directly from STD signal intensities because there is no simple correlation between the intensity and  $k_{\text{off}}$  and  $K_D$  (Jayalakshmi & Krishna, 2002). Low or absent STD signals can be observed for very strong interactions ( $k_{\text{off}}$  low). A long complex lifetime limits the accumulation of saturated ligands in solution. However, the same observation can be made for very weak complexes, i.e. very high  $k_{\text{off}}$ . The resulting very short residence time of the ligand in the binding pocket prevents efficient cross-saturation to bound ligand and its accumulation in solution. STD signals are readily observable for complexes with micro- to millimolar  $K_D$  values. Affinities in this range are often observed for carbohydrate-protein interactions (Dam & Brewer, 2007) and are also expected for HBGAs binding to NoV VLPs.

$K_D$  values can in principle be determined by STD titration experiments. Typically, the ligand concentration is gradually increased while the protein concentration is kept constant (Angulo *et al.*, 2010; Fielding, 2007). The data obtained have to be analyzed with care, and results depend on the design of the experiment. Low excess of ligand over protein binding sites and ligand relaxation can deliver erroneous  $K_D$  values that are usually false too high (Angulo *et al.*, 2010; Yan *et al.*, 2003). If other error sources can be excluded, STD titration experiments therefore at least provide an upper estimation of the  $K_D$  value. In cases where direct titration experiments are not applicable due to a shortage of material or too strong binding (i.e. absent STD effects), competitive STD titration experiments can be employed. Depletion of a reporter ligand with the ligand of interest provides its inhibitory efficiency ( $IC_{50}$ ) and –if the affinity of the reporter ligand is known– its  $K_D$ .

In this work STD titration experiments with HBGAs and inhibitors of NoV VLPs will be attempted and discussed. In case of multivalent inhibitors with high expected affinities competition experiments with L-fucose as reporter ligand will be employed. Knowledge on the affinities of HBGAs is important to understand the mode of attachment factor binding in detail. A comparison of the binding strength of prototype inhibitors with that of HBGAs is of fundamental importance for evaluation of inhibitor efficacies and further drug design.

*Transferred NOESY experiments.* The conformation of a ligand bound to a large receptor molecule can be investigated by transferred NOESY (trNOESY) NMR spectroscopy (Casset *et al.*, 1997; Clore & Gronenborn, 1982; Neuhaus & Williamson, 2000). TrNOESY experiments are based on the observation of NOEs between spatially neighboring spins. Protons of the ligand coming into close proximity (typically  $<5 \text{ \AA}$ ) experience cross relaxation via zero- and double quantum transitions due to dipole-dipole coupling. This gives rise to cross peaks in two-dimensional NOESY spectra. The detectable intensity change, the NOE enhancement, is dependent on the spin-spin distance. In the extreme narrowing limit (i.e. for rapidly tumbling molecules) the maximum NOE enhancement  $\eta_{\max}$  is directly proportional to the spin-spin distance ( $\sim r^{-6}$ ). The intensity of NOESY cross peaks also depends on the molecular tumbling rate (i.e. molecular weight). Small molecules with fast tumbling rate display positive NOE enhancements, while for large molecules negative and more intense NOE effects can be observed (Figure 1.9 a)). The region of zero NOE applies to mid-sized molecules and is also dependent on the magnetic field strength. Furthermore, large molecules display a much faster build-up of the NOE effect than small molecules (Figure 1.9 b)).

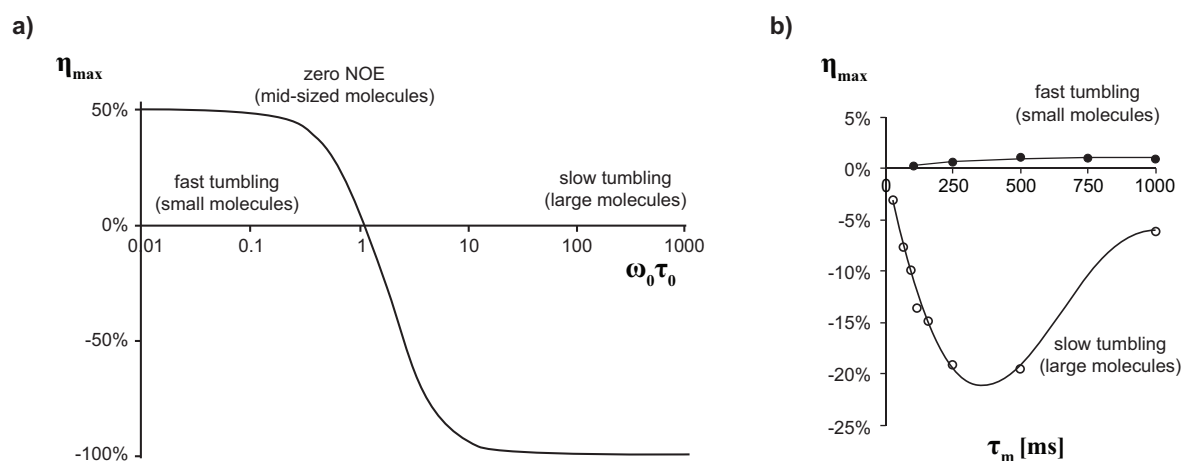


Figure 1.9. Theoretical steady-state NOE enhancement for a two-spin system. a) Maximum NOE enhancement  $\eta_{\max}$  of a spin upon saturation of the couple spin as a function of the molecular tumbling rate  $\tau_0$  and the spectrometer frequency  $\omega_0$  [MHz]; the figure was adapted from (Claridge, 2000). b) Typical NOE build-up curves of small molecules (filled circles) and large molecules or small molecules bound to a macromolecular receptor (i.e. trNOEs) (empty circles);  $\tau_m$ : NOESY mixing time.

TrNOESY experiments make use of the fact that, upon binding to a large protein, small ligands behave like the protein for the life time of the complex. In particular, they adopt the motional characteristics of the complex. The resulting transferred NOEs (trNOEs) report

on the conformation of the bound ligand and can be discriminated from NOEs of the free ligand by their size and build-up behavior. TrNOESY cross peaks are dependent on the exchange kinetics between free and bound state and on the size of the protein.

In this work trNOESY experiment are applied to study the conformation of HBGAs bound to NoV VLPs (Figure 1.10).

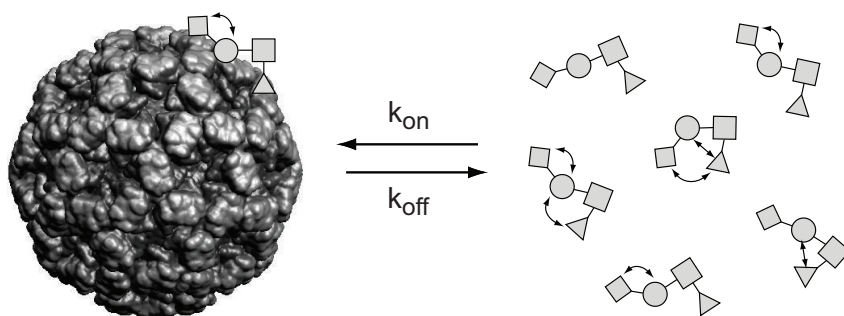


Figure 1.10. Schematic principle of trNOESY experiments with VLPs and HBGAs. In the free state the ligand (e.g. tetrasaccharide) is present in different conformations each with a characteristic NOE pattern. VLPs bind to a single or a subset of ligand conformations giving rise to the respective (averaged) trNOE pattern.

Most of the ABH and Lewis antigens studied in this work are relatively rigid (Imberty *et al.*, 1995; Lemieux *et al.*, 1980; Otter *et al.*, 1999; Yuriev *et al.*, 2005). The torsion angles along the rotatable glycosidic bonds are highly constricted for most oligosaccharides due to the exoanomeric effect. An exception is the  $\alpha(2,3)$ -linkage between Neu5Ac and Gal present in sLe<sup>x</sup> and sLe<sup>a</sup>. Previous studies demonstrated that sLe<sup>x</sup> can adopt multiple conformations in solution and different subsets thereof are recognized by carbohydrate binding proteins (Harris *et al.*, 1999; Haselhorst *et al.*, 2001; Poppe *et al.*, 1997; Scheffler *et al.*, 1997; Scheffler *et al.*, 1995). TrNOESY experiments are therefore conducted to investigate the bound conformation of sLe<sup>x</sup> in the presence of Ast6139 VLPs. The results will be compared with molecular dynamics (MD) simulations of sLe<sup>x</sup> in the NoV binding pocket to provide a comprehensive and experimentally verified model for the recognition of sLe<sup>x</sup> by Ast6139 VLPs (Fiege *et al.*, 2012).

### 1.11.2 Surface Plasmon Resonance Spectroscopy

Surface Plasmon Resonance (SPR) spectroscopy is a technique that exploits the so-called surface plasmon effect to analyze interaction of molecules (Earp & Dessy, 1998; Jason-Moller *et al.*, 2006; Lieberg *et al.*, 1983; Piliarik *et al.*, 2009). The SPR effect is generated in a conducting film at the interface of two media with different refractive indices. The conducting film is usually a ca. 50 nm thin gold film on the glass layer of an SPR sensor chip. One of the interaction partners –called the ligand– is immobilized on the surface of the sensor chip that is functionalized correspondingly e.g. with carboxyl groups or hydrophobic chains. The exchangeable sensor chip and the integrated microfluidic cartridge (IFC) of the SPR instrument form the flow cells filled with nL volumes of buffer. The second interaction partner –the analyte– is injected into the IFC and passes the flow cells under continuous flow allowing association and dissociation to the immobilized interaction partner.

The sensor chip is coupled to an opto-electronic device with a light source (near-infrared LED) and a detector array. The incident light is focused on the sensor chip under conditions of total internal reflection. This condition is observable at the interface of two media with different refractive indices, i.e. the glass layer of the sensor chip and the medium of the flow cell. With the angle of the incident light beam matching exactly the total internal reflection angle  $\theta_{\text{spr}}$ , an electric field –the evanescent wave field– is created in the conducting gold film of the sensor chip (Earp & Dessy, 1998). It reaches into the medium with lower refractive index, i.e. the medium of the flow cell. Binding of analytes to the ligand immobilized on the chip surface changes the refractive index of the medium and consequently  $\theta_{\text{spr}}$ . The change of  $\theta_{\text{spr}}$  is detected on the photo-detector array and is proportional to the bound mass. The response is expressed in RU (response units, 1 RU = 1 picogram per  $\text{mm}^2$  on the sensor surface). The form of the response is dependent on the affinity and the kinetic parameters of the respective interaction (Myszka, 2000).

In order to remove background responses from unspecific binding of buffer components, the analyte is simultaneously injected on a reference flow cell to which no binding should occur. Subtraction of the response on the reference flow cell from that of the flow cell with immobilized ligand provides the actual response. The binding event with association, equilibrium and dissociation phases is monitored in a so-called sensorgram (Figure 1.11 b)) in real time. In this work a Biacore 3000 instrument (formerly Biacore, now GE Healthcare) is utilized that displays a data collection rate of up to 10 Hz.

Immobilization of the ligand is either accomplished by directly immobilized using a covalent coupling approach, or by indirect capturing techniques (cf. e.g. Biacore Sensor Surface Handbook, GE Healthcare). The latter takes advantage of the high affinity interaction between streptavidine (or one of its descendants) and biotin of the accordingly functionalized ligand. Ready-to-use sensor chips with pre-coupled streptavidine are commercially available. Covalent immobilization involves covalent bond formation with amine, thiol or aldehyde groups of the ligand. In the most widely used amine coupling a carboxymethylated sensor chip surface is activated by injection of NHS (*N*-hydroxysuccinimide) and EDC (1-ethyl-3-(3-dimethylaminopropyl) carbodiimide). The formed *N*-hydroxysuccinimide esters react with primary amino groups of the injected ligand leading to amide bond formation and release of free NHS (Earp & Dessy, 1998). Remaining NHS esters are deactivated by injecting a high concentration of ethanolamine.

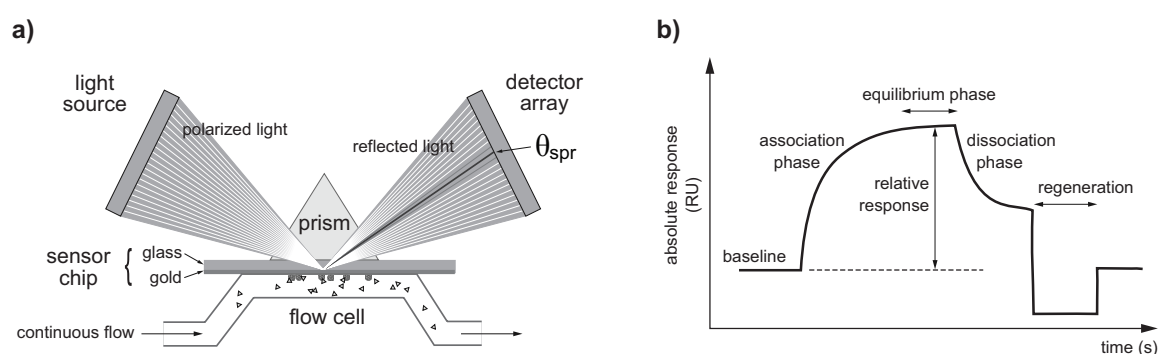


Figure 1.11. Principles of SPR spectroscopy. a) Schematic build-up of the SPR detection system. Incident light at the total internal reflection angle  $\theta_{spr}$  creates an evanescent field that induces surface plasmons in the gold film.  $\theta_{spr}$  is detected as a reduction in the intensity of the reflected light. b) Schematic illustration of a sensorgram. Affinity data can be obtained by monitoring the responses at the equilibrium phases versus injected analyte concentration. The association and dissociation phases report on the kinetics. The figure was adapted from the Biacore Sensor Surface Handbook (GE Healthcare).

SPR can be used to study the interaction of proteins with proteins, peptides and small molecules (Day *et al.*, 2002; Seet *et al.*, 2003), proteins with carbohydrates (Haselhorst *et al.*, 2001; Munoz *et al.*, 2008; Plath *et al.*, 2006), proteins with (glyco)lipids (de Haro *et al.*, 2004; Lopez & Schnaar, 2006), proteins with nucleic acids (Katsamba *et al.*, 2002) or even the interaction of whole cells and viruses with receptor molecules (Abad *et al.*, 2002; Dubs *et al.*, 1992; Nam *et al.*, 2006; Shirato *et al.*, 2008; Wang *et al.*, 2010).

In this work, binding of HBGAs and prototype inhibitors to Ast6139 VLPs is investigated. Two basic assay formats are applied. In the direct binding assay VLPs are covalently coupled to the surface of SPR sensor chips and HBGAs or inhibitors are in the mobile phase (Figure 1.12 a)). Concentration series furnish the affinity of the interactions from monitoring the response at equilibrium versus the injected analyte concentration. Kinetic parameters are in principle accessible from analysis of association and dissociation phases provided that the interaction is within the specified range for SPR (i.e.  $k_{\text{off}}$  between  $10^{-1}$  and  $5 \cdot 10^{-6} \text{ s}^{-1}$  for the Biacore 3000 instrument).

In a competitive assay format carbohydrates conjugated to either polyacrylamide (PAA) or BSA (neoglycoproteins) are immobilized on sensor chips (Figure 1.12 b) and c)). HBGAs or inhibitors are pre-incubated with VLPs and compete with the immobilized carbohydrate conjugates for VLP binding when co-injected. Appropriate concentration series can provide inhibition efficiencies ( $\text{IC}_{50}$  values) of the co-injected analytes.

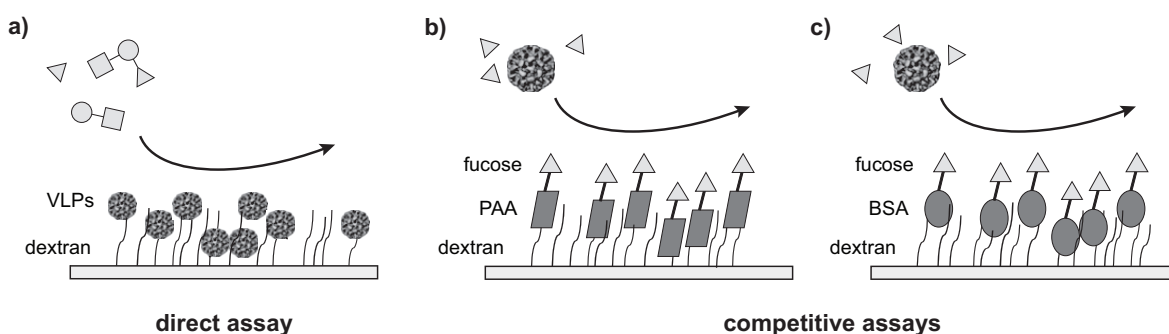


Figure 1.12. SPR assay formats with NoV VLPs. a) Direct binding assay with VLPs immobilized on the sensor chip and HBGAs or inhibitors applied in the mobile phase. b)-c) Competitive assays with PAA- (b) or BSA- (c) sugar conjugates immobilized on the sensor chip; VLPs are co-injected with HBGAs or inhibitors.

Competitive SPR assays with either monovalent carbohydrates or neoglycoproteins captured on sensor chips have been utilized before to obtain qualitative and semi-quantitative information on NoV VLP binding to HBGAs (Choi *et al.*, 2008; de Rougemont *et al.*, 2011; Shirato *et al.*, 2008). However no affinity data have been reported so far from SPR assays. Such information is highly desirable to further understand the attachment factor binding and facilitate the development of entry-inhibitors against NoV.

### 1.11.3 Hemagglutination Assays

Agglutination refers to the ability of certain molecules to bind to red blood cells (RBCs). If a dilution RBCs from a crude blood extract is placed in a well plate, RBCs sediment after 30 min at 4°C. This can be visually identified as a clearing of the previously homogeneous red solution. Molecules that bind to surface molecules of RBCs can their sedimentation, a process called hemagglutination (Figure 1.13). The respective solution will stay red. After a few hours or days the RBCs degrade and the cell debris sediments irrespective of the presence of agglutinating molecules. Agglutination of RBCs by viruses has been shown before (Brown & Cohen, 1992; Rogers & Paulson, 1983; Ruvoen-Clouet *et al.*, 2000) and can be used to analyze receptor specificities or determine virus titers from patients' samples or environmental sources.

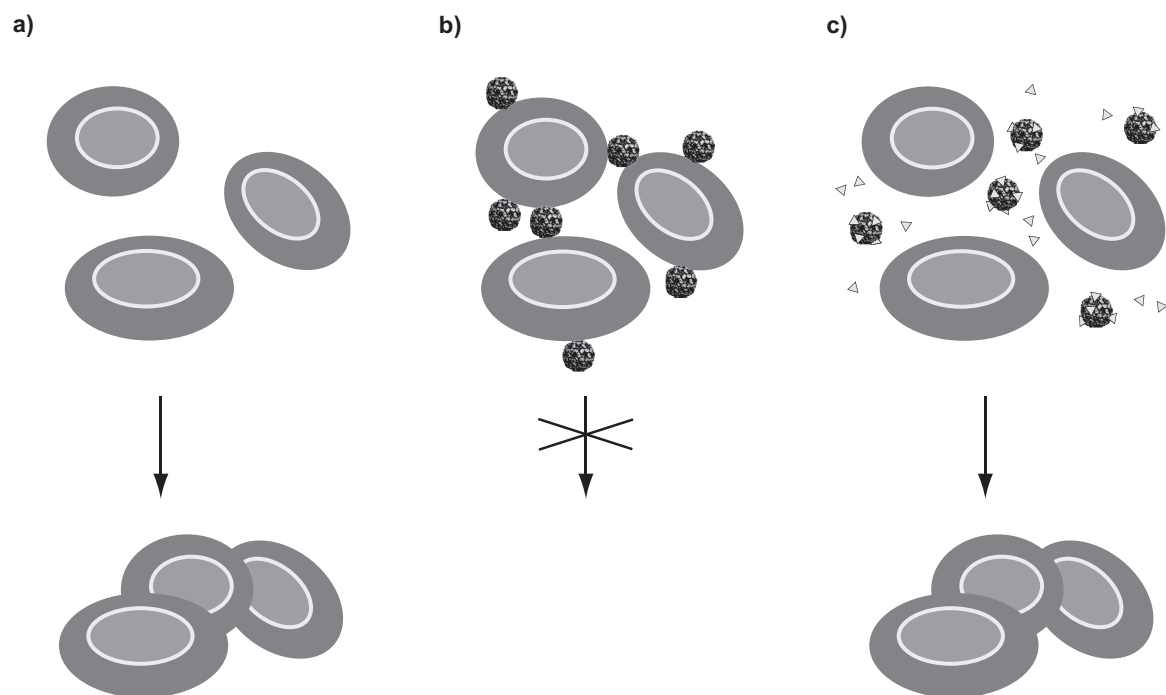


Figure 1.13. Principles of hemagglutination by VLPs. a) Red blood cells (RBCs) sediment from crude blood extracts. b) VLPs agglutinate RBCs via binding to HBGAs their surfaces. c) HBGAs or inhibitors (grey triangles) bind to VLPs and allow RBC sedimentation.

Agglutination is dependent on the RBC concentrations and the surface density of the responsible molecule. For a given RBC concentration the titer of hemagglutination for a certain virus preparation can be determined by serial dilution experiments. The titer of hemagglutination is equal to the reciprocal of the highest dilution of the molecule that still has the capability to agglutinate (i.e. prevent sedimentation of) RBCs.



NoV VLPs can agglutinate RBCs by binding to ABH blood group antigens on the surface of RBCs (Hutson *et al.*, 2003). In this work, hemagglutination assays are used to determine the inhibitory effect of multivalent polyacrylamide-based inhibitors. Competition with the ABH antigens on the RBCs leads to inhibition of agglutination (Figure 1.13 b)). In serial dilution experiments RBCs and VLPs at a concentration above the titer of hemagglutination are incubated with various concentrations of polymeric inhibitors. Comparison of the lowest inhibitor concentrations that still inhibit agglutination of RBCs by VLPs allows qualitative ranking of these prototype inhibitors in a quasi-biological assay. Although binding to RBCs is not relevant to NoV pathogenesis the hemagglutination assay investigates VLP binding to intact cells that present HBGAs similar to those on the gastrointestinal mucosa.



## 2 Objectives

Non-infectious virus-like particles (VLPs) of NoV are very well suited for a range of *in vitro* experiments. Qualitative information on the binding of NoV VLPs to their attachment factors, histo-blood group antigens (HBGAs), has been obtained by ELISA and SPR assays. Structural data on the HBGA binding site is available from X-ray crystallography, albeit under rather non-physiological conditions and for a very limited number of NoV-HBGA complexes. In this work, a range of experiments employing NMR and SPR spectroscopy will provide a very detailed view on HBGA recognition by VLPs of the human NoV strain Ast6139 yielding both qualitative and quantitative information:

- STD NMR experiments of synthetic HBGA fragments in presence of NoV VLPs provide a detailed picture of the specificity and the minimal structural binding requirements. Group epitope mapping of HBGA fragments furnishes binding epitopes at atomic resolution indicating important functional groups that can be compared to structural data of related NoV strains.

STD NMR may also be used to elucidate binding affinities. Therefore, an additional aim is to explore the applicability of STD titration experiments to determine binding affinities of selected NoV-HBGA interactions.

- TrNOESY experiments may yield information on the bioactive conformation of HBGA bound to NoV VLPs. This is of particular interest in case of flexible ligands such as sialyl-Lewis<sup>x</sup> (sLe<sup>x</sup>). TrNOESY experiments identify which subset of sLe<sup>x</sup> conformations is recognized by the VLPs from solution yielding important information on the mode of attachment factor binding.
- SPR experiments provide complementary information on HBGA binding to NoV VLPs. Experimental setup for this system has been proven to be non-trivial by us and by others. In general, two assay formats are applicable. An indirect (competitive) assay format employing immobilization of carbohydrate conjugates of polyacrylamide (PAA) or BSA has been previously reported for NoV. It provides inhibitory efficiencies (IC<sub>50</sub> values) of competing molecules, e.g. attachment factors. A direct binding assay with immobilized NoV VLPs will be reported for the first time and furnishes affinities data for selected HBGA fragments.
- Based on the identified attachment factor specificity of NoV VLPs, the design of mono- and multivalent inhibitors directed against the HBGA binding site, so-called

entry-inhibitors, should be possible. Lead compounds for drug design were obtained from different screening approaches against NoV VLPs and were used for the synthesis of multivalent PAA-based prototype entry-inhibitors.

- Prototype inhibitors will be tested for binding and inhibition of NoV VLPs with STD NMR and SPR. Competitive titration experiments will provide  $IC_{50}$  values for inhibition of NoV-HBGA interaction. Direct titration experiments may yield affinity information that can be compared to those of monovalent HBGAs.
- Finally, hemagglutination assays with red blood cells (RBCs) and NoV VLPs are applied to study the efficiency of multivalent inhibitors on a qualitative level. Although binding of NoV to RBCs (i.e. hemagglutination) via blood group antigens is not relevant to disease pathogenesis, this assay allows evaluation of NoV-HBGA inhibition by prototype inhibitors in a cell-based assay.

Briefly, the study aims at elucidation of NoV binding to ‘natural’ attachment factors and inhibitors thereof at atomic resolution under physiological conditions. Therefore NMR experiments are employed along with other biophysical methods as outlined above.

### 3 Material and Methods

#### 3.1 Expression of Norovirus VLPs

The GII.4 NoV strain investigated in this work was the Spanish isolate Ast6139/01/Sp (GenBank entry: AJ583672.2) (Ng *et al.*, 2004). VLPs of Ast6139 were recombinantly expressed in insect cells using a baculoviral expression system (Jiang *et al.*, 1992). The coding region of the major capsid protein VP1 (ORF2: bp 2500-4119) was cloned into the NcoI and XhoI restriction sites of the baculovirus transfer vector pTriEx-Sfil (Novagen) (Pengelley *et al.*, 2006). The pTriEx-VP1 construct was transformed into *E.coli* XL10-Gold cells (Stratagene) and plated onto LB-Carbenicillin Agar plates. Colonies were picked and expressed overnight in LB medium. The pTriEx-VP1 plasmid was purified with the help of the Plasmid Purification Kit (Qiagen) and the sequence was confirmed by nucleotide sequencing. Modified bacmid DNA was linearized by Eco81I restriction enzyme (Takara) and was cotransfected with the pTriEx-VP1 construct into Sf9 cells using Cellfectin reagent (Invitrogen). Cotransfected Sf9 cells were incubated at 28°C in insect Xpress (BioWhittaker) protein free medium and recombinant baculovirus Bac-Tri-VP1 was obtained. The respective protocols were published previously (Pengelley *et al.*, 2006; Zhao *et al.*, 2003). Protein expression was confirmed by Western blotting using polyclonal rabbit serum antibodies raised by immunizing rabbits with NoV VLPs purified from baculoviral expression (unpublished data).

For VLP production, High Five cells (Invitrogen) were grown to a confluent monolayer in cell culture dishes and infected with Bac-Tri-VP1 at a multiplicity of infection of five. Infected cell cultures were grown in Insect-Xpress (BioWhittaker) protein free medium with Penicillin and Streptomycin for ca. four days at 28°C. Cells were harvested by scraping and centrifuged at 500xg for 10 min at 4°C. The supernatant was discarded and the cell pellets were resuspended in PBS pH 7.2. The cells were homogenized by sonication. Cell lysates were centrifuged at 16000 rpm for 30 min at 4°C using a Kontron A8.24 rotor (r=50 mm) in an Allegra 64R centrifuge (Beckman Coulter). The supernatant including recombinant VLPs was ultracentrifuged at 26000 rpm for 150 min at 4°C using a Beckman SW28 rotor (r=161 mm) in a Beckman Coulter ultracentrifuge. The sediment including the VLPs was resuspended in PBS and extracted twice with trichlorotrifluoroethane (Freon 113). The extract was purified by ultracentrifugation in a CsCl gradient (0.39 g/mL) at 35000 rpm for 24 h at 4°C using a Beckman SW60 rotor. The

gradients containing VLPs were removed with a syringe, diluted in PBS pH 7.2 and centrifuged at 27000 rpm for 2 h at 4°C using a Beckman SW40 rotor. The supernatant was discarded and the sediment containing the VLPs was resuspended in PBS pH 7.2. The protein was investigated by reducing SDS gel electrophoresis following Coomassie blue staining and the concentration was determined by Bradford testing. The sample was stored at 4°C until use.

### 3.1.1 Cloning of Single Site Mutants

For insight into the role of single amino acids on the HBGA recognition by NoV, four mutants of Ast6139 VLPs, R345A, D374A, D391A and H395A, were cloned by site-directed mutagenesis. R345 and D374 are directly involved in a range of hydrogen contacts with A and B trisaccharide in the crystal structures of the related NoV strain VA387 (Cao *et al.*, 2007) (see Figure 1.7 for the structure of the binding pocket). Mutation of these residues is expected to strongly weaken or abolish HBGA binding activity. For D391 a water-mediated contact to  $\beta$ -Gal of ABH antigens is predicted. Its mutation allows evaluation of the importance of this contact. In the mentioned crystal structures H395 makes a stacking interaction with Y443 that forms the hydrophobic pocket for the methyl group of Fuc. The mutant H395A allows to evaluate the role of this potentially stabilizing stacking interaction.

A recombinant vector construct with full length VP1 of the Ast6139 isolate in a pBacPAK8 vector (Clontech) (see above) served as template for site-directed mutagenesis. Mutagenic PCR primers were purchased from Sigma (sequences shown in Table 3.1).

*Table 3.1. Primers used for site-directed mutagenesis of VP1. Two primers (forward and reverse) carrying the desired mutation are applied for each mutant. Mutated nucleotides are shown in red bold letters.*

Mutant	Mutated codon	Direction	Primer sequence
R345A	CGC > <b>GCC</b> (bp 1033-1035)	forward	GGATGGCTCGACC <b>GC</b> CGGCCACAAAGCTACAG
		reverse	CCCCTACCGAGCTGG <b>CG</b> GCCGGTGTTTCG
D374A	GAT > <b>GCT</b> (bp 1120-1122)	forward	CACCACTGACACAAACAATG <b>CT</b> CTTGAAGCTGGCC
		reverse	GTGACTGTGTTTGTTAC <b>G</b> AGAACTTCGACCGGTTTCG
D391A	GAT > <b>GCT</b> (bp 1171-1173)	forward	CCAGTCGGTGTCTGTCAGG <b>CT</b> TGGTAATAACCACC
		reverse	CCACAGCAGGTCC <b>G</b> ACCATTATTGGTGGTTTACTTGGG
H395A	CAC > <b>GGC</b> (bp 1183-1185)	forward	GGTGTCTGTCAGGATGGTAATAAC <b>GC</b> CCAAAATGAACCC
		reverse	GGTCCTACCATTATTG <b>CG</b> GGTTTACTTGGGGTTGTTACCC

PCR was performed with 100 ng of mutagenic primers and 100 ng of DNA template using the QuikChange Site-Directed Mutagenesis Kit (Stratagene). PCR products were digested with Dpn1 followed by transformation into XL10-Gold cells (Stratagene). The cells were plated onto LB-Carbenicillin Agar plates and grown overnight at 37°C. Plasmids were purified with the help of the HighPure Plasmid Isolation Kit (Roche) and the sequence was confirmed by nucleotide sequencing.

For recombinant baculovirus and VLP production, mutant VP1 was cloned from the pBacPAK8 vector into the pTriEx vector as described (Pengelley *et al.*, 2006). PCR fragments containing the mutant VP1 were obtained by PCR of the mutant pBacPAK8-VP1 using the excision primers 5'-CATGCATGCAGGTCTCACATGAAGATGGCGTCG AATGACG-3' (forward) and 5'-GTCATGCATGCTCGAGTAATGCACGTCTACGCC-3' (reverse). The PCR fragments were digested with BsaI and XhoI restriction enzymes (Fermentas) and cloned into the NcoI and XhoI sites of the pTriEx-1.1 vector (Novagen). The ligated mutant pTriEx-VP1 constructs were transformed into XL1-Blue cells (Stratagene), plated on LB-Carbenicillin Agar plates and grown overnight at 37°C. Plasmids were purified using the HighPure Plasmid Isolation Kit (Roche) and verified by nucleotide sequencing and restriction digest. Recombinant baculovirus containing mutant VP1 and mutant VLPs were obtained as described for the wildtype.

## 3.2 Molecules Studied for Binding to Norovirus VLPs

### 3.2.1 Carbohydrates

For analysis of the HBGA binding pattern of NoV VLPs synthetic carbohydrates from mono- to tetrasaccharides were available for testing. The carbohydrates are grouped into ABH and Lewis antigens and according to the presence or absence of an L-Fuc moiety.

*ABH antigens containing L-Fuc.* L-Fuc (**1**) and  $\alpha$ -L-Fuc-(1,*O*)-CH<sub>3</sub> (**2**) were purchased from Sigma. H-disaccharides  $\alpha$ -L-Fuc-(1,2)- $\beta$ -D-Gal-(1,*O*)-R (**3**) with R=<sup>13</sup>CH<sub>3</sub> (**3a**) and R=(CH<sub>2</sub>)<sub>5</sub>COOCH<sub>3</sub> (**3b**) were chemically synthesized by Wilfried Hellebrandt (University of Lübeck, unpublished data). A antigen trisaccharide  $\alpha$ -D-GalNAc-(1,3)-[ $\alpha$ -L-Fuc-(1,2)]- $\beta$ -D-Gal-(1,*O*)-(CH<sub>2</sub>)<sub>7</sub>CH<sub>3</sub> (**4**) and B antigen trisaccharide  $\alpha$ -D-Gal-(1,3)-[ $\alpha$ -L-Fuc-(1,2)]- $\beta$ -D-Gal-(1,*O*)-R (R=(CH<sub>2</sub>)<sub>7</sub>CH<sub>3</sub>) (**5a**) were enzymatically synthesized utilizing human blood group glycosyltransferases (Seto *et al.*, 2000) and were kind gifts from Monica Palcic (Carlsberg Laboratory, Copenhagen). B antigen *O*-methyl glycoside (R=CH<sub>3</sub>) (**5b**) was enzymatically synthesized by Inken Schmutde (University of Lübeck, unpublished data). B trisaccharide with R=(CH<sub>2</sub>)<sub>8</sub>COOC<sub>2</sub>H<sub>5</sub> (**5c**) was a kind gift from David R. Bundle (University of Alberta, Edmonton). H antigen type 1 *O*-octyl glycoside  $\alpha$ -L-Fuc-(1,2)- $\beta$ -D-Gal-(1,3)- $\beta$ -D-GlcNAc-(1,*O*)-(CH<sub>2</sub>)<sub>7</sub>CH<sub>3</sub> (**6**) and H antigen type 2 with a Lemieux spacer  $\alpha$ -L-Fuc-(1,2)- $\beta$ -D-Gal-(1,4)- $\beta$ -D-GlcNAc-(1,*O*)-(CH<sub>2</sub>)<sub>8</sub>COOCH<sub>3</sub> (**7**) were kind gifts from Ole Hindsgaul (Carlsberg Laboratory, Copenhagen). H antigen type 6  $\alpha$ -L-Fuc-(1,2)- $\beta$ -D-Gal-(1,4)-D-Glc (**8**) in the reducing form was purchased from Dextra. 8-methoxycarbonyloctyl glycoside of H antigen type 6 (R=(CH<sub>2</sub>)<sub>8</sub>COOCH<sub>3</sub>,  $\beta$  anomer) (**8a**) was a kind gift from David R. Bundle (University of Alberta, Edmonton).

*Lewis antigens containing L-Fuc.*  $\alpha$ -L-Fuc-(1,3)- $\beta$ -D-GlcNAc-(1,*O*)-CH<sub>3</sub> (**9**) was synthesized by Wilfried Hellebrandt (University of Lübeck, unpublished data). *O*-methyl glycosides of Le<sup>x</sup>  $\beta$ -D-Gal-(1,4)-[ $\alpha$ -L-Fuc-(1,3)]- $\beta$ -D-GlcNAc-(1,*O*)-CH<sub>3</sub> (**10**) and Le<sup>a</sup>  $\beta$ -D-Gal-(1,3)-[ $\alpha$ -L-Fuc-(1,4)]- $\beta$ -D-GlcNAc-(1,*O*)-CH<sub>3</sub> (**11**) were obtained from Toronto Research Chemical. *O*-nethyl of Le<sup>y</sup>  $\alpha$ -L-Fuc-(1,2)- $\beta$ -D-Gal-(1,4)-[ $\alpha$ -L-Fuc-(1,3)]- $\beta$ -D-GlcNAc-(1,*O*)-CH<sub>3</sub> (**12**) and Le<sup>b</sup>  $\alpha$ -L-Fuc-(1,2)- $\beta$ -D-Gal-(1,3)-[ $\alpha$ -L-Fuc-(1,4)]- $\beta$ -D-GlcNAc-(1,*O*)-CH<sub>3</sub> (**13**) were kind gifts from Todd Lowary (University of Alberta, Edmonton) and Monica Palcic (Carlsberg Laboratory, Copenhagen), respectively.



SLe<sup>x</sup>  $\alpha$ -D-Neu5Ac-(2,3)- $\beta$ -D-Gal-(1,4)-[ $\alpha$ -L-Fuc-(1,3)]- $\beta$ -D-GlcNAc-(1,*O*)-CH<sub>3</sub> (**14**) was purchased from Toronto Research Chemical. SLe<sup>a</sup> with a benzyl carbamoyl spacer  $\alpha$ -D-Neu5Ac-(2,3)- $\beta$ -D-Gal-(1,3)-[ $\alpha$ -L-Fuc-(1,4)]- $\beta$ -D-GlcNAc-(1,*O*)-(CH<sub>2</sub>)<sub>3</sub>NH-COO-CH<sub>2</sub>-C<sub>6</sub>H<sub>5</sub> (**15**) was a gift from Beat Ernst (University of Basel).

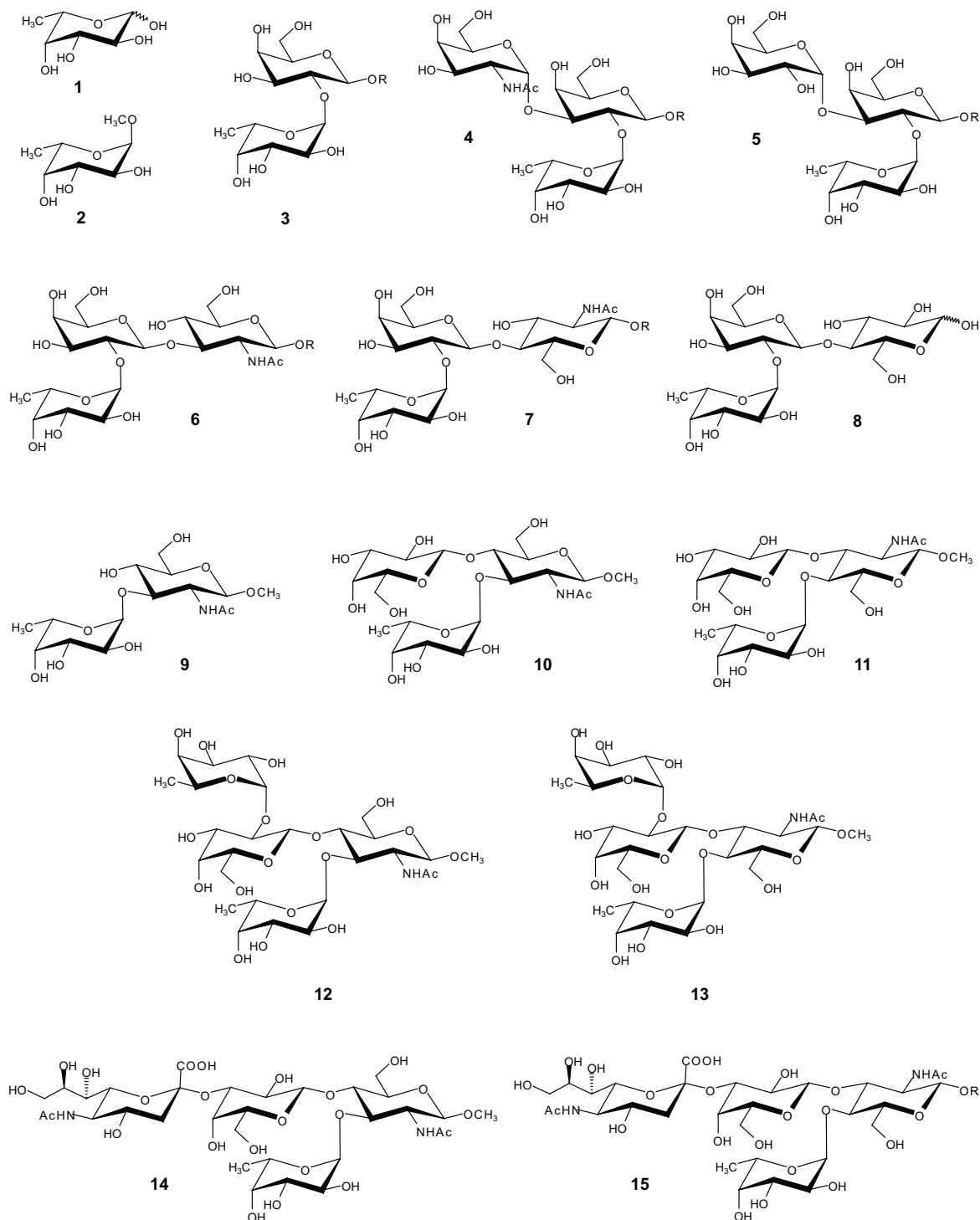


Figure 3.1. Structures of ABH and Lewis antigens containing an L-Fuc moiety.

*Carbohydrates without L-Fuc.* D-Gal (**16**), D-ManNAc (**20**), L-Gal (**22**),  $\beta$ -D-Gal-(1,4)-D-GlcNAc (type 2 precursor) (**24**),  $\beta$ -D-Gal-(1,3)-D-GalNAc (type 3 precursor) (**25**) and  $\beta$ -D-Gal-(1,4)- $\beta$ -D-Glc-(1,*O*)-CH<sub>3</sub> (type 6 precursor) (**26**) were purchased from Sigma. D-GalNAc (**17**), D-Glc (**18**) and D-GlcNAc (**19**) were obtained from Fluka, Merck and Aldrich, respectively. D-Fuc (**21**) and  $\beta$ -D-Gal-(1,3)-D-GlcNAc (type 1 precursor) (**23**) as well as reducing forms of 3'-sialyllactose  $\alpha$ -D-Neu5Ac-(2,3)- $\beta$ -D-Gal-(1,4)-D-Glc (**27**) and 6'-sialyllactose  $\alpha$ -D-Neu5Ac-(2,6)- $\beta$ -D-Gal-(1,4)-D-Glc (**28**) were obtained from Dextra. Xenoantigen  $\alpha$ -D-Gal-(1,3)- $\alpha$ -D-Gal-(1,*O*)-CH<sub>3</sub> (**29**) was purchased from Calbiochem.

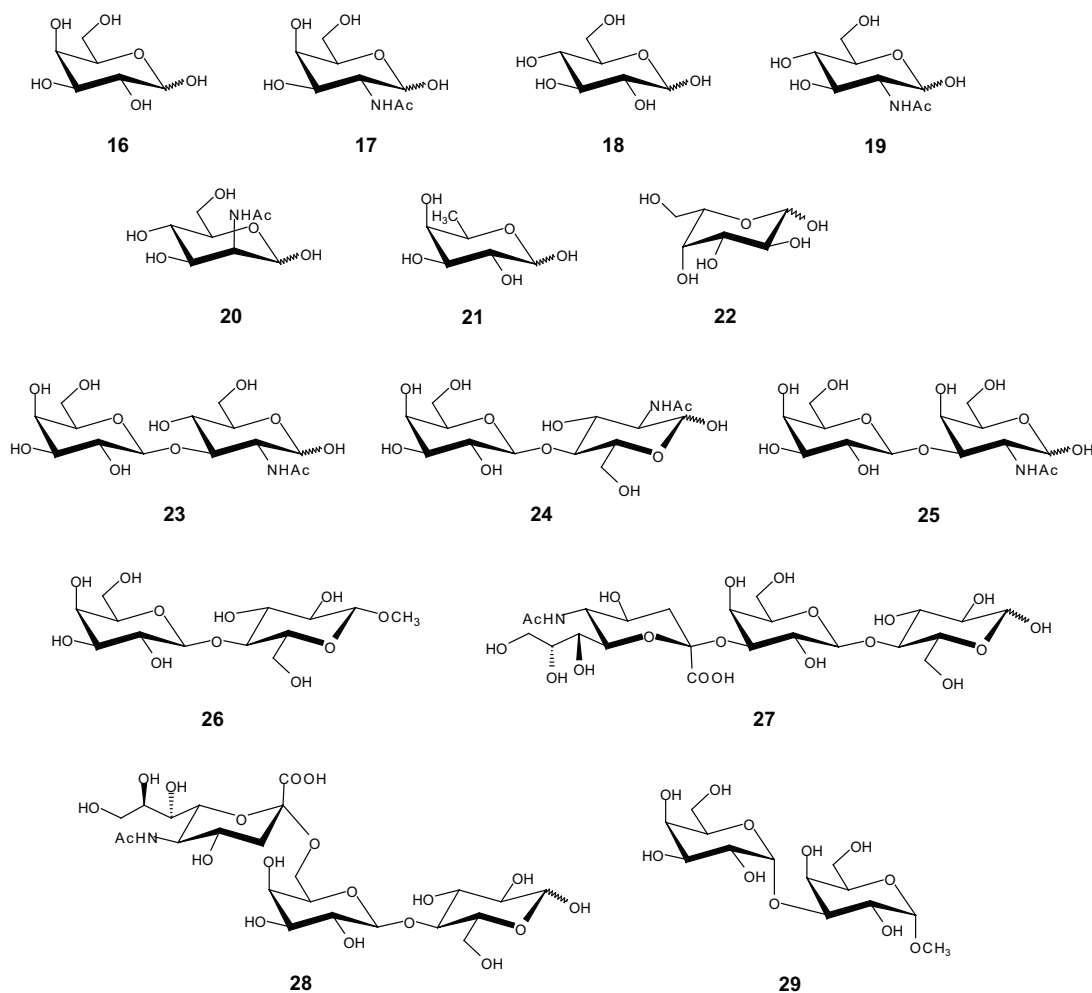


Figure 3.2. Structures of HBGAs without an L-Fuc moiety.

### 3.2.2 Synthetic Inhibitors Based on HBGA Fragments

Based on a high specificity of GII.4 NoV VLPs for L-Fuc (cf. sections 1.3 and results) as well as on different library screening approaches inhibitors directed against the HBGA binding site are designed (cf. section 1.10). Nearly all inhibitors contain L-Fuc for specificity and additional functional groups.

The difucosylated compound **30** (MW: 546.5 g/mol) was synthesized using click chemistry (Best, 2009; Hein *et al.*, 2008) resulting in a linker with two triazole rings and a central glycerol unit (Figure 3.3). The heterobifunctional compound **31** (MW: 636.7 g/mol) was synthesized in the same way but linking Fuc to fragment 160 from the Maybridge library. Fragment 160 was classified as competitive hit in NMR screening against NoV Ast6139 VLPs (Rademacher *et al.*, 2011) (cf. section 1.10). **32** (MW: 289.3 g/mol) and **33** (379.5 g/mol) furnish each ‘one half’ of the heterodivalent compound **31**, i.e. Fuc and fragment 160, respectively, coupled to a triazole ring with an ethanol residue. All compounds were synthesized by Dr. Julie Guiard in the laboratory of Professor David R. Bundle and Dr. Pavel I. Kitov (University of Alberta, Edmonton). The synthesis of **31** to **33** is published elsewhere (Guiard *et al.*, 2011).

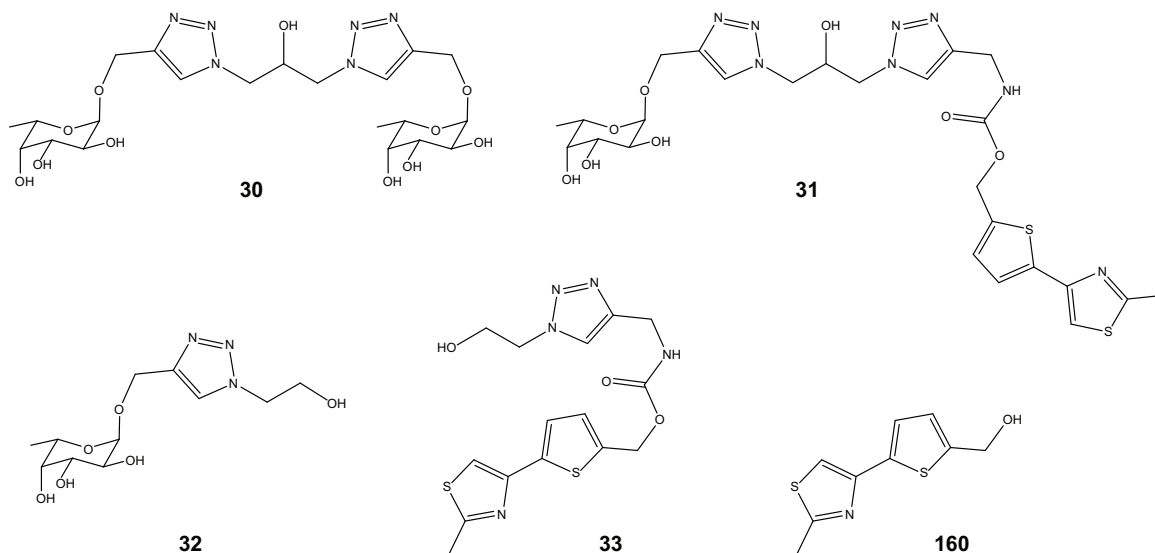


Figure 3.3. Structures of inhibitors with L-Fuc and/ or fragment 160. **30** and **31** constitute homo- and heterodivalent fucosylated compounds, respectively. **32** and **33** resemble the two functional groups of **31** coupled to a part of the linker. The structure of fragment 160 is also shown.

Using a click chemistry protocol, polymeric inhibitors based on the polyacrylamide (PAA) **34** ('backbone', MW: 2740 g/mol per N<sub>3</sub>) were synthesized that contain L-Fuc and/or fragment 160: **35** (L-Fuc, MW: 2842 g/mol per Fuc), **36** (fragment 160, MW: 3030 g/mol per 160) and **37** (L-Fuc and fragment 160, MW: 3160 g/mol per Fuc) (Figure 3.4). All molecular weights are given per monomeric repeating unit, i.e. per Fuc or fragment 160 residues or per N<sub>3</sub> in case of the PAA backbone **34**. The number of monomeric repeats 'n' in each polymer is 20 to 30 resulting in a total molecular weight of 60 to 100 kDa. For comparability, concentrations of polymers will be given 'per monomeric unit' in this work. **35** to **37** were synthesized by Dr. Julie Guiard (Guiard *et al.*, 2011). **34** was synthesized by Dr. Eugenia Paszkiewicz (University of Alberta, Edmonton) from the same laboratory.

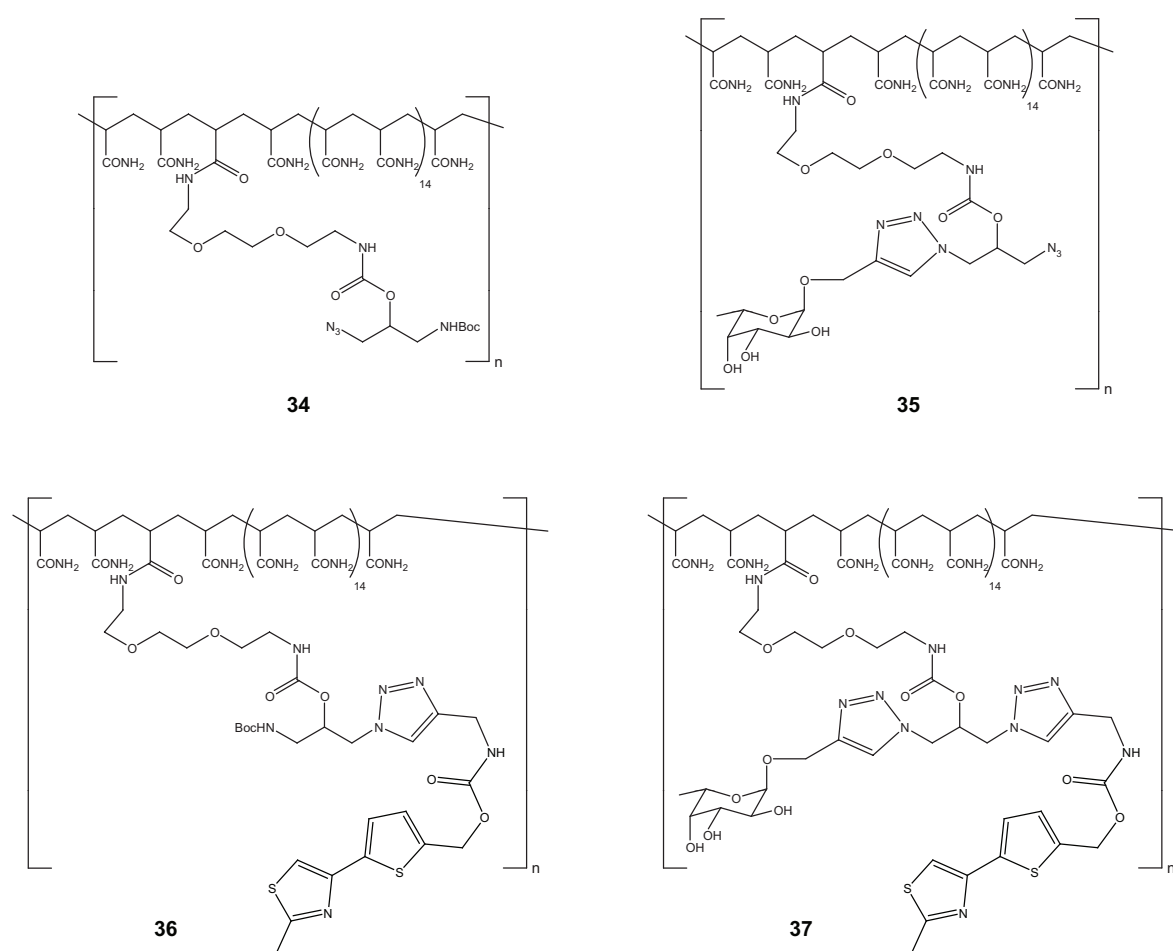


Figure 3.4. Polymeric PAA-based inhibitors with L-Fuc and/or fragment 160. Each polymer consists of 20 to 30 monomeric repeating units ('n') resulting in total molecular weights from 60 to 100 kDa.

Chemical structures of polymers 38, 39, 40, and 41 are shown. Each structure features a poly(amide-ether) backbone with a repeating unit of 14 methylene groups. The side chain contains a glucose moiety linked via an ether bond to a 1,2,4-triazole ring, which is further linked to a 1,3,4-oxadiazole ring. The terminal group of the side chain varies: 38 has a 4-(pyridin-2-yl)benzamide group, 39 has a 4-(furan-2-yl)benzamide group, 40 has a 4-phenyl-1,3,4-oxadiazole-2-carbonyl group, and 41 has a 4-phenyl-1,3,4-thiadiazole-2-carbonyl group.

Figure 3.5. Polymeric inhibitors containing L-Fuc and ‘adjacent site’ fragments. The attached aromatic fragments display inter-ligand NOEs to  $\alpha$ -L-Fuc-(1,*O*)-CH<sub>3</sub> in the presence of Ast6139 VLPs.

An *in silico* screening approach of a virtual library by molecular docking to the HBGA binding pocket of NoV VLPs complemented the hits from NMR screening (cf. section 1.10). All compounds in the library contained an L-Fuc moiety and were easy to synthesize applying Ugi reactions. The four compounds with the highest predicted free energy of the docking model were synthesized by Dr. Julie Guiard (University of Alberta, Edmonton, unpublished data): **42** (MW: 673.7 g/mol), **43** (MW: 525.6 g/mol), **44** (MW: 476.4 g/mol) and **45** (MW: 669.7 g/mol) (Figure 3.6). Two polymeric versions of the “virtual screening”-hit **42** with different linker compositions based on the PAA backbone **34** were synthesized by Dr. Eugenia Paszkiewicz (University of Alberta, Edmonton, unpublished data): **46** (MW: 2453.7 g/mol) and **47** (2394.6 g/mol) (bottom panel in Figure 3.6).

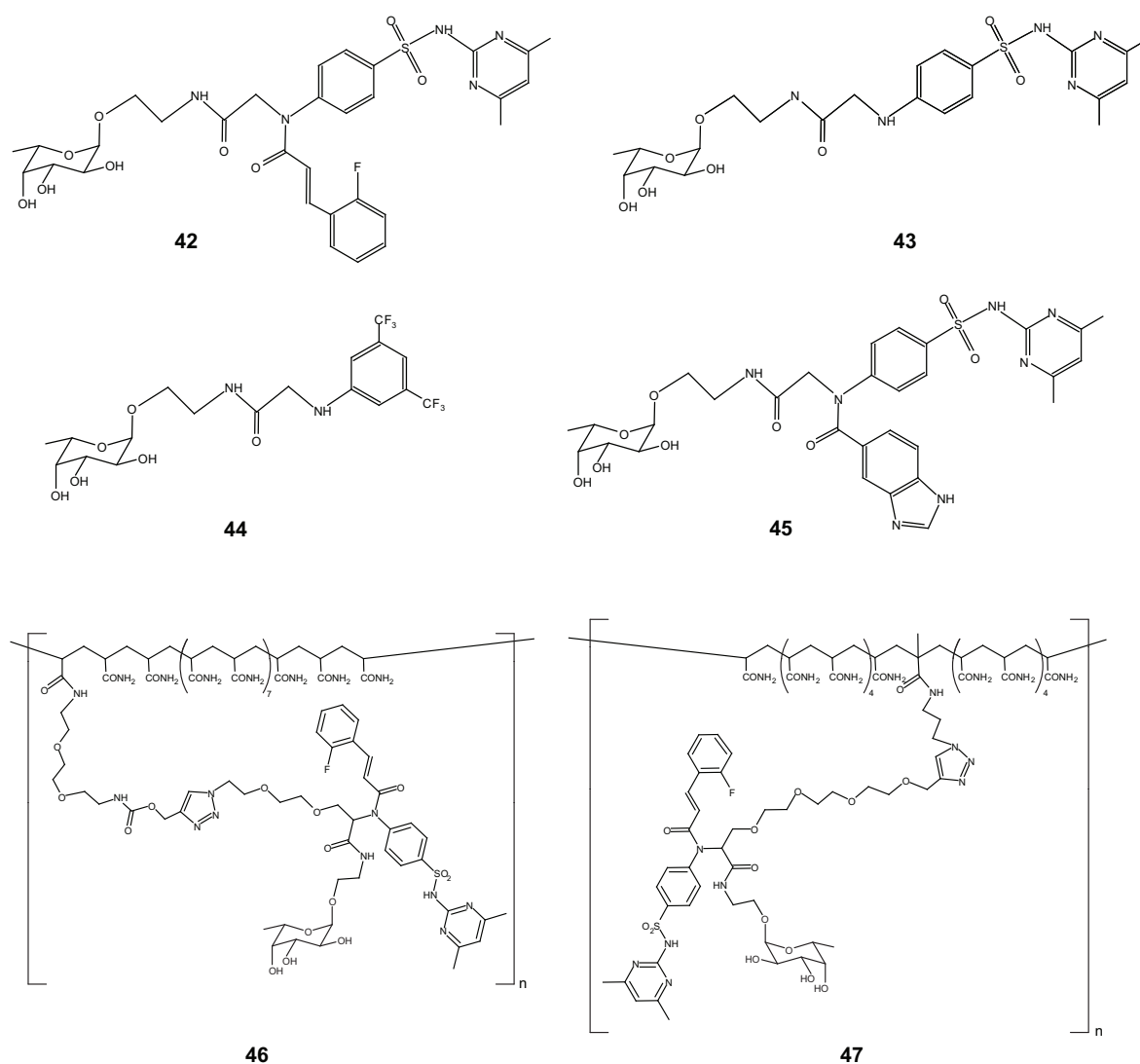


Figure 3.6. Structures of inhibitors obtained from virtual library screening. **42** to **45** are the four best hits according to predicted free energy of docking models. **46** and **47** are polymeric versions of **42** differing in the design of the linker to the PAA backbone.

### 3.3 NMR Spectroscopy

All experiments were performed on a Bruker Avance DRX or AV III 500 MHz NMR spectrometer equipped with a TCI cryogenic probe. Bruker Topspin 2.1 and 3.0 were used for data acquisition, processing and analysis. All experiments were measured in 23 mM deuterated phosphate buffer pH 7.0 with 154 mM sodium chloride, if not stated otherwise (pH adjusted in water). *d4*-trimethylsilyl-2,2,3,3-tetradeuteriopropionic acid (TSP-*d4*) (Cambridge Isotope Laboratories, Inc.) was used as internal standard. The temperature was set to 282 K except 298 K applied in NOESY experiments.

#### 3.3.1 Assignment Experiments

Chemical shift assignment of carbohydrates and selected inhibitors was accomplished employing standard one- and two-dimensional NMR experiments.  $^1\text{H}$ ,  $^1\text{H}$ -COSY,  $^1\text{H}$ ,  $^{13}\text{C}$ -HSQC,  $^1\text{H}$ ,  $^{13}\text{C}$ -HMBC and  $^1\text{H}$ ,  $^1\text{H}$ -TOCSY experiments were performed using standard Bruker pulse sequences. 1D gradient enhanced chemical shift selective filter (ge cssf) TOCSY and NOESY experiments were used for assignment of overlapping spectra regions (Robinson *et al.*, 2004) (pulse sequences and parameters can be found in section 7.6.7 in the appendix). Carbohydrates and inhibitors were dissolved in  $\text{D}_2\text{O}$  at a concentration of 1 to 5 mM and measured at 282 K. Compound **42** displayed broad, heterogeneous signals and decomposition in aqueous solution and was therefore in addition measured in methanol-*d4* (Aldrich). Proton  $T_1$  relaxation times were measured by inversion recovery experiments using a standard Bruker pulse sequence with 13 delays and a relaxation delay of 20 s. Data were extracted from non-linear curve fitting using Origin 7.0 (Microcal).

#### 3.3.2 STD NMR Spectroscopy

##### *Binding Epitopes from Group Epitope Mapping*

Samples for STD NMR experiments with carbohydrates and inhibitors contained 0.12 to 0.89 mg/mL Ast6139 VLPs corresponding to 11 to 80 nM VLPs or 1.9 to 14.8  $\mu\text{M}$  binding sites (assuming 180 binding sites per VLP). Ligands were present at concentrations from 0.5 to 1.7 mM (see Table 7.3 for a detailed description of sample composition and experimental parameters). The resulting ligand to binding site ratio was 30:1 to 260:1. Mutant

Ast6139 VLPs D391A and H395A (cf. section 3.1.1) were measured with  $\alpha$ -L-Fuc-(1,*O*)-CH<sub>3</sub> **2** and B trisaccharide **5b**. Samples of bovine NoV Bo/Newbury2/1976/UK (NB2) (Oliver *et al.*, 2003; Woode & Bridger, 1978) contained 0.24 mg/mL VLPs and 0.5 mM of xenoantigen **29** or other carbohydrates (see Table 7.3). NB2 VLPs were provided by Dr. Didier Poncet (CNRS Gif-sur-Yvette, France).

STD NMR experiments were measured with a pseudo-2D setup with interleaved acquisition of on- and off-resonance spectra (see section 7.6.7 in the appendix for pulse programs). On- and off-resonance frequencies were chosen as -4 and 300 ppm. The inter-scan delay was set to 25 s if not stated otherwise according to (Rademacher & Peters, 2008). Suppression of the residual water signal was achieved using a 3-9-19 WATERGATE sequence. A train of Gaussian pulses (45 to 50 dB attenuation level) with a single length of 49 ms and 1 s inter-pulse delay was used for selective saturation of VLPs. For some ligands whole STD build-up curves were recorded with saturation times between 0.25 and 4 s: A and B trisaccharides **4**, **5b** and **5c** as well as compounds **31**, **42**, **43**, **44**, **45** and fragment 160 in presence of wildtype Ast6139 VLP; mutants D391A and H395A in presence of **5b**; xenoantigen **29** in presence of NB2 VLPs. For all other binding ligands single experiments were measured at saturation times of 0.5 s. According to typically measured  $T_1$  relaxation times, this should still be in the linear range of the build-up of the STD effect. STD spectra of non-binding carbohydrates were recorded with a longer saturation time of 2 s. The number of scans varied largely from 64 to 8k depending on the sample composition and the size of observed STD signals (cf. Table 7.3).

Absolute STD effects in percent of the reference signal have been determined by overlay of difference spectra with the corresponding reference spectra ('manual' analysis) or by integration of the signals in the difference spectra relative to that in the corresponding reference spectra.

Whole STD build-up curves were subjected to non-linear curve fitting to a mono-exponential equation using Origin 7.0 (Microcal):

$$STD(t) = STD_{max}(1 - e^{(-k_{sat}t)}) \quad (1)$$

with  $STD(t)$  being the STD signal intensity at saturation time  $t$ ,  $STD_{max}$  being the maximum STD signal intensity assuming infinity saturation times, and  $k_{sat}$  being the observed saturation rate constant (Mayer & James, 2004). Instead of the absolute STD effect in percent of the reference signal, the product  $STD_{max} * k_{sat}$  is used to derive binding epitopes.



In order to account for the presence of a “lag phase” of the STD build-up (Jayalakshmi & Krishna, 2002), an additional parameter  $b$  (y-shift) was included:

$$STD(t) = STD_{max}(1 - e^{(-k_{sat}t)}) + b \quad (2)$$

The intersection of the curve with the x axis as a measure for the lag phase is calculated by  $\ln(1+b/STD_{max})/(-k_{sat})$ .

Binding epitopes for group epitope mapping were obtained by normalizing the proton with the highest absolute STD effect or the largest product  $STD_{max} * k_{sat}$  to 100% and calculating the relative STD effects of all other signals as fraction of the highest STD signal.

### *Direct STD Titration Experiments*

The virtual screening hit **42** was titrated to Ast6139 VLPs for affinity determination. The starting NMR sample contained 0.22 mg/mL VLPs (20 nM VLPs, 3.7  $\mu$ M binding sites) and 0.1 mM TSP-*d4* as internal reference. It was used to dissolve ~0.9 mg of **42** to final concentrations of 25, 10, 2 and 0.5 mM that served as stocks for stepwise titration to the starting sample without **42**. The concentrations of VLPs and TSP were therefore kept constant. For each titration step with final concentrations of **42** from 1.9  $\mu$ M to 5.3 mM an STD NMR experiment was performed using a Bruker pulse sequence with a 3-9-19 WATERGATE solvent suppression scheme. The saturation time was set to 4 s with an additional relaxation delay of 1 s. The number of scans was ranging from 5k for the first titration step (1.9  $\mu$ M) to 32 for the last steps in the mM range. Four dummy scans were recorded. For each spectrum signals of **42** were integrated and the STD amplification factors (STD AF) were determined:

$$STD\ AF = \frac{I_0 - I_{sat}}{I_0} \times \text{ligand excess} \quad (3)$$

with  $I_0$  and  $I_{sat}$  being the signal intensities in the reference and STD spectrum, respectively. Plots of STD amplification factors versus concentrations  $c$  of **42** were fitted to a Langmuir binding isotherm to yield dissociation constants  $K_D$ :

$$STD\ AF(c) = \frac{STD\ AF_{max} * c}{K_D + c} \quad (4)$$

with  $STD\ AF_{max}$  being the STD amplification factor at infinite ligand concentration and  $K_D$  being the equilibrium dissociation constant. The equation is valid for systems in fast

exchange on the NMR chemical shift and relaxation time scale ( $\mu\text{M}$  to  $\text{mM}$  affinities). In this case, the signal of the free ligand (STD AF) reports on the bound state.

Bovine NoV NB2 VLPs were titrated with the xenoantigen **29** for affinity determination. A sample of 0.02 mg/mL VLPs (1.8 nM VLPs, 0.33  $\mu\text{M}$  binding sites) was titrated with **29** from 510  $\mu\text{M}$  to 8 mM in five steps. For each titration step an STD spectrum was measured using a Bruker pulse sequence with an excitation sculpting scheme for solvent suppression (pulse sequence not shown). The saturation time was 2 s with an additional relaxation delay of 0.1 s. 5k scans (first titration step) to 256 scans (last step) and four dummy scans were recorded. The VLP concentration was not held constant during the titration and was diluted by 9% until the end of the titration. Because of this, equation 4 was modified in such a way that 'c' is the ligand excess instead of the ligand concentration and ' $K_D$ ' is the ligand excess at which the ligand concentration corresponds to the true  $K_D$  value. The  $K_D$  value was estimated from the ratio of ligand excess to ligand concentration that was known for each titration step.

#### *Competitive STD Titration Experiments*

For competitive titration experiments, first starting NMR samples were prepared that contained 0.15 to 0.22 mg/mL Ast6139 VLPs (14 to 20 nM VLPs, 2.5 to 3.7  $\mu\text{M}$  binding sites) and 1 mM of the carbohydrate ligand that is to be displaced, called the reporter ligand from here on. Competing ligands were dissolved in the same buffer (deuterated phosphate buffer pH 7.0, 154 mM NaCl) at stock concentrations that depended on the solubility and the anticipated titrated concentration range. If not stated otherwise, the competing ligand was added in dilutions containing the same concentration of VLPs and reporter ligand as the starting sample keeping their concentrations constant.

Competitive titrations with HBGAs and non-polymeric inhibitors were done employing  $\alpha\text{-L-Fuc-(1,}O\text{)-CH}_3$  **2** as competing ligand that was available in large quantities. A trisaccharide **4**, B trisaccharide **5b**, sLe<sup>x</sup> **14**, the difucosylated compound **30** and the heterodivalent compound **31** were used as reporter ligands.  $\alpha\text{-L-Fuc-(1,}O\text{)-CH}_3$  was titrated stepwise at final concentrations ranging from 1  $\mu\text{M}$  to 95 mM.  $\alpha\text{-L-Fuc-(1,}O\text{)-CH}_3$  was also used as reporter ligand for competitive titrations of B trisaccharide *O*-methyl glycoside **5b** and virtual screening hit **42** with titration ranges from 1  $\mu\text{M}$  to 1 mM and from 0.25  $\mu\text{M}$  to 1 mM, respectively.

Competitive titrations of polymeric PAA-based inhibitors were performed using  $\alpha$ -L-Fuc-(1,*O*)-CH<sub>3</sub> **2** as reporter ligand. Polymers were dissolved in NMR buffer at stock concentrations from 1 to 4 mM calculated per monomeric repeating unit (i.e. ‘per Fuc’ in most cases). Polymers were titrated from 1 nM to 20  $\mu$ M (**39**), 50  $\mu$ M (**38**), 90  $\mu$ M (**46**) or 200  $\mu$ M (**35**, **40** and **41**). In case of **38** and **39** the concentrations of reporter ligand and VLPs were not kept constant and were diluted adding up to 8% and 5%, respectively, at the end of the titration.  $\alpha$ -L-Fuc-(1,*O*)-CH<sub>3</sub> was also titrated with BSA-H type 2 trisaccharide conjugate, that was a kind gift from Ole Hindsgaul (Carlsberg Laboratory, Copenhagen). A stock solution of BSA-H type 2 conjugate in NMR buffer contained 90  $\mu$ M BSA conjugate corresponding to 1 mM H type 2 trisaccharide moieties (12 saccharide units on average per BSA molecule, determined by the manufacturer). The titration range was 1.1 nM to 20  $\mu$ M calculated per H type 2 trisaccharide moieties.

For each titration steps an STD experiment was acquired using a Bruker pulse sequence with 3-9-19 WATERGATE solvent suppression. A saturation time of 2 s was used. The interscan delay was set to 2 s (titration of **4**, **5b**, **14** with  $\alpha$ -L-Fuc-(1,*O*)-CH<sub>3</sub>; titration of  $\alpha$ -L-Fuc-(1,*O*)-CH<sub>3</sub> with **5b**, **38**, **39** and BSA-H type 2 conjugate) or 5 s (titration of **30** and **31** with  $\alpha$ -L-Fuc-(1,*O*)-CH<sub>3</sub>; titration of  $\alpha$ -L-Fuc-(1,*O*)-CH<sub>3</sub> with **35**, **40**, **41** and **46**). 64 to 1k scans were acquired depending on the size of the STD signals of the reporter ligand.

The absolute STD effects  $STD(I)$  of the reporter ligand signals were obtained manually by spectra scaling (*vide supra*).  $STD(I)$  was plotted against the competing ligand concentration and fitted against equation 5:

$$STD(I) = STD_{min} + \frac{STD_0 - STD_{min}}{1 + \left(\frac{IC_{50}}{[I]}\right)^{Hill}} \quad (5)$$

where  $STD_0$  is the absolute STD effect of the reporter ligand in absence of competing ligand,  $STD_{min}$  is the (fitted) minimal STD effect of the reporter ligand in presence of high concentrations of competing ligand,  $IC_{50}$  is the half maximum inhibitory concentration of the competing ligand, and  $Hill$  is the Hill slope of the inhibition curve reporting on cooperativity (Fersht, 1999). A Hill slope of 1 is equivalent to independent binding sites (no cooperativity). Hill slopes below and above 1 indicate positive and negative cooperativity, respectively. (In inhibition experiments  $Hill$  has a negative sign, but for clarity the positive values will be discussed throughout this work.)

Obtained  $IC_{50}$  values are used to compare the binding strengths of HBGAs and inhibitors for NoV VLPs in a qualitative way.

In cases where either the  $K_D$  of the displaced ligand or the  $K_I$  of the competing ligand are known, the missing value can in principle be calculated according to (Wang *et al.*, 2004) and (Dalvit, 2008):

$$\frac{STD(I)}{STD_0} = \frac{[P_T] + [L_T] + K_D \left(1 + \frac{[I]}{K_I}\right) - \sqrt{\left\{[P_T] + [L_T] + K_D \left(1 + \frac{[I]}{K_I}\right)\right\}^2 - 4[P_T][L_T]}}{[P_T] + [L_T] + K_D - \sqrt{\{[P_T] + [L_T] + K_D\}^2 - 4[P_T][L_T]}}$$

where  $STD(I)$  and  $STD_0$  are the absolute STD effects of the reporter ligand in presence and absence of the competing ligand, respectively,  $[P_T]$  is the total concentration of protein binding sites,  $[L_T]$  is the total concentration of reporter ligand,  $K_D$  and  $K_I$  are the dissociation constants of the reporter and competing ligand, respectively, and  $[I]$  is the concentration of competing ligand.

More easily,  $K_I$  was calculated from the  $IC_{50}$  value calculated from equation 5 applying the Cheng-Prusoff equation (Cheng & Prusoff, 1973):

$$K_I = \frac{IC_{50}}{1 + \frac{[L]}{K_D}} \quad (6)$$

with  $IC_{50}$  being the half maximum inhibitory concentration of the competing ligand, and  $[L]$  and  $K_D$  being the concentration and the dissociation constant of the reporter ligand, respectively. In particular, the  $K_D$  of  $\alpha$ -L-Fuc-(1,*O*)-CH<sub>3</sub> **2** experimentally determined by direct STD titration was used to calculate the  $K_D$  of HBGAs and inhibitors.

For the two complementary competitive titrations of  $\alpha$ -L-Fuc-(1,*O*)-CH<sub>3</sub> **2** with B trisaccharide **5b** and *vice versa* a mathematical approach was applied to calculate their  $K_D$  values from the two  $IC_{50}$  values by conversion and substitution operations of the Cheng-Prusoff equation (cf. section 7.6.2 in the appendix for details).

### 3.3.3 Transferred NOESY Experiments

Transferred NOESY (trNOESY) experiments were recorded with standard Bruker pulse sequences with gradient pulses and phase sensitivity. 3-9-19 or W5 WATERGATE sequences were applied to suppress the residual solvent signal. Free sLe<sup>x</sup> **14** in absence of VLPs was measured at a concentration of 1 mM in D<sub>2</sub>O at different temperatures ranging from 283 K to 310 K in 5 K increments. NOE build-up curves for this sample were measured at 310 K with mixing times ranging from 100 to 5000 ms and at 298 K with mixing times ranging from 100 to 1000 ms. The sample of sLe<sup>x</sup> **14** for trNOESY experiments contained 1.2 mg/mL Ast6139 VLPs (110 nM VLPs, 20 μM binding site) and 0.25 mM sLe<sup>x</sup> resulting in a ligand to binding site ratio of 12.5:1. TrNOE build-up curves were measured with mixing times ranging from 25 ms to 5 s at a temperature of 298 K. Further experimental details are summarized in Table 7.4 in the appendix.

For calculation of trNOE build-up curves NOESY cross peaks were integrated relative to the diagonal peak of H1<sup>Fuc</sup> in the spectrum with the shortest mixing time (25 ms). TrNOE build-up curves were fitted to a double-exponential equation:

$$I_{NOE}(\tau_m) = \frac{P_1}{(P_1 - P_2)} (e^{(-P_2 \times \tau_m)} - e^{(-P_1 \times \tau_m)}) \quad (7)$$

with  $I_{NOE}$  being the NOE intensity at NOESY mixing time  $\tau_m$  and  $P_1$  and  $P_2$  being exponential coefficients. The mixing time at which maximum NOE intensity  $I_{max}$  is reached is calculated as:

$$\tau_{m(I_{max})} = \frac{\ln(P_2) - \ln(P_1)}{(P_2 - P_1)}$$

The trNOESY sample with sLe<sup>x</sup> and Ast6139 VLPs was also subjected to 1D gradient-enhanced cssf TOCSY and NOESY experiments with varying mixing times for analysis of regions with spectral overlap (see section 7.6.7 for pulse programs).

### 3.3.4 ROESY Experiments

Transferred ROESY (trROESY) experiments of sLe<sup>x</sup> **14** in presence of Ast6139 VLPs were measured using a Bruker pulse sequence with 3-9-19 WATERGATE solvent suppression. The sample contained 1.2 mg/mL VLPs (20 μM binding sites) and 800 μM sLe<sup>x</sup> **14**, resulting in a ligand to binding site ratio of 40:1. Experiments were measured at a

temperature of 298 K with 2 s relaxation delay and a mixing time of 150 ms. 64 scans were acquired with 512 increments and 2k data points in the direct dimension resulting in an experimental time of about 21 h (cf. Table 7.4).

### 3.3.5 Stability Measurements of Carbamates

Compounds **31** and **33** containing a carbamate linkage were tested for stability by NMR measurement over a certain time range. Compound **31** was dissolved in D<sub>2</sub>O at a concentration of 0.5 mM and TSP-*d4* was added to a final concentration of 0.1 mM. 1D <sup>1</sup>H NMR spectra were measured with 32 scans and 4 dummy scans with a relaxation delay of 20 s over a period of ca. four months (114 days). Compound **33** displayed a low solubility. From a saturated solution of **33** with a nominal concentration of 5 mM the supernatant was taken and TSP-*d4* was added to a final concentration of 0.1 mM. 1D <sup>1</sup>H NMR spectra were measured with 16 scans, 4 dummy scans and a relaxation delay of 20 s over a period of 20 days. From the first spectrum measured directly after solving an initial concentration of **33** of ca. 1.1 mM was estimated by signal integration using the TSP signal as reference. In each measured spectrum spectrally isolated signals of **31** and **33** were integrated and normalized to the integral of the TSP signal. The plots of the normalized integrals versus the time in log scale were fitted to an exponential decay function:

$$I(t) = I_0 * e^{(-t/\tau)} + b \quad (8)$$

where  $I(t)$  is the signal integral at time  $t$ ,  $I_0$  is the initial integral directly after solving,  $\tau$  is the lifetime of the compound and  $b$  is a correction factor for baseline distortions or disturbing signals that were included in the integral ranges.

### 3.4 Surface Plasmon Resonance

The interaction of Ast6139 VLP with synthetic HBGA fragments and prototype inhibitors is investigated with SPR spectroscopy using two basic experimental setups: a direct binding assay (sections 3.4.1) and a competition assay (section 3.4.2). All experiments were performed on a Biacore 3000 instrument (GE Healthcare). Details on the general instrument handling can be found in the Biacore 3000 Handbook.

#### 3.4.1 Direct Immobilization of Norovirus VLPs

In the direct assay format VLPs are immobilized on a CM5 sensor chip surface and carbohydrates and inhibitors are tested as analytes in the mobile phase (cf. Figure 1.12). Titration experiments with increasing concentrations of the analyte allow determination of the affinity constant of the interactions.

*Immobilization of NoV VLPs.* CM5 sensor chips (GE Healthcare) providing a 100 nm carboxy-methylated dextran matrix were covered with Ast6139 VLPs using the Amine Coupling Kit (GE Healthcare). Therefore, the chips were docked and primed with 10 mM sodium acetate buffer pH 5.0, 154 mM sodium chloride and 0.01% sodium azide as running buffer. The chip surface was prepared for immobilization by two injections of 20  $\mu$ L 0.1 M glycine in NaOH pH 12 and 0.3% Triton X-100 and then activated by injection of 150  $\mu$ L of a freshly prepared mixture of NHS and EDC at a flow rate of 10  $\mu$ L/min. A 3 mg/mL stock solution of VLPs in PBS pH 7.2 was diluted in 10 mM sodium acetate buffer pH 4 or 4.5 to a concentration of 5 to 10  $\mu$ g/mL and injected. Remaining activated groups were deactivated by injection of ethanolamine with a total volume of at least 300  $\mu$ L. The amount of immobilized VLPs was 1600 to 12000 RU. The reference flow cell was only activated and deactivated. Carbohydrates and inhibitors were dissolved in running buffer and injected at varying concentrations.

*Titration experiments with HBGAs and inhibitors.* 10 mM sodium acetate buffer pH 5.0 with 154 mM sodium chloride and 0.01% sodium azide was used as running buffer if not stated otherwise. Non-polymeric compounds were dissolved in running buffer at the following concentrations: L-Fuc, D-Gal, D-Glc and D-Man: 200 mM; H-disaccharide **3b**: 500 mM; H type 6 trisaccharide **8a**: 40 mM; **30**, **42**, **43**, **44** and **45**: 20 mM; **31**: 5 mM. Titrations of non-polymeric compounds were performed by injection of 10 to 80  $\mu$ L

sample (flow rate 5 to 20  $\mu\text{L}/\text{min}$ ). In case of **30**, **31**, **42**, **43**, **44** and **45** the chip surfaces were regenerated by two 1 minute injections of 25 mM sodium phosphate buffer pH 7.4. Polymeric inhibitors **34**, **35**, **36**, **38**, **39**, **40**, **41**, **46** and **47** were dissolved in running buffer at a concentration of 1 to 4 mM directly before measurement. Titrations were performed by injection of 15 to 30  $\mu\text{L}$  of sample (flow rate of 10  $\mu\text{L}/\text{min}$ ). In case of **46** and **47** the chip surface was regenerated by two injections of 1 minute duration of phosphate buffer pH 7.4. The difference responses (RU) at the end of the injections were monitored and plotted against the injected analyte concentration. A Langmuir binding isotherm for 1:1 binding was fitted to the titration curves using Origin 7.0 (Microcal):

$$RU(c) = \frac{RU_{max} * c}{c * n + K_D} + b \quad (9)$$

where  $c$  is the concentration of the analyte,  $RU_{max}$  is the maximum response assuming saturation of binding sites,  $n$  is the steric interference factor (in all cases assessed as 1),  $K_D$  is the dissociation constant of the polymeric inhibitor and  $b$  is a correction factor to account for imperfections in the reference subtraction. In case of polymeric inhibitors  $c$  corresponds to the concentration of monomeric repeating unit (cf. section 3.2.2).

For virtual screening hit **42** and polymeric inhibitor **38** the titration curves were fitted to a two-site binding model with two independent dissociation constants:

$$RU(c_{lig}) = \frac{RU_{max,1} * c_{lig}}{c_{lig} * n_1 + K_{D,1}} + \frac{RU_{max,2} * c_{lig}}{c_{lig} * n_2 + K_{D,2}} + b \quad (10)$$

with  $K_{D,1}$  and  $K_{D,2}$  being the dissociation constants of the high and the low affinity component, respectively.

*Influence of buffer and pH on carbohydrate binding to VLPs.* To study the influence of different buffers and pH on analyte binding to VLPs, a range of different buffers was prepared: 10 mM sodium acetate buffer with pH ranging from 3.8 to 5.6 in steps of 0.2 p; 25, 50 and 100 mM sodium acetate buffer at pH 5.0; 50 mM MES buffer with pH 5.6, 5.8, 6.0, 6.2, 6.4 and 6.6; 25 mM sodium phosphate buffer pH 6.2 – 7.6 (steps of 0.2 pH units); 100 mM BisTris buffer with pH 5.8, 6.0, 6.2, 6.4, 6.6 and 6.8. All buffers contained 154 mM sodium chloride, 0.01% sodium azide and 0.005% Surfactant P-20 (GE Healthcare). H-disaccharide with 5-methoxycarbonylpentyl spacer **3b** was used as analyte since it provided positive responses under various conditions. **3b** was dissolved in 10 mM sodium acetate buffer pH 5.0 at a concentration of 500 mM and then diluted in the various buffers to a final concentration of 10 mM. Because of the high dilution factor the influence



of the stock buffer in the final solution was assumed to be negligible. The system was primed to one of the various buffers and 10  $\mu$ L of the 10 mM solution of H-disaccharide **3b** in the same buffer were injected in duplicate (flow rate 10  $\mu$ L/min). The difference response (RU) in the steady state was monitored.

### 3.4.2 Competitive Assay for Estimation of IC<sub>50</sub> Values

For the competitive or indirect assay SPR sensor chips are covered with carbohydrate conjugates of PAA or BSA to simulate a glycosylated cell surface to which NoV VLPs can bind. The competition efficiencies of carbohydrates and inhibitors are determined in titration experiments by co-injecting VLPs with increasing ligand concentrations.

#### *Competitive Assay using PAA Sugar Conjugates*

*Stock solutions.* 50 mM MES buffer pH 6.0 with 154 mM sodium chloride, 0.01% sodium azide and 0.005% Surfactant P-20 (GE Healthcare) was used as running buffer. PAA-biotin (short: PAA),  $\alpha$ -L-Fuc-(1,*O*)-PAA-biotin (PAA-fucose), H-disaccharide-PAA-biotin (PAA-H-disaccharide) and B-trisaccharide-PAA-biotin (PAA-B-trisaccharide) (Glycotech) were dissolved in H<sub>2</sub>O to a final concentration of 1 mg/ml. A 200  $\mu$ g/ml stock solution of Neutravidin (Pierce) in 10 mM sodium acetate buffer pH 4.0 was prepared. A 3  $\mu$ g/ $\mu$ L stock solution of Ast6139 VLPs in PBS pH 7.2 was used for all experiments.

*Immobilization of PAA sugar conjugates.* The immobilization was performed in HBS-P buffer pH 7.4 (GE Healthcare). A C1 sensor chip (GE Healthcare) providing a gold surface functionalized with carboxyl groups was used. The chip surface was prepared and activated using the Amine Coupling Kit (GE Healthcare) as described for immobilization of VLPs (*vide supra*). 80  $\mu$ L Neutravidin (Pierce) was injected (flow rate 10  $\mu$ L/min) to a final amount of ca. 2000 RU. Remaining activated carboxyl groups were deactivated by injection of 60  $\mu$ L ethanolamine. 5 to 7  $\mu$ L of 1  $\mu$ g/ml solutions of biotinylated PAA-sugars in HBS-P buffer pH 7.4 (GE Healthcare) were injected at a flow rate of 5  $\mu$ L/min to a final amount of 210 RU PAA-fucose on flow cell 2, 220 RU PAA-H-disaccharide on flow cell 3 and 210 RU PAA-B trisaccharide on flow cell 4. All flow cells including the reference flow cell were blocked by 2x25  $\mu$ L injections of 10  $\mu$ g/mL PAA-biotin in HBS-P buffer pH 7.4 (GE Healthcare), adding 230 RU PAA-biotin to the reference flow cell 1 and ca. 100 RU PAA-biotin to the three flow cells covered with PAA-sugars.

*Concentration and flow rate dependent VLP binding.* 20  $\mu\text{L}$  VLPs at concentrations ranging from 0.12 to 120  $\mu\text{g/mL}$  were injected on the sensor chip (flow rate 10  $\mu\text{L/min}$ ). During the dissociation phase 15  $\mu\text{L}$  100 mM L-Fuc (**1**) was injected. Finally the chip surface was regenerated by two injections of 10  $\mu\text{L}$  25 mM phosphate buffer pH 7.4. For the test of VLP binding as a function of the contact time 20  $\mu\text{L}$  30  $\mu\text{g/mL}$  VLPs in running buffer were injected at flow rates of 1, 2, 4, 8, 16 and 32  $\mu\text{L/min}$  resulting in contact times of 20, 10, 5, 2.5, 1.25 and 0.625 min, respectively. The chip surface was regenerated by two injections of 10  $\mu\text{L}$  25 mM phosphate buffer pH 7.4.

*Competition titration experiments with polymeric inhibitors.* Samples with 15  $\mu\text{g/mL}$  Ast6139 VLPs were preincubated with increasing concentrations of polymeric inhibitor in running buffer for 2 h at room temperature. 20  $\mu\text{L}$  of each sample were injected at a flow rate of 5  $\mu\text{L/min}$  and the response in the steady state was monitored. Titration curves were fitted to equation 11 using Origin 7.0 (Microcal) in analogy to equation 5 for competitive STD titrations:

$$RU(c) = RU_{min} + \frac{RU_{max} - RU_{min}}{1 + \left(\frac{IC_{50}}{c}\right)^{Hill}} \quad (11)$$

With  $c$  being the inhibitor concentration,  $RU_{max}$  and  $RU_{min}$  being the response in absence and high excess of inhibitor, respectively,  $IC_{50}$  being the half maximum inhibitory concentration of the inhibitor and  $Hill$  being the Hill slope of the inhibition curve reporting on cooperativity (Fersht, 1999).

#### *Competitive Assay using BSA Sugar Conjugates*

*Stock solutions.* 10 mM sodium acetate buffer pH 5.0 or 25 mM phosphate buffer pH 6.2 were used as running buffers. 25 mM sodium phosphate buffer pH 7.6 was used for regeneration of the chip surface. All buffers contained 154 mM sodium chloride and 0.01% sodium azide. BSA sugar conjugates were dissolved in NMR buffer (23 mM deuterated phosphate buffer pH 7.0, 154 mM sodium chloride) at concentrations of 6 to 7 mg/mL corresponding to 90  $\mu\text{M}$  BSA and approximately 1 mM carbohydrates (depending on the average number of carbohydrates per BSA molecule). A stock solution of Ast6139 VLPs (3 mg/mL in PBS pH 7.2) was used for titration experiments. Carbohydrate stock solutions (200 to 500 mM) were dissolved in running buffer directly before the measurement.

*Immobilization of BSA sugar conjugates.* CM5 sensor chips (GE Healthcare) were primed with acetate buffer pH 5.0 as running buffer. The chip surface was prepared and activated using the Amine Coupling Kit (GE Healthcare) as described above. BSA sugar conjugates or BSA (reference flow cell) were diluted to concentrations of 60 to 70  $\mu\text{g/mL}$  in 10 mM sodium acetate buffer pH 4 without NaCl and injected. The resulting coverage for two CM5 chips was 10000 RU and 2400 RU BSA, respectively, on the reference flow cells and 240 to 4800 RU BSA-H type 2 on the first chip and 1500 RU BSA-H type 2, 1370 RU BSA-H type 6 and 3860 RU BSA-LacNAc on the second chip. The BSA conjugates were kind gifts from Ole Hindsgaul (Carlsberg Laboratory, Copenhagen) (BSA-H type 2 and BSA-LacNAc) and David R. Bundle (University of Alberta, Edmonton) (BSA-H type 6).

*Qualitative binding experiments.* VLPs were diluted to concentrations of 3.75 to 30  $\mu\text{g/mL}$  in running buffer and injected at flow rates from 2 to 32  $\mu\text{L/min}$ . For test of pH dependency 10  $\mu\text{L}$  of 15  $\mu\text{g/mL}$  VLPs in sodium acetate buffer pH 5.0 were injected (flow rate 5  $\mu\text{L/min}$ ) followed by injection of 10  $\mu\text{L}$  of different buffers: 10 mM sodium acetate buffer at pH 3.8, 4.2, 4.6, 5.0, 5.4 and 5.6; 25 mM sodium phosphate buffer at pH ranging from 5.8 to 7.2 (steps of 0.2 pH units). All buffers contained 154 mM sodium chloride and 0.01% sodium azide. The amount of bound VLPs after buffer injection was monitored. Remaining VLPs were removed by injection of 25 mM phosphate buffer pH 7.6.

*Competitive titration experiments.* In a sequential assay format constant amounts of VLPs (10  $\mu\text{L}$  of 15  $\mu\text{g/mL}$ ) were injected at a flow rate of 5  $\mu\text{L/min}$  with phosphate buffer pH 6.2 as running buffer. After 3 min 10  $\mu\text{L}$  of increasing concentrations of L-Fuc (**1**) were injected and the fraction of removed VLPs was monitored. In the direct competition assay VLPs (15  $\mu\text{g/mL}$ ) were mixed with L-Fuc or D-Gal (**16**) at concentrations from 490  $\mu\text{M}$  to 250 mM. 10  $\mu\text{L}$  of the mixtures were injected (flow rate 5 to 10  $\mu\text{L/min}$ ) and the amount of bound VLPs was monitored. The chip surface was regenerated by 10  $\mu\text{L}$  injections of phosphate buffer pH 7.6. The direct competition assay was performed in both running buffers (acetate buffer pH 5.0 and phosphate buffer pH 6.2).

### 3.5 Hemagglutination Assay

A 1.5 mg/mL Ast6139 VLP sample and a 5 mg/ml RHDV VLP sample, both in PBS pH 7.5, were used for hemagglutination assays with RBCs and polymeric inhibitors. Whole blood samples of blood group O donors were obtained from the blood donation service of the Hospital Universitario General Asturias in Oviedo, Spain. Blood samples were centrifuged at 750 g for 5 min. The supernatant containing the serum was removed from the fraction of red blood cells (RBCs) by decanting and washed with PBS. The procedure was repeated 3 times and the RBCs were stored at 4°C until use. A serial dilution of VLPs in PBS pH 7.2 was prepared in a 96 well plate at final volumes of 50  $\mu$ L and incubated for ½ h at 4°C. 50  $\mu$ L of 0.75% RBCs in PBS pH 7.2 were added to the VLP dilutions and incubated for 1 h at 4°C. The titer of hemagglutination (i.e. the reciprocal of the highest dilution of VLPs that still has the capacity to agglutinate RBCs) is determined by visual inspection.

For inhibition assays serial dilutions of polymers **34**, **35**, **36**, **37**, **38**, **39**, **40** and **41** were prepared in PBS pH 7.2 in 96 well plates at final volumes of 25  $\mu$ L. 25  $\mu$ L of VLPs at a concentration above the titer of hemagglutination were added resulting in final concentrations of the polymers from 250  $\mu$ M to 0.06 nM. Polymers and VLPs were incubated for ½ h at 4°C. Then 50  $\mu$ L of 0.75% RBCs in PBS pH 7.2 were added and incubated for 1 h at 4°C. The titer of inhibition of hemagglutination (i.e. the reciprocal of the highest concentration of inhibitor that still has the capacity to inhibit agglutination of RBCs by the VLPs) is visually determined.

### 3.6 Molecule Visualization

Solution conformations of HBGA fragments were produced with the help of the SWEET2 database (<http://www.glycosciences.de/modeling/sweet2/>). Stick and space-filling (CPK) models of carbohydrates in mono- or stereo-chemical view were produced with the program PyMOL (Schrödinger, <http://www.pymol.org/>) in the free version 0.98 (2005). Models of protein-ligand interactions with protein surface presentations were created with PyMOL or with Sybyl-X 1.2 (Tripos).

## 4 Results

### 4.1 Expression of Wildtype and Mutant Norovirus VLPs

For the *in vitro* characterization of NoV binding to HBGAs using different biophysical methods, non-infectious VLPs were expressed in insect cells with the help of baculovirus expression systems according to published protocols (Jiang *et al.*, 1992; Pengelley *et al.*, 2006; Zhao *et al.*, 2003). Samples of wildtype VLPs of the GII.4 NoV strain Ast6139/01/Sp (Ng *et al.*, 2004) have been obtained at concentrations of 3 and 8 mg/mL in PBS pH 7.2.

Recombinant baculoviruses of four mutants R345A, D374A, D391A and H395A were obtained by site-directed mutagenesis of the wildtype VP1 (cf. section 3.1.1). Since expression of sufficient amounts of VLPs requires laborious optimization procedures, samples of only two mutants were obtained and available for testing in this work: D391A (sample concentrations of 1.6 mg/mL) and H395A (1.1 mg/mL).









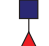
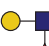















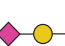


### 4.2 STD NMR Experiments with HBGA Fragments

#### 4.2.1 HBGA Binding Specificity from STD NMR

The binding of synthetic HBGA fragments to Ast6139 VLPs was investigated by STD NMR (Fiege *et al.*, 2012; Langpap, 2008). In general, STD effects can be observed for ligand-receptor complexes in the  $\mu\text{M}$  to  $\text{mM}$  range. Low or absent STD effects could in principle indicate strong binding with a very low  $k_{\text{off}}$ -rate (cf. section 3.3.2 in the Introduction). The interaction of HBGA fragments with VLPs is however expected to be rather weak in the  $\text{mM}$  or at best high  $\mu\text{M}$  range. STD titration of  $\alpha\text{-L-Fuc-(1,}O\text{)-CH}_3$  in presence of Ast6139 VLPs yielded a  $K_D$  in the low millimolar range (unpublished results, see section 7.6.1 in the appendix). Therefore it is safe to assume that absence of STD effects corresponds to missing or very weak (high  $\text{mM}$ ) binding.

STD experiments were measured for a broad range of ABH and Lewis-type antigens in presence of Ast6139 VLPs. They were classified into binders and non-binders according to presence and absence, respectively, of STD signals (Table 4.1). The HBGA binding profile determined in this way immediately reveals a strict requirement of an L-Fuc moiety for binding to Ast6139 VLPs. L-Fuc can be either  $\alpha(1,2)$ -linked (ABH antigens) or  $\alpha(1,3)/\alpha(1,4)$ -linked (Lewis antigens). STD spectra of a representative from each of the two groups (A trisaccharide and  $\text{sLe}^x$ ) are shown exemplarily in Figure 4.1.

Table 4.1. HBGA binding specificity of Ast6139 VLPs determined by STD NMR.

No.	Carbohydrate structure	Common name	Symbol <sup>[a]</sup>
<b>binding HBGA fragments</b>			
1, 2	L-Fuc, $\alpha$ -L-Fuc-(1, <i>O</i> )-CH <sub>3</sub>		
3a	$\alpha$ -L-Fuc-(1,2)- $\beta$ -D-Gal	H-disaccharide	
4	$\alpha$ -L-Fuc-(1,2)-[ $\alpha$ -D-GalNAc-(1,3)]- $\beta$ -D-Gal	A antigen trisaccharide	
5	$\alpha$ -L-Fuc-(1,2)-[ $\alpha$ -D-Gal-(1,3)]- $\beta$ -D-Gal	B antigen trisaccharide	
6	$\alpha$ -L-Fuc-(1,2)- $\beta$ -D-Gal-(1,3)- $\beta$ -D-GlcNAc	H antigen type 1	
7	$\alpha$ -L-Fuc-(1,2)- $\beta$ -D-Gal-(1,4)- $\beta$ -D-GlcNAc	H antigen type 2	
8	$\alpha$ -L-Fuc-(1,2)- $\beta$ -D-Gal-(1,4)-D-Glc	H antigen type 6	
9	$\alpha$ -L-Fuc-(1,3)- $\beta$ -D-GlcNAc-(1, <i>O</i> )-CH <sub>3</sub>		
10	$\beta$ -D-Gal-(1,4)-[ $\alpha$ -L-Fuc-(1,3)]- $\beta$ -D-GlcNAc	Le <sup>x</sup>	
11	$\beta$ -D-Gal-(1,3)-[ $\alpha$ -L-Fuc-(1,4)]- $\beta$ -D-GlcNAc	Le <sup>a</sup>	
12	$\alpha$ -L-Fuc-(1,2)- $\beta$ -D-Gal-(1,4)-[ $\alpha$ -L-Fuc-(1,3)]- $\beta$ -D-GlcNAc	Le <sup>y</sup>	
13	$\alpha$ -L-Fuc-(1,2)- $\beta$ -D-Gal-(1,3)-[ $\alpha$ -L-Fuc-(1,4)]- $\beta$ -D-GlcNAc	Le <sup>b</sup>	
14	$\alpha$ -D-Neu5Ac-(2,3)- $\beta$ -D-Gal-(1,4)-[ $\alpha$ -L-Fuc-(1,3)]- $\beta$ -D-GlcNAc	sLe <sup>x</sup>	
15	$\alpha$ -D-Neu5Ac-(2,3)- $\beta$ -D-Gal-(1,3)-[ $\alpha$ -L-Fuc-(1,4)]- $\beta$ -D-GlcNAc	sLe <sup>a</sup>	
<b>non-binding HBGA fragments</b>			
16	D-Gal		
17	D-GalNAc		
18	D-Glc		
19	D-GlcNAc		
20	D-ManNAc		
21	D-Fuc		
22	L-Gal		
23	$\beta$ -D-Gal-(1,3)-D-GlcNAc	type 1 precursor	
24	$\beta$ -D-Gal-(1,4)-D-GlcNAc	type 2 precursor	
25	$\beta$ -D-Gal-(1,3)-D-GalNAc	type 3 precursor	
26	$\beta$ -D-Gal-(1,4)- $\beta$ -D-Glc-(1, <i>O</i> )-CH <sub>3</sub>	type 6 precursor	
27	$\alpha$ -D-Neu5Ac-(2,3)- $\beta$ -D-Gal-(1,4)-D-Glc	3'-sialyllactose	
28	$\alpha$ -D-Neu5Ac-(2,6)- $\beta$ -D-Gal-(1,4)-D-Glc	6'-sialyllactose	
29	$\alpha$ -D-Gal-(1,3)- $\alpha$ -D-Gal-(1, <i>O</i> )-CH <sub>3</sub>	Galili epitope, xenoantigen	

[a] Symbols according to the CFG nomenclature (<http://www.functionalglycomics.org/>)

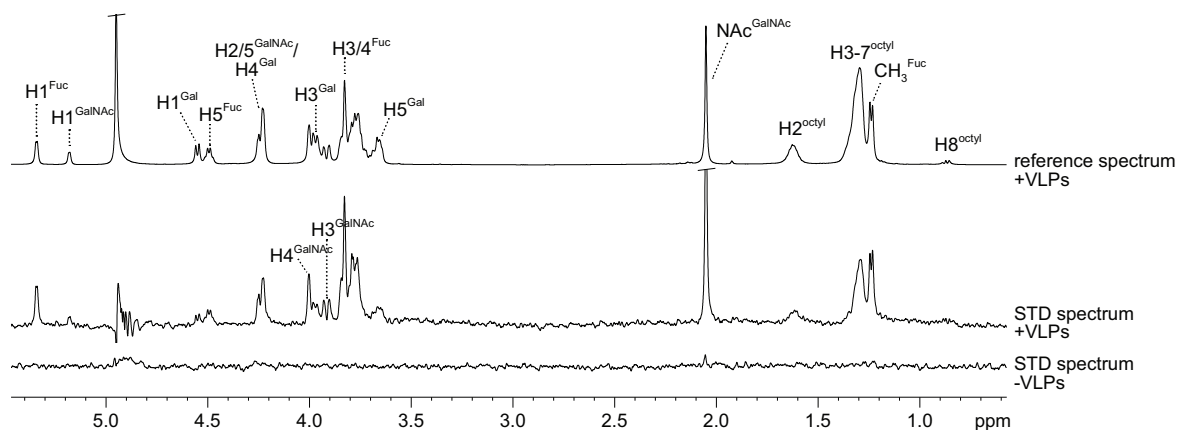
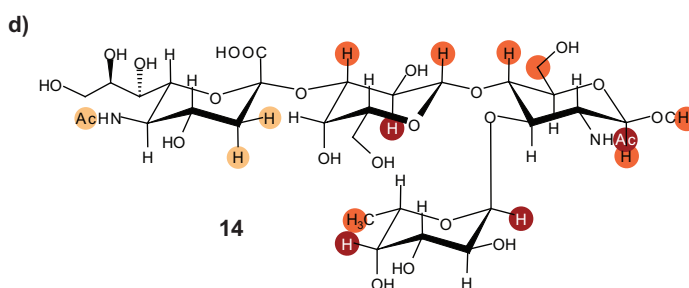
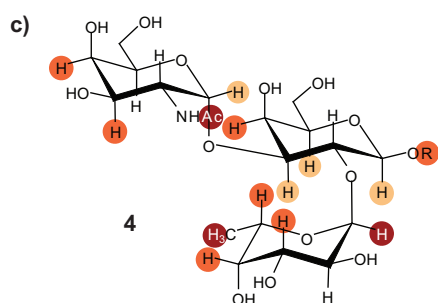
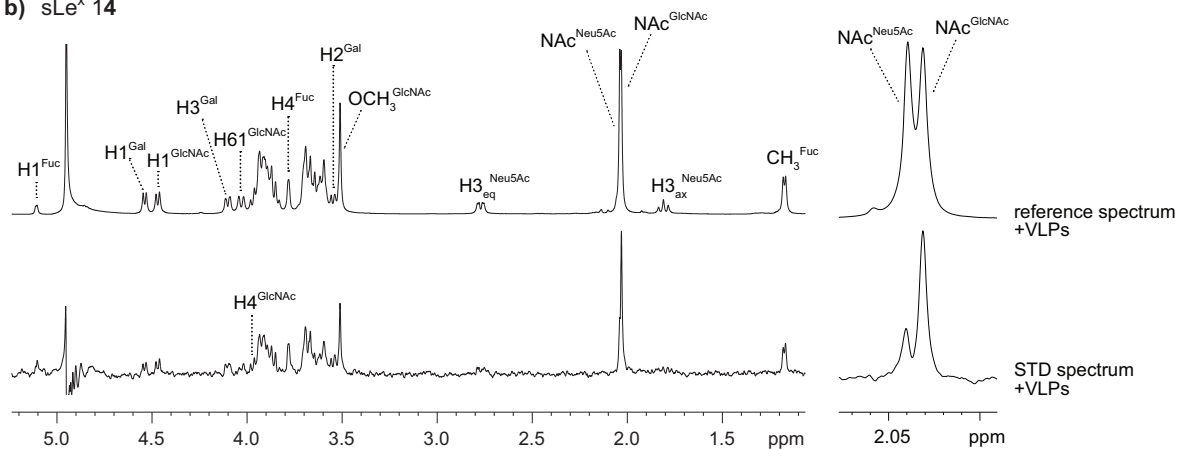
a) A trisaccharide **4**b) sLe<sup>x</sup> **14**

Figure 4.1. STD experiments and binding epitopes of A trisaccharide and sLe<sup>x</sup>. a) Reference and STD spectra of 0.5 mM A trisaccharide **4** (a) and sLe<sup>x</sup> **14** (b) in presence of 0.22 mg/mL VLPs; STD spectra were recorded at 500 MHz, 282 K and with a saturation time of 0.5 s. c),d) Binding epitopes obtained from whole STD build-up curves (**4**) or a single STD experiment at 0.5 s saturation time (**14**); Red, orange and pale yellow circles indicate strong (>80%), medium (40-80%) and weak (<40%) relative STD effects. Protons without a circle could not be analyzed due to spectral overlap.

The specificity for L-Fuc is very distinct as demonstrated by the absence of STD signals for L-Gal **22** that differs from L-Fuc only in the presence of a hydroxyl group at carbon 6. Binding of other monosaccharides (**16** to **21**) was neither observed under the limitations discussed above.

The smallest oligosaccharide furnishing  $\alpha$ 1,2-linked L-Fuc is H-disaccharide **3**. Trisaccharides with additional moieties on H3<sup>Gal</sup> (i.e. A and B antigens **4** and **5**) or on the reducing end (i.e. H antigens) were also bound. All three H antigen types 1, 2 and 6 (**6**, **7** and **8**) that differ in the kind of backbone linkage show STD signals. Removal of the L-Fuc moieties yielding the corresponding disaccharides type 1, 2 and 6 (**23**, **24** and **26**) abolished binding to Ast6139 VLPs indicated by the absence of STD effects.

Analogue to H-disaccharide, the smallest Lewis disaccharide **9** bound to VLPs. Extension to trisaccharides (Le<sup>x</sup> and Le<sup>a</sup>) and difucosylated (Le<sup>y</sup> and Le<sup>b</sup>) or sialylated tetrasaccharides (sLe<sup>x</sup> and sLe<sup>a</sup>) was tolerated. The non-fucosylated counterpart of sLe<sup>x</sup>, 3'-sialyllactose **27**, was not recognized.

#### 4.2.2 Binding Epitopes from Group Epitope Mapping

STD NMR experiments also furnished the binding epitopes of HBGAs in which the highest STD signal was set to 100% and all other signals were normalized accordingly (Mayer & Meyer, 2001). A comparison of the binding epitopes of all bound HBGA fragments reveals a strong saturation of all Fuc moieties (Figure 4.2). For the monosaccharidic L-Fuc saturation transfer to both monomers was observed. Since mutarotation of L-Gal is slow on the NMR time scale under the chosen conditions, both anomers must be recognized independently. This is further confirmed by observation of two distinct binding epitopes for the two anomers. H1, H2 and H3 of the  $\alpha$ -anomer received medium to high fractions of saturation transfer. In contrast no STD signal was observed for the  $\beta$ -anomeric proton. From stereochemical presentations of  $\alpha$ - and  $\beta$ -L-Fuc it should be possible that both anomers were bound in a similar overall orientation in the binding pocket allowing the  $\alpha$ -anomeric proton to be recognized while that of the  $\beta$ -anomer points away from the protein surface (Figure 4.3). The methyl group at position 6 of both anomers received only small fractions of saturation. Nevertheless this group plays a critical role for the specificity of Ast6139 VLPs. Addition of a hydroxyl group yielding L-Gal completely abolished binding (Figure 4.3). In co-crystal structures of the closely related GII.4 NoV strain VA387 with A and B trisaccharides the methyl group of Fuc faced a tyrosine residue, Y443 (Cao *et al.*, 2007) (Figure 4.4). This hydrophobic pocket could impose steric hindrance against the hydroxyl group of L-Gal without necessarily causing strong saturation of the methyl group of L-Fuc (considering that the on-resonance is set in the aliphatic region).



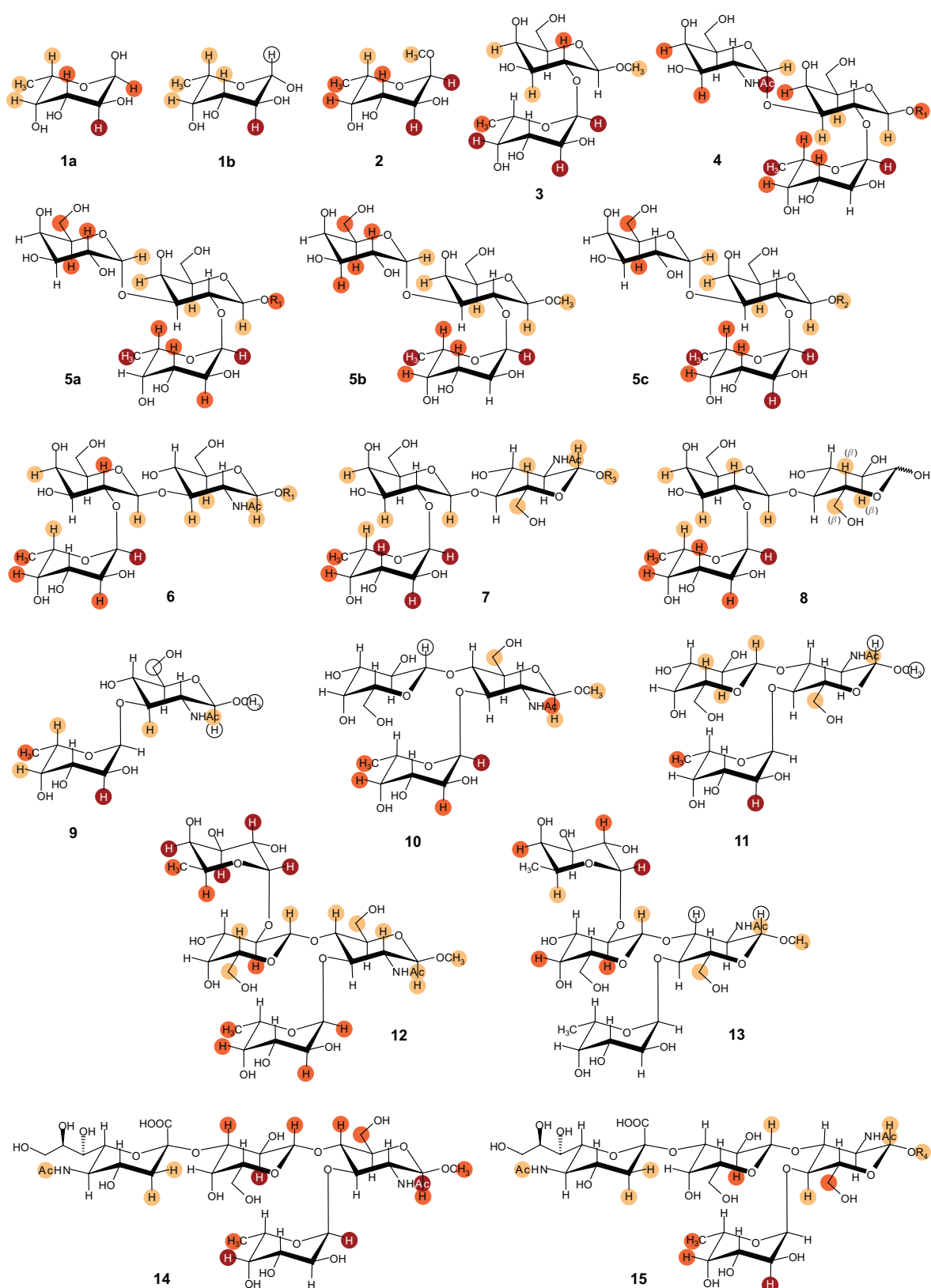


Figure 4.2. Binding epitopes of HBGAs in presence of Ast6139 VLPs. Red, orange, pale yellow and empty circles indicate strong, medium, weak and absent relative STD effects. Protons without a label could not be analyzed due to spectral overlap.  $R_1=(CH_2)_7CH_3$ ;  $R_2=(CH_2)_8COOC_2H_5$ ;  $R_3=(CH_2)_8COOCH_3$ ;  $R_4=(CH_2)_3NHCOOCH_2C_6H_5$ .

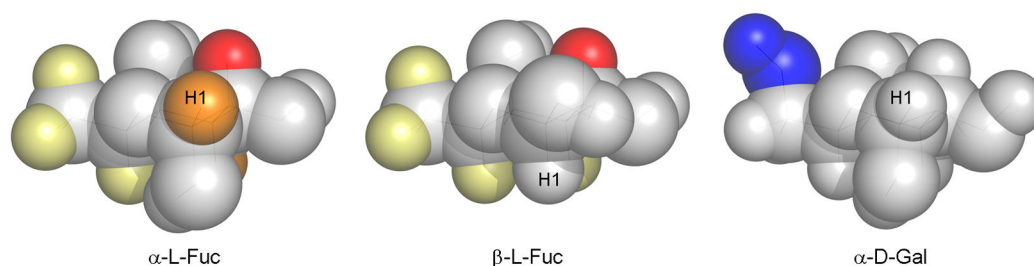


Figure 4.3. The stereochemistry of L-Fuc and L-Gal. CPK representations of  $\alpha$ -L-Fuc (left),  $\beta$ -L-Fuc (middle) and  $\alpha$ -L-Gal (right). Red, orange and pale yellow color indicates strong (>80%), medium (40-80%) and weak (<40%) relative STD effects in presence of Ast6139 VLPs. The  $\alpha$ - and  $\beta$ -anomeric protons of L-Fuc are labeled. The additional hydroxyl group at carbon 6 in L-Gal is colored in blue.

The crystal structures of VA387 with A and B trisaccharides (Cao *et al.*, 2007) is also in accordance with the observed high saturation transferred to the L-Fuc moieties of HBGAs in presence of Ast6139 VLPs. Beside the mentioned van der Waals contacts from Y443 a dense hydrogen bonding network to the Fuc was established by residues T344, R345, D374 and G442' ( ' indicates the second monomer) (Figure 4.4, Figure 1.7 in the Introduction). The  $\alpha$ -GalNAc and  $\alpha$ -Gal moieties of A and B trisaccharide, respectively, also received significant saturation transfer. In the aforementioned crystal structures both residues were predicted to make several water-mediated contacts with protein residues (Cao *et al.*, 2007). However, binding of H-disaccharide (lacking the  $\alpha$ -Gal/GalNAc) and non-binding of the xenoantigen **29** (lacking the Fuc) demonstrated that the  $\alpha$ -Gal residue is neither necessary nor sufficient for binding to Ast6139 VLPs.

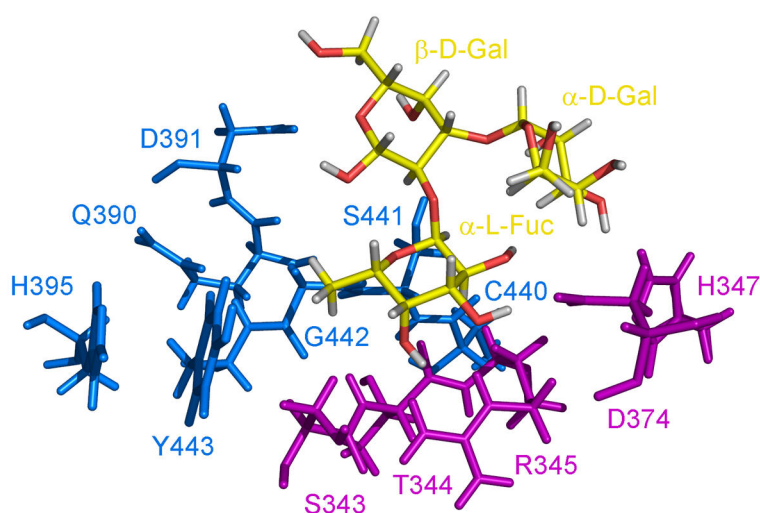


Figure 4.4. Binding pocket of GII.4 NoV capsids with B trisaccharide. Stick representation of residues at the P dimer interface with monomers colored in magenta and blue, respectively, from the co-crystal structure of NoV strain VA387 with B trisaccharide (pdb code: 2OBT) (Cao *et al.*, 2007). All depicted residues are conserved in Ast6139.

The binding epitopes of H trisaccharides type 1, 2 and 6 (**6**, **7** and **8**) displayed only weak saturation transfer to the backbone disaccharides suggesting a minor role for recognition (Figure 4.2). The overall binding epitopes were very similar.

Lewis antigens exhibit strong saturation transfer to L-Fuc and rather low STD effects for the other residues. Differences were observed for the *N*-acetyl groups of Lewis antigens with  $\alpha(1,3)$  and  $\alpha(1,4)$ -linked Fuc, respectively (Figure 4.5). Le<sup>x</sup> **10** and sLe<sup>x</sup> **14** displayed medium to strong saturation and Le<sup>a</sup> **11** and sLe<sup>a</sup> **15** only very weak saturation of the *N*-acetyl groups caused by opposite orientation relative to the binding pocket. When the Fuc residues are superimposed the *N*-acetyl group of Le<sup>x</sup> is oriented similar to that of A trisaccharide which received high fractions of saturation (compare Figure 4.5 c) and e)).

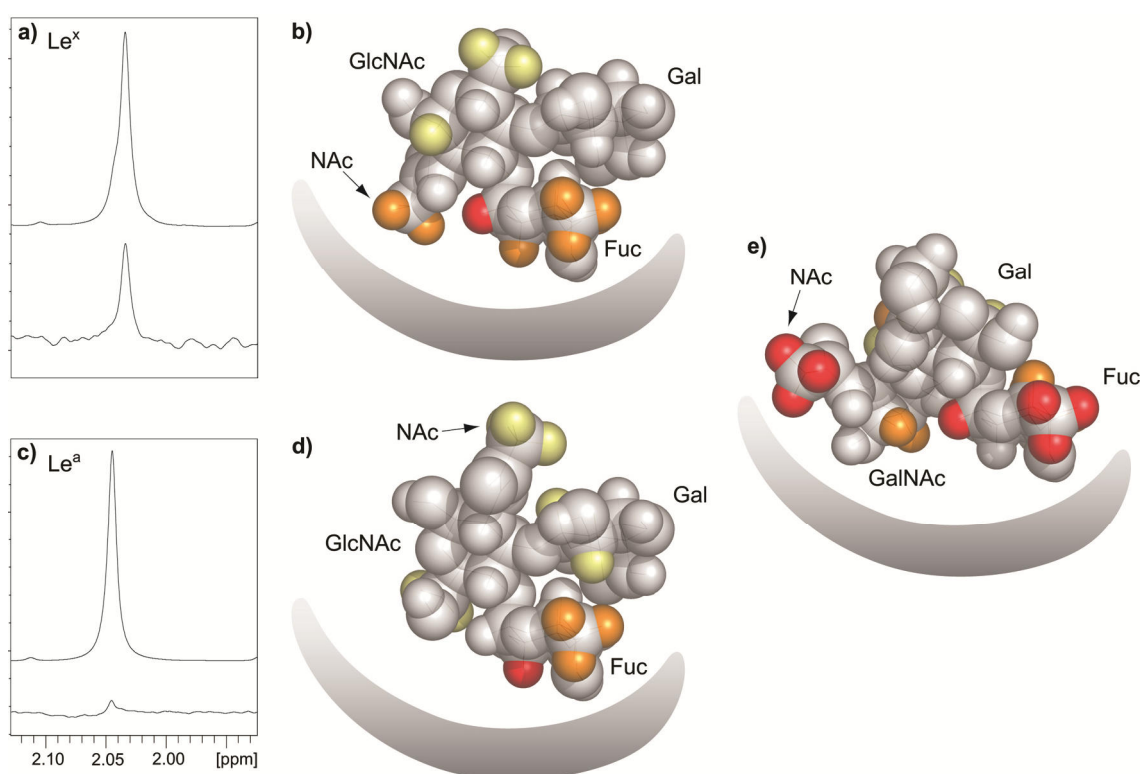


Figure 4.5. Differences in the STD effect of *N*-acetyl groups of Le<sup>x</sup> and Le<sup>a</sup>. a),b) Reference (top) and STD spectra (bottom, scaled to 2% of the reference) of Le<sup>x</sup> **10** (a) and Le<sup>a</sup> **11** (b) depicting the *N*-acetyl region. c)-e) CPK views of Le<sup>x</sup> (c), Le<sup>a</sup> (d) and A trisaccharide **4** (e); colors indicate strong (red), medium (orange) and weak (pale yellow) relative STD effects. The relative orientation of the protein is schematized in grey. Capping structures at the reducing ends were omitted for clarity.

In case of difucosylated Le<sup>y</sup> **12** both Fuc moieties received saturation transfer (Figure 4.2). The  $\alpha(1,3)$ -Fuc receives only ~70% of the saturation transferred to the  $\alpha(1,2)$ -Fuc. It can be hypothesized that the observed binding epitope represents a weighted average of two distinct binding epitopes with each of them resembling the binding mode of the

trisaccharide components  $\text{Le}^x$  and H type 2. In the major solution conformation of  $\text{Le}^y$  both Fuc moieties are oriented towards the same interface (Figure 4.6) in principle allowing saturation of both fucoses from a single binding mode. In case of  $\text{Le}^b$  **13** STD signals for  $\alpha(1,4)$ -Fuc could not be evaluated unambiguously due to spectral overlap.

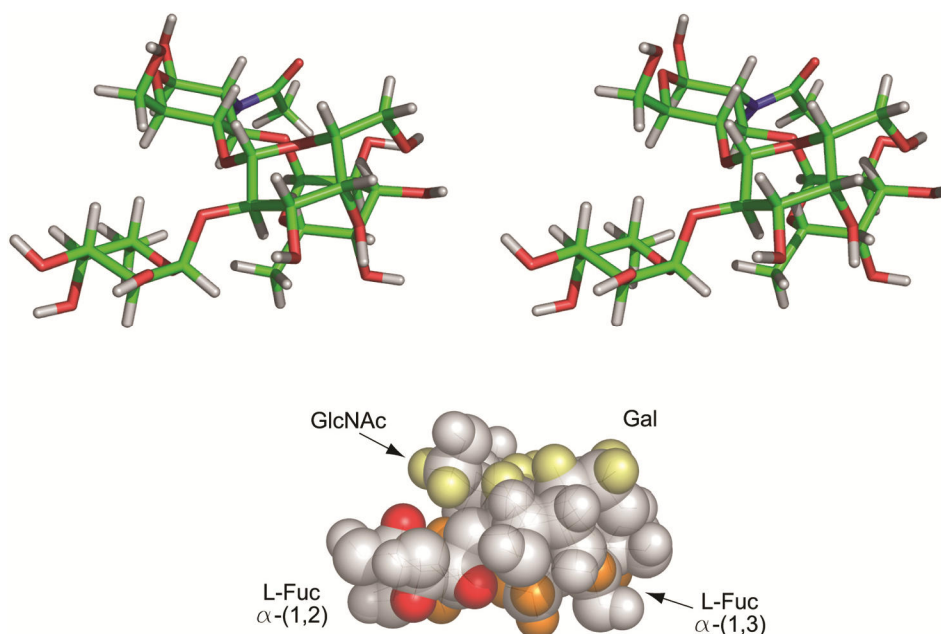


Figure 4.6. Structure and binding epitope of  $\text{Le}^y$ . (Top) crossed-eye stereo view in stick representation. (Bottom) CPK representation with colors indicating strong (red), medium (orange) and weak (pale yellow) STD effects of  $\text{Le}^y$  **12**.

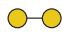
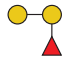




STD binding epitopes of tetrasaccharides  $\text{sLe}^x$  **14** and  $\text{sLe}^a$  **15** displayed significant saturation transfer to the  $\text{Le}^x$  and  $\text{Le}^a$  core trisaccharides. In contrast, signals of the neuraminic acid residues ( $\text{H3}_{\text{eq/ax}}$ , NAc) were only weakly saturated and therefore not in close contact to saturated protein protons. The other resonances of this residue could not be analyzed due to spectral overlap and may potentially receive stronger saturation. The absence of STD signals for 3'-sialyllactose and the recognition of  $\text{Le}^x$  and  $\text{Le}^a$  with similar binding epitopes however suggest a minor role of the neuraminic acid. A more detailed analysis of  $\text{sLe}^x$  recognition by Ast6139 VLPs will employ transferred NOESY experiments in presence of Ast6139 VLPs (sections 4.3) as well as computational studies (section 4.4).

As sidenote, some of the tested carbohydrates carry a hydrophobic spacer for purification (residues  $\text{R}_1$  to  $\text{R}_4$  in Figure 4.2). Comparison of the binding epitopes of B trisaccharide with (**5a** and **5c**) or without (**5b**) spacer shows only minor differences that are within the error of measurement. The influence of the hydrophobic spacer on the binding epitope of HBGAs is therefore regarded to be negligible.

### 4.2.3 Comparative STD NMR studies of Bovine NoV

Knowledge on the structural basis of attachment factor binding is very limited for animal caliciviruses. STD NMR offers the possibility to study attachment factor binding to VLPs at atomic resolution even if structural details on the binding site are unknown, e.g. in case of the rabbit calicivirus RHDV (Rademacher *et al.*, 2008). In cases of similar attachment factor specificities of different viruses it allows to judge on the possibility of interspecies transmission. In the course of this work, VLPs of bovine norovirus Bo/Newbury2/1976/UK (NB2) from genogroup III were subjected to STD experiments. Previous studies with tissue samples, knock-out animals and ELISA assays conducted by the groups of Jacques Le Pendu (Nantes, France) and Didier Poncet (Gif sur Yvette, France) indicated that binding of NB2 VLPs depends on the presence of the Galili epitope Gal- $\alpha$ (1,3)-Gal- $\beta$ (1,4)-GlcNAc (Zakhour *et al.*, 2009). This epitope is present in all mammalian species except in humans, gorillas and chimpanzee due to inactivation of the  $\alpha$ 1,3-galactosyltransferase enzyme. It is therefore also referred to as xenoantigen. STD experiments with NB2 VLPs elucidated its HBGA binding pattern (Table 4.2).

Table 4.2. HBGA specificity of bovine NoV NB2 determined by STD NMR.

No.	HBGA structure	Common name	Structure
<b>binding HBGA structures</b>			
<b>29</b>	$\alpha$ -D-Gal-(1,3)- $\alpha$ -D-Gal-(1, <i>O</i> )-CH <sub>3</sub>	Galili epitope, xenoantigen	
<b>non-binding HBGA structures</b>			
<b>5</b>	$\alpha$ -L-Fuc-(1,2)-[ $\alpha$ -D-Gal-(1,3)]- $\beta$ -D-Gal-(1, <i>O</i> )-R, R=(CH <sub>2</sub> ) <sub>7</sub> CH <sub>3</sub> ( <b>5a</b> ) or R=CH <sub>3</sub> ( <b>5b</b> )	B antigen trisaccharide	
<b>10</b>	$\beta$ -D-Gal-(1,4)-[ $\alpha$ -L-Fuc-(1,3)]- $\beta$ -D-GlcNAc-(1, <i>O</i> )-CH <sub>3</sub>	Lewis <sup>x</sup>	
<b>16</b>	D-Gal		
<b>23</b>	$\beta$ -D-Gal-(1,3)-D-GlcNAc	type 1 precursor	
<b>24</b>	$\beta$ -D-Gal-(1,4)-D-GlcNAc	type 2 precursor	

NB2 specifically bound to Gal- $\alpha$ (1,3)-Gal- $\alpha$ (1,*O*)-CH<sub>3</sub> but not to carbohydrates with terminal  $\beta$ -D-Gal moieties in 1,3- or 1,4-linkage neither to monosaccharidic D-Gal. Addition of L-Fuc to the Gal at the reducing end yielding B trisaccharide completely abolished the binding. Weak STD effects observed for the octyl protons of B trisaccharide **5a** likely represent unspecific binding since addition of an excess of **29** did not change the intensities of the respective STD signals (data not shown).

The disaccharide Gal- $\alpha$ (1,3)-Gal was therefore identified as minimal structural binding requirement. Group epitope mapping from STD build-up curves of **29** in presence of NB2 VLPs revealed pronounced saturation transfer to the protons around the glycosidic linkage (Figure 4.7). The presence of a Fuc residue in B antigen (Figure 4.7 c)) was not tolerated implicating steric hindrance from the binding pocket. Considering the absence of the xenoantigen in humans, zoonotic infection with bovine NoV NB2 therefore seems unlikely.

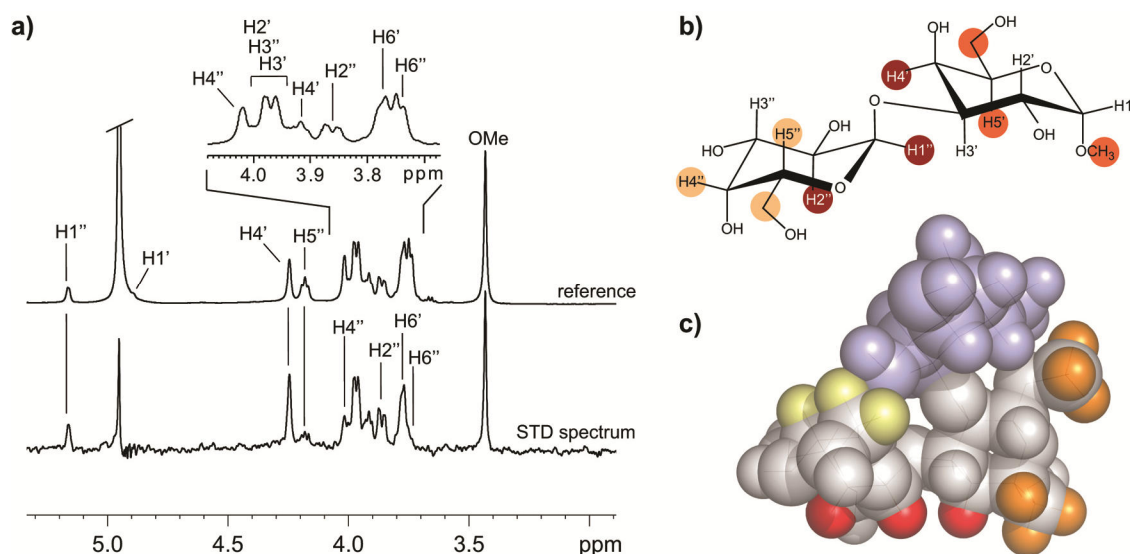


Figure 4.7. STD experiment of xenoantigen with NB2 VLPs. a) Reference (top) and STD spectrum (bottom, scaled to 8% of the reference) of **29** measured at 500 MHz, 282 K and a saturation time of 2 s. b) Binding epitope obtained from whole curve fitting of STD build-up curves (0.5 to 4 s saturation time) indicating strong (red), medium (orange) and weak (pale yellow) relative STD effects. c) CPK representation of B trisaccharide **5b** with the coloring indicating the binding epitope of **29** (cf. b)). Addition of  $\alpha$ (1,2)-L-Fuc colored in pale blue abolished the binding to NB2.

NB2 VLPs were also subjected to STD titration experiments with the xenoantigen **29** in order to determine the dissociation constant of the interaction. Titration of **29** from 510  $\mu$ M to 8 mM in 5 steps yielded binding curves that were fitted to a Langmuir isotherm (Figure 4.8). Depending on the data range included in the fitting,  $K_D$  values from ca. 2 to 8 mM were obtained (Table 4.3). Exclusion of the last data point (dotted lines in Figure 4.8) led to slight improvement of the fit especially for H1'' and provided lower  $K_D$  values (Table 4.3). However, the reliability of such data selection is questioned considering the low number of data points. Also taking into account the fact that the VLP concentration was not held constant during the titration, the  $K_D$  obtained from STD titration of xenoantigen **29** in presence of NB2 VLPs is considered to be only a very rough estimation of the affinity.



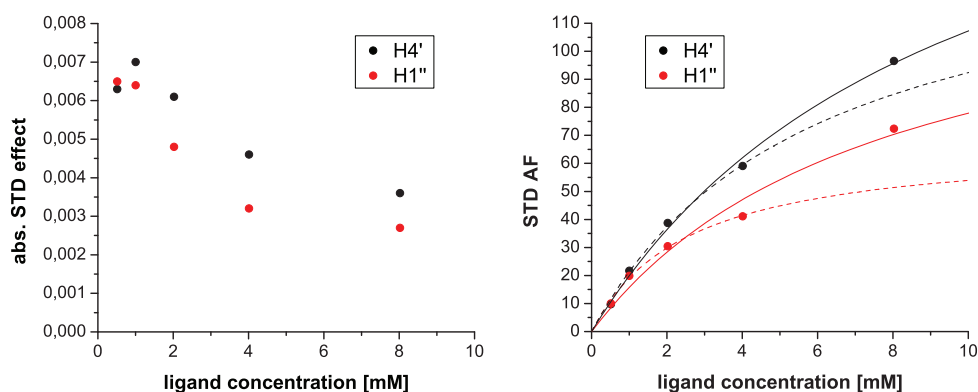


Figure 4.8. STD titration of xenoantigen in presence of NB2 VLPs. Plots of absolute STD effects (left) and STD amplification factors (right) versus **29** concentrations. Titration curves were fitted to a Langmuir isotherm (straight lines: all data points included; dotted lines: excluding the last data point) (cf. Table 4.3). The ligand excess instead of ligand concentration was used as independent variable (see Materials and Methods). For clarity, the figures show the STD effects as a function of **29** concentration.

Table 4.3. Results of STD titration of xenoantigen with NB2.

Proton	Range fitted	$K_D$	STD AF <sub>max</sub>	$R^2/\chi^2$
H4'	0 – 8 mM	<b>7.9 mM</b> ( $\pm 1.3$ mM)	190 ( $\pm 18$ )	0.9663/ 5.80
	0 – 4 mM	5.1 mM ( $\pm 1.0$ mM)	136 ( $\pm 18$ )	0.9966/ 2.38
H1''	0 – 8 mM	<b>6.7 mM</b> ( $\pm 2.6$ mM)	128 ( $\pm 28$ )	0.9725/ 21.17
	0 – 4 mM	2.4 mM ( $\pm 0.3$ mM)	65 ( $\pm 4$ )	0.9963/ 1.01

#### 4.2.4 STD NMR Experiments with Mutant NoV VLPs

Ast6139 VLP mutants D391A and H395A were subjected to STD NMR experiments with synthetic HBGA fragments to evaluate the role of the mutated amino acids on attachment factor binding. Both mutants bound to  $\alpha$ -L-Fuc-(1,*O*)-CH<sub>3</sub> **2** and B trisaccharide **5b** indicated by observation of STD signals. The binding epitopes were obtained from whole curve fitting of STD build-up curves (**5b**) or from single STD experiments (**2**) (Figure 4.9). Comparison with corresponding binding epitopes in presence of wildtype VLPs reveals only minor deviations. For instance, in the binding epitopes of B trisaccharide in presence of the mutants the relative STD effect of the methyl group of L-Fuc is reduced relative to the anomeric proton. Such a reduction may change the normalization of the STD effects of the other protons and could explain the slightly increase in saturation transfer to the  $\alpha$ -Gal residues in presence of mutant VLPs. In particular, relative STD effects of H5 and H6 of  $\alpha$ -Gal deviate by more than 20% in for wildtype and mutant H395A.

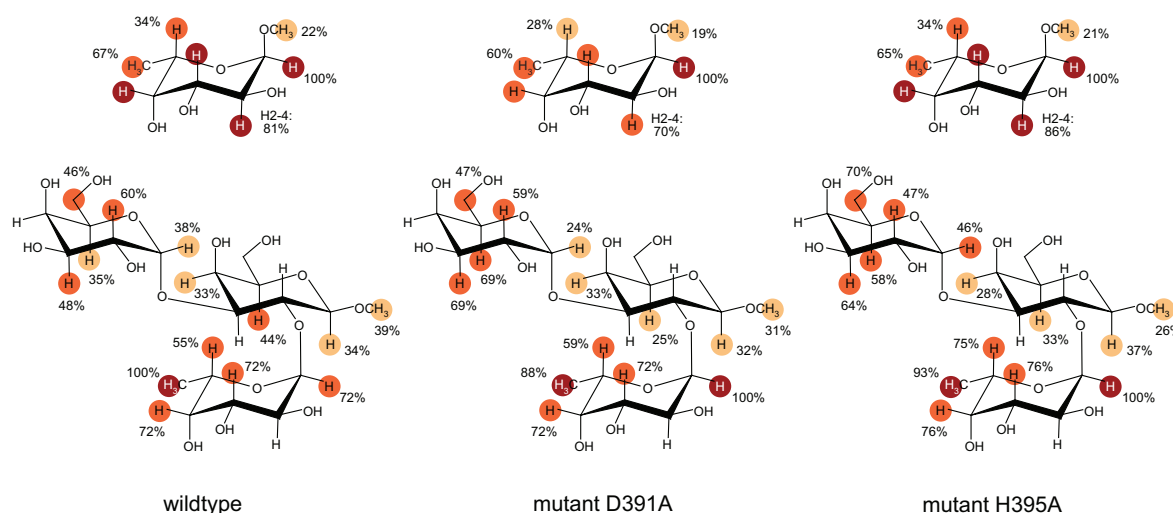


Figure 4.9. Binding epitopes for wildtype and mutant Ast6139 VLPs. Epitopes of  $\alpha$ -L-Fuc-(1,*O*)-CH<sub>3</sub> **2** (top panel) and B trisaccharide *O*-methyl glycoside **5b** were obtained from single STD experiments with a saturation time of 0.5 s (**2**) or from whole STD build-up curves (**5b**).

Most of the deviations in the binding epitopes may be explained by the inherent measurement error (typically ~10%). Major changes in the binding site geometry are therefore excluded. Minor changes may not be detected by STD NMR, but could nevertheless have impact on the binding affinity.



### 4.3 TrNOESY Experiments of sLe<sup>x</sup>

In contrast to other HBGAs that are relatively rigid (Imberty *et al.*, 1995; Lemieux *et al.*, 1980), the tetrasaccharide sLe<sup>x</sup> is characterized by a distinct flexibility around the  $\alpha(2,3)$ -glycosidic linkage (Haselhorst *et al.*, 2001; Poppe *et al.*, 1997). Therefore, trNOESY NMR experiments of sLe<sup>x</sup> in presence of Ast6139 VLPs are conducted to identify the bioactive conformation of sLe<sup>x</sup> and thereby gain insight on its recognition by VLPs.

To facilitate presentation of results, an introduction to the known solution conformations of sLe<sup>x</sup> will be given. In accordance with the exoanomeric effect, two major conformational families of sLe<sup>x</sup> are present in solution called ‘aA’ and ‘bA’ (Haselhorst *et al.*, 2001) (see Table 4.4 for torsion angles and Figure 4.10 for stereo views). ‘A’ refers to the global minimum conformation of Le<sup>x</sup> in solution. It features a stacked orientation of Fuc and Gal giving rise to interglycosidic NOEs  $H1^{\text{Fuc}} - \text{NAc}^{\text{GlcNAc}}$ ,  $H5^{\text{Fuc}} - H2^{\text{Gal}}$  and  $H6^{\text{Fuc}} - H2^{\text{Gal}}$ . Two low populated Le<sup>x</sup> conformations termed ‘B’ and ‘D’ were predicted by Metropolis Monte Carlo (MMC) simulations (Peters *et al.*, 1993; Stuike-Prill & Meyer, 1990). They display slightly distorted orientation of Fuc and Gal causing an interglycosidic NOE  $H1^{\text{Fuc}} - H2^{\text{Gal}}$  and the disappearance of NOE  $H5^{\text{Fuc}} - H2^{\text{Gal}}$ . ‘B’ and ‘D’ were shown to be recognized by *Aleuria aurantia* agglutinin and isolectin A from *Lotus tetragonolobus*, respectively (Haselhorst *et al.*, 2001).

‘a’ and ‘b’ describe the highest populated orientations along the  $\alpha(2,3)$ -glycosidic linkage. ‘a’ is characterized by the NOE  $H3^{\text{Gal}} - H8^{\text{Neu5Ac}}$  and a large distance ( $>4 \text{ \AA}$ ) between  $H3_{\text{eq}}^{\text{Neu5Ac}}/H3_{\text{ax}}^{\text{Neu5Ac}}$  and  $H3^{\text{Gal}}$ . In conformation ‘b’ the Neu5Ac residue is rotated in such a way that  $H3_{\text{eq}}$  and  $H3_{\text{ax}}$  of Neu5Ac come in close contact with  $H3^{\text{Gal}}$  giving rise to NOEs, whereas the distance  $H8^{\text{Neu5Ac}} - H3^{\text{Gal}}$  becomes large. MMC simulations predicted that conformation ‘a’ is favored over ‘b’ so that ‘aA’ is the major conformation in solution (Haselhorst *et al.*, 2001). Several studies demonstrated that ‘aA’ is recognized by E-selectin (Harris *et al.*, 1999; Poppe *et al.*, 1997; Scheffler *et al.*, 1997; Scheffler *et al.*, 1995).

Table 4.4. Major solution conformational families of sLe<sup>x</sup>. Dihedral angles predicted by MMC simulations (Haselhorst *et al.*, 2001) follow the NMR definition of  $\phi$  ( $H_1-C_1-O_1-C'_x$ ) and  $\psi$  ( $C_1-O_1-C'_x-H'_x$ ).

Conformation	Neu5Ac- $\alpha(2,3)$ -Gal $\phi/\psi$	Gal- $\beta(1,4)$ -GlcNAc $\phi/\psi$	Fuc- $\alpha(1,3)$ -GlcNAc $\phi/\psi$	relative energy (kcal/mol)
‘aA’	–68/ –3	49/ 12	51/ 23	0.0
‘bA’	–171/ –8	52/ 10	50/ 24	1.3

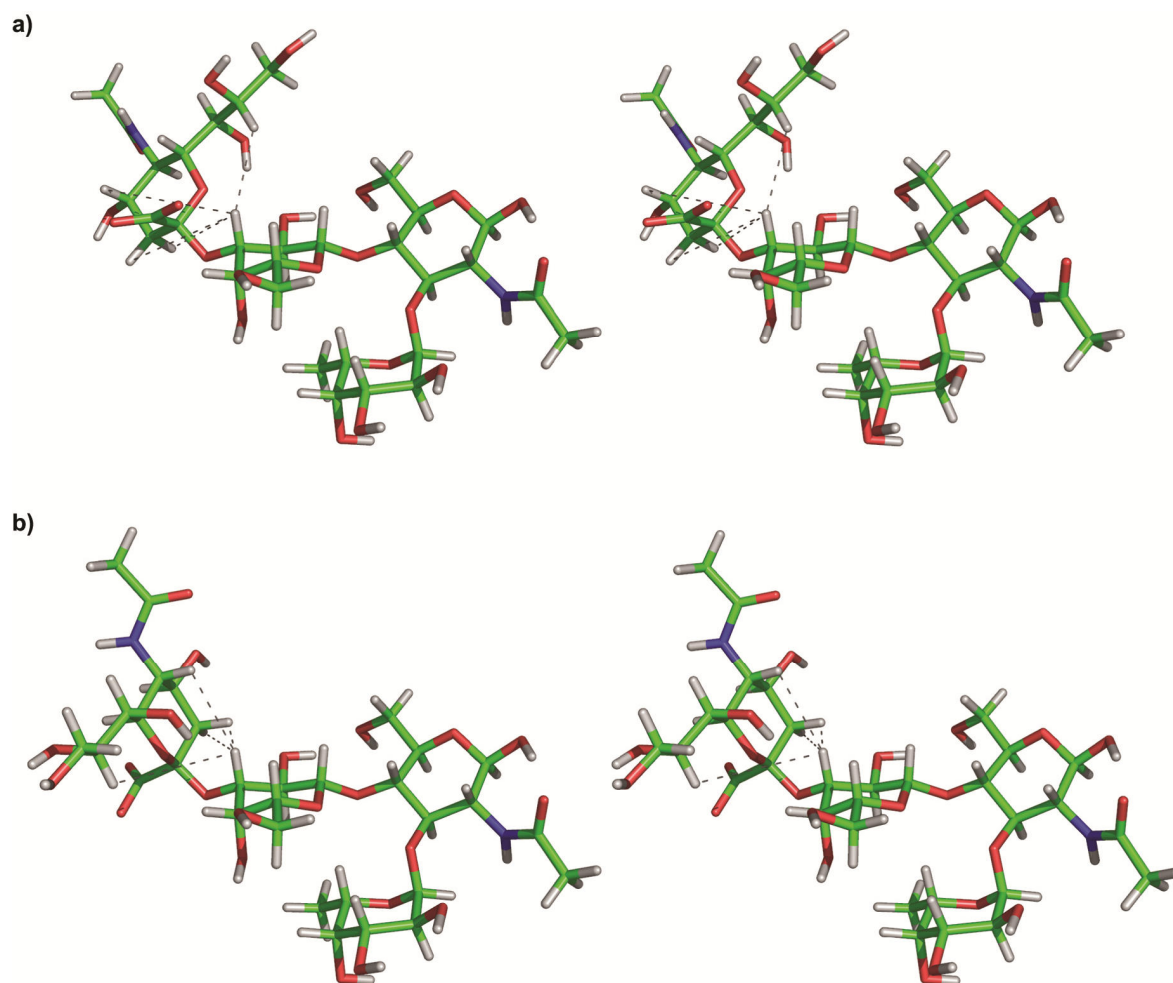
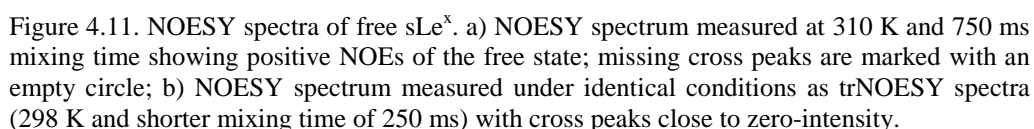


Figure 4.10. Stereochemical presentation of  $sLe^x$  major solution conformations. Crossed-eye stereo views of conformation 'aA' (a) and 'bA' (b) (cf. Table 4.4). Informative interglycosidic distances ('aA'/'bA') are  $H3_{eq}^{Neu5Ac} - H3^{Gal}$  (4.37 Å/ 3.19 Å),  $H3_{ax}^{Neu5Ac} - H3^{Gal}$  (4.09 Å/ 1.73 Å),  $H5^{Neu5Ac} - H3^{Gal}$  (4.93 Å/ 2.93 Å) and  $H8^{Neu5Ac} - H3^{Gal}$  (2.93 Å/ 4.43 Å).

Analysis of trNOESY spectra can be disturbed by the presence of NOEs of the free ligand. Therefore, NOESY spectra of  $sLe^x$  were acquired in absence of VLPs at different temperatures to find the condition of zero NOE that is a function of the correlation time (varies with temperature) and the magnetic field (fixed at 500 MHz) (cf. section 1.11.1 in the Introduction). At 310 K positive NOEs were observed that reflect the weighted average of conformations in solution at this temperature (Figure 4.11 a)). NOE cross peak  $CH_3^{Fuc} - H2^{Gal}$  reported on conformation 'A' of the  $Le^x$  part. The other two characteristic cross peaks  $H1^{Fuc} - NAc^{GlcNAc}$  and  $H5^{Fuc} - H2^{Gal}$  could not be observed at the conditions chosen. A weak NOE cross peak  $H3_{ax}^{Neu5Ac} - H3^{Gal}$  indicated conformation 'b' of the neuraminic acid residue. At 298 K NOE cross peaks of free  $sLe^x$  were close to the "zero-crossing" (Figure 4.11 b)). This temperature was chosen for trNOESY experiments to allow undisturbed analysis of cross peaks.



TrNOESY spectra of sLe<sup>x</sup> **14** recorded at 298 K in the presence of Ast6139 VLPs displayed a large set of negative cross peaks at short mixing times (Figure 4.12). The observation of interglycosidic trNOEs H1<sup>Fuc</sup> – NAc<sup>GlcNAc</sup>, H5<sup>Fuc</sup> – H2<sup>Gal</sup> and H6<sup>Fuc</sup> – H2<sup>Gal</sup> and the absence of cross peak H1<sup>Fuc</sup> – H2<sup>Gal</sup> unambiguously reflected the presence of Le<sup>x</sup> conformation ‘A’ that is the predominant conformation in solution. TrNOE cross peaks H3<sub>eq</sub><sup>Neu5Ac</sup> – H3<sup>Gal</sup>, H3<sub>ax</sub><sup>Neu5Ac</sup> – H3<sup>Gal</sup> and H5<sup>Neu5Ac</sup> – H3<sup>Gal</sup> along the α(2,3) glycosidic linkage indicated short distances between these proton pairs and are associated with conformation ‘bA’ (red squares in Figure 4.12). To evaluate the possibility of spin-diffusion on the observed trNOEs, a trROESY spectrum of sLe<sup>x</sup> in presence of VLPs was measured (see Figure 7.6 in the appendix). ROESY experiments show transient ‘rotating frame NOE’ effects that are always positive and eliminate spin diffusion effects (Claridge, 2000). TrROE cross peak H3<sub>ax</sub><sup>Neu5Ac</sup> – H3<sup>Gal</sup> was clearly observed (green squares in Figure 7.6) indicating that this cross peak did not originate from spin diffusion but indeed reflects close proximity. The two cross peaks H3<sub>eq</sub><sup>Neu5Ac</sup> – H3<sup>Gal</sup> and H5<sup>Neu5Ac</sup> – H3<sup>Gal</sup> were not observed in the trROESY spectrum probably due to a low signal-to-noise ratio. The cross peak H8<sup>Neu5Ac</sup> – H3<sup>Gal</sup> characteristic for conformation ‘aA’ was also observed in trNOESY spectra (blue square in Figure 4.12), although it was weak and lies in a strongly overlapping region. To further analyze this region, 1D chemical shift selective filter (cssf) TOCSY and NOESY experiments were measured using the same NMR sample.

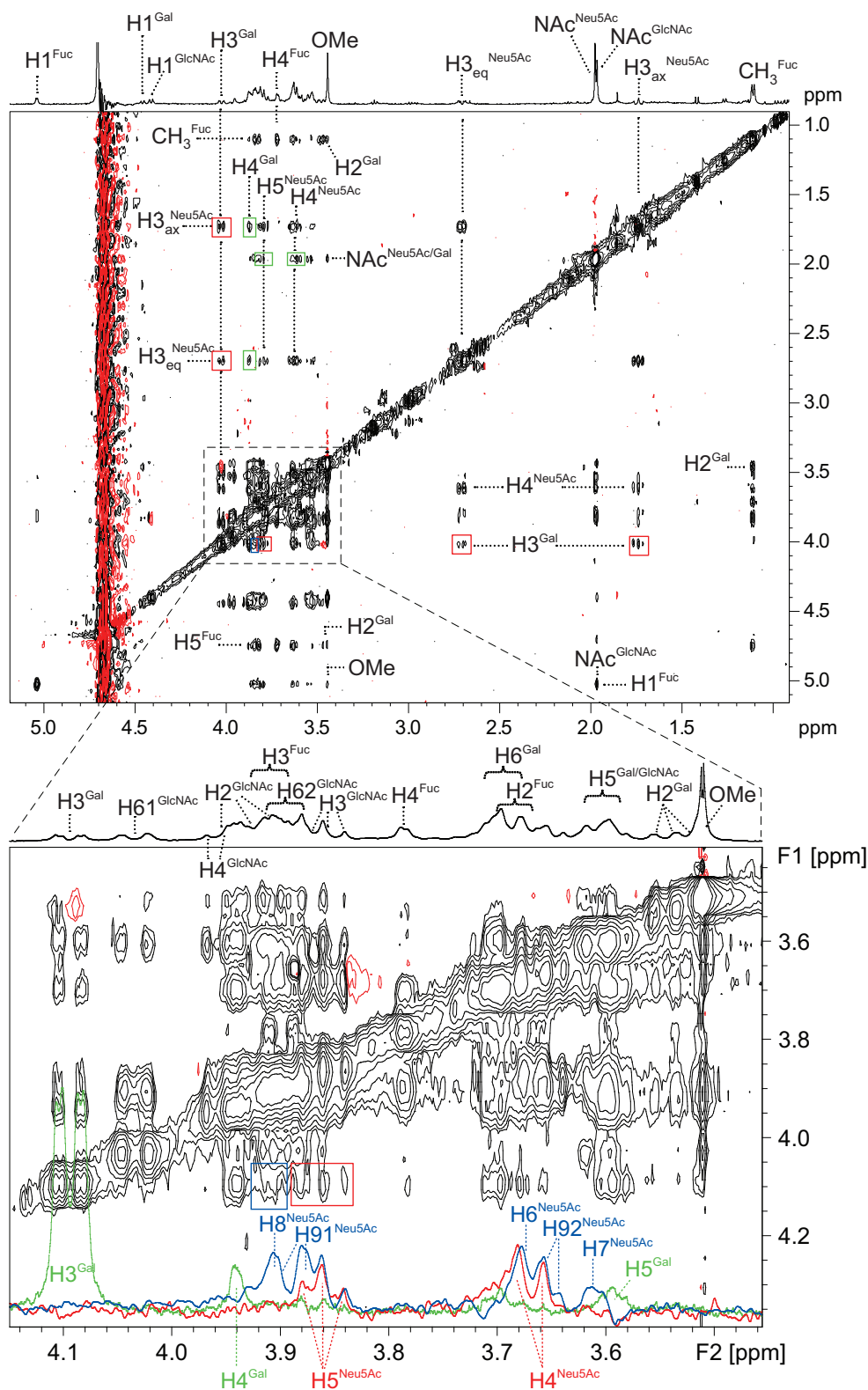


Figure 4.12. TrNOESY spectrum of sLe<sup>x</sup> in presence of Ast6139 VLPs. The spectrum was recorded at 500 MHz, 298 K and with a mixing time of 750 ms. Interglycosidic trNOEs reporting on conformations 'aA' and 'bA' are indicated by blue and red squares, respectively. Green squares mark potentially long-range trNOEs. The extension (bottom) shows the peak region of the ring protons as an overlap 1D cssf TOCSY spectra with irradiation of H3<sup>ax</sup><sup>Neu5Ac</sup> (red,  $\tau_m$ =200 ms) and H4/H6/H92<sup>Neu5Ac</sup> (blue,  $\tau_m$ =60 ms) and a 1D cssf NOESY spectrum with selective irradiation of H3<sup>Gal</sup> (green,  $\tau_m$ =250 ms).

1D cssf TOCSY spectra with selective irradiation of  $\text{H3}_{\text{ax}}^{\text{Neu5Ac}}$  or  $\text{H4/H6/H92}^{\text{Neu5Ac}}$  and a 1D cssf NOESY spectrum with selective irradiation of  $\text{H3}^{\text{Gal}}$  revealed the chemical shifts of Neu5Ac and Gal protons in this region (see extension of the trNOESY spectrum in Figure 4.12).  $\text{H8}^{\text{Neu5Ac}}$  did not directly overlap with  $\text{H4}^{\text{Gal}}$ ,  $\text{H91}^{\text{Neu5Ac}}$  or  $\text{H5}^{\text{Neu5Ac}}$ . Other ring protons in this region cannot give rise to the observed trNOE cross peak that was therefore supposed to be indeed  $\text{H8}^{\text{Neu5Ac}} - \text{H3}^{\text{Gal}}$ . However, in the 1D cssf NOESY spectrum with irradiation of  $\text{H3}^{\text{Gal}}$  corresponding trNOE enhancement of  $\text{H8}^{\text{Neu5Ac}}$  was not observed. The strong intensity of  $\text{H5/H3}_{\text{eq}}/\text{H3}_{\text{ax}}^{\text{Neu5Ac}} - \text{H3}^{\text{Gal}}$  cross peaks suggests that conformation ‘bA’ was significantly populated in the bound state. ‘aA’ may constitute a minor fraction of the bound population of  $\text{sLe}^x$  and the corresponding trNOE  $\text{H8}^{\text{Neu5Ac}} - \text{H3}^{\text{Gal}}$  may hence be too weak to be detected in 1D cssf NOESY experiments.

With respect to efficient cross relaxation due to the large molecular weight of VLPs, it cannot be excluded that weak trNOE cross peaks of  $\text{sLe}^x$  result from spin diffusion effects in the bound state. In support of this hypothesis some observed trNOE cross peaks potentially reflect long distances ( $>4 \text{ \AA}$ ) from both intra- and interglycosidic interactions (green squares in Figure 4.12). For instance, intraresidual trNOEs  $\text{H5} - \text{NAc}$  and  $\text{H4} - \text{NAc}$  of Neu5Ac correspond to distances of 4.4 to 5.5  $\text{\AA}$  (Figure 4.13 and Table 4.5). Analysis of the trNOE build-up curves revealed that they reached their maximum intensity at relatively long mixing times  $>600 \text{ ms}$ . This is an indication for indirect interactions and therefore likely reflects spin diffusion.

*Table 4.5. Analysis of selected  $\text{sLe}^x$  trNOE build-up curves. Interatomic distances are determined for the major solution conformations ‘aA’ and ‘bA’ (Haselhorst et al., 2001). TrNOESY mixing times  $\tau_m$  at which maximum cross peak intensity is reached are obtained from non-linear curve fitting (cf. Figure 4.13).*

TrNOE (F2 – F1)	Distance	$\tau_m(I_{\text{max}})$	Comments
$\text{H2}^{\text{Gal}} - \text{CH}_3^{\text{Fuc}}$	2.6 – 4.2 $\text{\AA}$	330 ms	reference cross peak, reports on conformation ‘A’
$\text{H3}_{\text{eq}}^{\text{Neu5Ac}} - \text{H4}^{\text{Neu5Ac}}$	2.51 $\text{\AA}$	340 ms	reference cross peak
$\text{H3}_{\text{eq}}^{\text{Neu5Ac}} - \text{H3}^{\text{Gal}}$	4.37 $\text{\AA}$ (‘aA’)/ 3.19 $\text{\AA}$ (‘bA’)	270 ms	reports on conformation ‘bA’
$\text{H3}^{\text{Gal}} - \text{H3}_{\text{ax}}^{\text{Neu5Ac}}$	4.09 $\text{\AA}$ (‘aA’)/ 1.73 $\text{\AA}$ (‘bA’)	220 ms	reports on conformation ‘bA’
$\text{H5}^{\text{Neu5Ac}} - \text{NAc}^{\text{Neu5Ac}}$	4.4 – 4.7 $\text{\AA}$	680 ms	spin diffusion
$\text{H4/H6/H92}^{\text{Neu5Ac}} - \text{NAc}^{\text{Neu5Ac}}$	4.4 – 5.5 $\text{\AA}$	630 ms	spin diffusion
$\text{H4}^{\text{Gal}} - \text{H3}_{\text{eq}}^{\text{Neu5Ac}}$	4.49 $\text{\AA}$ (‘aA’)/ 5.05 $\text{\AA}$ (‘bA’)	330 ms	very poor fit, spin diffusion?

In contrast, interglycosidic trNOEs  $\text{H3}_{\text{eq}}^{\text{Neu5Ac}} - \text{H3}^{\text{Gal}}$  and  $\text{H3}_{\text{ax}}^{\text{Neu5Ac}} - \text{H3}^{\text{Gal}}$  reached maximum trNOE intensity at mixing times between 200 and 300 ms in a similar range as

intraresidual reference cross peaks (Table 4.5). Both cross peaks are therefore regarded to be direct trNOEs and indeed reported on sLe<sup>x</sup> conformation ‘bA’.

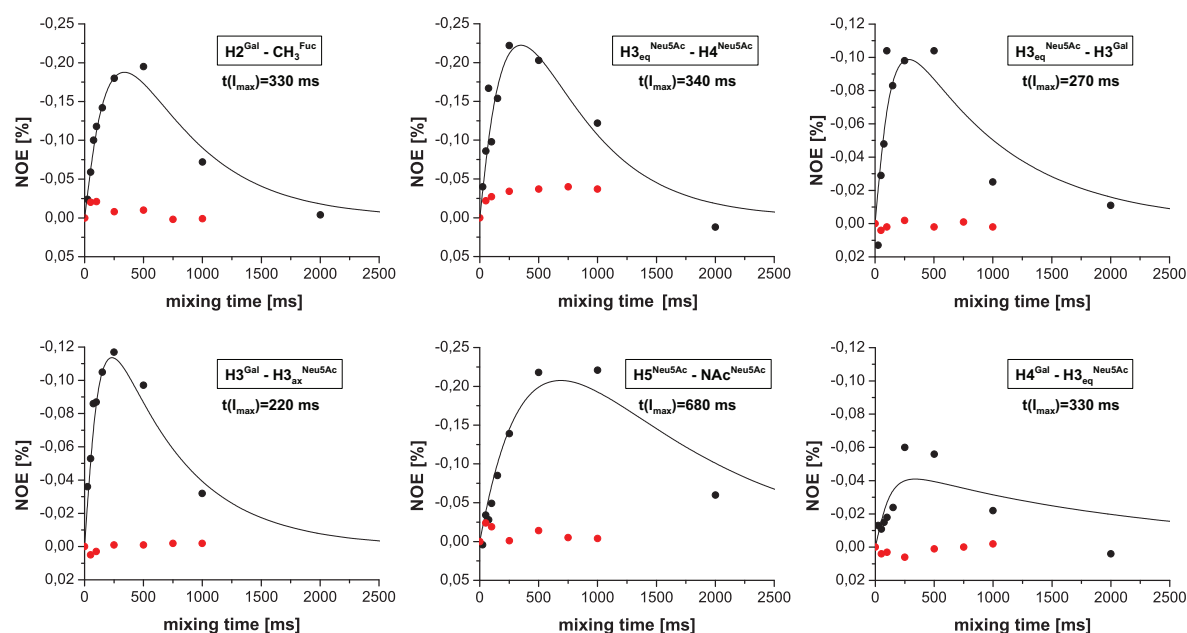


Figure 4.13. Build-up curves of selected sLe<sup>x</sup> trNOE cross peaks. Normalized cross peak intensities of NOESY experiments in presence of Ast6139 VLPs (trNOEs, black circles) and for free sLe<sup>x</sup> (NOEs, red circles) measured at 298 K. TrNOE build-up curves were fitted to a double-exponential equation (black lines); mixing times at maximum intensity are denoted.

In summary, trNOESY experiments of sLe<sup>x</sup> in the presence of Ast6139 VLPs furnished cross peaks of two distinct conformations ‘aA’ and ‘bA’ (Figure 4.14). Either the VLPs recognize different preformed conformations of sLe<sup>x</sup> or, alternatively, the neuraminic acid residue remains flexible in the bound form. Further insight on the mode of recognition was gained by molecular dynamics (MD) simulations as discussed in the next section.

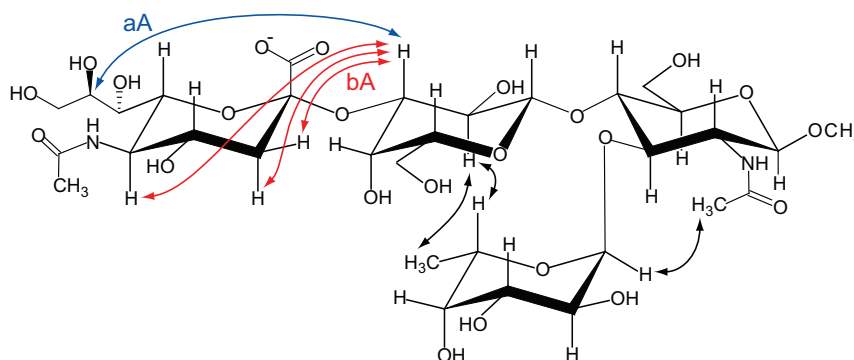


Figure 4.14. Schematic presentation of informative trNOEs of sLe<sup>x</sup>. Cross peaks along the  $\alpha(2,3)$  glycosidic linkage report on conformation ‘aA’ (blue arrows) and ‘bA’ (red arrows). Black arrows show cross peaks reporting on Le<sup>x</sup> conformation ‘A’.



#### 4.4 Docking Studies and MD Simulations of HBGAs

In order to obtain representative models of HBGA recognition by Ast6139 VLPs analyzed with STD NMR, molecular docking studies and in case of sLe<sup>x</sup> molecular dynamics (MD) simulations were carried out by Dr. Pavel Kitov and Jonathan Cartmell (University of Alberta, Edmonton) (Fiege *et al.*, 2012). Briefly, HBGA structures were generated applying Amber and Glycam parameters (<http://www.glycam.com>). Docking was performed using Autodock Vina (Trott & Olson, 2010). The crystal structure of the GII.4 strain VA387 in complex with B trisaccharide (pdb code 2obt) (Cao *et al.*, 2007) was chosen as model for docking, as this strain has 96% sequence identity with Ast6139 investigated in this work (see Figure 7.1 for sequence alignment). Only docking poses with reasonable torsion angles and with the Fuc moiety overlapping that of the crystal structure were considered. Representative docking poses of ABH and Lewis antigens are compiled in Figure 4.15.

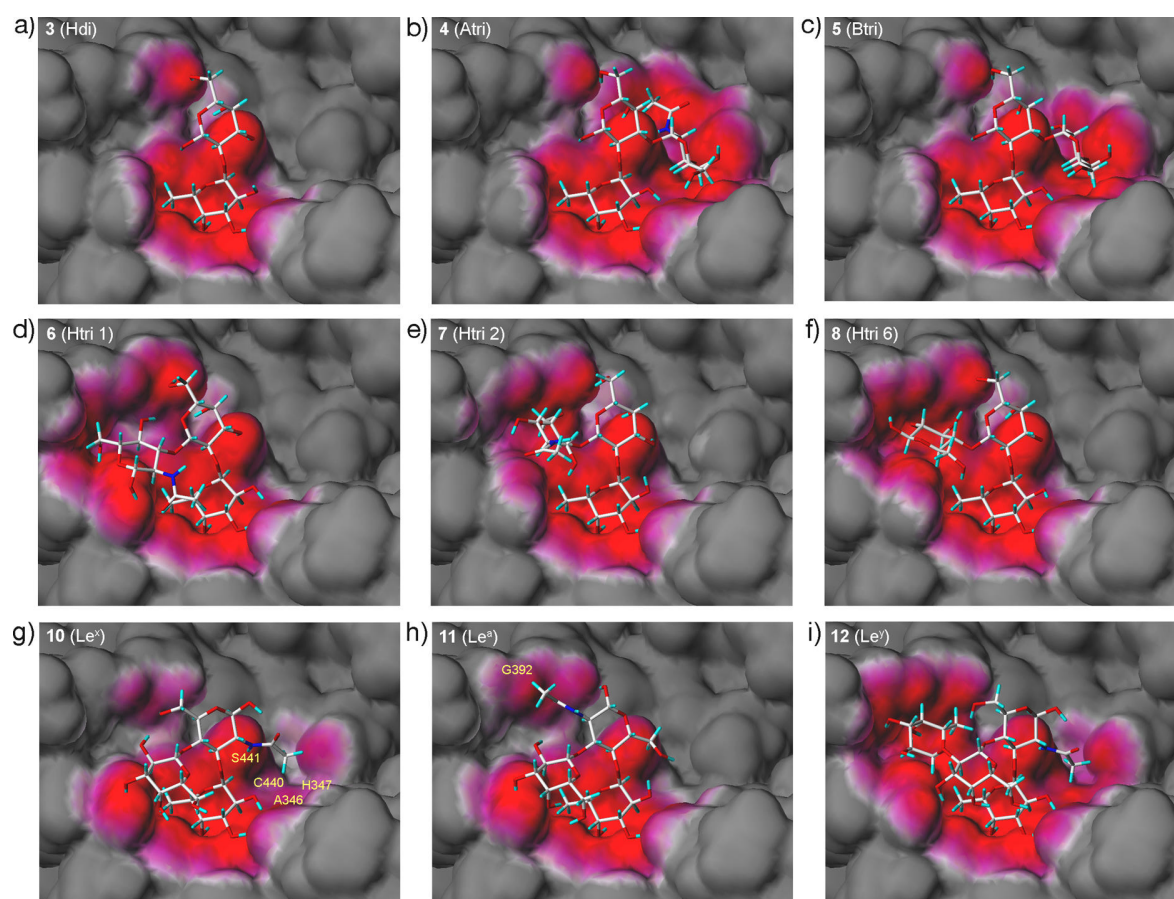


Figure 4.15. Docking poses of selected HBGA in the VA387 binding pocket. a) H-disaccharide; b) A trisaccharide; c) B trisaccharide; d) H trisaccharide type 1; e) H trisaccharide type 2; f) H trisaccharide type 6; g) Le<sup>x</sup>; h) Le<sup>a</sup>; i) Le<sup>y</sup>. In figures g) and h) residues potentially contacting to the *N*-acetyl groups of Le<sup>x</sup> and Le<sup>a</sup> are labeled. Structures were prepared with Sybyl-X 1.2 (Tripos).

In case of ABH trisaccharides the H-disaccharide core was well defined while the additional glycoside moieties were less defined (data not shown). Although results from docking studies have to be taken with care, this potentially reflects a weak recognition of the backbone moieties and is in accordance with the observed low saturation transferred to these residues.

Docking poses of Le<sup>x</sup> **10** and Le<sup>a</sup> **11** were analyzed with regard to STD NMR results that showed significant differences in the saturation transferred to the *N*-acetyl groups (cf. Figure 4.5). In the docking structure, the *N*-acetyl group of Le<sup>x</sup> pointed towards the binding pocket where it potentially could interact with and receive saturation from residues A346, H347, C440' and S441' (Figure 4.15 g)). In case of Le<sup>a</sup> the GlcNAc residue was oriented in such a way that the *N*-acetyl group pointed into the opposite direction and could make only one contact to G392' (Figure 4.15 h)). This is in excellent agreement with the STD binding epitopes.

Difucosylated Le<sup>y</sup> **12** was docked with the  $\alpha(1,3)$ -linked Fuc matching the Fuc in the crystal structure (Figure 4.15 i)). The second Fuc moiety came in close proximity to the protein surface. This pose could potentially lead to the observed STD effects for both Fuc moieties. Docking runs failed to produce valid poses of Le<sup>y</sup> with  $\alpha(1,2)$ -Fuc placed in the binding site. For Le<sup>b</sup> **13** no docking poses with correct torsion angles were produced. Building Le<sup>b</sup> from the docking model of Le<sup>a</sup> **11** resulted in severe clashes of the  $\alpha(1,2)$ -Fuc with the protein surface. However this might be due to missing minimization of the complex structure that would allow slight changes of protein side chains.

Docking poses obtained for sLe<sup>x</sup> **14** and sLe<sup>a</sup> **15** showed unusual  $\psi$  angles ( $\sim 180^\circ$  instead of  $20$  to  $40^\circ$  as predicted by GlyTorsion, <http://www.glycosciences.de/tools/glytorsion/>) along the glycosidic bond between Fuc and GlcNAc. Since the mode of sLe<sup>x</sup> binding to NoV VLPs is particularly interesting considering its flexibility, sLe<sup>x</sup> was subjected to MD simulations in order to obtain a reasonable binding model that explains the experimental STD and trNOESY NMR data (*vide supra*). The distribution of sLe<sup>x</sup> torsion angles during a 20 ns MD run with explicit water revealed sampling of multiple conformations both in the free form and bound to VA387 (Figure 4.16). In the free state sLe<sup>x</sup> most frequently adopted torsion angles corresponding to conformation 'aA' ( $\phi/\psi_{\text{Neu5Ac-Gal}} = -68^\circ/-3^\circ$ ). In the bound form the distribution of sampled conformations was shifted towards 'bA' ( $\phi/\psi_{\text{Neu5Ac-Gal}} = -171^\circ/-8^\circ$ ) (cf. Table 4.4). Bound sLe<sup>x</sup> also stayed in conformation 'bA' for a longer range of MD snap shots than free sLe<sup>x</sup> (Fiege *et al.*, 2012). Importantly, conformational switch between both conformations occurred during the MD run.



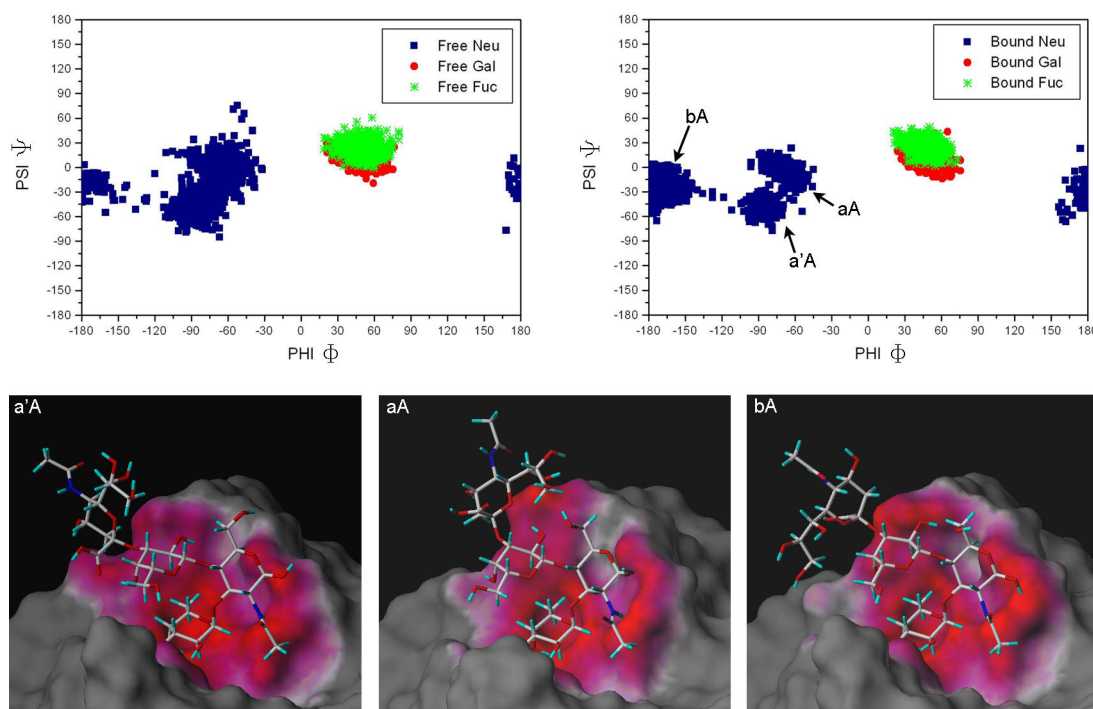


Figure 4.16. Bound conformations of sLe<sup>x</sup> from MD simulation. Top panel: scattered plots of a 20 ns MD simulation with explicit water showing torsion angles from individual snap shots (collection every 2 ps) for the free state (left) and bound to VA387 (right). Bottom panel: representative conformations of three major conformations of sLe<sup>x</sup> from MD simulations with the following torsion angles  $\phi(\text{H}_1\text{-C}_1\text{-O}_1\text{-C}'_x)$  and  $\psi(\text{C}_1\text{-O}_1\text{-C}'_x\text{-H}'_x)$  along the  $\alpha(2,3)$  linkage: a'A:  $\phi/\psi = -80^\circ/50^\circ$ ; aA:  $\phi/\psi = -55^\circ/-0^\circ$ ; bA:  $\phi/\psi = -167^\circ/-31^\circ$ . Conformations aA and bA most closely correspond to 'aA' and 'bA' reported previously (Haselhorst *et al.*, 2001).

To summarize, MD simulations of sLe<sup>x</sup> bound to VA387 suggested preferential recognition of sLe<sup>x</sup> in a conformation similar to 'bA'. In addition, flexibility of the neuraminic acid residue was implied from the interchange between conformations of this residue during the MD run. This provided a reasonable explanation and validation of STD and trNOESY data obtained for sLe<sup>x</sup> in presence of Ast6139 VLPs. Observation of only weak STD effects to Neu5Ac is in accordance with flexibility of this residue and a dominating conformation 'bA' that is rather far from the protein surface (Figure 4.16). Strong trNOEs observed for cross peaks reporting on conformation 'bA' and a weaker cross peak for 'aA' were nicely reproduced by a 20 ns MD run.

## 4.5 STD NMR Experiments with Inhibitors based on L-Fuc

### 4.5.1 Compounds with Fragments from NMR Screening

First lead compounds for the design of entry-inhibitors against Ast6139 VLPs were derived from an NMR screening of the Maybridge fragment library (Rademacher, 2008; Rademacher *et al.*, 2011) (see section 1.10). Competitive hits that bind to the HBGA binding sites as well as ‘adjacent site binders’ displaying inter-ligand NOEs to L-Fuc in the presence of VLPs were obtained. The competitive hit 160 was coupled to L-Fuc, the minimal structural requirement for binding to Ast6139 VLPs (*vide supra*). The STD binding epitope of this heterodivalent compound **31** is shown in Figure 4.17 e). Strong saturation transfer was observed to the fragment moiety as well as to the L-Fuc residue. The saturation transfer to the fragment moiety was relatively homogeneous as already observed for the fragment 160. Detailed analysis of STD data of Maybridge fragments revealed that their binding epitopes are correlated to the  $T_1$  relaxation of the protons (Rademacher, 2008; Yan *et al.*, 2003). The reason for this can be stronger binding and hence faster spin diffusion within the fragments in the bound form leading to loss of the binding epitope information. The intramolecular spin diffusion is facilitated by strongly coupled spin systems of the aromatic fragments. Only minor saturation transfer occurred to the triazole rings and the glycerol chain of the linker of **31** indicating that only the functional groups mediate the binding. The binding epitope of the divalent compound **30** presenting two L-Fuc moieties with the same linker arrangement as compound **31** is shown in Figure 4.17 g). Similar to **31** the linker received only very little saturation transfer and is hence unlikely to significantly contribute to the binding.

The heterodivalent compound **31** underwent decomposition in aqueous solution at neutral pH (Guiard *et al.*, 2011) (Figure 4.17). NMR spectroscopy and mass spectrometry identified the carbamate linkage between the fragment moiety and the triazole linker as the breaking point. Reaction products are fragment 160 and –after carbon dioxide loss– the amine of L-Fuc plus linker. Analysis of NMR spectra of a 0.5 mM sample of **31** in D<sub>2</sub>O revealed a half-life of 11 days. Compound **33** that lacks the L-Fuc and one of the triazole rings underwent decomposition with a half-life of only 4 day indicating that the L-Fuc is not involved in the reaction. Other carbamates that were tested for stability under the same conditions neither showed decomposition so that the instability of **31** must be a peculiarity

of the linkage to fragment 160 (Guiard *et al.*, 2011). The decomposition of **31** did not occur in the solid phase or in MeOH (data not shown).

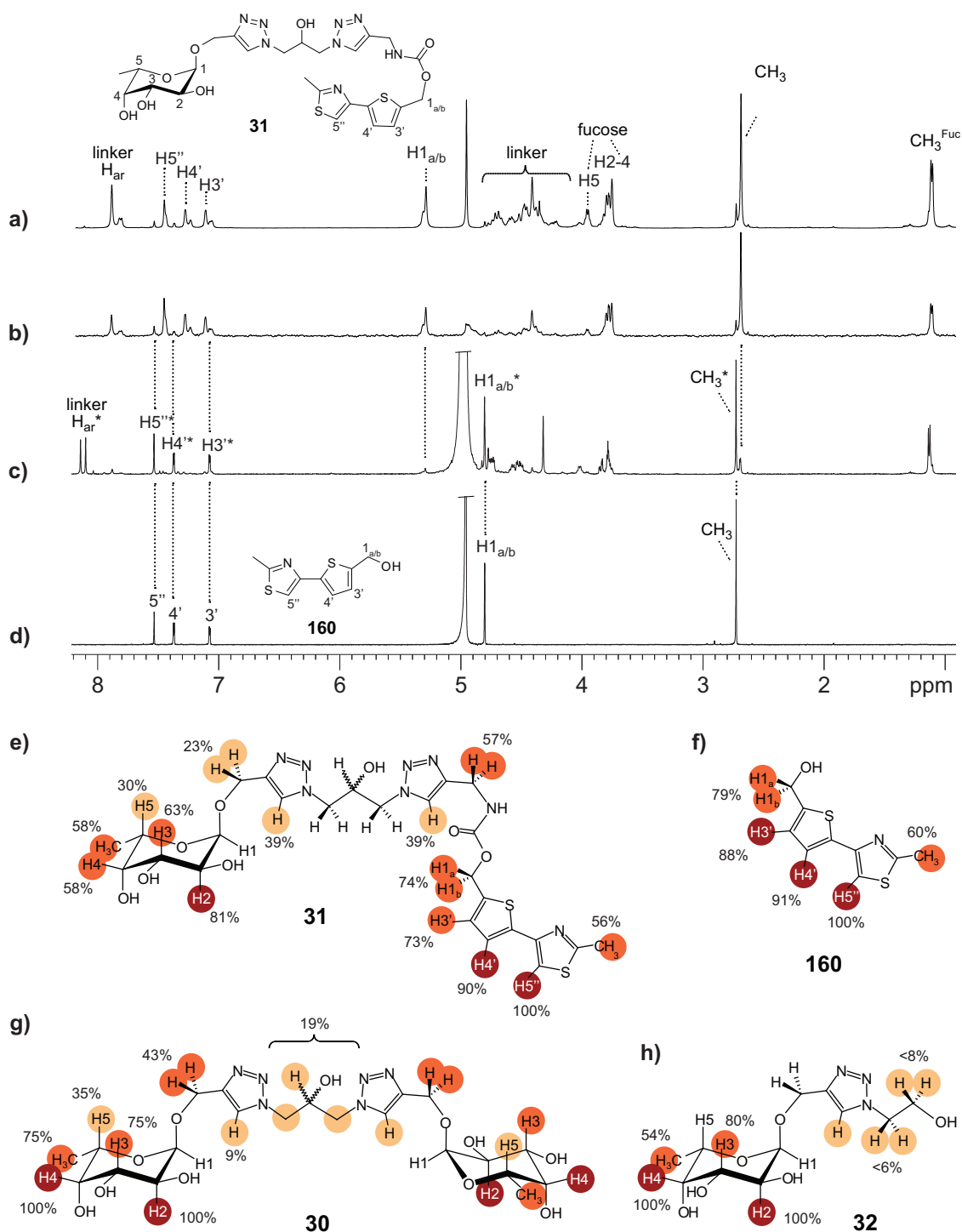


Figure 4.17. Binding epitope of heterodivalent inhibitor **31**. a)-c) NMR spectra of compound **31** containing L-Fuc and fragment 160; reference spectrum (a) and STD spectrum (b) in presence of Ast6139 VLPs measured within 24 h of solving; reference spectrum after 3 weeks in D<sub>2</sub>O in absence of VLPs (c); d) reference spectrum of fragment 160; e)-h) binding epitopes of hetero-divalent compound **31** (e), fragment 160 (f), divalent compound **30** (g) and compound **32** (h).

In the NMR spectrum of **31** additional sets of broad peaks were observed for the aromatic protons in aqueous buffer (cf. Figure 4.17 a)) that became dominant at higher concentrations (data not shown). In MeOH only a single set of sharp signals was observed for these protons. The broad signals are considered to arise from concentration-dependent oligomerization of **31** presumably via the aromatic rings. In support of this, compound **33** consisting of fragment 160 and a triazole is poorly soluble in water. Fragment 160 is soluble at 2 mM concentration and displayed one set of sharp NMR signals (Figure 4.17 d)). Contribution of the triazole rings to oligomerization of **31** is therefore implicated.

#### 4.5.2 Hits from Virtual Library Screening

Further inhibitor candidates were obtained from a virtual screening of fucosylated compounds against the HBGA binding site of a related GII.4 NoV strain (see section 1.10). The four hits **42**, **43**, **44** and **45** with the highest predicted affinity were synthesized and subjected to STD NMR experiments furnishing binding epitopes (Figure 4.18).

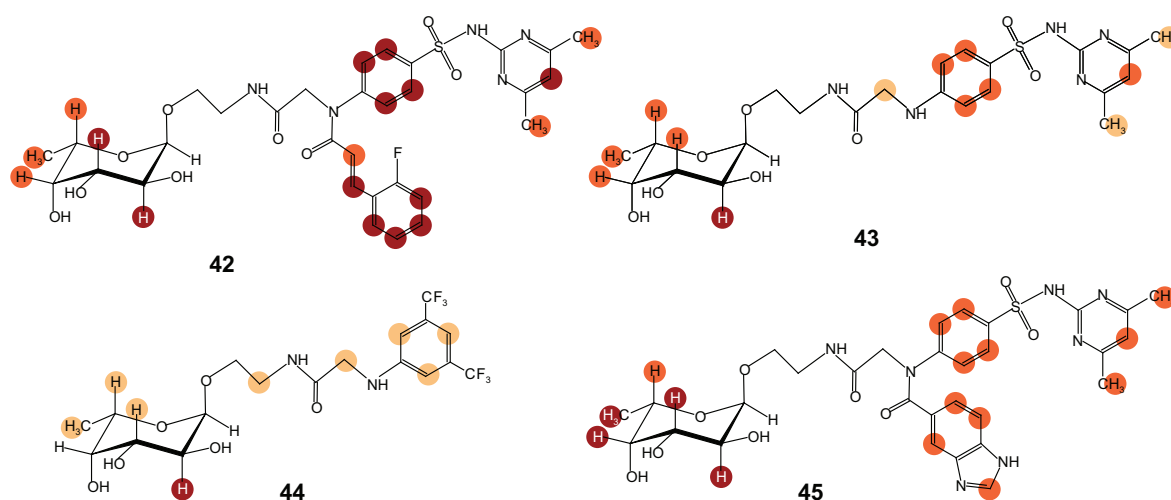


Figure 4.18. STD binding epitopes of hits from virtual screening. Binding epitopes were obtained from whole-curve fitting of STD build-up curves (saturation time 0.35 to 4 s). 5 s relaxation delay was applied. Red, orange and pale yellow circles indicate strong (>80%), medium (40-80%) and weak (<40%) relative STD effects. Protons without label were not analyzed due to spectral overlap.

The binding epitope of compound **42** displayed strong and relative homogeneous saturation transfer to the fucose moiety and to the three aromatic rings. As discussed above, spin diffusion within the aromatic rings but not between the individual rings and the fucose is likely. Close contact of all functional groups to the viral capsid surface is therefore

implicated. The proton with the strongest STD signal is H4 of the fluorobenzene ring. The overlapping signal H2/H3 of Fuc has ca. 90% relative STD effect. In case of the other three compounds the highest STD effects are seen for H2 of L-Fuc. The aromatic rings of **43** and **45** displayed medium saturation transfer indicating moderate proximity to the protein surface relative to the L-Fuc moiety. Especially compound **45** that is very similar to **42** received lower saturation transfer to its aromatic rings compared with **42**. Compound **44** exhibited only weak STD effects for protons except H2 of L-Fuc suggesting that the 1,3-di(trifluoromethyl)benzene ring was not substantially recognized in the binding pocket.

#### 4.5.3 STD Titration of Virtual Screening Hit **42**

Direct SPR titration experiments with immobilized VLPs presented in section 4.7.3 indicated a  $\mu\text{M}$  affinity for compound **42** while the other three compounds from virtual screening as well as HBGA fragments displayed only weak binding. For comparison and validation, compound **42** was subjected to STD titration experiments. Compound **42** was titrated stepwise to Ast6139 VLPs up to a final concentration of 5.3 mM. The concentrations of VLPs and the internal reference TSP were kept constant. The obtained titration curves of STD amplification factor versus **42** concentrations were fitted against a Langmuir 1:1 binding model (Figure 4.19 and Table 4.6).

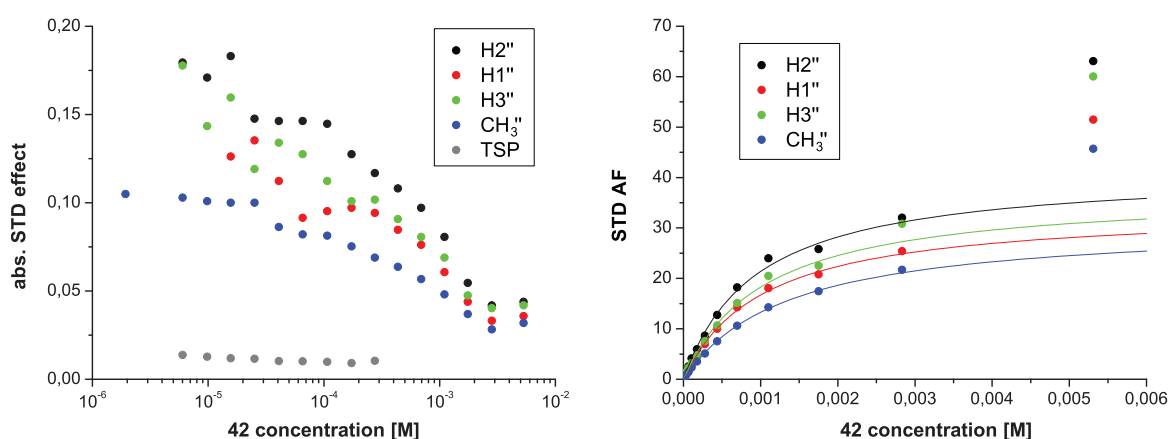


Figure 4.19. STD titration of virtual screening compound **42**. Absolute STD effects (left) and STD amplification factors (right) versus **42** concentrations for reporter signals of **42** and TSP as reference. STD experiments were measured with 4 s saturation time and 5 s relaxation delay at 282 K. Lines (right) show curve fitting to a 1:1 Langmuir isotherm excluding the last two data points (2.8 and 5.3 mM).

The STD amplification factors of all analyzed signals displayed a dramatic increase at the highest concentration (5.3 mM) that cannot be explained by non-saturable unspecific binding encompassed by a two-site binding model (cf. Figure 4.31). It is rather assumed that the increase originated from concentration-dependent oligomerization of compound **42**. This is deduced from the chemical shift changes observed during the titration. The chemical shifts of a 2 mM sample of **42** in absence of VLPs were exactly between those of the data points with 1.8 and 2.8 mM **42** in presence of VLPs (see Figure 7.8 in the appendix). Hence the chemical shift changes were obviously unrelated to binding to VLPs. The trend of increased STD amplification factors was already obvious for the second-highest concentration (2.83 mM). The two sets of data points were therefore excluded from non-linear curve fitting. A  $K_D$  value of ca. 1 mM for **42** binding to Ast6139 VLPs was obtained (Table 4.6). Taking into account the effect of ligand relaxation in STD experiments reported in the literature (Angulo *et al.*, 2010; Yan *et al.*, 2003), the  $K_D$  value from STD titration with a saturation time of 4 s is regarded to be only a very rough estimation and an upper limit of the true  $K_D$ .

Table 4.6.  $K_D$  values from STD titration of compound **42**. Curves of STD amplification factor versus **42** concentration were fitted to a 1:1 Langmuir isotherm.

Proton	$K_D$	STD AF <sub>max</sub>	$R^2/\chi^2$
H2''	<b>0.94 mM</b> ( $\pm 0.10$ mM)	41.5 ( $\pm 2.2$ )	0.9951/ 0.44
H1''	<b>1.03 mM</b> ( $\pm 0.09$ mM)	33.8 ( $\pm 1.5$ )	0.9972/ 0.17
H3''	<b>1.04 mM</b> ( $\pm 0.11$ mM)	37.3 ( $\pm 2.0$ )	0.9957/ 0.29
CH <sub>3</sub> ''	<b>1.34 mM</b> ( $\pm 0.04$ mM)	31.1 ( $\pm 0.6$ )	0.9996/ 0.01

## 4.6 Competitive STD Titration Experiments

For direct STD titration experiments with the aim of affinity determination two requirements have to be met. First, a sufficient amount of ligand is required to cover a concentration range up to ten times the estimated  $K_D$ . With respect to an estimated affinity of monovalent HBGAs in the mM range this adds up to mg quantities that are not available for most of the ligands. Therefore qualitative information on the affinity of monovalent HBGAs was gained from competitive titration experiments using a competing ligand that is available in larger quantities, i.e.  $\alpha$ -L-Fuc-(1,*O*)-CH<sub>3</sub> (**2**) in most case (section 4.6.1) The second fundamental requirement is that the ligand of interest must show STD signals in the presence of the macromolecular receptor. This condition is not met for very strong interactions such as binding of polymeric inhibitors to NoV VLPs. Qualitative information on the relative binding strengths could be gained from competitive titration of a weaker reporter ligand by the polymeric compounds (section 4.6.2).

### 4.6.1 Experiments with HBGAs and Divalent Inhibitors

Three monovalent HBGAs and two divalent inhibitors were titrated with  $\alpha$ -L-Fuc-(1,*O*)-CH<sub>3</sub> **2**. For each titration step an STD spectrum was measured and the absolute STD effects of the depleted ligands were determined. Inhibition curves were subjected to non-linear curve fitting providing IC<sub>50</sub> values for  $\alpha$ -L-Fuc-(1,*O*)-CH<sub>3</sub> (Table 4.7). A higher IC<sub>50</sub> thereby implicated a stronger binding of the depleted ligand that was not as easily displaced by  $\alpha$ -L-Fuc-(1,*O*)-CH<sub>3</sub>. IC<sub>50</sub> values from depletion of A trisaccharide **4** (5.4 mM) and B trisaccharide **5b** (4.3 mM) suggest that A trisaccharide is a slightly better binder although the values have to be treated with care considering the large inherent experimental error. Interestingly, IC<sub>50</sub> values obtained for A trisaccharide reporter signals H3-7 and H8 of its octyl spacer were considerably higher than that obtained for signals of Fuc and GalNAc. This is an indication for the presence of a second binding mode mediated by the octyl spacer that was less effectively depleted by  $\alpha$ -L-Fuc-(1,*O*)-CH<sub>3</sub>. It most likely represents unspecific binding to hydrophobic patches on the VLP surface. An increased IC<sub>50</sub> value for reporter signal H4 <sup>$\beta$ -Gal</sup> and a gradual increase of IC<sub>50</sub> values from H4 <sup>$\beta$ -Gal</sup> over H3-7 to the terminal H8 was observed (Table 4.7 and Figure 4.20). Despite this data, the general influence of spacer-mediated binding on STD binding epitopes of HBGAs is regarded to

be minor as indicated by nearly identical binding epitopes for B trisaccharides with (**5a** and **5c**) and without (**5b**) hydrophobic spacer (cf. Figure 4.2).

The  $IC_{50}$  value of  $\alpha$ -L-Fuc-(1,*O*)-CH<sub>3</sub> obtained for depletion of sLe<sup>x</sup> **14** (ca. 3.9 mM) argued for a slightly weaker affinity of sLe<sup>x</sup> compared to A and B trisaccharides. This was substantiated by observation of weaker absolute STD effects in presence of VLPs for sLe<sup>x</sup> (e.g. ~2.2% for H1<sup>Fuc</sup>) compared to A and B trisaccharides (~3.6% for H1<sup>Fuc</sup>).

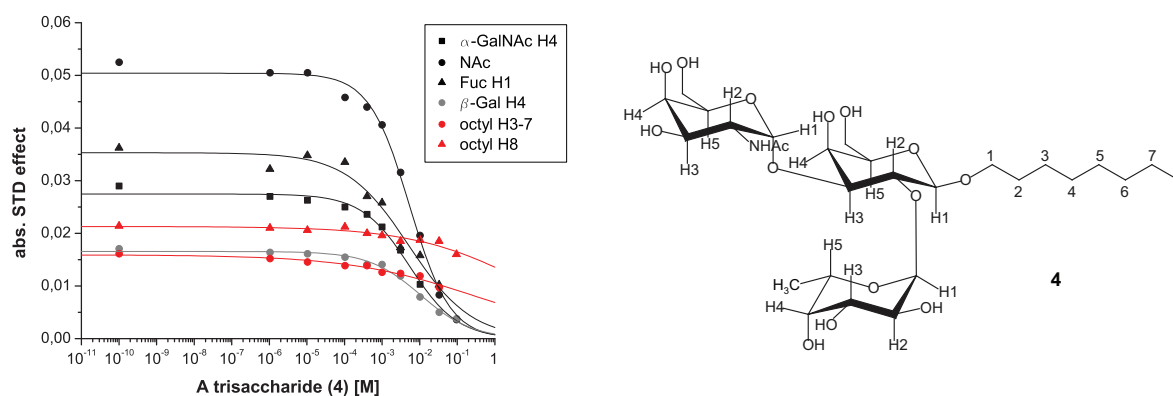


Figure 4.20. Competitive STD titration of A trisaccharide with  $\alpha$ -L-Fuc-(1,*O*)-CH<sub>3</sub>. (Left) titration curves for A trisaccharide (**4**) reporter signals and curve fitting to equation 5 (lines) (cf. Table 4.7). (Right) structural formula of A trisaccharide *O*-octyl glycoside.

In a reversed assay constellation,  $\alpha$ -L-Fuc-(1,*O*)-CH<sub>3</sub> was used as reporter ligand for competitive titration with B trisaccharide **5b**. The  $IC_{50}$  values obtained for reporter signals H5 ( $0.66 \text{ mM} \pm 0.16 \text{ mM}$ ) and CH<sub>3</sub> ( $1.45 \text{ mM} \pm 0.57 \text{ mM}$ ) were by a factor of four lower than the  $IC_{50}$  value for titration of B trisaccharide with  $\alpha$ -L-Fuc-(1,*O*)-CH<sub>3</sub>. This data constitute direct experimental proof that Ast6139 VLPs bind to fucosylated oligosaccharides with a higher affinity compared to monosaccharidic Fuc. In general,  $IC_{50}$  values allow only a qualitative comparison of binding affinities since they are dependent on the experimental setup, e.g. the protein concentration.  $K_D$  values can in principle be calculated from  $IC_{50}$  values with the help of the Cheng-Prusoff equation if the affinity of one ligand is known. Therefore the  $K_D$  value of  $\alpha$ -L-Fuc-(1,*O*)-CH<sub>3</sub> determined by STD titration (cf. section 7.6.1 in the appendix) was taken to calculate  $K_D$  values for HBGAs (see Table 7.2 in the appendix for results). Assuming a  $K_D$  of 1.7 mM for  $\alpha$ -L-Fuc-(1,*O*)-CH<sub>3</sub>, calculated  $K_D$  values were ~0.5 mM for A trisaccharide, 0.6 to 0.7 mM for B trisaccharide and ~0.8 mM for sLe<sup>x</sup>. A second approach using mathematical conversions and substitution of the Cheng-Prusoff equation was employed for calculation of  $K_D$  values of  $\alpha$ -L-Fuc-(1,*O*)-CH<sub>3</sub> and B trisaccharide **5b** from the two  $IC_{50}$  values from competitive titration of one with



the other (see section 7.6.2). The calculated  $K_D$  values were very close to those obtained from the other approach (0.7 mM for B trisaccharide, 1.7 mM for  $\alpha$ -L-Fuc-(1,*O*)-CH<sub>3</sub>). To compare the binding strengths of ‘natural’ HBGA fragments and inhibitors, divalent compounds **30** and **31** were titrated with  $\alpha$ -L-Fuc-(1,*O*)-CH<sub>3</sub> (Figure 4.21 and Table 4.7). The data indicate that difucosylated compound **30** was easier depleted and hence weaker bound to VLPs than A and B trisaccharides and sLe<sup>x</sup>. Obviously a potential multivalency effect of **30** did not outweigh the higher affinities of ABH and Lewis antigens that are the result from evolution of the HBGA binding site towards optimized accommodation of oligosaccharides.

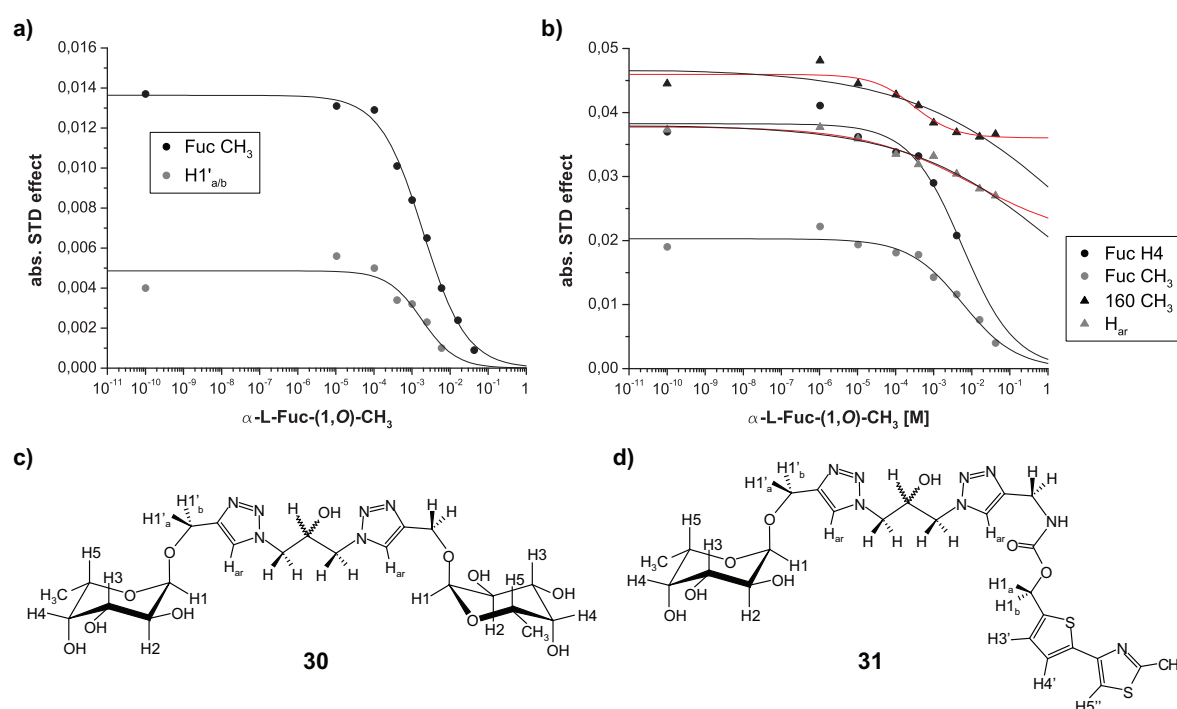


Figure 4.21. Competitive STD titration of divalent inhibitors with  $\alpha$ -L-Fuc-(1,*O*)-CH<sub>3</sub>. a),b) Inhibition curves for compounds **30** (a) and **31** (b) (first data points were measured in absence of  $\alpha$ -L-Fuc-(1,*O*)-CH<sub>3</sub>); non-linear curve fitting to a dose-response curve (equation 5) keeping STD<sub>min</sub> fixed to 0 (black lines) or allowing STD<sub>min</sub> to be >0 (red lines) (cf. Table 4.7). c),d) Structural formulas of **30** and **31**.

Inhibition curves of the heterodivalent compound **31** displayed different behaviors for its two functional groups L-Fuc and fragment 160 (Figure 4.21). Fuc signals of **31** were depleted by  $\alpha$ -L-Fuc-(1,*O*)-CH<sub>3</sub> with an IC<sub>50</sub> values comparable to that for titration of A trisaccharide indicating similar affinities (Table 4.7). STD effects of Fuc were reduced by 80% at the end of the titration in presence of 42 mM  $\alpha$ -L-Fuc-(1,*O*)-CH<sub>3</sub>. In contrast, the CH<sub>3</sub> signal of fragment moiety 160 was reduced by only 20%. Fitting of the inhibition

curve for this signal assuming partial depletion was in very good agreement with the experimental data and yielded an  $IC_{50}$  of 300  $\mu$ M (red line in Figure 4.21). Fragment 160 was classified as competitive binder to Ast6139 VLPs (Rademacher *et al.*, 2011) (see section 1.10), but obviously a large part of the saturation transfer to fragment 160 resulted from binding to sites not targeted by L-Fuc. According to the Cheng-Prusoff equation,  $K_I = IC_{50}/(1+[L]/K_D)$ ,  $IC_{50}$  is an upper limit of the  $K_I$  of the competing ligand. This suggests that  $\alpha$ -L-Fuc-(1,*O*)-CH<sub>3</sub> binds with an affinity of at least 300  $\mu$ M to certain binding sites of VLPs. In STD titration experiments of  $\alpha$ -L-Fuc-(1,*O*)-CH<sub>3</sub> a  $K_D$  of ca. 2 mM was determined. This raises the question if the 160 binding site depleted by  $\alpha$ -L-Fuc-(1,*O*)-CH<sub>3</sub> represents the HBGA binding site observed in crystal structures. Further experiments are necessary to assess the differences in the binding modes of Fuc and (fragment) inhibitors.

*Table 4.7.  $IC_{50}$  values from competitive STD titration of HBGAs. 1 mM of the ligand was titrated with  $\alpha$ -L-Fuc-(1,*O*)-CH<sub>3</sub> up to 95 mM. Inhibition curves of STD signals of depleted ligand were fitted to equation 5. Errors of fitted Hill slopes were usually <10%.*

Ligand displaced	Reporter signal	$IC_{50}$ value	Hill slope	$R^2$	Comments
A trisaccharide octyl glycoside ( <b>4</b> )	$\alpha$ -GalNAc H4	5.4 mM ( $\pm$ 0.8 mM)	0.68	0.9840	
	NAc	5.4 mM ( $\pm$ 0.6 mM)	0.81	0.9945	
	Fuc H1	5.2 mM ( $\pm$ 1.5 mM)	0.52	0.9649	
	$\beta$ -Gal H4	10.6 mM ( $\pm$ 1.5 mM)	0.63	0.9903	influenced by octyl binding
	octyl H3-7	330 mM ( $\pm$ 210 mM)	0.25	0.9600	weak binding via octyl spacer
	octyl H8	6.9 M ( $\pm$ 9.2 M)	0.29	0.9047	weak binding via octyl spacer
B trisaccharide methyl glycoside ( <b>5b</b> )	$\alpha$ -Gal H3	4.1 mM ( $\pm$ 0.9 mM)	0.67	0.9706	
	Fuc H1	4.7 mM ( $\pm$ 1.0 mM)	0.69	0.9772	
	Fuc CH <sub>3</sub>	4.2 mM ( $\pm$ 0.9 mM)	0.71	0.9789	
sLe <sup>x</sup> ( <b>14</b> )	NAc	3.9 mM ( $\pm$ 0.4 mM)	0.68	0.9938	overlap of GlcNAc/ Neu5Ac
<b>30</b> (difucosylated compound)	Fuc CH <sub>3</sub>	2.0 mM ( $\pm$ 0.2 mM)	0.77	0.9959	
	H1' <sub>a/b</sub>	1.8 mM ( $\pm$ 0.8 mM)	0.97	0.8703	
<b>31</b> (heterodivalent compound with fragment 160 and Fuc)	H <sub>ar</sub>	2.1 M ( $\pm$ 1.8 M)	0.22	0.9584	
		11 mM ( $\pm$ 54 mM)	0.30	0.9612	partial depletion by 50%
	160 CH <sub>3</sub>	8.7 M ( $\pm$ 20.5 M)	0.20	0.8359	
		300 $\mu$ M ( $\pm$ 180 $\mu$ M)	0.81	0.9394	partial depletion by 20%
	Fuc H4	5.7 mM ( $\pm$ 2.1 mM)	0.63	0.9364	
	Fuc CH <sub>3</sub>	5.8 mM ( $\pm$ 1.5 mM)	0.61	0.9712	

A hint for such divergent binding modes was the observation of significantly different Hill slopes for carbohydrate reporter signals (0.6 to 0.8) opposed to that of fragment 160 or spacer signals of A trisaccharide (0.2 to 0.3).

Finally,  $\alpha$ -L-Fuc-(1,*O*)-CH<sub>3</sub> was titrated with compound **42** from virtual screening. IC<sub>50</sub> values for reporter signals H2-4 (3.6 mM  $\pm$  0.8 mM) and CH<sub>3</sub> (1.9 mM  $\pm$  0.4 mM) indicated that  $\alpha$ -L-Fuc-(1,*O*)-CH<sub>3</sub> was more efficiently displaced by B trisaccharide than by **42**. In support of this, the K<sub>D</sub> value of **42** from direct STD titration ( $\sim$ 1 mM, section 4.5.3) was slightly higher than the assumed K<sub>D</sub> of B trisaccharide (0.7 mM, *vide supra*).

#### 4.6.2 Experiments with Polymeric Inhibitors

Polymeric PAA-based inhibitors featuring L-Fuc and fragment hits from NMR screening do not display STD effects in presence of Ast6139 VLPs likely due to a low  $k_{\text{off}}$  of the interaction. Therefore, polymers were subjected to competitive STD titrations using  $\alpha$ -L-Fuc-(1,*O*)-CH<sub>3</sub> **2** as reporter ligand to determine inhibition efficiencies (Figure 4.22).

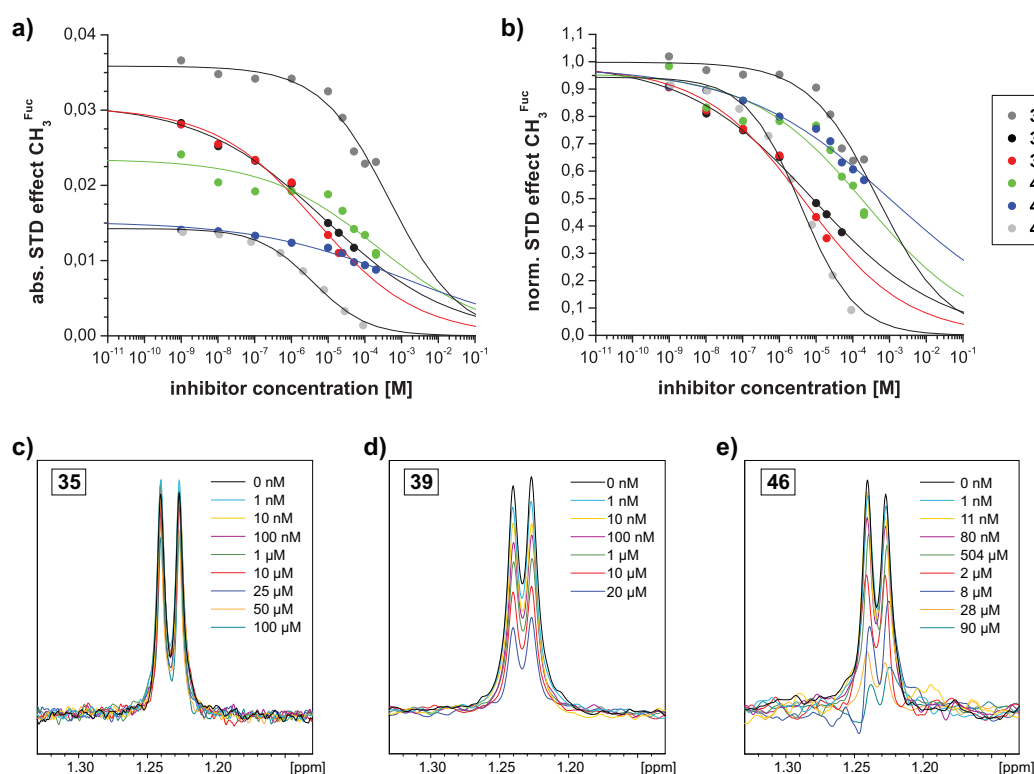


Figure 4.22. STD competition experiments with polymeric inhibitors. a),b) absolute STD effects (a) and reduction of STD effects (b) of  $\alpha$ -L-Fuc-(1,*O*)-CH<sub>3</sub> **2** reporter signal CH<sub>3</sub><sup>Fuc</sup> as a function of polymer concentration (calculated per monomeric repeating unit); lines show non-linear curve fitting to equation 5 (STD<sub>min</sub> fixed to 0). c)-e) Spectral region of the CH<sub>3</sub><sup>Fuc</sup> signal in presence of increasing concentrations of three polymers.

Fitting of the inhibition curves yielded  $IC_{50}$  values in the  $\mu\text{M}$  range as calculated per monomeric repeating unit (Table 4.8). Polymer **46** containing compound **42** from virtual screening had the highest inhibition efficiency ( $4\ \mu\text{M}$ ). Slightly weaker were polymers **39** ( $5$  to  $8\ \mu\text{M}$ ) and **38** ( $8$  to  $20\ \mu\text{M}$ ) with Fuc and ‘adjacent site’ fragments, i.e. fragments showing ILOEs to  $\alpha\text{-L-Fuc-(1,}O\text{)-CH}_3$  (see section 1.10). **40**, **41** and polymer **35** (only Fuc) had  $IC_{50}$  values in the higher  $\mu\text{M}$  range. In all samples, visible precipitation occurred during the titrations, in case of strong inhibitors (**38**, **39** and **46**) already at nM concentrations. Polymers in absence of VLPs did not precipitate as tested for a  $250\ \mu\text{M}$  sample of **38**. Likewise, no precipitation was observed in NMR samples of VLPs and HBGAs without polymer over a period of months. Therefore the observed precipitates were likely complexes of VLPs and polymer. The underlying inhibition mechanism is very efficient since precipitation occurred already at nM concentration of polymers.

Table 4.8.  $IC_{50}$  values of polymeric inhibitors from competitive STD titrations. The titration curves using  $\text{CH}_3^{\text{Fuc}}$  (cf. Figure 4.22) and  $\text{H2-4}^{\text{Fuc}}$  of  $\alpha\text{-L-Fuc-(1-}O\text{)-CH}_3$  as reporter signals were fitted to equation 5 keeping  $\text{STD}_{\text{min}}$  (STD effect at excess of inhibitor) fixed to 0. Concentrations are given ‘per Fuc’.

Competing ligand	Functionalities	Reporter signal: $\text{CH}_3^{\text{Fuc}}$		Reporter signal: $\text{H2-4}^{\text{Fuc}}$	
		$IC_{50}$	Hill slope	$IC_{50}$	Hill slope
<b>35</b>	L-Fuc	$490\ \mu\text{M} (\pm 200\ \mu\text{M})$	0.46	$810\ \mu\text{M} (\pm 320\ \mu\text{M})$	0.46
<b>38</b>	L-Fuc, fragment 191	$8.3\ \mu\text{M} (\pm 1.6\ \mu\text{M})$	0.25	$20\ \mu\text{M} (\pm 4\ \mu\text{M})$	0.28
<b>39</b>	L-Fuc, fragment 473	$4.8\ \mu\text{M} (\pm 1.7\ \mu\text{M})$	0.32	$8.1\ \mu\text{M} (\pm 2.7\ \mu\text{M})$	0.38
<b>40</b>	L-Fuc, fragment 151	$230\ \mu\text{M} (\pm 120\ \mu\text{M})$	0.28	$180\ \mu\text{M} (\pm 50\ \mu\text{M})$	0.40
<b>41</b>	L-Fuc, fragment 231	$1.2\ \text{mM} (\pm 0.5\ \text{mM})$	0.21	$380\ \mu\text{M} (\pm 150\ \mu\text{M})$	0.20
<b>46</b>	compound <b>42</b>	$3.9\ \mu\text{M} (\pm 0.7\ \mu\text{M})$	0.59	$4.7\ \mu\text{M} (\pm 0.9\ \mu\text{M})$	0.63

A general difference in the form of the inhibition curves was seen for polymers containing Fuc (**35**) or compound **42** (**46**) on the one hand (light and medium grey circles in Figure 4.22) and polymers containing Fuc and ‘adjacent site’ fragments on the other hand. The major difference was found in the Hill slopes. Inhibition curves of polymers **35** and **46** had Hill slopes from 0.46 to 0.63 (the error was typically <10%). The hill slopes for the polymers with ‘adjacent site’ fragments were significantly lower (0.20 to 0.40). This prompted to different inhibition mechanisms of the tested polymers. A Hill coefficient <1 for all polymers suggested negative cooperativity of the inhibition of Fuc binding to VLPs. Probably the binding of polymers to VLPs sterically hindered the approach and binding of further polymeric molecules but not that of the smaller  $\alpha\text{-L-Fuc-(1,}O\text{)-CH}_3$ . Polymers may also aggregate at higher concentrations leading to their depletion from solution.

For comparison, BSA sugar conjugate containing on average 12 H type 2 trisaccharide residues per BSA molecules was also subjected to competitive STD titration (Figure 4.23). The  $IC_{50}$  value for depletion of  $\alpha$ -L-Fuc-(1,*O*)-CH<sub>3</sub> binding to Ast6139 VLPs was in the sub- $\mu$ M range calculated per H type 2 residue (Table 4.8). This indicated higher inhibition efficiency per functional (carbohydrate) group compared to the polymeric inhibitors. A reason for this might be an increased multivalency effect in case of the BSA sugar conjugate. It exhibits a globular fold with a molecular weight of ca. 74 kDa to which the carbohydrate moieties are attached in relatively close proximity. In contrast the polymeric inhibitors with an overall molecular weight of 60 to 100 kDa present their functional groups along a linear but flexible PAA backbone (20 to 30 monomeric units) like a “rope of pearls”. In case of the BSA conjugate a low Hill coefficient of ca. 0.2 indicated negative cooperativity similar to that observed for polymers with ‘adjacent site’ fragments.

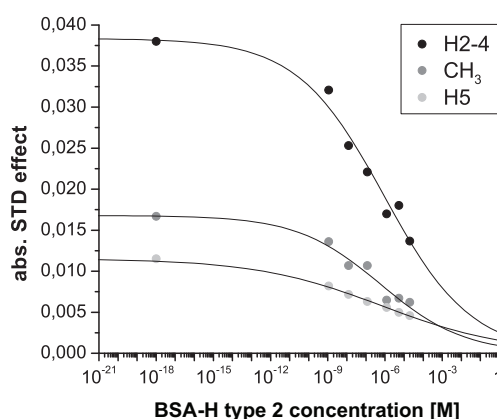


Figure 4.23. Competitive STD titration of BSA sugar conjugate. Plots of absolute STD effects of  $\alpha$ -L-Fuc-(1,*O*)-CH<sub>3</sub> reporter signals versus BSA-H type 2 concentration (calculated per H type 2) were fitted to equation 5 (lines). The data points at the lowest concentration represent measurement in absence of BSA conjugate.

Table 4.9.  $IC_{50}$  values from competitive STD titration of BSA-H type 2 conjugate. Inhibition curves of  $\alpha$ -L-Fuc-(1,*O*)-CH<sub>3</sub> reporter signals were fitted to equation 5 keeping  $STD_{min}$  (STD effect at excess of inhibitor concentrations) fixed to 0. The concentrations are calculated ‘per H type 2 trisaccharide residue’.

Reporter ligand	$IC_{50}$	Hill slope
H2-4	0.89 $\mu$ M ( $\pm$ 0.65 $\mu$ M)	0.19
CH <sub>3</sub>	0.59 $\mu$ M ( $\pm$ 0.51 $\mu$ M)	0.20
H5	0.71 $\mu$ M ( $\pm$ 0.14 $\mu$ M)	0.13



#### 4.7 Direct SPR Binding Assays with Immobilized VLPs

With the aim to analyze binding of HBGAs and prototype inhibitors to Ast6139 VLPs with an alternative biophysical method, VLPs were immobilized on SPR sensor chips for a direct binding assay. Beside qualitative binding information, concentration-dependent measurements can provide dissociation constants. In contrast to NMR, SPR detects VLP-analyte interactions under continuous flow. Seven CM5 sensor chips A to G were covered with VLPs adding up to 14 flow cells (Fc) with 1600 to 12000 RU VLPs. In single cases, bovine serum albumin (BSA) and human galactosyltransferase B (GTB) (Patenaude *et al.*, 2002) were immobilized for comparison.

A) Fc1: activated/ deactivated (reference)

Fc2: 3500 RU VLPs

Fc3: 7300 RU VLPs

Fc4: 5200 RU VLPs

B) Fc1: activated/ deactivated (reference)

Fc2: 12000 RU VLPs

Fc3: 8900 RU BSA

C) Fc1: 7050 RU VLPs

Fc2: 5260 RU VLPs

Fc3: activated/ deactivated (reference)

D) Fc1: activated/ deactivated (reference)

Fc2: 4200 RU GTB

Fc4: 5370 RU VLPs

E) Fc1: activated/ deactivated (reference)

Fc2: 11600 RU VLPs

Fc3: 7600 RU VLPs

Fc4: 5030 RU VLPs

F) Fc1: activated/ deactivated (reference)

Fc2: 1600 RU VLPs

Fc3: 5100 RU VLPs

Fc4: 3700 RU VLPs

G) Fc1: activated/ deactivated (reference)

Fc2: 5300 RU VLPs

### 4.7.1 Binding Studies with HBGA Fragments

Monosaccharidic L-Fuc was injected on six different sensor chips with immobilized VLPs. If binding of analytes to immobilized ligand occurs in SPR, one normally expects a positive response difference (i.e. after subtraction of the reference flow cell signal) that is proportional to the netto mass increase on the sensor surface (see Figure 1.11 for a typical sensorgram). However, injection of L-Fuc on most flow cells led to negative response differences that were proportional to the injected L-Fuc concentration and to the VLP coverage (Figure 4.24). As an exception, one flow cell on sensor chip C with a coverage of 5260 RU VLPs showed a positive response difference (marked with an arrow in Figure 4.24 d)). Since the responses were reproducible on this chip, it was used for titration of L-Fuc and other HBGAs (see Figure 4.27 and Figure 4.28).

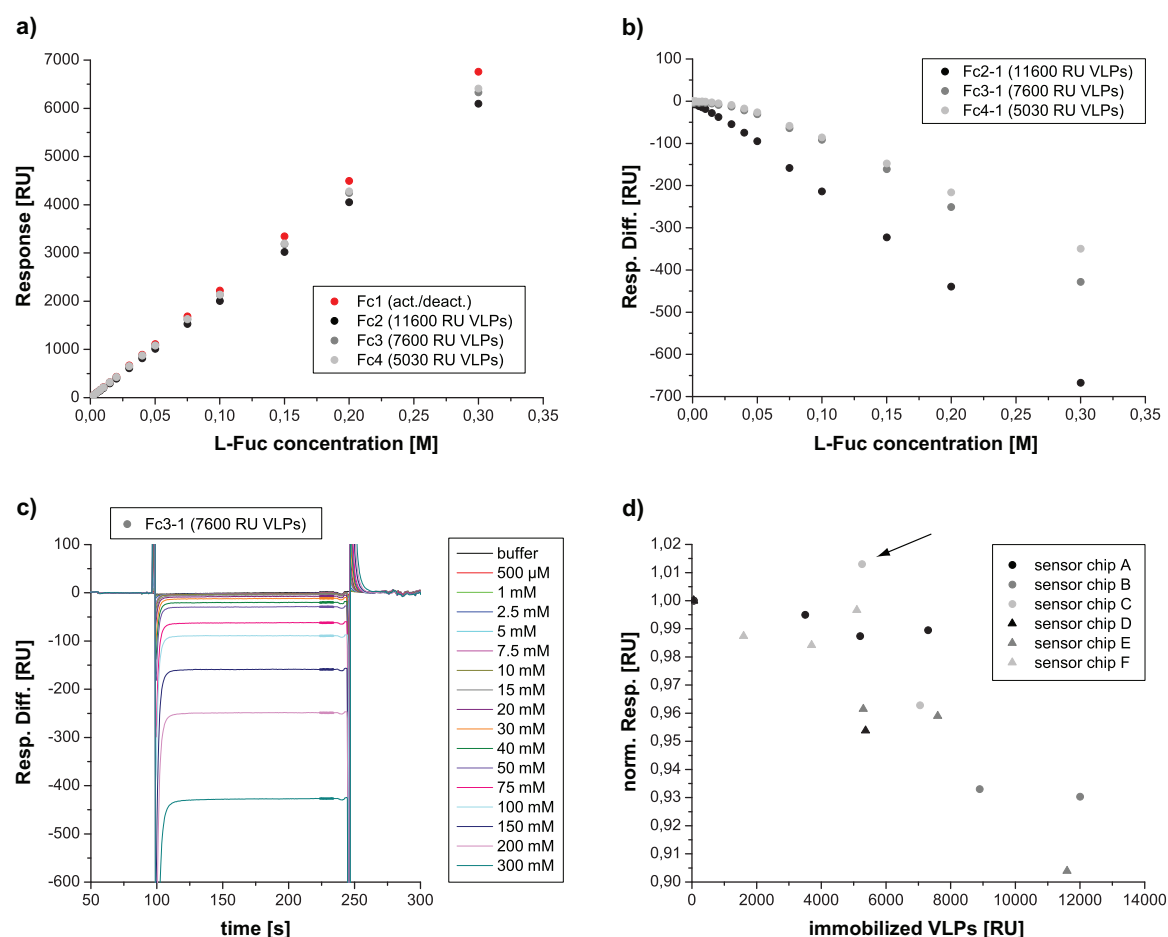


Figure 4.24. SPR experiments with L-Fuc at different coverage rates of VLPs. a)-c) Absolute responses (a), response differences (b) and difference curves (Fc3) (c) of L-Fuc injections on sensor chip E. d) Response differences as a function of VLP coverage on different sensor chips normalized to the response of the corresponding reference flow cell; the data point for Fc2 on sensor chip C (5260 RU VLPs) with positive response differences is indicated with an arrow.



Other HBGAs also showed negative response differences on at least one sensor chip: two other monosaccharides D-galactose (**16**) and D-mannose, H-disaccharide *O*-methyl glycoside (**3a**), B antigen trisaccharide *O*-methyl and *O*-octyl glycosides (**5a** and **5b**), H trisaccharide type 6 *O*-(8-methoxycarbonyl)-octyl glycoside (**8a**), type 6 precursor (**26**) and the difucosylated compound **30** (Figure 4.25 and Figure 4.26). Similar to L-Fuc, the negative response differences were linear proportional to the injected concentrations. The reason for negative response differences is likely refractive index artifacts observed for flow cells with very different surface compositions, i.e. an empty reference flow cell and a few thousand RU VLPs on the test flow cells (see manual “Surface plasmon resonance” by P.A. van der Merwe, University of Oxford). Immobilized VLPs occupy a certain volume that will not be displaced by the analyte. If the injected analyte solution has a very high refractive index such as high mM solution of carbohydrates the absolute response can be therefore higher on the empty reference flow cell. In cases where the expected response is small due to a low molecular weight of analytes (<1000 g/mol for mono- to trisaccharides) and a low expected affinity requiring sampling of high analyte concentrations, refractive index artifacts are especially likely to obscure the positive response of binding analyte.

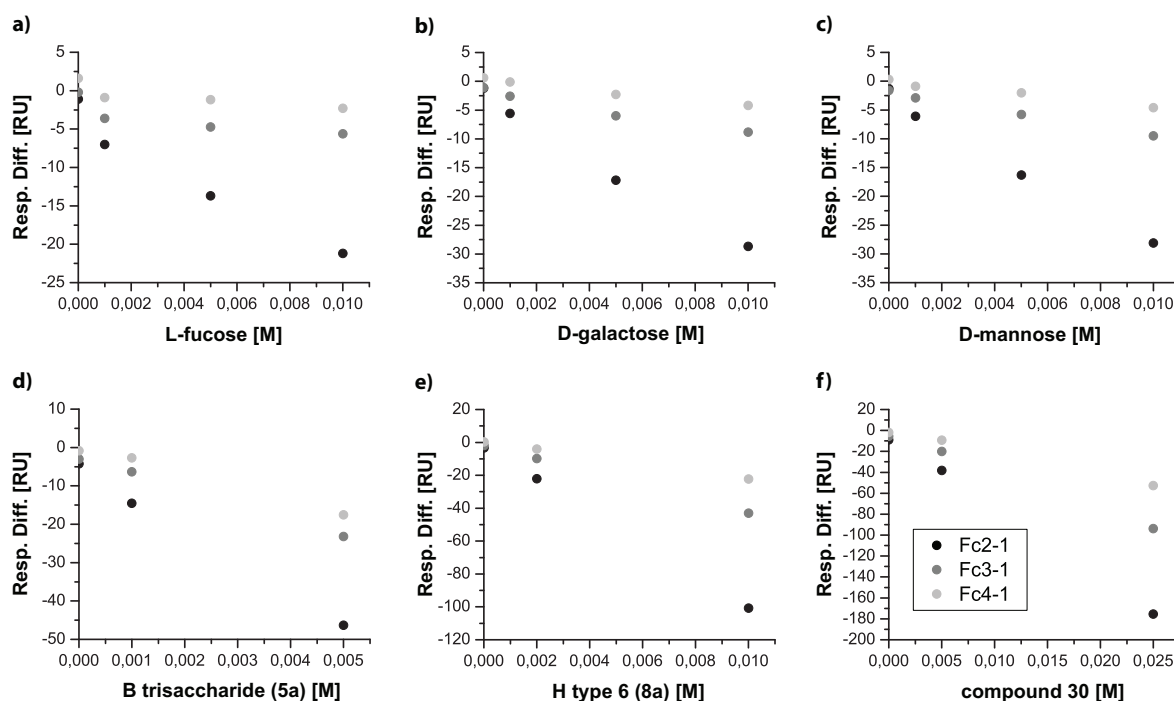


Figure 4.25. SPR experiments with HBGAs showing negative response differences. All substances were measured on sensor chip E with VLP coverage rates of 11600 RU (Fc2), 7600 RU (Fc3) and 5030 RU (Fc4).

As an exception, H-disaccharide *O*-5-methoxycarbonylpentyl glycoside (**3b**) showed positive responses on all sensor chips (see Figure 4.26 and Figure 4.29). To test if the hydrophobic spacer of **3b** mediates unspecific binding to the chip surface, two H disaccharides and two B trisaccharides each with and without hydrophobic spacer were injected on sensor chip B covered with VLPs (12000 RU black lines in Figure 4.26) and BSA (8900 RU, red lines in Figure 4.26).

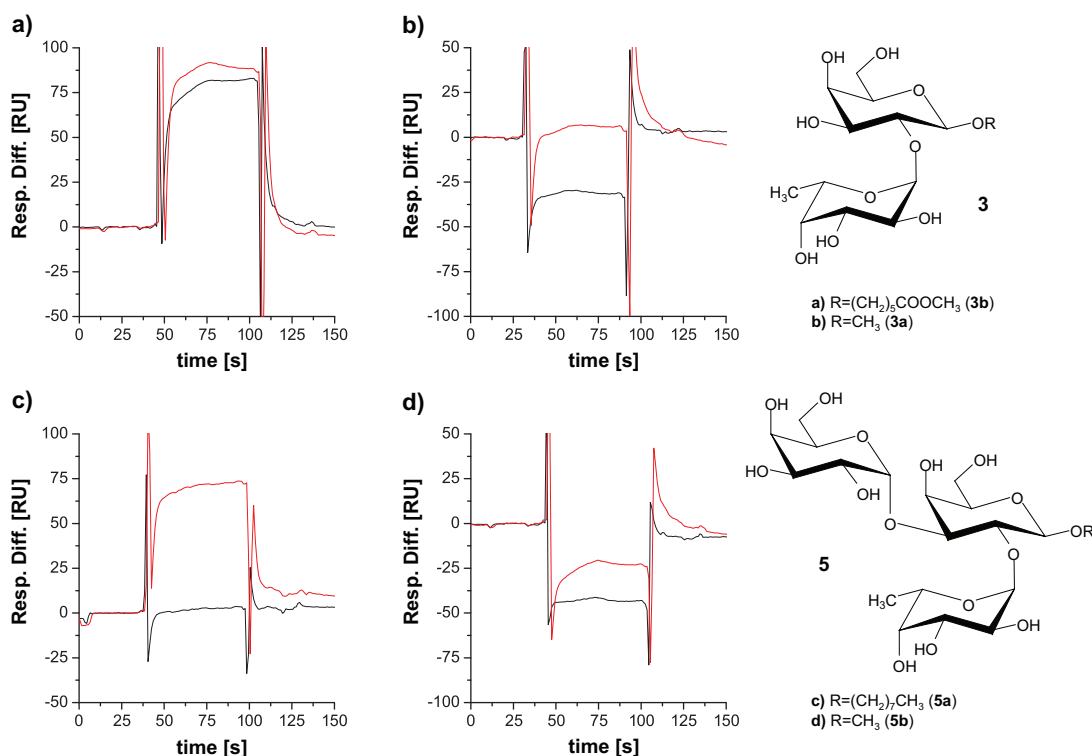


Figure 4.26. Injections of H-disaccharide and B trisaccharide. Difference curves for H-disaccharides **3b** (a) and **3a** (b) (10 mM) and B trisaccharides **5a** (c) and **5b** (d) (4 mM) on Fc2 (12000 RU VLPs, black) and Fc3 (8900 RU BSA, red) of sensor chip B.

Difference curves from injection of B trisaccharide *O*-octyl glycoside (**5a**) showed no response on immobilized VLPs, indicating that the presence of a hydrophobic spacer alone does not mediate unspecific binding. The *O*-methyl glycosides **3a** and **5b** displayed negative responses on VLPs again suggesting refractive index artifacts. Both **3b** and **5a** containing hydrophobic spacer groups had significant positive responses on immobilized BSA while the responses for corresponding *O*-methyl glycosides were close to zero or negative. This suggests that hydrophobic spacer of carbohydrates mediate unspecific binding to BSA but not to VLPs. The binding of H-disaccharide **3b** to immobilized VLPs is therefore considered to be specific. However uncertainty on the nature of this binding remains considering the absence of positive responses for other carbohydrates.

Only one out of 14 flow cells covered with VLPs, namely Fc2 of sensor chip C covered with 5260 RU VLPs, yielded positive response differences for L-Fuc and carbohydrates other than H-disaccharide **3b**. In particular, Fc1 of the same sensor chip covered with 7050 RU VLPs displayed negative response differences. The reason for this discrepancy is not known. However the measurements on Fc2 were reproducible and yielded reasonable binding curves (Figure 4.27 and Figure 4.28). The sensorgrams of L-Fuc injections reached the equilibrium level instantaneously after injection start. Likewise the baseline level was recovered after injection stop without the necessity for a regeneration step. This is an indication for fast kinetic of the interaction (Figure 7.9 in the appendix). The resulting rectangular sensorgram form does not allow evaluation of association and dissociation phases in order to obtain kinetic constants. Binding curves for L-Fuc and other HBGAs were obtained from monitoring the response differences in the equilibrium phase as a function of injected concentration. The curves were fitted to a Langmuir binding isotherm for 1:1 binding (equation 9) and results are summarized in Table 4.10.

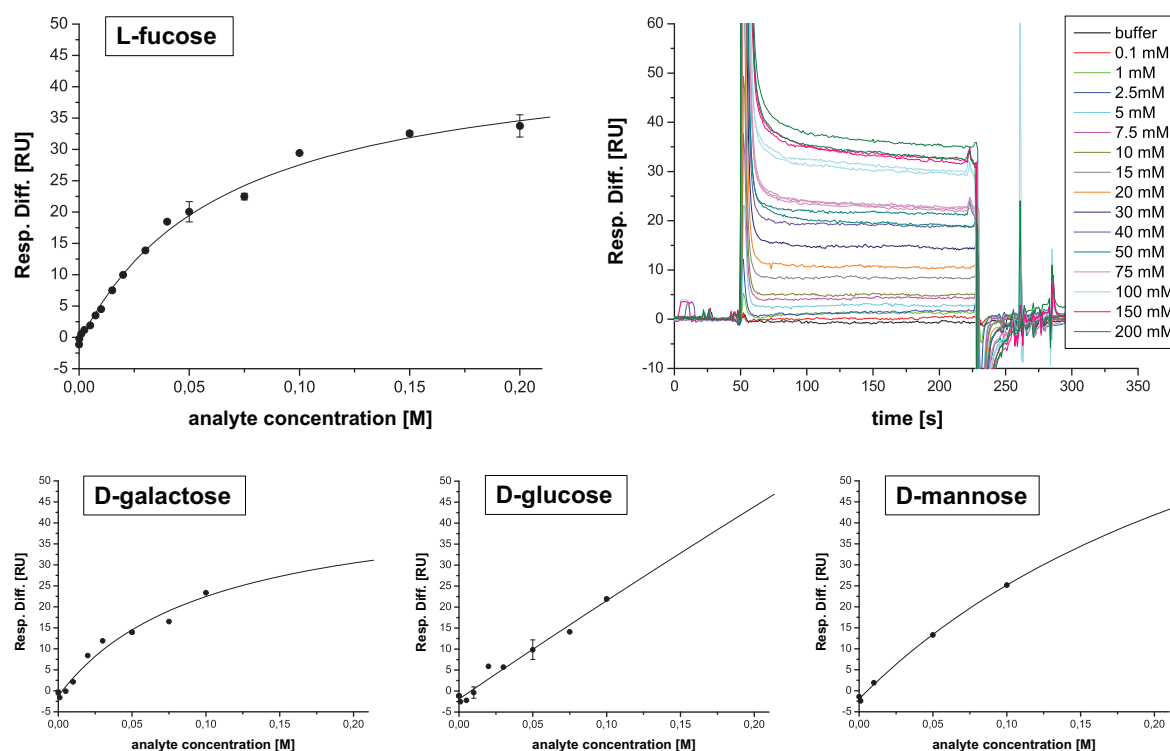


Figure 4.27. SPR experiments with monosaccharides yielding binding curves. Top panel: binding curve (left) and difference curves (right) from injections of increasing L-Fuc concentrations on Fc2 of sensor chip C (5260 RU VLPs); spikes at the beginning and end of injections result from imperfect reference curve subtraction. Bottom panel: binding curves for three other monosaccharides on the same flow cell. Lines represent Langmuir fits (cf. Table 4.10).

The  $K_D$  value calculated for L-Fuc was between 60 and 70 mM which is in the range of weak monovalent carbohydrate-protein interactions. The fitted  $RU_{\max}$  value was ca. three times larger than the theoretical  $RU_{\max}$  value calculated from the coverage (5260 RU corresponding to ca. 300 Mio. VLPs/mm<sup>2</sup>), the molecular weight of L-Fuc (164.2 g/mol) and assuming saturation of all binding sites (180 per VLP). This suggested the presence of more than one binding site per VP1 monomer of VLPs. However, curve fitting to a two site binding model accounting for presence of two binding sites with different affinities (cf. STD titration of  $\alpha$ -L-Fuc-(1,*O*)-CH<sub>3</sub>, section 7.6.1 in the appendix) was not justified by the data. The obtained  $K_D$  is hence the weighted average of the  $K_D$  values of all binding sites.

Three other monosaccharides were tested for binding to VLPs (Figure 4.27). The form of the sensorgrams was similar to that of L-Fuc, e.g. the equilibrium state was reached instantaneously (sensorgrams not shown). Fitted  $K_D$  values for all three monosaccharides were higher than that for L-Fuc (Table 4.10). For D-glucose and D-mannose no saturation of the binding occurred and the  $R_{\max}$  values vastly outreach the theoretical values for 1:1 binding. The observed responses could thus result from unspecific i.e. non-saturable binding. In contrast the  $R_{\max}$  value for D-galactose is in the range of that of L-Fuc. A  $K_D$  of ~100 mM for D-galactose could therefore represent weak but specific binding that is not observed in STD experiments. Observation of significant saturation transfer to the terminal D-galactose of B trisaccharide (cf. Figure 4.2) could be an indication for a weak recognition site for D-galactose next to that of L-Fuc.

$K_D$  values of other fucosylated HBGAs and divalent inhibitors were also determined from concentration series on sensor chip C (Figure 4.28 and Table 4.10). For H trisaccharide type 6 (**8a**) a  $K_D$  of 10 mM was obtained that is seven times smaller than the  $K_D$  of L-Fuc. The fitted  $RU_{\max}$  value was in the range of the theoretical value for a 1:1 binding. It is thus possible that the observed response results solely from binding to the HBGA site identified in the crystal structure of the GII.4 strain VA387 in complex with A and B trisaccharide (Cao *et al.*, 2007). The additional hexose moieties may cause that H trisaccharide **8a** can only be accommodated in the known HBGA binding site while L-Fuc and H disaccharide also bind to other sites on the VLP surface.

Interestingly, difucosylated compound **30** and heterodivalent compound **31** with L-Fuc and fragment 160 yielded positive response differences on both flow cells of sensor chip C covered with VLPs (Figure 4.28). In contrast to the previously discussed carbohydrates, compound **30** had to be injected for a longer time in order to reach the equilibrium state (cf. Figure 7.11 in the appendix for the original sensorgrams). Additionally, large portions

of substance remained on the VLP covered surfaces after injection stop. Only small fractions thereof were removed by regeneration with phosphate buffer pH 7.4 which in other cases allowed efficient regeneration due to weakening of binding to VLPs at this pH.

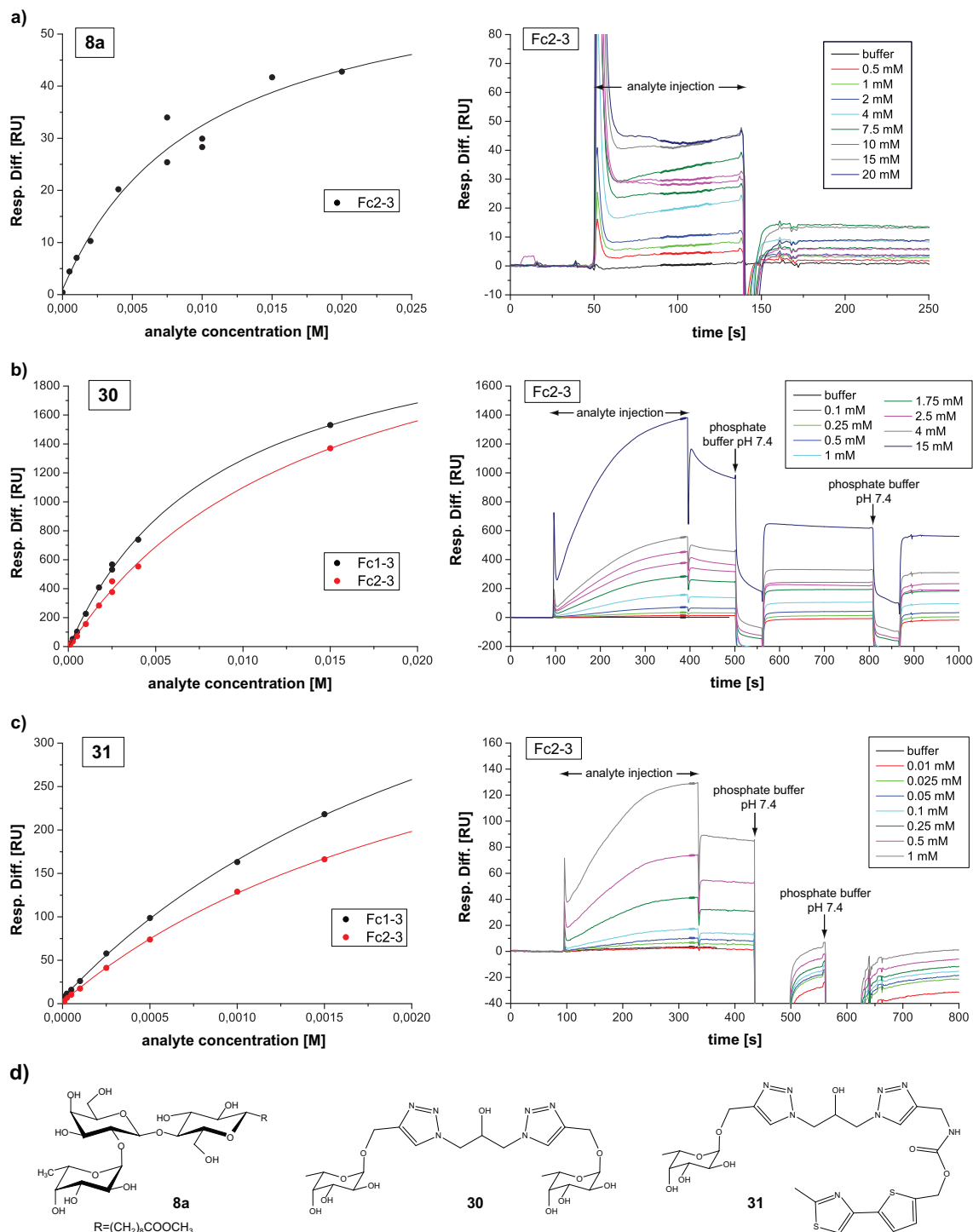


Figure 4.28. SPR experiments with fucosylated compounds. a)-c) (Left) binding curves fitted to a 1:1 Langmuir isotherm (lines) and (right) difference curves (bold curve regions were averaged) for H trisaccharide type 6 (**8a**) (a), difucosylated compound **30** (b) and hetero-divalent compound **31** (c) on sensor chip C covered with 7050 RU (Fc1) and 5260 RU (Fc2) VLPs; reference flow cell: Fc3. d) Structural formulas.

Other regeneration methods (high salt content, high concentrations of L-Fuc) were neither successful (data not shown). Non-linear fitting of the titration curves to a 1:1 Langmuir binding isotherm yielded a  $K_D$  value of 8 to 16 mM for compound **30** (Table 4.10). However, the fitted  $RU_{max}$  values vastly exceeded the theoretical values for a 1:1 binding by factors of 40 to 60. Considering also the form of the sensorgrams, a complex binding behavior of **30** with multiple binding modes is assumed. The inability to regenerate the surface with buffer at pH 7.4 which normally leads to strong weakening of VLP-HBGA interaction (cf. sections 4.7.2 and 4.8.2) indicates, that binding of **30** to immobilized VLPs was mediated by a process different from that of other HBGAs. STD NMR experiments, albeit measured at a different pH, displayed significant saturation transfer only for L-Fuc protons but not for the linker. The nature of **30** binding seen in SPR measurements with immobilized VLPs therefore remains unknown.

Table 4.10. Results from SPR measurements with HBGAs and divalent inhibitors.

Compound	$K_D$ [mM]	$RU_{max}$ [RU]	$R^2/\chi^2$	Chip/ flow cell	Coverage [RU]	Theor. $RU_{max}$
L-fucose	<b>65.9</b> ( $\pm 7.5$ )	47.1 ( $\pm 1.8$ )	0.9908/ 1.60	C/Fc2	5260	14.4
D-galactose	<b>101</b> ( $\pm 38$ )	47.7 ( $\pm 9.5$ )	0.9774/ 2.24	C/Fc2	5260	15.8
D-glucose	<b>4340</b> ( $\pm 38000$ )	1040 ( $\pm 9040$ )	0.9726/ 2.55	C/Fc2	5260	15.8
D-mannose	<b>320</b> ( $\pm 180$ )	115 ( $\pm 50$ )	0.9980/ 0.56	C/Fc2	5260	15.8
H-disaccharide ( <b>3b</b> )	<b>46.4</b> ( $\pm 3.0$ )	162.9 ( $\pm 6.9$ )	0.9995/ 0.24	A/Fc2	3500	26.5
	<b>111.8</b> ( $\pm 13.8$ )	274 ( $\pm 20$ )	0.9968/ 5.53	A/Fc2	3500	26.5
	<b>39.2</b> ( $\pm 2.2$ )	436 ( $\pm 10$ )	0.9986/ 16.0	A/Fc3	7300	55.3
	<b>56.9</b> ( $\pm 2.9$ )	351.5 ( $\pm 8.3$ )	0.9991/ 5.26	A/Fc4	5200	39.4
	<b>58.2</b> ( $\pm 3.2$ )	1108 ( $\pm 36$ )	0.9997/ 13.2	B/Fc2	12000	90.9
H trisaccharide type 6 ( <b>8a</b> )	<b>10.1</b> ( $\pm 4.1$ )	63.4 ( $\pm 10.2$ )	0.9643/ 9.88	C/Fc2	5260	57.7
<b>30</b> (difucosylated)	<b>8.6</b> ( $\pm 0.6$ )	2424 ( $\pm 69$ )	0.9988/ 351	C/Fc1	7050	64.2
	<b>14.3</b> ( $\pm 1.9$ )	2687 ( $\pm 187$ )	0.9968/ 698	C/Fc2	5260	47.9
<b>31</b> (L-Fuc + fragment 160)	<b>2.8</b> ( $\pm 0.3$ )	604 ( $\pm 41$ )	0.9996/ 3.50	C/Fc1	7050	74.8
	<b>2.6</b> ( $\pm 0.2$ )	455 ( $\pm 25$ )	0.9997/ 1.57	C/Fc2	5260	55.8

For the heterodivalent compound **31** a  $K_D$  values of 2.6 to 2.8 mM was obtained which indicates stronger binding compared to all other tested HBGAs (Table 4.10). The theoretical  $RU_{max}$  was exceeded by a factor of  $\sim 8$  suggesting multiple binding sites per VP1. Like for compound **30** significant amounts of substance remained bound after injection stop and

the sensorgram form indicated multiple binding modes. But in contrast to **30**, injection of phosphate buffer pH 7.4 completely removed bound compound **31** and recovered the baseline level suggesting that the observed binding was related to HBGA recognition. For L-Fuc three binding sites per VP1 monomer were implicated from curve fitting. A corresponding factor of eight for compound **31** suggests the existence of yet other binding sites on the VLP surface. This might be related to binding via the fragment moiety 160. Fragment 160 was identified as competitive binder of Ast6139 VLPs (Rademacher, 2008; Rademacher *et al.*, 2011) (see section 1.10). However competitive STD titrations suggested that 160 also binds to sites that are not competed with L-Fuc (cf. Figure 4.21). H-disaccharide **3b** was titrated on sensor chip A with three different VLP coverage rates. In a first titration on Fc2 covered with 3500 RU VLPs, **3b** was measured in triplicate up to 30 mM. For the second and third measurements, a shift of the whole binding curves towards smaller RU values was observed (Figure 7.13 in the appendix). The RU shift was independent from the injected concentration and was seen also for buffer injections. It was thus regarded as an artifact from imperfect curve subtraction. The shifts were cancelled out by global fitting of the three binding isotherms to a single  $K_D$  value but allowing different  $RU_{max}$  values and y-shifts (Figure 7.13). The titration was repeated on all three flow cells of sensor chip A and on sensor chip B with 12000 RU VLPs (Figure 4.29).

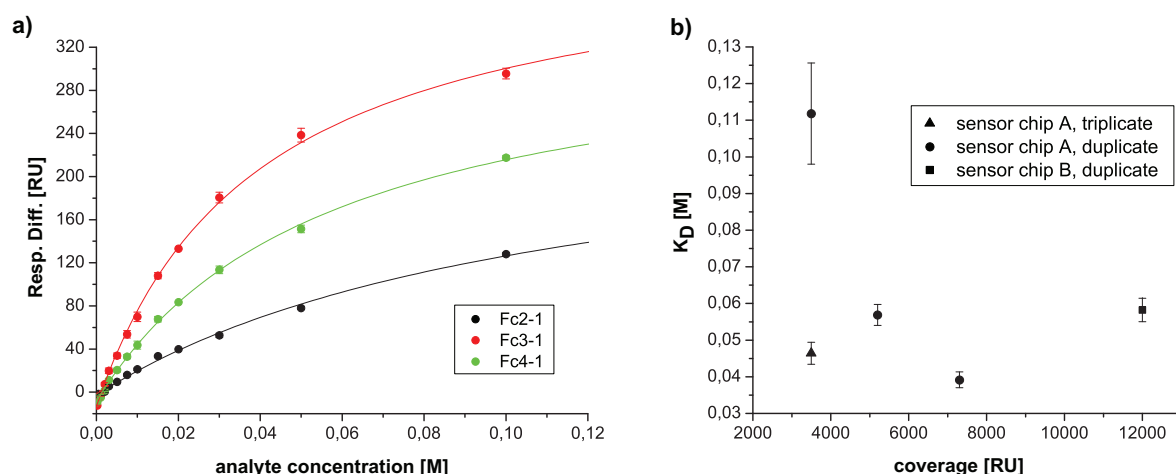


Figure 4.29. SPR experiment of H-disaccharide with immobilized VLPs. a) Binding curves for H disaccharide **3b** on sensor chip A with VLP coverage rates of 3500 RU (Fc2), 7300 RU (Fc3) and 5200 RU (Fc4) from duplicate; lines show curve fittings to a 1:1 Langmuir isotherm (equation 9). b) Determined  $K_D$  value on different flow cells versus VLP coverage.

The results yield a  $K_D$  value of H disaccharide **3b** between 40 to 60 mM independent from the VLP coverage (Figure 4.29 b)). A higher  $K_D$  value determined from the second

measurement on Fc2 of sensor chip A (ca. 110 mM) is regarded as outlier considering the large error (>10%). In addition, a previous titration on this flow cell yielded a lower  $K_D$  (46 mM) indicating that the life time of sensor chips with immobilized VLPs is limited. The results place the affinity of H-disaccharide (40 to 60 mM) between that of L-Fuc (60-70 mM) and H trisaccharide **8a** (8-16 mM). This is reasonable considering the different number of possible carbohydrate-protein interaction. The fitted  $RU_{max}$  is six times higher than the theoretical value suggesting multiple binding sites as seen for compound **31** (factor ~8) and to a smaller extend for L-Fuc (factor ~3).

#### 4.7.2 Investigation of pH and Buffer Dependence

H-disaccharide *O*-5-methoxy-carboxypentyl glycoside (**3b**) was used to probe the pH and buffer dependence of the binding to immobilized Ast6139 VLPs, despite the doubt concerning the exact nature this interaction (*vide supra*). **3b** was diluted in each buffer to a concentration of 10 mM and injected on sensor chip A equilibrated with the same buffer. The results for flow cell 3 with 7300 RU immobilized VLPs are shown in Figure 4.30.

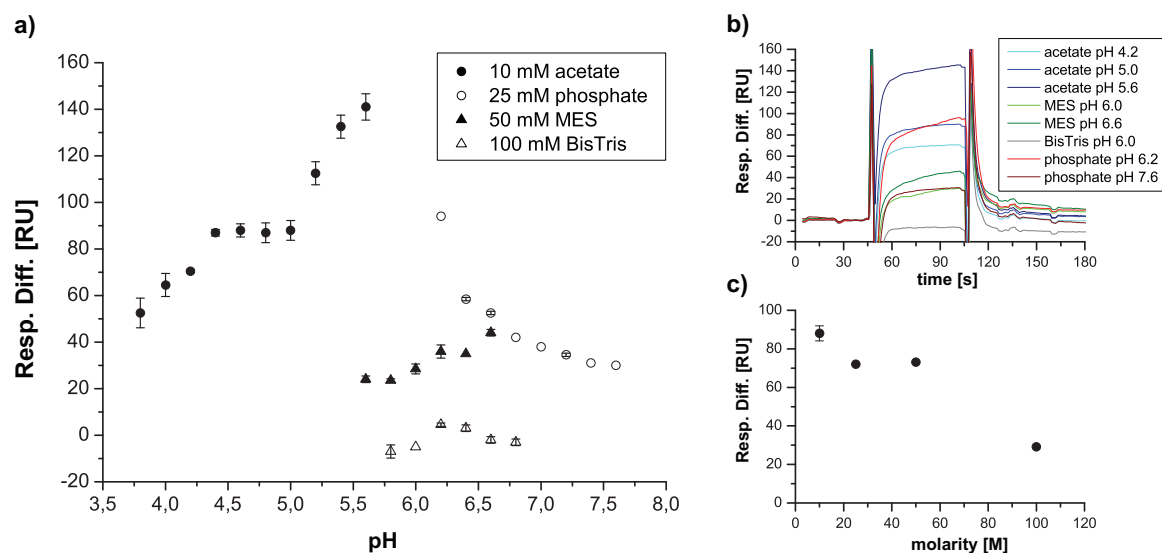


Figure 4.30. Binding of H-disaccharide as a function of pH and buffer. a) Response difference for H disaccharide **3b** injections on Fc3 (7300 RU VLPs) on sensor chip A under various buffering conditions. b) Corresponding difference curves for selected buffering conditions. c) Response difference as a function of the molarity of 10 mM sodium acetate buffer pH 5.0.

The highest responses were reached with 25 mM sodium acetate buffer at pH 5.6. Combining the responses for 10 mM sodium acetate and 25 mM sodium phosphate buffers, a pH optimum for the binding at pH 6 is seen. Acetate and phosphate buffers at exactly



pH 6 were not applied considering the low buffering strength of both buffers at this pH ( $pK_a$  values 4.75 and 7.21, respectively). MES buffer covers this range very well, but only weak responses were seen for H disaccharide binding in this buffer. Additionally, a limited stability was found for VLPs stored in MES buffer (reduction of the response by 30% within one day and by 50% within 12 days, data not shown). For BisTris buffer pH 5.8 to 6.8 the responses were close to zero.

A strong linear dependence of the response on the buffer concentration was found for sodium acetate buffer (Figure 4.30 c)). At 100 mM buffer concentration the response is reduced to one third compared 10 mM concentration. Therefore, the different molarities of the tested buffers may reduce the comparability of the measurements.

### 4.7.3 Experiments with Hits from Virtual Library Screening

Compounds **42**, **43**, **44** and **45** are the four best-ranked hits obtained from *in silico* screening of a virtual library of fucosylated compounds against the HBGA binding site of GII.4 strain VA387 (see section 1.10). Compounds were dissolved at 20 mM concentration in 10 mM sodium acetate buffer pH 5.0 and titrated on sensor chips C and F (Figure 4.31 and Table 4.11). Compound **45** was very poorly soluble and was therefore not measured.

The form of the titration curves for compound **42** was indicative for the presence of multiple binding modes. In addition to fitting to a 1:1 Langmuir isotherm (equation 9) the curves were therefore also fitted to a two-site binding model (equation 10). The latter provided significantly reduced  $\chi^2$  values and a much better visual conformity of the fit with the experimental data (Table 4.11). The two-site model is therefore valid to describe binding of **42** to immobilized VLPs. Measurement on sensor chip C yielded a high affinity component for **42** of 170 to 180  $\mu\text{M}$ , albeit with a high error. The chip surface had to be regenerated by two injections of phosphate buffer pH 7.4 (see Figure 7.16 in the appendix for sensorgrams). On sensor chip F the high affinity component was 240 to 280  $\mu\text{M}$  with a relative error below 10%. Regeneration of the chip surface was not necessary (Figure 4.31). The  $\text{RU}_{\text{max}}$  values for the high affinity components were below the theoretical  $\text{RU}_{\text{max}}$  values for a 1:1 binding to VLPs.

The low affinity components could not be determined accurately since the highest injected concentration was only 5 mM. In case of measurement on sensor chip C, the low affinity component ( $K_{D,2}$ ) had to be kept constant to allow reliable fitting. The  $\chi^2$  and  $R^2$  values

were relatively stable for a wide range of  $K_{D,2}$  from 20 to 500 mM. Table 4.11 shows the fitting results for  $K_{D,2}$  kept constant at 500. In case of measurement on sensor chip F,  $K_{D,2}$  was fitted to 60 to 70 mM. The  $RU_{max}$  values for the low affinity component exceed the theoretical  $RU_{max}$  by far suggesting unspecific binding interaction of the aromatic rings with hydrophobic patches on the VLP surface.

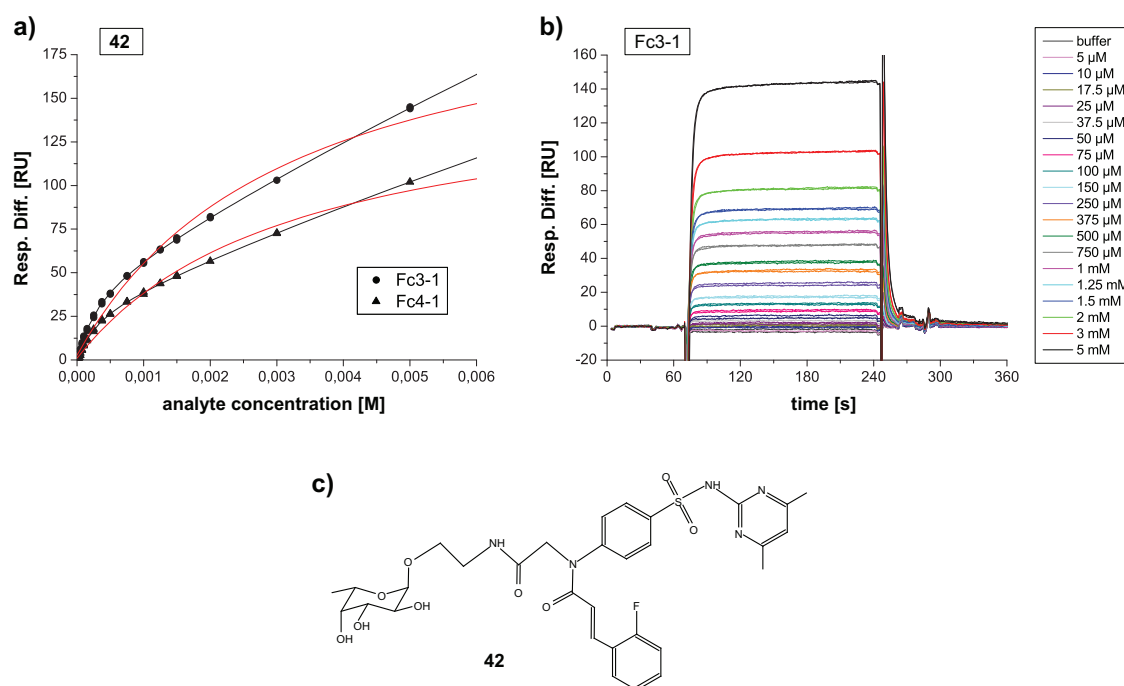


Figure 4.31. SPR experiment with virtual screening hit **42**. a) Binding isotherms for Fc3 (5100 RU VLPs) and Fc4 (3700 RU VLPs) on sensor chip F from duplicate; curve fitting to a 1:1 binding model (red lines, equation 9) and a two-site binding model (black lines, equation 10). b) Difference curves for Fc3; injection of 30  $\mu$ l **42** (flow rate 10  $\mu$ L/min); regeneration was not necessary. c) Structural formula of **42**.

Table 4.11. Results from SPR measurement of virtual screening hit **42**.

$K_{D,1}$ [mM]	$RU_{max,1}$ [RU]	$K_{D,2}$ [mM]	$RU_{max,2}$ [RU]	$R^2/\chi^2$	Chip/ flow cell	Coverage [RU]	Theor. $RU_{max}$
6.3 ( $\pm$ 1.3)	636 ( $\pm$ 100)	–	–	0.9802/ 91.7	C/Fc1	7050	79.2
<b>0.18</b> ( $\pm$ 0.12)	36.3 ( $\pm$ 8.9)	500 ( $\pm$ 0)	28250 ( $\pm$ 1610)	0.9870/ 62.7			
6.5 ( $\pm$ 1.2)	535 ( $\pm$ 75)	–	–	0.9846/ 48.9	C/Fc2	5260	59.1
<b>0.17</b> ( $\pm$ 0.09)	29.3 ( $\pm$ 5.7)	500 ( $\pm$ 0)	23500 ( $\pm$ 1050)	0.9916/ 27.8			
3.2 ( $\pm$ 0.4)	221 ( $\pm$ 13)	–	–	0.9870/ 21.7	F/Fc3	5100	57.3
<b>0.28</b> ( $\pm$ 0.02)	46.7 ( $\pm$ 2.4)	70 ( $\pm$ 48)	1550 ( $\pm$ 940)	0.9997/ 0.60			
3.3 ( $\pm$ 0.4)	159 ( $\pm$ 10)	–	–	0.9857/ 12.1	F/Fc4	3700	41.5
<b>0.24</b> ( $\pm$ 0.02)	31.8 ( $\pm$ 1.5)	60 ( $\pm$ 32)	970 ( $\pm$ 460)	0.9997/ 0.31			

Compounds **43** and **44** did not follow a two-site binding behavior (Figure 4.32 and Figures 7.17 and 7.18 in the appendix).  $K_D$  values of 3.3 mM and ca. 6 mM, respectively, were determined by curve fitting to a 1:1 binding isotherm (Table 4.12). This indicated rather weak binding compared to **42**, but still much stronger binding compared to L-Fuc. For **44** the responses were very small and the relative error was large. The  $RU_{max}$  values were in the range of the theoretical  $RU_{max}$  values for a 1:1 binding to VP1 of VLPs. The attached functional groups may prevent binding of the L-Fuc moieties of **43** and **44** to other sites hypothesized for monosaccharidic L-Fuc.

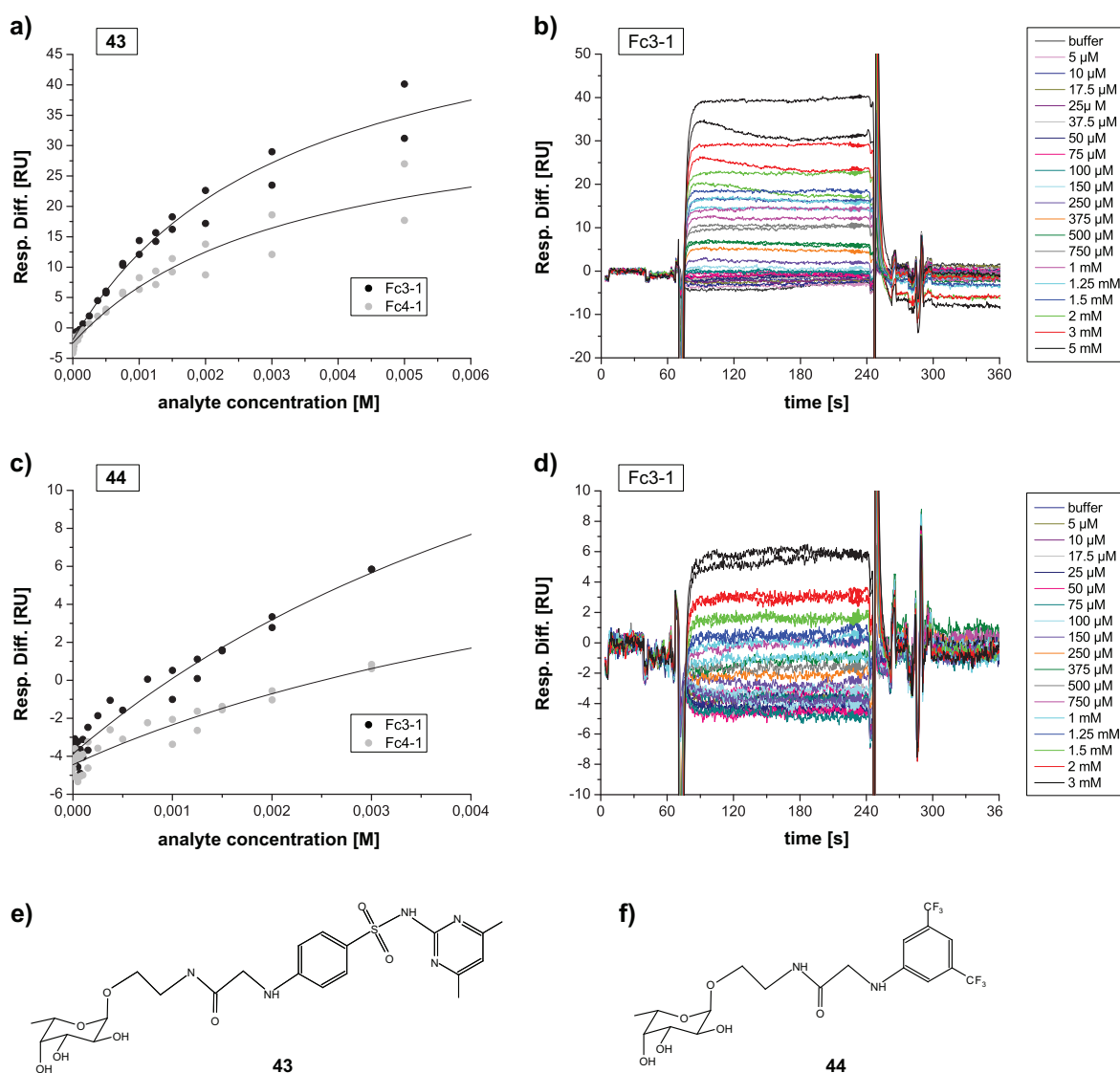


Figure 4.32. SPR experiment with virtual screening hits **43** and **44**. a),c) Binding isotherms for **43** (a) and **44** (c) measured in duplicate on Fc3 (5100 RU VLPs) and Fc4 (3700 RU VLPs) of sensor chip F, curve fitting to a 1:1 binding model (black lines, equation 9). b), d) Difference curves for Fc3 for **43** (b) and **44** (d); injection of 30  $\mu$ l of compound (flow rate 10  $\mu$ L/min); regeneration of the chip surface was not necessary. e),f) Structural formulas.

Measurements of **43** and **44** on sensor chip C yielded much higher  $K_D$  values and the theoretical  $RU_{\max}$  values were by far outreached (cf. Table 7.6). However the experimental errors were very high likely because the sensor chip was already in use for a relative long time (ca. 1 week). The data are therefore not reliable.

Table 4.12. Results from SPR measurement of other virtual screening hits.

Compound	$K_D$ [mM]	$RU_{\max}$ [RU]	$R^2/\chi^2$	Chip/ flow cell	Coverage [RU]	Theor. $RU_{\max}$
<b>43</b>	<b>3.3</b> ( $\pm 0.5$ )	61.1 ( $\pm 4.7$ )	0.9802/ 2.7	F/Fc3	5100	44.7
	<b>3.3</b> ( $\pm 0.8$ )	39.8 ( $\pm 5.0$ )	0.9487/ 3.0	F/Fc4	3700	32.4
<b>44</b>	<b>6.3</b> ( $\pm 2.9$ )	29.7 ( $\pm 10.1$ )	0.9578/ 0.44	F/Fc3	5100	40.5
	<b>6.1</b> ( $\pm 4.6$ )	15.5 ( $\pm 8.4$ )	0.8948/ 0.33	F/Fc4	3700	29.4
<b>45</b>	low solubility/ not determined					

#### 4.7.4 Experiments with Polymeric Inhibitors

Multivalent polyacrylamide-(PAA)-based polymeric inhibitors were synthesized from two different screening approaches against NoV VLPs (see section 1.10). In order to determine affinity constants the polymers were injected on SPR sensor chips covered with Ast6139 VLPs. 10 mM sodium acetate pH 5.0 was used as running buffer

Polymer **34** represents the PAA backbone that was the basis for the synthesis of all other polymeric compounds. Injection on sensor chip F at concentrations from 10 to 200  $\mu\text{M}$  yielded zero or even negative responses (Figure 4.33).

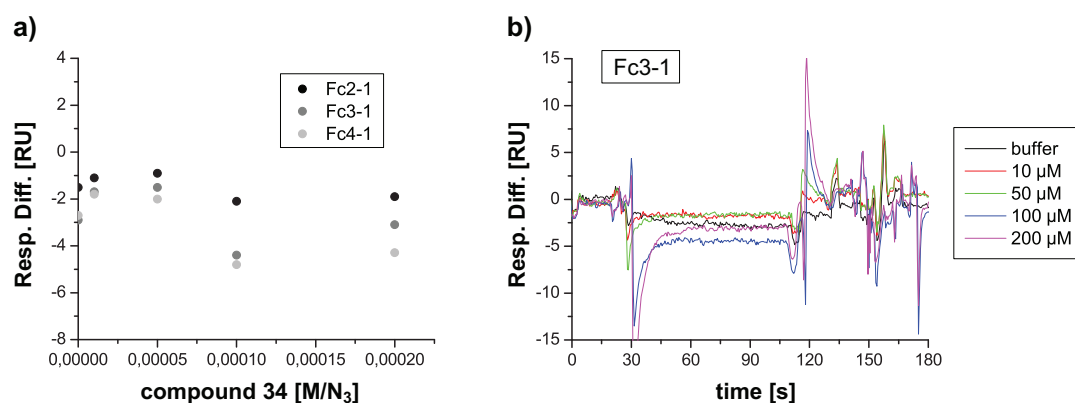


Figure 4.33. SPR experiments with the polyacrylamide backbone **34**. a) Response differences on Fc2 (1600 RU VLPs), Fc3 (5100 RU VLPs) and Fc4 (3700 RU VLPs) of sensor chip F. b) Difference curves for Fc3.

The injections were repeated on other sensor chips with the same result. As a conclusion binding of the PAA polymer **34** to VLPs cannot be detected by the direct SPR assay under the chosen conditions.

Polymer **35** contains  $\alpha$ -L-Fuc covalently linked to the PAA backbone via a triazole linker. Measurement of **35** on sensor chip G furnished a linear response increase in the range of injected concentrations (Figure 4.34). Consequently curve fitting to a one-site binding model yielded very high  $K_D$  and  $RU_{max}$  values with very high errors. Considering the range of injected concentrations up to 750  $\mu$ M (given per monomeric repeating unit) a binding of **35** in the low mM range may not be detected with this assay format.

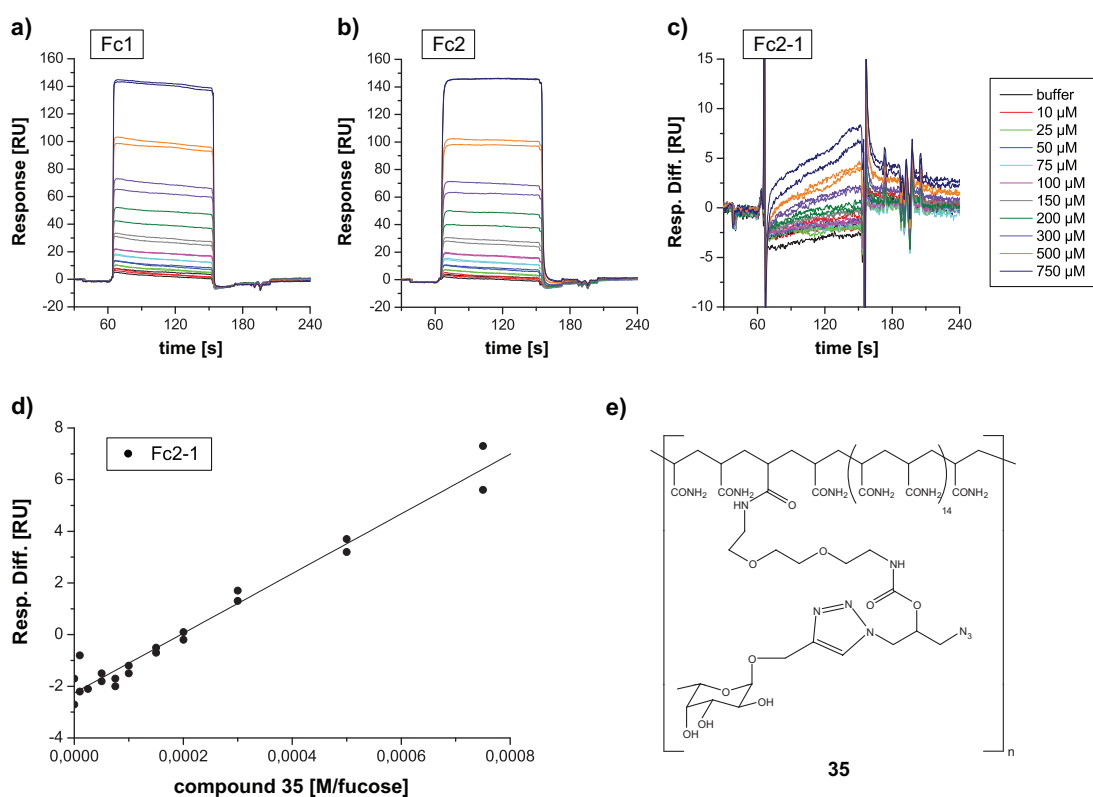


Figure 4.34. SPR experiments with polymeric compound **35** with L-Fuc. a),b) Sensorgrams for Fc1 (reference) and Fc2 (5300 RU VLPs) on sensor chip G. c),d) Difference curves (c) and binding curves (d) for Fc2. e) Structural formula,  $n=20-30$ .

Polymeric compounds containing aromatic fragments obtained from NMR screening (see section 1.10) were tested on sensor chip F with VLP coverage rates of 1600 RU, 5100 RU and 3700 RU on flow cells 2, 3 and 4, respectively. Sensorgrams and binding curves of polymer **36** containing fragment 160 are shown in Figure 4.35. Binding curves for all other polymers are shown in Figure 4.36 while the respective sensorgrams can be found in the appendix (Figures 7.19 to 7.25). All polymers containing a fragment from the Maybridge

library (**36**, **38**, **39**, **40** and **41**) or the virtual screening hit **42** (**46** and **47**) showed saturable binding to immobilized VLPs. Polymers **36**, **38**, **39**, **40** and **41** were injected 1.5 to 2 minutes (flow rate 10  $\mu\text{L}/\text{min}$ ) to reach the equilibrium level. After injection stop the sensorgram was allowed to reach the baseline level by ca. 30 minute waiting time. In contrast, polymers **46** and **47** had to be injected 3 minutes to reach the equilibrium to an acceptable level suggesting slower binding kinetics. In addition, the baseline levels were not recovered in a reasonable time after injection of **46** and **47**. The chip surface had to be recovered by injections of phosphate buffer pH 7.4.

Binding curves of polymeric compounds were subjected to non-linear curve fitting to a 1:1 Langmuir isotherm (results compiled in Table 4.13). Values obtained for the flow cell with the lowest VLP coverage (Fc2, 1600 RU) had very high errors and were hence excluded.

Polymer **36** contains the fragment 160 identified as competitive binder to the HBGA site of Ast6139 VLPs (Rademacher, 2008; Rademacher *et al.*, 2011). Non-linear curve fitting of its binding isotherm yielded a  $K_D$  of 590 to 640  $\mu\text{M}$ .

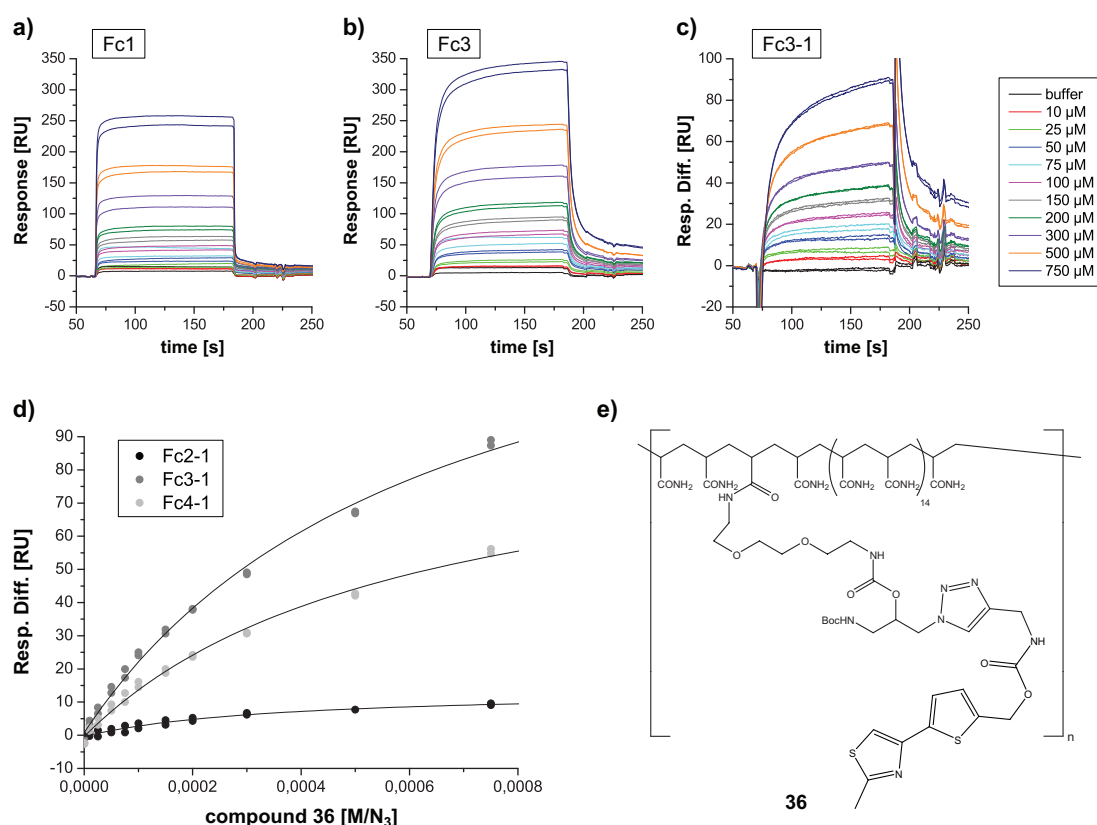


Figure 4.35. SPR experiments with polymeric compound **36** with fragment 160. a),b) Sensorgrams for Fc1 (reference) and Fc3 (5100 RU VLPs) on sensor chip F. c) Difference curves for Fc3. d) Binding curves for Fc2 (1600 RU VLPs), Fc3 (5100 RU VLPs) and Fc4 (3700 RU VLPs); curve fitting to a 1:1 binding model (lines). e) Structural formula,  $n=20-30$ .

Attachment of fragment 160 in polymer **36** in contrast to L-Fuc in polymer **35** therefore led to a significantly increased affinity for binding to immobilized VLPs. Competitive STD titration of the heterodivalent compound **31** containing L-Fuc linked to fragment 160 indicated that fragment 160 also binds to sites that are not displaced by  $\alpha$ -L-Fuc-(1,*O*)-CH<sub>3</sub> (cf. Figure 4.21). The higher affinity of polymer **36** might thus result from binding of fragment 160 to additional sites on the VLPs surface.

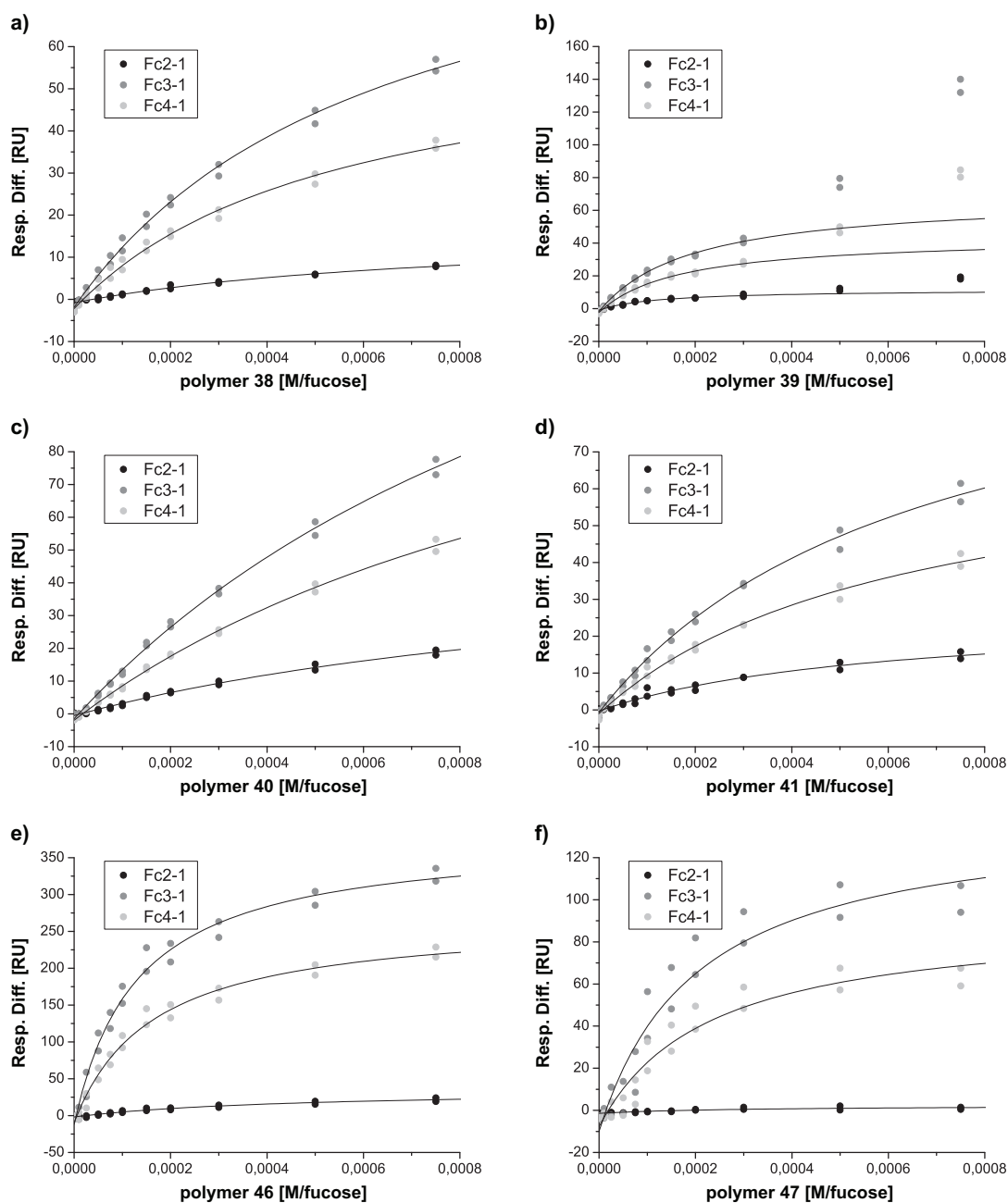


Figure 4.36. SPR experiments with other polymeric compounds. Response differences for polymers **38**, **39**, **40**, **41**, **46** and **47** on Fc2 (1600 RU VLPs), Fc3 (5100 RU VLPs) and Fc4 (3700 RU VLPs) on sensor chip F; curve fitting to a 1:1 binding model (lines); in case of **39** (b) data points above 300  $\mu$ M were ignored.

Polymers **38** to **41** contain ‘adjacent site’ binders from fragment screening in addition to L-Fuc (see section 1.10). The obtained  $K_D$  values were in the  $\mu\text{M}$  and low mM range spanning almost one order of magnitude (Table 4.13). Polymer **39** with fragment 473 is the strongest binder (170 – 190  $\mu\text{M}$ ) followed by **38** (550 – 640  $\mu\text{M}$ ) and **41** (630 – 670  $\mu\text{M}$ ). **40** is the weakest binder (1.3 mM). For **39** a drastic increase of the responses above concentrations of 300  $\mu\text{M}$  was observed that cannot be explained by a two-site binding model (compare Figure 4.31 for a typical curve form of two-site binding). The respective data points were therefore excluded from the fit.

Polymer **46** containing the virtual screening hit **42** displayed the highest affinity of all tested polymers (130 – 160  $\mu\text{M}$ ). Considering the experimental error, polymer **39** with the ‘ILOE’ fragment 473 is almost in the same range. The affinity of **46** given per monomeric repeating unit is not significantly increased compared to the affinity of compound **42** (170 – 280  $\mu\text{M}$ , Table 4.11) which is the functional group of **46**.

Table 4.13. Results from SPR measurement of polymeric inhibitors. The flow cells on sensor chip F were covered with 1600 RU, 5100 RU and 3700 RU VLPs on Fc2, Fc3 and Fc4, respectively.

Polymer	Functionalities	$K_D$ [ $\mu\text{M}$ ]	$\text{RU}_{\text{max}}$ [RU]	$R^2/\chi^2$	Flow cell
<b>36</b>	fragment 160	<b>350</b> ( $\pm 80$ )	14.2 ( $\pm 1.3$ )	0.9621/ 0.44	Fc2
		<b>640</b> ( $\pm 70$ )	158.0 ( $\pm 9.1$ )	0.9944/ 4.6	Fc3
		<b>590</b> ( $\pm 70$ )	97.3 ( $\pm 6.0$ )	0.9926/ 2.5	Fc4
<b>38</b>	L-Fuc + fragment 191	<b>800</b> ( $\pm 140$ )	17.9 ( $\pm 1.8$ )	0.9884/ 0.10	Fc2
		<b>640</b> ( $\pm 70$ )	105.1 ( $\pm 5.7$ )	0.9950/ 1.8	Fc3
		<b>550</b> ( $\pm 70$ )	66.4 ( $\pm 3.9$ )	0.9924/ 1.3	Fc4
<b>39</b>	L-Fuc + fragment 473	<b>130</b> ( $\pm 30$ )	12.6 ( $\pm 1.0$ )	0.9750/ 0.26	Fc2
		<b>190</b> ( $\pm 20$ )	70.4 ( $\pm 3.3$ )	0.9950/ 1.2	Fc3
		<b>170</b> ( $\pm 20$ )	46.4 ( $\pm 2.2$ )	0.9934/ 0.76	Fc4
<b>40</b>	L-Fuc + fragment 151	<b>1330</b> ( $\pm 280$ )	53.7 ( $\pm 7.5$ )	0.9914/ 0.36	Fc2
		<b>1320</b> ( $\pm 150$ )	211.4 ( $\pm 16.3$ )	0.9973/ 1.8	Fc3
		<b>1280</b> ( $\pm 130$ )	144.3 ( $\pm 9.8$ )	0.9978/ 0.71	Fc4
<b>41</b>	L-Fuc + fragment 231	<b>580</b> ( $\pm 130$ )	26.7 ( $\pm 3.1$ )	0.9733/ 0.72	Fc2
		<b>670</b> ( $\pm 80$ )	112.0 ( $\pm 6.9$ )	0.9940/ 2.4	Fc3
		<b>630</b> ( $\pm 70$ )	75.5 ( $\pm 4.5$ )	0.9936/ 1.3	Fc4
<b>46</b>	<b>42</b>	<b>460</b> ( $\pm 130$ )	37.8 ( $\pm 4.6$ )	0.9569/ 2.9	Fc2
		<b>130</b> ( $\pm 20$ )	391.8 ( $\pm 13.3$ )	0.9849/ 218.5	Fc3
		<b>160</b> ( $\pm 20$ )	277.9 ( $\pm 10.4$ )	0.9847/ 102.4	Fc4
<b>47</b>	<b>42</b>	<b>310</b> ( $\pm 170$ )	3.9 ( $\pm 0.8$ )	0.7978/ 0.23	Fc2
		<b>200</b> ( $\pm 60$ )	151.0 ( $\pm 13.7$ )	0.9311/ 130.2	Fc3
		<b>230</b> ( $\pm 60$ )	99.4 ( $\pm 9.4$ )	0.9329/ 51.9	Fc4



Polymer **47** that differs from **46** only in the linker assembly was only poorly soluble. The variability in the double measurement was very high with the second injections showing lower responses. It is assumed that not all of the substance was dissolved and/or that the polymer partly sedimented during the measurement. In that case the fitted  $K_D$  values are false too high.

The results from titration of polymeric compounds were evaluated for the occurrence of mass transport limitation. This effect refers to the maximum rate at which the analyte can be transferred from the laminar flow phase of the constantly injected buffer to the surface and *vice versa*. It is frequently observed for large ligands with slower diffusion and can alter the influence binding parameters. In particular, the apparent association and dissociation rates on densely covered flow cells will be limited by mass transport leading to an apparent increase of the affinity. For all titrated polymers no linear dependence of the obtained  $K_D$  value above the experimental error was observed (cf. Table 4.13). Mass transport was hence not a problem at the applied flow rate of 10  $\mu\text{L}/\text{min}$ .

For all polymers,  $K_D$  values obtained for Fc2 on sensor chip F covered with 1600 RU VLPs had very large errors ( $>20\%$ ). Evaluation of the observed response difference versus VLP coverage tested for polymer **38** suggested that at least 3000 to 4000 RU VLPs should be immobilized on a sensor chip to obtained reliable results (Figure 4.37).

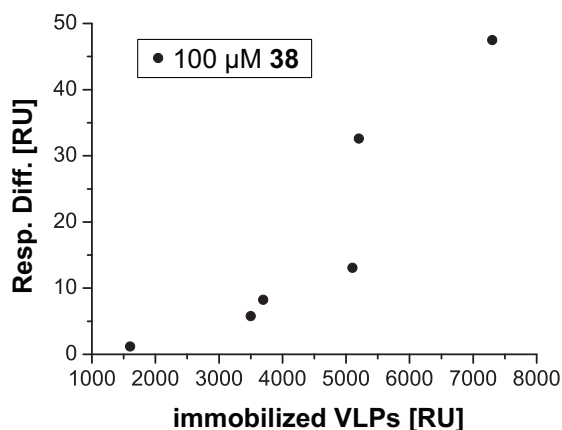


Figure 4.37. SPR response for polymeric compound as a function of VLP coverage. Polymer **38** with L-Fuc and 'ILOE' fragment 191 at a concentration of 100  $\mu\text{M}$  was injected (10 to 15  $\mu\text{L}$ ) on Fc2 (3500 RU), Fc3 (7300 RU) and Fc4 (5200 RU) of sensor chip A and Fc2 (1600 RU), Fc3 (5100 RU) and Fc4 (3700 RU) on sensor chip F.

Polymeric compound **40** was also titrated on sensor chip D with immobilized VLPs as well as immobilized GTB enzyme (Figure 4.38). Non-linear curve fitting of the binding curve for VLP binding yields a  $K_D$  value of 1.4 mM ( $\pm 0.2$  mM) which is in the range of previous measurements of **40** (Table 4.13). The fitted  $RU_{max}$  value is 175 RU ( $\pm 19$  RU). In contrast, the responses for binding to immobilized GTB showed a linear increase with the injected concentrations of **40**. Consequently the fitted  $K_D$  value was very large above 1 M and assigned to unspecific binding. L-Fuc was not identified as a binder for GTB (unpublished results). Likewise, NMR screening of the Maybridge library against GTB did not yield fragment 473 as hit (Rademacher *et al.*, 2011). The observed response may thus be related to unspecific interaction of the PAA backbone with GTB.

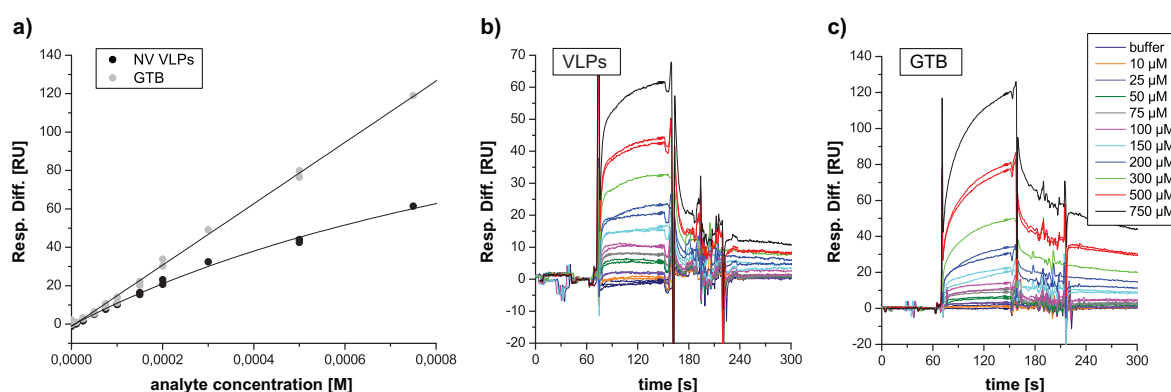


Figure 4.38. Binding of polymeric compound to VLPs and GTB. a) Response differences for injections of polymer **40** (contains L-Fuc and 'ILOE' fragment 151) on Fc4 (5370 RU VLPs) and Fc2 (4200 RU GTB) on sensor chip D; curve fitting to a 1:1 binding model (lines). b),c) Corresponding difference curves.

## 4.8 Competitive SPR Experiments

In a competitive assay format HBGA fragments conjugated to a PAA backbone (section 4.8.1) or to BSA as carrier protein (section 4.8.2 ) were immobilized on SPR sensor chips. Ast6139 VLPs were in the mobile phase. Competition experiments furnished  $IC_{50}$  values of co-injected HBGA and inhibitors that can be compared on a qualitative level

### 4.8.1 Measurements on PAA Sugar Conjugates

Biotinylated PAA sugar conjugates were captured with Neutravidin on C1 sensor chips. No binding of VLPs was observed in phosphate buffer pH 7.0 (Rademacher *et al.*, 2008). 50 mM MES pH 6.0 provided high responses and was therefore chosen as running buffer. VLP dilutions in running buffer were prepared directly before the measurement since VLPs had a limited stability under these conditions (50% signal loss over ten days storage at 4°C). Binding of VLPs to immobilized PAA sugars was concentration dependent (Figure 4.39 and Figure 7.27 in the appendix).

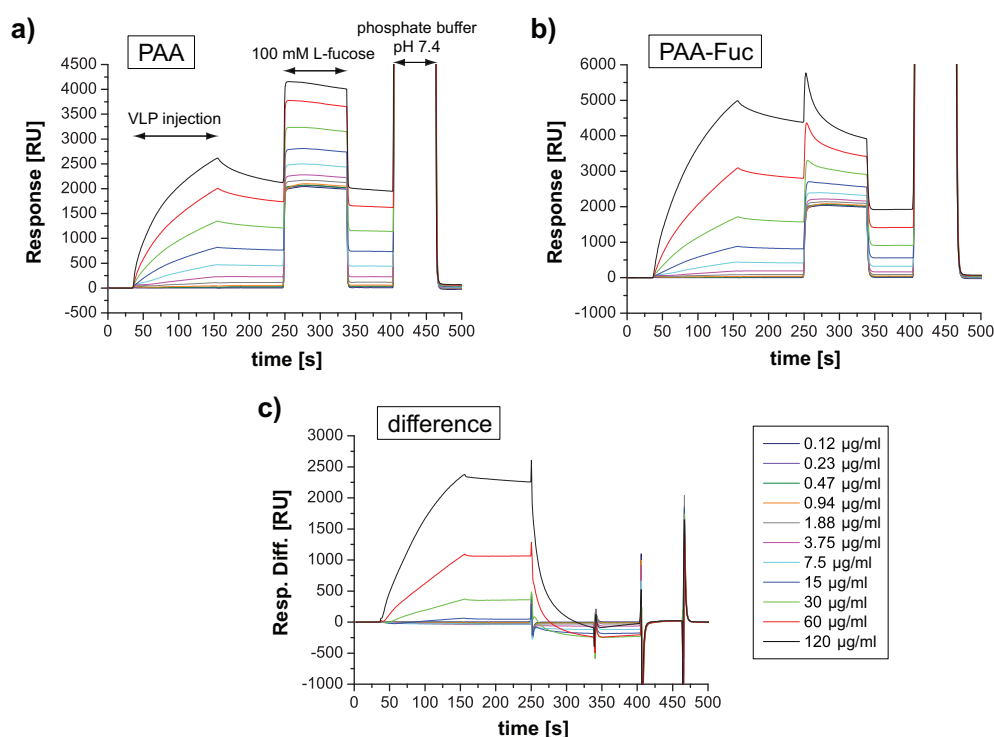


Figure 4.39. Concentration-dependent VLP binding to PAA-fucose. a),b) Sensorgrams for injection of 20 µL VLPs at increasing concentrations (flow rate 10 µL/min) on a C1 chip covered with 230 RU PAA on the reference flow cell (a) and 210 RU PAA-Fuc and 110 RU PAA on the second flow cell (b). c) Difference curves for the flow cell with PAA-Fuc.

The response on the reference flow cell with PAA is very high. In fact, only at high injected VLP concentrations above 15  $\mu\text{g/mL}$  positive difference responses were obtained for PAA-Fuc (Figure 4.39 c)). Injection of L-Fuc removed a part of the VLPs from the flow cell with PAA-fucose, but not from the reference flow cell with PAA. In the difference curves the baseline level was recovered after L-Fuc injection. The remaining bound VLPs are therefore regarded as background response from unspecific binding to PAA independent from HBGA recognition.

In a published work (Rademacher *et al.*, 2011) competition experiments with Ast6139 VLPs and polymeric compounds **35** and **37** on immobilized PAA-Fuc were presented. A C1 chip was covered with 151 RU PAA on the reference flow cell and 90 RU PAA-Fuc on the second flow cell. Constant concentrations of VLPs were incubated with increasing concentrations of polymers for 2 h at room temperature. The mixtures were injected and the equilibrium responses were plotted against the polymer concentration (given per monomeric repeating unit) (Figure 4.40). Non-linear curve fitting of the difference curves for PAA-Fuc yielded  $\text{IC}_{50}$  values of 240  $\mu\text{M}$  for **35** (containing Fuc) and 0.9  $\mu\text{M}$  for **37** (containing Fuc and fragment 160) (Table 4.14). For both polymers the absolute responses showed drastic increase above ca. 20  $\mu\text{M}$  that likely originates from agglomeration of polymers. The respective data points were excluded from the curve fitting and are not shown in Figure 4.40.

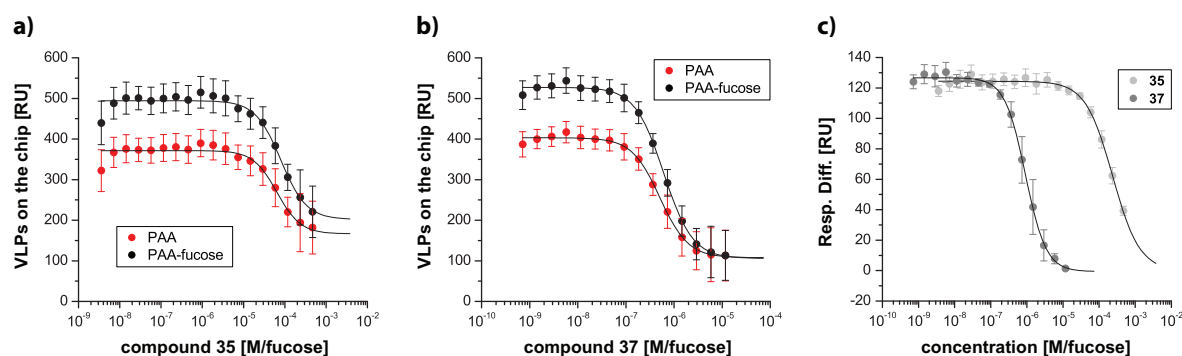


Figure 4.40. Competitive SPR experiments with polymers **35** and **37** on PAA-Fuc. a),b) Absolute responses for injections of 15  $\mu\text{g/mL}$  VLPs with increasing concentrations of **35** (a) and **37** (b) on immobilized PAA (red, reference) and PAA-Fuc (black). c) Response differences after reference subtraction; lines show curve fitting to equation 11 (Table 4.14).

A second C1 sensor chip was covered with 230 RU PAA on the Fc1 (reference), 210 RU PAA-Fuc on Fc2, 220 RU PAA-H-disaccharide on Fc3 and 210 RU PAA-B trisaccharide on Fc4. Polymeric compounds **38**, **39**, **40** and **41** as well as the PAA backbone **34** were

tested on this sensor chip for their ability to inhibit VLP binding to the chip surface (Figure 4.41). All polymers except **34** displayed inhibition of VLP binding that could be fitted to  $IC_{50}$  values in the  $\mu M$  range (Table 4.14). However, curve fitting for the reference flow cell with PAA provided very similar  $IC_{50}$  values compared to the flow cells with PAA sugar conjugates (see Figure 7.28 and Table 7.7 in the appendix) as in case of polymers **35** and **37**. In contrast to **35** and **37**, the difference curves for polymers **38**, **39**, **40** and **41** did not exhibit a typical sigmoid form. Instead, an initial decrease in the response was seen for nM concentrations. At ca.  $1 \mu M$  a ‘peak’ of the response was observed followed by final strong decrease down to zero binding at further increased concentrations.

The titration curves for the backbone **34** showed a decrease of VLP binding by ca. 30% at nM concentrations. This suggested an unspecific inhibitory effect of the PAA backbone that also occurred for the other polymers. But a strong inhibition of VLP binding with  $IC_{50}$  values in the  $\mu M$  range was only observed for polymers with additional functional groups. A small inhibitory effect was seen for **34** at very high concentrations and is probably due to unspecific VLP-PAA complex formation.

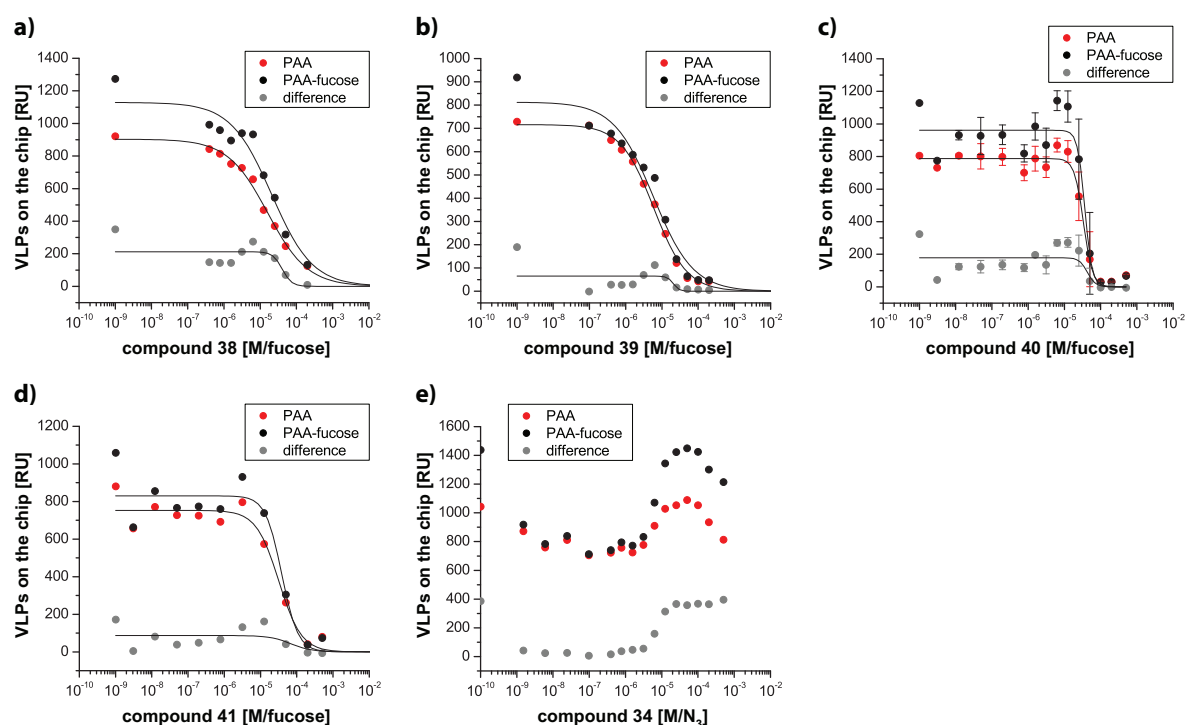


Figure 4.41. Competitive SPR experiments with other polymers on PAA-Fuc. Absolute responses for injections of  $15 \mu g/mL$  VLPs with increasing concentrations of polymer on immobilized PAA (red, reference) and PAA-Fuc (black) and response differences for PAA-Fuc after reference subtraction (grey); lines show curve fitting to equation 11 (Table 4.14); the first points represent injections of VLPs without polymer.

The polymeric compound **35** containing L-Fuc and fragment 160 was also measured on the same sensor chip as polymers **34**, **38**, **39**, **40** and **41** (curves not shown). The fitted  $IC_{50}$  value was  $4.0\ \mu\text{M}$  ( $\pm 0.7\ \mu\text{M}$ ) and thereby one order of magnitude lower than determined on the first sensor chip. However the low number of six data points reduced the reliability of the measurement. The data are therefore not included in the following table.

*Table 4.14. Competitive SPR measurements with polymers on PAA-fucose.  $IC_{50}$  values are given per monomeric repeating unit. Polymers **35** and **37** were measured on a sensor chip covered with 151 RU PAA and 90 RU PAA-Fuc. Other polymers were measured on a chip covered with 230 RU PAA and 210 RU PAA-Fuc.*

Polymer	Functionalities	$IC_{50}$ (PAA)	$IC_{50}$ (PAA-Fuc)	$IC_{50}$ (difference)
<b>34</b>	PAA backbone	no inhibition curve	–	–
<b>35</b>	L-Fuc	<b><math>60\ \mu\text{M}</math></b> ( $\pm 20\ \mu\text{M}$ )	<b><math>80\ \mu\text{M}</math></b> ( $\pm 30\ \mu\text{M}$ )	<b><math>240\ \mu\text{M}</math></b> ( $\pm 10\ \mu\text{M}$ )
<b>37</b>	L-Fuc + fragment 160	<b><math>0.51\ \mu\text{M}</math></b> ( $\pm 0.03\ \mu\text{M}$ )	<b><math>0.61\ \mu\text{M}</math></b> ( $\pm 0.03\ \mu\text{M}$ )	<b><math>0.91\ \mu\text{M}</math></b> ( $\pm 0.04\ \mu\text{M}$ )
<b>38</b>	L-Fuc + fragment 191	<b><math>20\ \mu\text{M}</math></b> ( $\pm 1.7\ \mu\text{M}$ )	<b><math>20\ \mu\text{M}</math></b> ( $\pm 6.5\ \mu\text{M}$ )	<b><math>40\ \mu\text{M}</math></b> ( $\pm 20\ \mu\text{M}$ )
<b>39</b>	L-Fuc + fragment 473	<b><math>5.9\ \mu\text{M}</math></b> ( $\pm 0.5\ \mu\text{M}$ )	<b><math>5.7\ \mu\text{M}</math></b> ( $\pm 1.6\ \mu\text{M}$ )	<b><math>20\ \mu\text{M}</math></b> ( $\pm 20\ \mu\text{M}$ )
<b>40</b>	L-Fuc + fragment 151	<b><math>30\ \mu\text{M}</math></b> ( $\pm 2.6\ \mu\text{M}$ )	<b><math>40\ \mu\text{M}</math></b> ( $\pm 5.5\ \mu\text{M}$ )	<b><math>40\ \mu\text{M}</math></b> ( $\pm 20\ \mu\text{M}$ )
<b>41</b>	L-Fuc + fragment 231	<b><math>30\ \mu\text{M}</math></b> ( $\pm 6.5\ \mu\text{M}$ )	<b><math>40\ \mu\text{M}</math></b> ( $\pm 10\ \mu\text{M}$ )	<b><math>60\ \mu\text{M}</math></b> ( $\pm 80\ \mu\text{M}$ )

#### 4.8.2 Measurements on BSA Sugar Conjugates

As an alternative to PAA sugar conjugates, the competitive SPR assay was also accomplished with BSA neoglycoconjugates. Binding of Ast6139 VLPs to BSA sugar conjugates was observed in phosphate buffer pH 6.2 as well as acetate buffer pH 5.0 (Figure 4.42). The VLPs specifically bound to BSA conjugates with Fuc moieties, i.e. with H trisaccharide type 2 or type 6 but not with LacNAc (type 2 precursor disaccharide) as it is expected from the HBGA specificity determined with STD NMR (see sections 4.2.1). The response of bound VLPs was nearly linear dependent on the injected VLP concentration in the tested range from 3.75 to 30  $\mu\text{g/mL}$ . It increased slightly for flow rates below 15  $\mu\text{L/min}$  likely due to mass transport limitations (data not shown). The response was also dependent on the coverage with BSA conjugate. In case of BSA-H type 2 conjugate a minimum coverage of ca. 2000 RU was required for a positive response in phosphate buffer pH 6.2. In contrast to PAA conjugates, nearly no binding occurred to the reference flow cell covered with BSA. This allows analysis of binding without a strong background response overlaying the specific interaction.

After injection stop, bound VLPs dissociated only very slowly indicating a strong avidity to the multivalent surface. Regeneration with phosphate buffer at pH of 7.6 was able to remove bound VLPs completely. High concentrations of L-Fuc efficiently removed bound VLPs in phosphate buffer pH 6.2 but not in acetate buffer pH 5.0 suggesting different binding modes for these two buffering conditions.

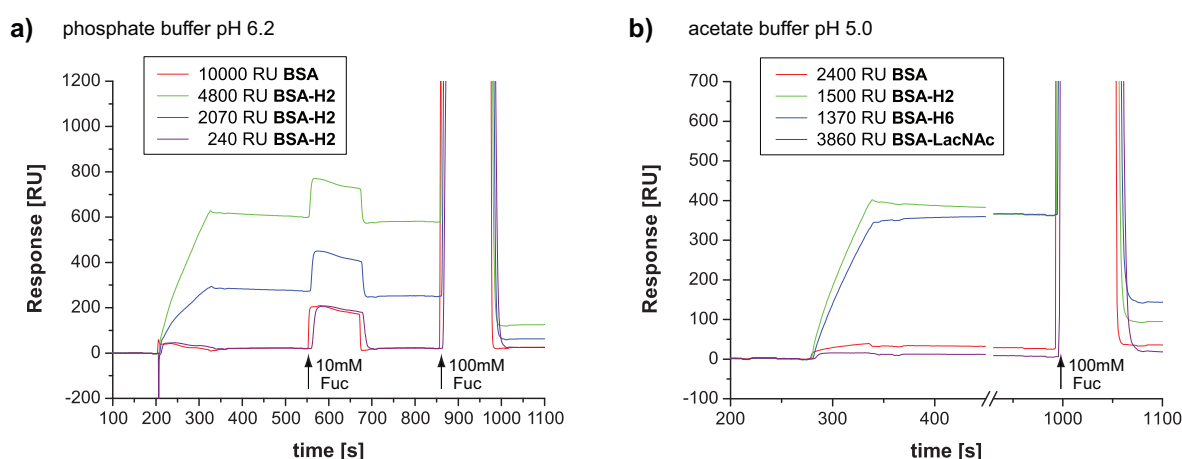


Figure 4.42. Responses of VLP injection on BSA sugar conjugates. a) Injection of 15  $\mu\text{g/mL}$  VLPs (10  $\mu\text{L}$ , flow 5  $\mu\text{L/min}$ ) on three different amounts of BSA-H type 2 conjugate (all flow cells blocked with BSA) in phosphate buffer pH 6.2. b) Injection of 15  $\mu\text{g/mL}$  VLPs (10  $\mu\text{L}$ , flow 10  $\mu\text{L/min}$ )

Furthermore a pH profile for VLP binding to BSA-H type 2 was determined. Identical amounts of VLPs were injected in acetate buffer pH 5.0 followed by injection of different buffers from pH 3.8 to 7.2 (Figure 4.43). Binding at acidic pH was relatively stable, while phosphate buffer above pH 6.4 removed large fractions of bound VLPs. An optimum around pH 6 was found confirming previous results from competitive binding assays with immobilized PAA sugars (Rademacher, 2008) and direct binding assays with immobilized VLPs (see section 4.7.2).

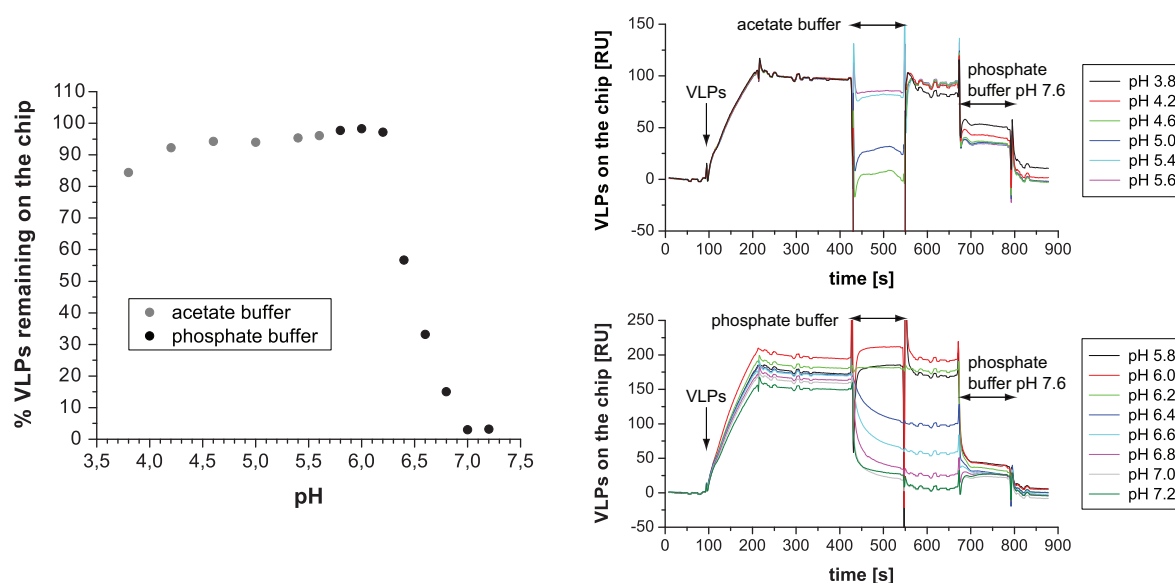


Figure 4.43. pH profile of VLP binding to BSA sugar conjugates. (Left) ratio of bound VLPs (RU after reference subtraction) after and before buffer injection on a flow cell covered with 2070 RU BSA-H2 and blocked with BSA. (Right) corresponding sensorgrams.

Competitive titration experiments with monovalent carbohydrates were conducted in phosphate buffer pH 6.2 in two different ways (Figure 4.44). In the first assay format identical amounts of VLPs were injected followed by injection of increasing amounts of L-Fuc ('sequential injection'). From monitoring of the amount of removed VLPs (in %) an  $IC_{50}$  value for L-Fuc of 30 to 40 mM was derived (Table 4.15). In the second assay, VLPs were pre-mixed with L-Fuc and then co-injected. The  $IC_{50}$  values derived in this way were lower than for the first assay. One source of error in the co-injection assay is the limited stability of VLPs in the buffer. This can be seen from a continuous reduction of bound VLPs during the course of the first assay (top left in Figure 4.44). In the sequential assay format this reduction can be cancelled out by monitoring the relative amount of VLPs removed by L-Fuc injection.



The sequential assay format was repeated in acetate buffer pH 5.0 and delivered an  $IC_{50}$  value for L-Fuc similar to that in phosphate buffer pH 6.2 (Table 4.15, curves not shown). The  $IC_{50}$  value of D-Gal was roughly estimated to be ca. three times higher (ca 60 mM) than that of L-Fuc in the sequential assay in acetate buffer pH 5.0 (data not shown).

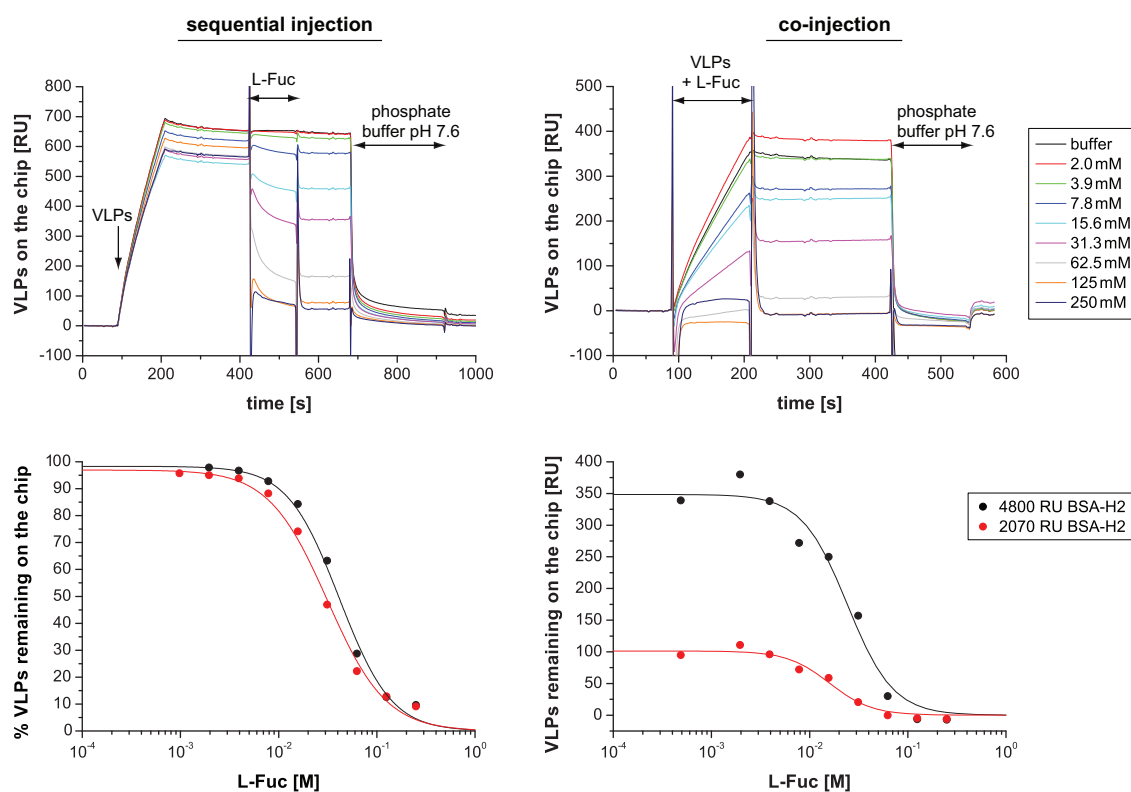


Figure 4.44. Competitive SPR experiments with VLPs with L-Fuc. Sensorgrams (top panel) and inhibition curves (bottom panel) for sequential injection of VLPs and L-Fuc (left) and for co-injection of pre-mixed VLPs and L-Fuc (right).

Table 4.15. Competitive SPR measurements on BSA-H2 conjugate.

Coverage	Buffer	$IC_{50}$ (L-Fuc)	Hill slope	$R^2/\chi^2$
<b>sequential injection</b>				
4800 RU BSA-H2	phosphate pH 6.2	41.7 mM ( $\pm$ 2.2 mM)	1.78	0.9957/ 8.2*10 <sup>-4</sup>
2070 RU BSA-H2	phosphate pH 6.2	31.4 mM ( $\pm$ 1.7 mM)	1.55	0.9958/ 7.4*10 <sup>-4</sup>
<b>co-injection</b>				
4800 RU BSA-H2	phosphate pH 6.2	24.3 mM ( $\pm$ 3.4 mM)	1.88	0.9772/ 740
2070 RU BSA-H2	phosphate pH 6.2	15.9 mM ( $\pm$ 2.4 mM)	2.03	0.9755/ 74
1500 RU BSA-H2	acetate pH 5.0	17.7 mM ( $\pm$ 4.1 mM)	1.47	0.9479/ 205



#### 4.9 Hemagglutination Assays

The inhibitory efficiency of PAA-based prototype inhibitors on HBGA binding to Ast6139 VLPs was determined in a third and most closely biological assay. NoV VLPs can agglutinate red blood cells (RBCs) via binding to HBGAs in the cell membrane of RBCs (Hutson *et al.*, 2003). A measure for the strength of this so-called hemagglutination is the titer characteristic for a certain VLP preparation. The titer is the lowest concentration of VLPs that still has the capability to agglutinate RBCs. For a 1.5 mg/mL preparation of Ast6139 VLP in PBS pH 7.2 the titer of hemagglutination was determined (Figure 4.45). For evaluation of specificity of VLP inhibition by polymeric inhibitors, a preparation of RHDV VLPs (5 mg/mL in PBS pH 7.2) was also included in the testing. The difference between hemagglutination and sedimentation of RBCs is clearly seen in Figure 4.45. Titers of hemagglutination were 400,000 for Ast6139 VLPs and 4,000,000 for RHDV VLPs.

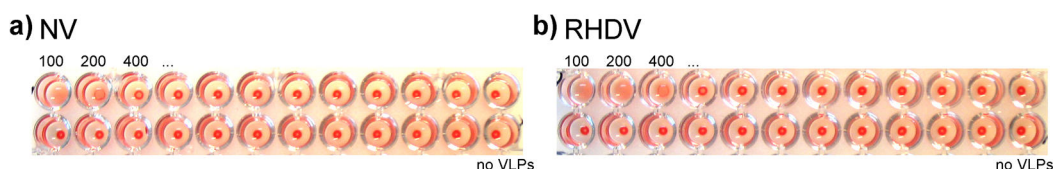


Figure 4.45. Determination of titer of hemagglutination of VLP samples. a) Hemagglutination assay with Ast6139 VLPs (1:2000 predilution) in log2 steps; numbers indicate dilution factors; hemagglutination in the first two wells corresponds to titer  $2000 \times 200 = 400,000$ . b) Hemagglutination assay with RHDV VLPs (1:10,000 predilution) in log2 steps; hemagglutination in first three wells corresponds to titer  $10,000 \times 400 = 4,000,000$ .

In the next step, serial dilutions of polymeric inhibitors were incubated with constant amounts of VLPs and RBCs to determine their inhibitory efficiencies (Figure 4.46 and Table 4.16). Binding of polymers to VLPs prevents binding to and thereby agglutination of RBCs. The polymers were allowed to preincubate with the VLPs for half an hour before addition of RBCs. The titer, i.e. the highest polymer concentration that still has the capacity to inhibit hemagglutination by VLPs, serves as a measure for the inhibitory efficiency of the polymers. For polymeric compounds **35** (containing L-Fuc) and **37** (containing L-Fuc and fragment 160) titers of 125  $\mu\text{M}$  and 3.9  $\mu\text{M}$ , respectively, were determined. These values are in the same range as  $\text{IC}_{50}$  values obtained from competitive SPR experiments with immobilized PAA sugars (80  $\mu\text{M}$  and 0.6  $\mu\text{M}$ , respectively, Table 4.14). Similar to the SPR experiments, addition of fragment 160 to polymer **35** yielding **37** led to significant increase of inhibition efficiency by almost two orders of magnitude (i.e. factor 32 or five dilution steps). It has to be mentioned that the constant dilution factor of two

provides only ‘quantized’ titers as measure for inhibitory efficiency. Polymers **38**, **39**, **40** and **41** containing ‘adjacent site’ fragments had titers from 244 nM to 2  $\mu$ M indicating slightly better inhibition of VLPs than **37**. The ranking of these titers is different from that obtained from competitive STD titrations (Table 4.8) and direct and competitive SPR titrations (Table 4.13 and Table 4.14). However, titers for these polymers from hemagglutination assays were relatively close (only three dilution steps or factor eight). The experimental error of hemagglutination assays is also regarded to be very high.

Polymer **36** containing only fragment 160 displayed a titer of 488 nM suggesting a stronger inhibition of VLPs compared to **37** fragment 160 and L-Fuc. Also considering the high titer of **35** (only L-Fuc), the influence of L-Fuc on inhibition of VLPs in this assay is regarded to be minor. Interestingly the PAA backbone **34** showed inhibition of hemagglutination at  $\mu$ M concentrations in the range of other polymers. The spots of sedimented RBCs were relatively broad indicating incomplete inhibition. Unspecific inhibition of VLPs at high  $\mu$ M concentrations of **34** was also seen in competitive SPR assays (Figure 4.41 e)). In contrast, direct SPR assays, that detect analyte binding under continuous flow, showed no binding of **34** to immobilized VLPs (Figure 4.33). This suggests that incubation time is critical for unspecific interaction.

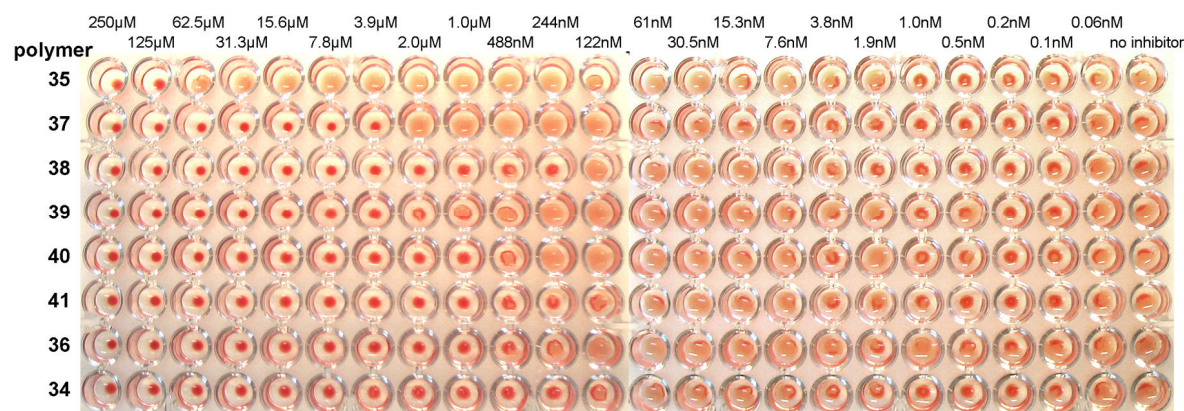


Figure 4.46. Hemagglutination assay with polymers and Ast6139 VLPs. Polymer concentrations are given for the samples containing VLPs and polymer; VLPs were diluted by a factor of 4000 corresponding to 100 units of hemagglutination (ratio of the titer of hemagglutination and the dilution factor of the VLPs); after ½ h RBCs were added resulting in further 1:2 dilution.

Moreover, all polymers including **34** also displayed a low degree of RBC sedimentation at low nM concentrations. This is in agreement with observations from competitive SPR measurements in which preincubation with nM concentrations of **34** led to ~30% inhibition of VLP binding to immobilized PAA-Fuc (Figure 4.41 e)). From this observation a second

inhibition mechanism is suggested that involves unspecific interaction of the PAA backbone with VLPs at nM concentrations. This inhibition mechanism is time dependent probably due to a slow complex formation that finally leads to precipitation.

Hemagglutination assays of polymers with RHDV VLPs yielded titers between 3.9 and 7.8  $\mu\text{M}$  for all polymers except **35** with a slightly higher titer of 62.5  $\mu\text{M}$  (Figure 4.47). In contrast to the experiments with Ast6139 VLPs, no sedimentation of RBCs is seen for concentrations below 100 nM (data not shown). A rather unspecific inhibition of RHDV VLPs by polymeric compounds is suggested. This is plausible considering that the fragments attached to the polymers were derived from NMR screening against Ast6139 VLPs. Similar to Ast6139 VLPs, RHDV recognizes L-Fuc and ABH antigens (Rademacher *et al.*, 2008). But attachment of L-Fuc to polymers seems to have no increasing effect on the inhibition (compare **36** and **37**).

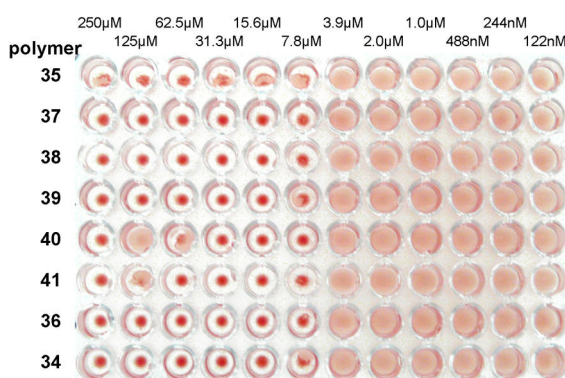


Figure 4.47. Hemagglutination assay with polymers and RHDV VLPs. The VLPs were diluted by a factor of 20000 corresponding to 200 units of hemagglutination.

Table 4.16. Results of hemagglutination assays with VLPs and polymeric inhibitors. Titers are defined as the lowest concentration of polymer that still has the capacity to inhibit agglutination of RBCs by VLPs.

Polymer	Functionalities	Titer (NoV VLPs)	Titer (RHDV VLPs)
<b>34</b>	PAA backbone	0.2 $\mu\text{M}$ (no full inhibition)	62.5 $\mu\text{M}$
<b>35</b>	L-Fuc	125 $\mu\text{M}$	7.8 $\mu\text{M}$
<b>36</b>	fragment 160	0.5 $\mu\text{M}$	7.8 $\mu\text{M}$
<b>37</b>	L-Fuc + fragment 160	3.9 $\mu\text{M}$	7.8 $\mu\text{M}$
<b>38</b>	L-Fuc + fragment 191	0.2 $\mu\text{M}$	7.8 $\mu\text{M}$
<b>39</b>	L-Fuc + fragment 473	2.0 $\mu\text{M}$	7.8 $\mu\text{M}$
<b>40</b>	L-Fuc + fragment 151	1.0 $\mu\text{M}$	7.8 $\mu\text{M}$
<b>41</b>	L-Fuc + fragment 231	0.2 $\mu\text{M}$	7.8 $\mu\text{M}$



## 5 Discussion

### 5.1 General Considerations for Studying NoV-HBGA Interaction

This work represents a detailed study of the binding of a human norovirus (NoV) to its attachment factors, so-called histo-blood group antigens (HBGAs). NMR spectroscopy along with other biophysical methods has been employed.

NoV from the family of caliciviruses cause acute gastroenteritis and are considered as an emerging viral threat. The constant increase of epidemic outbreaks since the first occurrence in the late 1960s is reflected in the huge efforts undertaken to unravel the pathology of the infection and in particular the mode of host cell attachment and entry. From early volunteer studies, HBGAs on the surface of the gastrointestinal mucosa were identified as attachment factors required for NoV infection (Harrington *et al.*, 2002; Hutson *et al.*, 2002; Marionneau *et al.*, 2005). Of high impact to the field was the ability to express the major capsid protein VP1 *in vitro* using recombinant baculovirus expression in insect cells or in *E.coli* (only for truncated versions of VP1). Virus-like particles (VLPs) obtained from expression of full length VP1 in insect cells have identical properties compared to whole viruses, but are not infectious and therefore much easier to handle (Hale *et al.*, 1998; Jiang *et al.*, 1992). A range of methods is available for the study of different aspects of NoV infection using VLPs. These include ELISA-based binding assays with saliva or synthetic oligosaccharides (de Rougemont *et al.*, 2011; Huang *et al.*, 2005; Tan & Jiang, 2005a) and SPR assays with either monovalent carbohydrates or neoglycoconjugates (Choi *et al.*, 2008; de Rougemont *et al.*, 2011; Shirato *et al.*, 2008). VLPs were also used in this study.

NoV display a large sequence diversity and are clustered into genogroups and genotypes on the basis of the VP1 gene sequence. The major capsid protein and in particular the outer P2 domain containing the HBGA binding site have a high mutation rate (Donaldson *et al.*, 2010; Lindesmith *et al.*, 2008). This is a consequence of the antigenic drift to escape host immune response but also an indication for the variation of HBGA binding patterns to invade new host populations (Donaldson *et al.*, 2008; Rydell *et al.*, 2011). Using ELISA and SPR assays, eight HBGA binding patterns were identified for NoV from different genogroups (Tan & Jiang, 2005a) (see Figure 1.4). While the prototype Norwalk virus from genogroup GI.1 had a limited specificity for A and H type antigens (Hutson *et al.*, 2002), ‘modern’ NoV strains display a broader binding to a range of ABH and Lewis antigens. This includes the cluster of GII.4 strains that cause the majority of epidemic

outbreaks since the early 1990s (Lindesmith *et al.*, 2008; Tan & Jiang, 2005a). To further understand the mechanisms of host cell attachment by this group of important viruses, NMR experiments were employed to study the binding of a GII.4 NoV strain (Ast6139 isolated 2001 in Asturias, Spain) to both ABH and Lewis antigens (Figure 5.1).

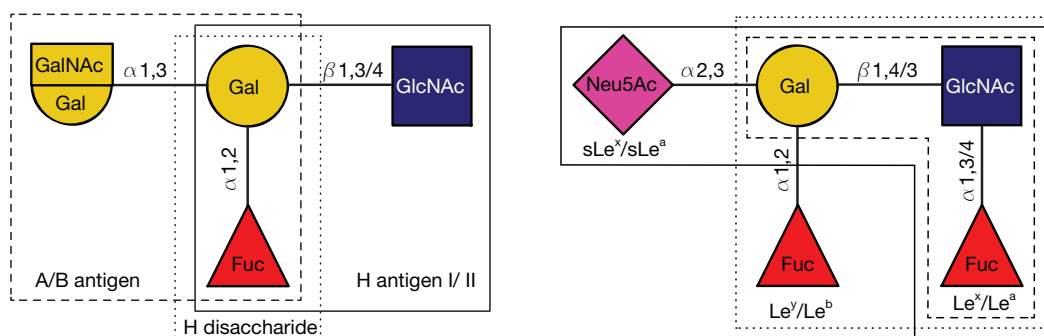


Figure 5.1: Schematic presentation of HBGA antigen. ABH antigens with  $\alpha(1,2)$ -linked L-Fuc (left) and Lewis antigens with  $\alpha(1,3)$ - or  $\alpha(1,4)$ -linked L-Fuc (right) were tested for binding to VLPs of the GII.4 NoV strain Ast6139.

Saturation transfer difference (STD) NMR experiments (Mayer & Meyer, 1999; Meyer & Peters, 2003) furnished binding epitopes of HBGAs that directly reflect recognition by VLPs at atomic level. The applicability of the method for very large systems like VLPs (MW  $\sim 10.8$  MDa) was demonstrated before (Benie *et al.*, 2003; Claasen *et al.*, 2005; Haselhorst *et al.*, 2011; Haselhorst *et al.*, 2008). In particular, VLPs of the animal calicivirus Rabbit Hemorrhagic Disease Virus (RHDV) provided binding epitopes for its attachment factors that are also HBGAs (Rademacher, 2008; Rademacher & Peters, 2008).

## 5.2 Optimization of Experimental Parameters for STD NMR

The aforementioned study with RHDV VLPs helped to ascertain experimental parameters for NMR experiments with VLPs. Their high molecular weight is beneficial for STD NMR because it results in very efficient cross relaxation rates within the protein as well as to bound ligands. As a consequence, saturation transfer to synthetic HBGA fragments has been observed at unusually high ligand excesses up to 260:1 (calculated per binding site, assuming 180 binding sites per VLP). In contrast, STD studies with other systems are usually performed with 20:1 to 50:1 ligand over protein ratio. One contribution to this efficient saturation of ligands is also the fast off rate of the weak VLP-HBGA interaction with dissociation constants in the millimolar or high micromolar range. The high off-rate



and consequently short residence time obviously prevented spin diffusion within HBGAs in the bound state despite the very fast transversal relaxation of the complex. This effect would lead to “blurring” of the binding epitope in the binding pocket. It is observed for small fragments of the Maybridge library that displayed STD effects proportional to their  $T_1$  relaxation times (Rademacher, 2008), an indication for disturbance by spin diffusion effects (Yan *et al.*, 2003). The strong coupling in the aromatic spin systems of the fragments likely facilitates this process. In contrast, no such correlation has been observed for RHDV or the NoV VLPs studied in this work (data not shown). STD experiments with NoV VLPs provide reproducible and reasonable binding epitopes for a range of carbohydrate ligands (see next section). Nevertheless, the binding epitopes should be analyzed only on a qualitative basis, since the unusually high molecular weight may settle VLPs outside of the classical relaxation theory.

As another consequence from the large molecular weight, slow longitudinal relaxation of VLPs requires application of long relaxation delays in STD experiments. With 25 s delay, ca. 92% signal intensity is recovered in the off-resonance spectrum in an interleaved setup of on- and off-resonance experiments (Rademacher & Peters, 2008). This caused a dramatic increase in required measuring time colliding with available instrumental resources. To gain sensitivity one could increase the protein concentration. But owing to relative laborious expression in insect cells the supply with VLPs was not unlimited. With the aim to test a large variety of HBGA fragments the amount of VLPs per NMR sample had to be reduced to 40  $\mu\text{g}$  corresponding to 0.22 mg/mL in 3 mm NMR tubes. In view of the available measuring time, STD spectra for some HBGAs were measured only at one saturation time (0.5 s) instead of whole STD build-up curves for determination of binding epitopes (see Materials and Methods). Considering typical  $T_1$  relaxation times of carbohydrate protons in the low second region this (data not shown) 0.5 s should still be in the linear slope region of STD build up curves. In support of this, binding epitopes obtained from single STD spectra and from STD build-up revealed only small deviations below 10% as exemplarily analyzed for A and B trisaccharides. Binding epitopes of HBGAs for qualitative analysis can thus be obtained from a single STD spectrum instead of whole build-up curves, provided that the signal to noise level of this spectrum is reasonably high (*nota bene* different relaxation times of other types of ligands).

### 5.3 HBGA Binding Patterns Vary with the Chosen Methods

STD experiments provided a detailed picture on the HBGA binding pattern of the NoV strain Ast6139 (see Table 4.1). L-Fuc was identified as minimal structural requirement for the binding. ABH antigens with  $\alpha(1,2)$ -Fuc as well as Lewis antigens with  $\alpha(1,3)$ - or  $\alpha(1,4)$ -linked Fuc (Figure 5.1) were recognized. This is contradictory to binding data for the closely related strain VA387 (1998 isolate with 95% sequence identity of VP1, see Figure 7.2 for alignment) determined by ELISA assays with saliva and oligosaccharides (Huang *et al.*, 2005). VA387 only bound to saliva of secretors and to A, B and H antigens as well as difucosylated Le<sup>y</sup> and Le<sup>b</sup>. Structural data from protein crystallography have shown that the  $\alpha(1,2)$ -Fuc of A and B trisaccharides is recognized in the HBGA binding pocket of VA387 by a dense network of hydrogen bonds and van der Waals interactions (Cao *et al.*, 2007) (see Figure 7.3 for a LigPlot analysis). In general, NoV have been classified into ‘A/B-binder’ and ‘Lewis-binder’ according to their HBGA binding patterns in ELISA assays (Huang *et al.*, 2005; Tan & Jiang, 2005a). Besides this, some strains did not show significant binding to any of the tested saliva or oligosaccharides indicating yet other attachment factors. None of the tested strains including VA387 exhibited strong binding to both non-secretor- and secretor-type antigens. In contrast, the STD experiments presented in this work demonstrated binding of the GII.4 strain Ast6139 to both ABH and Lewis antigens. The reason for this discrepancy may be the different sensitivity of the mentioned assay formats. STD NMR is especially suitable for the detection of weak ligand-receptor interactions with  $\mu\text{M}$  to  $\text{mM}$  dissociation constants. In contrast, ELISA assays have a higher detection threshold considering the various applied washing steps. STD experiments in presence of Ast6139 VLPs suggested a weaker binding of Lewis antigens compared to A and B antigens identified by smaller STD effects. In principle, this observation could also reflect a tighter binding with a low off rate that prevents efficient accumulation of saturated ligand in solution (Jayalakshmi & Krishna, 2002). However the affinity of HBGA is ascertained in the  $\text{mM}$  or at best  $\mu\text{M}$  range by both STD and SPR experiments (see later discussion). Lower STD effects are therefore very likely equivalent to weaker binding. A lower affinity of GII.4 VLPs for Lewis antigens may be the reason that such a binding has not been detected with ELISA assays for related strains of Ast6139. However, the pathophysiological relevance of such a weak binding may be questioned considering the strong secretor dependency of most GII.4 strains (Hutson *et al.*, 2005; Le Pendu *et al.*, 2006).

Only in a very recent study binding of both ABH- and Lewis-type antigens was described for more contemporary epidemic GII.4 strains (de Rougemont *et al.*, 2011). In ELISA assays, two strains from 2006 (Den Haag) and 2007 (Osaka) bound to saliva of secretors and Lewis-positive non-secretors. Both strains also bound to neoglycoproteins (BSA- or HSA-carbohydrate conjugates) of ABH antigens as well as Le<sup>x</sup> and sLe<sup>x</sup>. This finding may be confined to post-2002 GII.4 strains that feature an amino acid insertion T395 in the P2 domain of VP1 under positive selection. It was related to a broader specificity and stronger binding to HBGAs compared to older variants such as VA387 (de Rougemont *et al.*, 2011; Siebenga *et al.*, 2010). But most interestingly, the same study demonstrated binding of an early 1996 GII.4 strain (Dijon) to Le<sup>x</sup> and sLe<sup>x</sup> on human serum albumin (de Rougemont *et al.*, 2011; Rydell *et al.*, 2009). Saliva binding of this strain has shown a strict secretor dependency that classified Dijon as typical strain from the A/B binding group. An obvious explanation for these observed discrepancies is the avidity increase of neoglycoproteins due to multivalency effects from on average 12 to 13 Le<sup>x</sup> or sLe<sup>x</sup> molecules coupled per carrier protein. An avidity increase of ~1000 for BSA-neoglycoproteins compared to the monovalent interaction has been assessed by competitive STD titration experiments in this work (cf. Table 4.7 and Table 4.9). A weaker binding of monovalent Lewis antigens may fall below the threshold of ELISA assays. In contrast, STD NMR detect Lewis (and ABH) antigen binding to VLPs of GII.4 strain Ast6139. This emphasized the strong influence of the assay format and type of ligands on the observed HBGA binding pattern of NoV VLPs. A closer look is taken at the binding specificities obtained for Dijon from ELISA assays and for Ast6139 from STD NMR in this study. Dijon has 99% sequence identity with VA387 and 96% identity with Ast6139 suggesting that the HBGA binding patterns are very similar if not identical (see Figure 7.2 in the appendix for a sequence alignment). Despite this, some marked differences were observed in the binding profiles obtained with the different methods. All three strains bound Le<sup>b</sup> and Le<sup>y</sup> (neoglycoproteins in case of Dijon), but only Ast6139 and Dijon bound to Le<sup>x</sup> in STD NMR experiments and Le<sup>x</sup> neoglycoprotein in ELISA assays, respectively. More remarkably, while VA387 and Ast6139 bound to monovalent A and B trisaccharides in ELISA assays and STD NMR experiments, respectively, Dijon did not bind to A and B trisaccharide neoglycoproteins. Furthermore, Dijon bound to non-fucosylated sialylated type 1 or type 2 precursor neoglycoproteins but Ast6139 did not show STD effects for non-fucosylated 3'- or 6'-sialyl-lactose. One reason for this may be importance of presentation of carbohydrate epitopes to glycan binding proteins (DeMarco & Woods, 2008). Inappropriate presentation of the

$\alpha(1,2)$ -Fuc in A and B trisaccharide neoglycoproteins in ELISA assays may reduce recognition by Dijon VLPs while VA387 strongly bound to their monovalent counterparts (Huang *et al.*, 2005). STD NMR encircles the problem of epitope presentation by using monovalent carbohydrate ligands and moreover efficiently detects even weak binding of HBGAs. As a disadvantage, very strong binding such as of polyvalent neoglycoconjugates could not be detected directly but only in competitive titration experiments.

#### 5.4 NMR Furnished Binding Epitopes for HBGAs

Beside the obtained qualitative information, group epitope mapping of STD NMR spectra furnished binding epitopes of HBGAs in presence of Ast6139 VLPs at atomic resolution that directly reflect the proximity to protons in the HBGA binding pocket (Fiege *et al.*, 2012). Comparison of all binding epitopes revealed the strongest saturation transfer to the L-Fuc moieties. Some other residues also displayed strong STD effects such as  $\alpha$ -GalNAc and  $\alpha$ Gal of A and B trisaccharides. However, none of these additional residues was strictly required for binding nor was there any preference for a certain linkage type of Fuc. L-Fuc was therefore identified as the minimal structural requirement for binding to Ast6139. The exclusive specificity for L-Fuc was further substantiated by the absence of STD effects for L-Gal that has an additional hydroxyl group at position C6 compared to L-Fuc. The high specificity of Ast6139 VLPs for L-Fuc and the predominant saturation transfer to this residue are in agreement with structural data of the related GII.4 strain VA387 (Cao *et al.*, 2007). Co-crystallization of VA387 P protein with A and B trisaccharides identified a number of amino acids that contacted the Fuc and explain efficient saturation of this residue. In particular, residues T344, R345, D374 and G442 made hydrogen binding contacts to the hydroxyl groups and the ring oxygen of Fuc. The methyl group at C6 was involved in hydrophobic interactions with Y443. This hydrophobic pocket apparently imposes sterical hindrance with the hydroxyl group at position C6 of L-Gal causing the exclusive specificity of Ast6139 VLPs for L-Fuc. A stacking interaction was observed between Y443 and H395 that has been hypothesized to be important for stabilizing the hydrophobic pocket. However, STD binding epitopes of L-Fuc and B trisaccharide with Ast6139 VLPs carrying the mutation H395A were almost identical to that with the wildtype (Figure 4.9). A critical contribution of H395 on formation of the binding site geometry is therefore excluded. Nevertheless, the binding to other ABH or Lewis antigens

may be altered. In particular, it should be evaluated if removal of the stacking interaction allows recognition of L-Gal due to a “loosening” of the hydrophobic pocket.

The co-crystal structures of VA387 P protein with A and B trisaccharide also revealed a relative close proximity of the  $\alpha$ -GalNAc and  $\alpha$ -Gal residues to the capsid protein surface. Their orientation was stabilized by a range of water-mediated contacts. This is in excellent agreement with the significant saturation transfer to these residues observed by STD NMR in presence of Ast6139 VLPs. The  $\beta$ -Gal residue more or less pointed away from the VA387 pocket and made only one water-mediated contact with D391. For mutant Ast6139 VLPs with D391 exchanged into an alanine nearly identical STD binding epitopes have been observed for B trisaccharide and L-Fuc in this work. The binding site geometry was obviously unchanged for this mutant suggesting that the role of this contact is insignificant (Figure 4.9). Nevertheless, removal of a water-mediated contact can lead to a reduction of the binding energy in the range of a few kilojoule without necessarily changing the binding site conformation. Affinity measurements by NMR, SPR or other method are required to determine contribution of D391 on binding affinity for HBGAs not reflected by STD binding epitopes alone.

Further analysis of HBGA binding epitopes in presence of Ast6139 VLPs revealed that only very weak saturation transfer to the backbone disaccharides of H antigens. Important interaction sites with these residues causing proximity to the protein surface are therefore unlikely. In support of this, the VLPs did not discriminate between different backbone linkages as apparent from observation of STD effects for H trisaccharides of type 1 (R- $\beta$ (1,3)-D-GlcNAc), type 2 (R- $\beta$ (1,4)-D-GlcNAc) and type 6 (R- $\beta$ (1,4)-D-Glc) (R stands for  $\alpha$ -L-Fuc-(1,2)-D-Gal). The binding epitopes for all three antigens were very similar. In a glycan array testing of Ast6139 VLP binding to A, B and H antigens of each type 1 to 6 a significantly stronger binding to type 1 and type 3 antigens has been observed than to other types (unpublished results by Peter Meloncelli, University of Alberta, Edmonton). Binding data from glycan arrays should be treated with care since binding to the captured carbohydrates may be influenced by epitope presentation. Titration experiments using NMR or SPR should be conducted in the future to address this question. Previous ELISA and SPR assays with synthetic oligosaccharides suggested a stronger binding of GII.4 strains to type 1 antigens compared to type 2 (Shirato *et al.*, 2008). For Norwalk virus from genogroup GI.1 a dependence on H type 1 or type 3 antigens but not H type 2 was found for VLP binding to tissue sections of the gastroduodenal junctions and to saliva (Marionneau *et al.*, 2002). The completely distinct HBGA binding site locations of GI and

GII strains elucidated by protein co-crystallization forbids a direct structural comparison (Cao *et al.*, 2007; Choi *et al.*, 2008). Nevertheless the preference for type 1 and type 3 HBGAs by different NoV may reflect the predominant expression of these structures in the gastrointestinal mucosa, the entry site of NoV.

In the case of Lewis antigens, information from binding epitopes allowed to judge on their relative orientation in the Ast6139 binding pocket. In particular, the strong saturation transferred to the *N*-acetyl groups of Le<sup>x</sup> and sLe<sup>x</sup> implicated an orientation in the binding pocket that places their *N*-acetyl group in close proximity with the protein surface. Low saturation to this group in case of Le<sup>a</sup> and sLe<sup>a</sup> indicate an opposite orientation. Despite the inherent distance information of the STD effect, STD NMR cannot directly report on the protein structure and the residues involved in binding. Such information has been obtained by protein crystallography of NoV P protein in complex with HBGAs (Bu *et al.*, 2008; Cao *et al.*, 2007; Chen *et al.*, 2011; Choi *et al.*, 2008; Hansman *et al.*, 2011), mutation studies identifying important protein residues (de Rougemont *et al.*, 2011; Tan *et al.*, 2008b; Tan *et al.*, 2009; Tan, 2006) and computational studies (Koppisetty *et al.*, 2010). The latter approach has been applied to provide representative models for the explanation of the experimental STD NMR data on a structural level in more detail (see next section). In cases where structural data on the protein site are missing such as in case of RHDV and bovine NoV, important information on the binding mode and specificity can be gained from STD binding epitopes (see later discussion).

## 5.5 Comparison of STD Binding Epitopes with Docking Models

In order to produce representative models for HBGAs bound to Ast6139 VLPs molecular docking was performed by Pavel I. Kitov and Jonathan Cartmell (University of Alberta, Edmonton) (Fiege *et al.*, 2012). The crystal structure of the closely related GII.4 strain VA387 was used to dock ABH and Lewis antigens with Autodock Vina (Trott & Olson, 2010). Almost all HBGAs identified as binders of Ast6139 VLPs by STD NMR were conveniently docked into the binding pocket of VA387 without clashes (Figure 4.15). Interestingly, the  $\alpha(1,3)$ -Fuc of Le<sup>x</sup> and  $\alpha(1,2)$ -Fuc of Le<sup>a</sup> were docked in similar conformations as the secretor-type Fuc of ABH antigens. This contradicts the previous hypothesis of different binding sites for NoV of the A/B and Lewis binding groups (Huang *et al.*, 2005; Tan & Jiang, 2005a). All docking models were in reasonable accordance with

the binding epitopes from STD NMR. In particular, the docking models for Le<sup>x</sup> and Le<sup>a</sup> could explain the differences in observed saturation transferred to their *N*-acetyl groups. The *N*-acetyl group of Le<sup>x</sup> pointed towards a pocket formed by several amino acids that could allow efficient saturation transfer. In contrast, the *N*-acetyl group of Le<sup>a</sup> was in rather loose contact to only a single residue G392 next to D391 that coordinates  $\beta$ -Gal of ABH antigens via a water molecule (Figure 5.2). This example demonstrates that computational modeling and STD NMR data perfectly complement each other and provided experimentally validated models for HBGA binding to NoV.

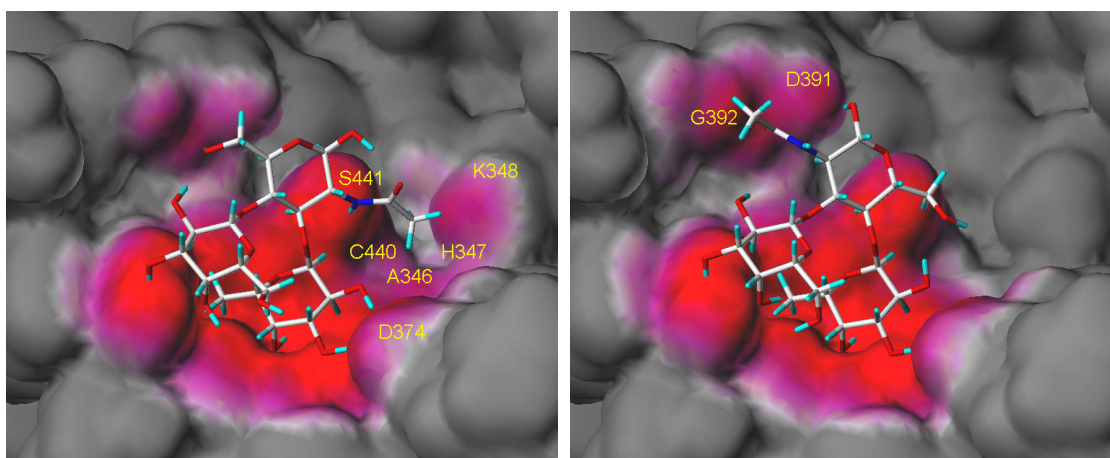


Figure 5.2. Docking models of Le<sup>x</sup> and Le<sup>a</sup>. Representative docking poses of Le<sup>x</sup> (left) and Le<sup>a</sup> (right) (Fiege *et al.*, 2012). Protein residues in proximity to the *N*-acetyl groups are labeled. The coloring indicates the proximity to the protein surface with 3 Å cutoff.

In another yet more elaborate study using docking and molecular dynamics (MD) simulations, the binding of ABH antigens up to pentasaccharides to VA387 was studied (Koppisetty *et al.*, 2010). All antigens including difucosylated Le<sup>b</sup>, ALe<sup>b</sup> and BLe<sup>b</sup> were forced to superimpose the secretor-Fuc with the position in the crystal structure (Cao *et al.*, 2007). However unpublished results by W. Nasir *et al.* from the same group (University of Stockholm, Sweden) also provided models for Le<sup>x</sup> and Le<sup>a</sup> and difucosylated Le<sup>y</sup> and Le<sup>b</sup> placed with the Lewis-type Fuc in the binding pocket (manuscript in preparation).

The STD binding epitope of difucosylated Le<sup>y</sup> in presence of Ast6139 VLPs exhibited strong saturation transfer to both Fuc moieties (see Figure 4.2) with saturation of the  $\alpha$ (1,3)-Fuc being ca. 70% of that of  $\alpha$ (1,2)-Fuc. Two explanations for this observation are possible: either a single binding mode leads to efficient saturation of both Fuc moieties. In support of this, the relatively constrained conformation of Le<sup>y</sup> brings both moieties in relative close proximity facing into similar directions (see Figure 4.6). Alternatively, two

binding modes may exist for Le<sup>y</sup> with either one of the Fuc residues recognized in the binding pocket causing a weighted average in the STD binding epitope. The latter hypothesis is supported by the previously mentioned MD simulations that provided models for recognition of both secretor- and non-secretor type Fuc by VA387 (W. Nasir et al., manuscript in presentation). The less sophisticated docking studies with Autodock Vina reported in this work failed to produce several of the binding models. For instance, Le<sup>y</sup> could not be docked with the  $\alpha(1,2)$ -Fuc moiety in conformations with correct torsion angles. This is likely due to an imperfection of the Autodock Vina algorithm that aims to optimize ligand protein interaction at the expense of correct torsion angles. In fact, the stronger saturation of the  $\alpha(1,2)$  Fuc residue indicated that a binding mode with the secretor-type Fuc placed in the binding pocket exists and is likely higher populated.

Structural data for recognition of Le<sup>y</sup> via the  $\alpha(1,3)$ -Fuc was obtained for the GII.9 strain VA207 from the Lewis binding group (Chen *et al.*, 2011). Despite having only 63% sequence identity with Ast6139, both strains share a common binding site with many conserved residues interacting with L-Fuc (see Figure 7.4 for LigPlot analysis). The  $\alpha(1,2)$ -Fuc residue of Le<sup>y</sup> was in relatively loose contact to the protein surface that would not result in sufficient saturation transfer to this residue. However, amino acid mutations in proximity of the binding pocket might change the situation in case of Ast6139. In contrast, a co-crystal structure of GII.10 strain Vietnam026 from the A/B binding group (64% sequence identity with Ast6139) in complex with Le<sup>y</sup> brings the second, Lewis-type fucose in close proximity to the protein surface (Hansman *et al.*, 2011) (see Figure 7.3 for LigPlot analysis). This structure could potentially explain the observed saturation transfer to both Fuc moieties of Le<sup>y</sup> in presence of Ast6139 VLPs. Le<sup>x</sup> and Le<sup>a</sup> were disordered in co-crystals with Vietnam026.

In conclusion, structural data for both the secretor- and the Lewis-position of Le<sup>y</sup> are available of which only the secretor-type position could explain the observed STD binding epitope presence of Ast6139 VLPs. Co-existence of both binding modes is suggested from MD simulations of the related GII.4 strain VA387. In general, this study showed that Ast6139 was capable of recognition of both ABH and Lewis antigens. Further experiments are necessary to elucidate the exact recognition mode of difucosylated HBGAs.



## 5.6 HBGA Specificities of other Caliciviruses

Results from STD NMR experiments of HBGAs with Ast6139 VLPs can be compared to results from analogue studies with two animal caliciviruses: RHDV from genus Lagovirus infecting rabbits (Rademacher *et al.*, 2008), and bovine NoV Newbury 2 (NB2) from genogroup III (Zakhour *et al.*, 2009). Both viruses share the specificity for HBGAs.

RHDV causes severe liver damage in rabbits and leads to death within 48 h of infection. It emerged from a less or avirulent ancestor by mutation in the 1980s (Kerr *et al.*, 2009). STD NMR experiments with RHDV VLPs furnished binding epitopes for ABH antigens. Similar to NoV Ast6139, L-Fuc was identified as minimal structural requirement for binding. Despite pronounced tertiary structure homology with GII.4 NoV (Barcena *et al.*, 2004; Katpally *et al.*, 2010) no structural information on the HBGA binding site is available. Binding epitopes from STD experiments therefore provide valuable otherwise inaccessible information on the binding site geometry. In contrast to protein crystallization, the experimental setup is relatively easy and allows measurements under physiological conditions. Subtle differences in the recognition of ABH antigens by RHDV and Ast6139 VLPs studied in this work were observed suggesting different recognition modes for both viruses. First, the specificity of L-Fuc recognition by RHDV VLPs seemed to be less confined demonstrated by significant saturation transfer to L-Gal. The hydrophobic pocket of the methyl group formed by Y443 of GII.4 NoV strains that prevents binding of L-Gal from steric hindrance is apparently not a structural feature of RHDV. Second, RHDV selectively bound to H trisaccharide type 2 but not type 1. The binding epitope of H type 2 in presence of RHDV VLPs revealed strong saturation transfer not only to the Fuc but also to the backbone disaccharide (Figure 5.3). This implicated important interaction sites of RHDV VLPs in the region of the backbone. H type 1 antigen is excluded from this binding site likely due to steric hindrance. Interestingly, even weak binding to non-fucosylated type 2 precursor was observed. Obviously, the additional interactions with the backbone can partly outbalance the absence of L-Fuc moiety.

In contrast, Ast6149 VLPs bound to H trisaccharides regardless of the backbone linkage, either type 1, 2 or 6 (see Figure 4.2). Only weak saturation of the backbone disaccharides suggested that H antigen recognition by this NoV is solely dependent on interaction with the L-Fuc moiety (Figure 5.3).

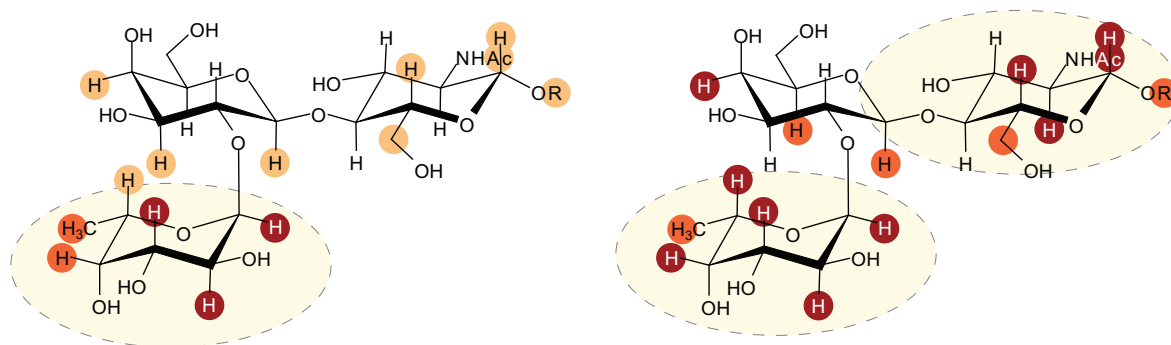


Figure 5.3. Binding epitopes of H trisaccharide type 2 with Ast6139 and RHDV. Binding epitope of **7** (R=Lemieux) in presence of Ast6139 VLPs (left) and RHDV VLPs (right) (Rademacher *et al.*, 2008). Colored circles indicate strong (>80%), medium (40-80%) and weak (<40%) relative STD effects. Yellow background color highlights structural groups important for recognition VLPs. The figure was adapted from (Fiege *et al.*, 2012).

The observed differences in HBGA binding epitopes and specificities of RHDV and NoV VLPs are likely correlated to different tissue specificity (Parra & Prieto, 1990). They may even explain the different host range and the absence of zoonotic RHDV infections in humans. However other factors like host enzymes required for viral replications are likely to contribute to this fact as well. The main replication of RHDV takes place in the liver and requires other infection routes and host factors than NoV that replicate in the mucosal epithelium of the gastrointestinal tract. Glycosyltransferase expression patterns in humans result in a selective presentation of type 1 and 3 HBGAs in the gut mucosa (Mollicone *et al.*, 1996; Oriol *et al.*, 1986) where they are exploited as attachment factors by NoV (Le Pendu, 2004; Marionneau *et al.*, 2002). The recognition of type 2 antigens by Ast6139 VLPs is therefore most probably not relevant for pathogenesis. It enables VLPs to agglutinate red blood cells carrying type 2 antigens (Hakomori, 1981; Le Pendu, 2004). This could be exploited in hemagglutination assays with VLPs and prototype inhibitions to study inhibitor efficiencies in a cell-based assay under quasi-biological conditions, though with a cell type unrelated to NoV pathogenesis.

The HBGA binding specificity of yet another calicivirus, bovine NoV NB2 from geno-group III, has been investigated with STD NMR (Zakhour *et al.*, 2009) (see section 4.2.3). In accordance with results obtained by other methods, NB2 VLPs specifically bound to the Galili epitope  $\alpha$ -Gal-(1,3)-Gal but not to ABH or Lewis antigens (Zakhour *et al.*, 2009). This epitope is also called xenoantigen, since it is found in all mammals except in humans, gorilla and chimpanzee due to inactivation of the  $\alpha$ 1,3-galactosyltransferase (Macher & Galili, 2008). Therefore, the probability of zoonotic infection of NB2 in humans seems unlikely. It would require major conformational changes in the binding

pocket in addition to the changes required to adapt to a new host. In summary, STD NMR experiments furnished the HBGA binding pattern of three caliciviruses in this and previous studies. The minimal structural binding motifs of Lagovirus RHDV and two NoV (Ast6139 and bovine NB2) demonstrated that the genetic relatedness is not a measure for the similarity of attachment factor binding (Figure 5.4).

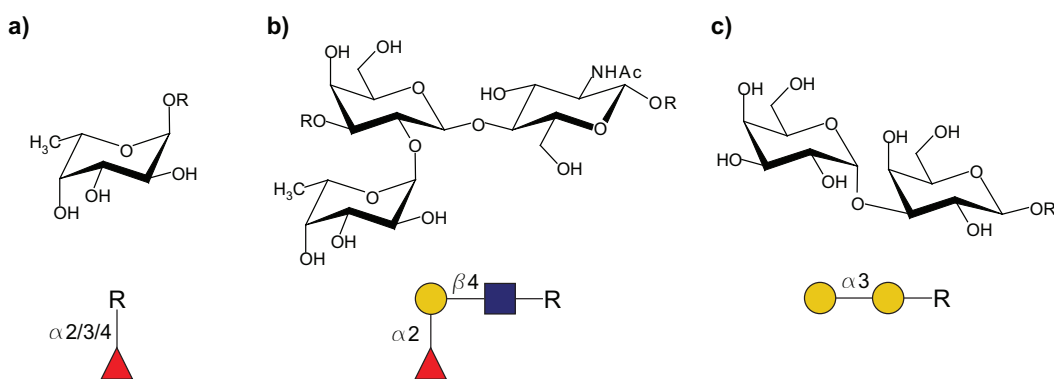


Figure 5.4. Minimal structural recognition motifs of three caliciviruses. Structural formulas (top panel) and symbol presentation (according to CFG nomenclature, bottom panel) of minimal structural requirements for binding to Ast6139 (a), RHDV (b) and NB2 (c).

## 5.7 Bioactive Conformation of sLe<sup>x</sup> from trNOESY Experiments

As an important note, Ast6139 VLPs also bound to sLe<sup>x</sup>. Sialylated glycans play pivotal roles in a range of biological processes including cell-cell signaling, the ‘homing’ of lymphocytes and tumor metastasis (Olofsson & Bergstrom, 2005; Schauer, 2009; Varki & Schauer, 2009). Due to their high abundance in all tissue types, many pathogens evolved to exploit sialic acids for host cell attachment, e.g. influenza viruses (Gamblin & Skehel, 2010), rotaviruses (Baker & Prasad, 2010) and polyomaviruses (Neu *et al.*, 2009). Importantly, sialic acids were identified as attachment factors for murine NoV (genogroup V) to macrophages and dendritic cells in the gut (Taube *et al.*, 2009). A detailed analysis of sLe<sup>x</sup> recognition by NoV was therefore desired.

SLe<sup>x</sup> has been shown to adopt multiple conformations in solution of which often only a subset of conformations is recognized by carbohydrate-binding proteins. E-selectin, that mediates adherence of lymphocytes to endothelial surface, binds to the major solution conformation ‘aA’ of sLe<sup>x</sup> (Harris *et al.*, 1999; Poppe *et al.*, 1997; Scheffler *et al.*, 1997; Scheffler *et al.*, 1995). In contrast, the plant lectin *Aleuria aurantia* agglutinin (AAA) binds to sLe<sup>x</sup> in a minor conformation ‘aD’ in which the Le<sup>x</sup> is slightly tilted (Haselhorst *et*

*al.*, 2001). This is based on a tight recognition of the Le<sup>x</sup> core by this lectin. Elucidation of the bioactive conformation of sLe<sup>x</sup> bound to NoV would provide important information on the mode of recognition.

Binding of human NoV GII.4 strains to of sLe<sup>x</sup> moieties was reported previously using ELISA-and SPR-binding assays (de Rougemont *et al.*, 2011; Rydell *et al.*, 2009). However the role of the neuraminic acid (Neu5Ac) in the binding process remained unclear. The STD binding epitope of sLe<sup>x</sup> with GII.4 strain Ast6139 presented in this work suggested that Neu5Ac was not in close proximity to the protein surface and thus plays only a minor role in the binding. This hypothesis is supported by crystal structure data of sLe<sup>x</sup> in complex with the P protein of NoV strain VA207 classified as a Lewis binder (Chen *et al.*, 2011). Despite being from another genotype (GII.9) VA207 recognizes the  $\alpha(1,3)$  Fuc moiety involving many conserved residues with GII.4 strains (see Figure 7.4). The *N*-acetyl group of GlcNAc and H2 of Gal are in close contact to the protein surface which is in accordance with a strong saturation transfer to these protons in presence of Ast6139. SLe<sup>x</sup> was present in the major solution conformation 'aA'. However a closer look at the electron density map revealed only very poor density for the Neu5Ac residue suggesting that it retained flexibility in the binding pocket of VA207.

To further assess the bioactive conformation of sLe<sup>x</sup> transferred NOESY experiments in presence of Ast6139 VLPs were performed. At 298 K strongly negative trNOE cross peaks were observed at a ligand to binding site ratio of 12.5:1 (assuming 180 binding sites per VLP) (Figure 4.12). In general trNOEs can be observed if the cross-relaxation rates  $\sigma^B$  and  $\sigma^F$  and the fractional populations  $N^B$  and  $N^F$  of the bound and free ligand fulfill the inequation  $|N^B\sigma_{IS}^B| \gg |N^F\sigma_{IS}^F|$  (Neuhaus & Williamson, 2000). The fraction of bound ligand is dependent on the  $K_D$  and  $k_{off}$  of the interaction as well as the ligand to protein ratio. For VLPs, the cross-relaxation rate  $\sigma^B$  of the bound ligand is extremely high, but the fraction of bound ligand is probably very low due to a fast  $k_{off}$  rate. With an estimated affinity of the monovalent carbohydrate interactions from 1 to 10 mM (Table 4.3 and Table 7.1) the  $k_{off}$  rate will be in a range of  $10^5$  to  $10^6$  Hz. Simulations for simple two-spin systems predict negative trNOE intensity for these parameters (cf. Figure 7.7). A further increase of  $k_{off}$  or alternatively an increase of the ligand excess would yield trNOEs close to zero or even weakly positive. Nevertheless it is still unclear if the classical relaxation theory applies to systems as large as VLPs (Rademacher, 2008).

The trNOE pattern of sLe<sup>x</sup> in presence of Ast6139 VLPs potentially showed the presence of two conformations that are also highly populated in solution (Figure 4.12). This either

reflects recognition of two distinct conformations from the set of solution conformations of  $sLe^x$ , or a retained flexibility of the Neu5Ac residue in the bound state. In support of the latter hypothesis, data from the co-crystal structure of VA207 P protein with  $sLe^x$  suggest a retained flexibility of the Neu5Ac residue (*vide supra*). Further insight on  $sLe^x$  recognition came from molecular dynamics (MD) simulations of  $sLe^x$  in the HBGA pocket of GII.4 strain VA387 carried out by Dr. Pavel Kitov and Jonathan Cartmell (University of Alberta, Edmonton) (Fiege *et al.*, 2012). A 20 ns MD run with explicit water revealed the presence of multiple conformations of the Neu5Ac residue in the bound state that interconverted during the run (Figure 4.16). This further supports the hypothesis of a retained flexibility of the Neu5Ac residue. Three major conformational families were sampled in both bound and free state in accordance with previous computational and experimental data for  $sLe^x$  (Haselhorst *et al.*, 2001; Poppe *et al.*, 1997). Importantly, in the bound state the relative populations were shifted from the major solution conformation ‘aA’ to conformation ‘bA’. A set of strong trNOE cross peaks characteristic for this conformation has been observed in presence of Ast6139 VLPs while the cross peak corresponding to conformation ‘aA’ was rather weak. The relatively higher abundance of ‘bA’ in the bound state may be explained by two hydrogen bonds from N393 stabilizing Neu5Ac in this conformation (Figure 5.5). The presence of multiple bioactive conformations for Neu5Ac was also in accordance with observed weak saturation transferred to protons of this residue, in particular to the *N*-acetyl group and H3<sub>ax</sub>/H3<sub>eq</sub>. In addition, in the predominant bound conformation ‘bA’ Neu5Ac is rather far from the protein surface. Only H3<sub>ax</sub> and H3<sub>eq</sub> come close to N393, but this would not lead to strong saturation due to mainly polar hydrogens in this region.

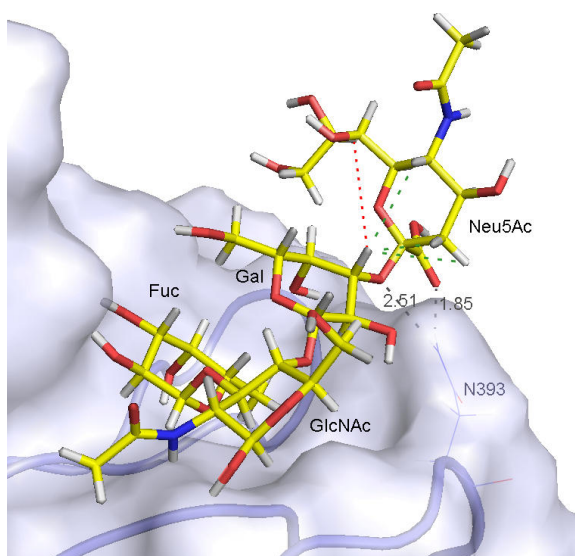


Figure 5.5. Predominant bound conformation of  $sLe^x$  from MD simulation. Ribbon and surface presentation of VA387; stick presentation of  $sLe^x$  in conformation ‘bA’ characterized by short distances between H3<sub>ax</sub>/H3<sub>eq</sub>/H5<sup>Neu5Ac</sup> and H3<sup>Gal</sup> (green lines, 2.1, 3.6 and 3.2 Å, respectively) and a long distance between H8<sup>Neu5Ac</sup> and H3<sup>Gal</sup> (red line, 5.9 Å). Neu5Ac is stabilized by a bidentate hydrogen bond from N393 (grey lines).

In conclusion MD simulations in conjunction with trNOESY and STD NMR data provided reasonable and experimentally validated binding models as demonstrated for the binding of sLe<sup>x</sup> to Ast6139 VLPs.

### 5.8 Affinity Data for HBGAs from STD NMR experiments

Monovalent carbohydrate protein interactions are usually rather weak with affinities in the mM or higher  $\mu$ M range (Dam & Brewer, 2007). Biologically relevant interactions e.g. of viruses with cell surface receptors are often substantially strengthened by multivalency effects. In case of NoV, a single virus particle contains up to 180 attachment factor binding sites (different conformations of ‘A/B’ and ‘C/C’ dimers in crystallized VLPs raised questions on the actual number of ‘active’ HBGA binding sites). In addition, a multitude of HBGAs are presented on the surfaces of the gastrointestinal epithelium. Virus attachment to the cell surface becomes literally irreversible despite weak monovalent interaction. Elucidation of dissociation constants for monovalent NoV-HBGA interactions is nevertheless desired to provide a more comprehensive view on HBGA recognition modes. Both STD and SPR experiments have furnished such affinity data in this work.

The dissociation constant for  $\alpha$ -L-Fuc-(1,*O*)-CH<sub>3</sub> binding to Ast6139 VLPs has been estimated in the low mM range by STD titration experiments (section 7.6.1 in the appendix). A similar study by others, a  $K_D$  of 460  $\mu$ M for L-Fuc binding to P protein dimers of the GII.10 strain Vietnam026 has been determined (Hansman *et al.*, 2012). The difference of factor three between the two  $K_D$  values may reflect different HBGA recognition by NoV strains from different genotypes. Furthermore, experimental error in case of Ast6139 is relatively high considering dilution of the protein during titration and the measurement of STD spectra at a single saturation time instead of whole STD build-up curves. Apparent  $K_D$  values from single saturation times have been shown to be usually false too high due to ligand relaxation and rebinding effects (Angulo *et al.*, 2010). Detection of whole STD build-up curves applied in case of Vietnam026 provides apparent  $K_D$  values that are closer to the true value. Finally, affinities of P protein (Vietnam026) could be different to that of VLPs (Ast6139) since the full virus particles may present further interaction sites for HBGAs. In particular, the presence of multiple binding sites for L-Fuc per VP1 monomer of Ast6139 VLPs was suggested from both STD titrations (section 7.6.1) and SPR experiments (section 4.7.1). Measurement of the weighted average of a high affinity site and other low affinity sites would reduce the observed apparent  $K_D$ .

To address this question, affinities should be determined for P dimers and VLPs of the same NoV strain. Alternatively, elimination of essential residues in the HBGA recognition site yielding “knock-out” mutants would allow to judge on the presence of HBGA-specific sites others than that known from crystal structures (Cao *et al.*, 2007). Two such mutants of Ast6139, R345A and D374A, have been cloned into recombinant baculoviruses and expression of VLPs is in preparation.

The affinity determination for other HBGA by STD titration was partly hampered due to the limited supply with oligosaccharidic HBGA fragments. For a reliable curve fitting, titrated ligand concentrations should cover a range from  $\sim 0.1$  up to ten times  $K_D$ . Considering estimated affinities in the mM or high  $\mu\text{M}$  range this adds up to milligram quantities of carbohydrate. Only in one more case a  $K_D$  has been determined by STD titration in this work, namely for xenoantigen binding to bovine NoV NB2. The obtained  $K_D$  (5 – 7 mM) was in a similar range of the previously mentioned data.

Relative binding data were also obtained by competitive STD titrations. Oligosaccharidic HBGA were used as reporter ligands (requiring only low amounts of substance) and applying  $\alpha\text{-L-Fuc-(1,}O\text{)-CH}_3$  as competing ligand available in large quantities. Obtained  $\text{IC}_{50}$  values allowed qualitative ranking of HBGA binding strengths (Figure 5.6). A weaker binding of Lewis antigen  $\text{sLe}^x$  compared to A and B antigens was suggested from the data. This was in accordance with observation of lower STD effects for Lewis antigens. Furthermore,  $\text{IC}_{50}$  values were converted to  $K_D$  values from the  $K_D$  of  $\alpha\text{-L-Fuc-(1,}O\text{)-CH}_3$  from direct STD titration and applying the Cheng-Prusoff equation. Calculated  $K_D$  values were in the medium to high  $\mu\text{M}$  range. STD titrations with strain Vietnam026 provided a  $K_D$  value for H type 2 trisaccharide (300  $\mu\text{M}$ ) in a similar range (Hansman *et al.*, 2012).

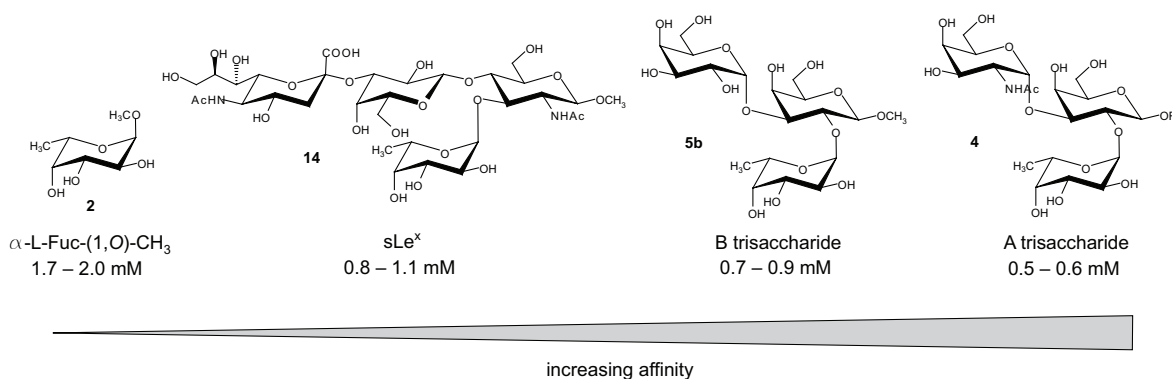


Figure 5.6. Ranking of HBGA binding strengths from STD NMR. Dissociation constants ( $K_D$ ) were obtained from direct STD titration ( $\alpha\text{-L-Fuc-(1,}O\text{)-CH}_3$ , Table 7.1) or from  $\text{IC}_{50}$  values with the help of the Cheng-Prusoff equation and assuming a  $K_D$  of 1.7 – 2.0 mM for L-Fuc-(1, *O*)-CH<sub>3</sub> (Table 7.2). R(4)=(CH<sub>2</sub>)<sub>7</sub>CH<sub>3</sub>.

IC<sub>50</sub> values from competitive titrations of B trisaccharide with  $\alpha$ -L-Fuc-(1,*O*)-CH<sub>3</sub> and vice versa were also converted into K<sub>D</sub> values from the Cheng-Prusoff equation by a mathematical approach without the necessity for any preassumptions (see section 7.6.2). The obtained K<sub>D</sub> values of 0.7 mM for B trisaccharide and 1.7 mM for  $\alpha$ -L-Fuc-(1,*O*)-CH<sub>3</sub> were very close to the K<sub>D</sub> values obtained from complement assays. The necessary assumption of K<sub>I</sub>=K<sub>D</sub> however limits this mathematical approach to pairs of ligands with exactly identical binding modes.

Divergent binding modes have been for example observed for the two functional groups of compound **31** in competitive STD titration by  $\alpha$ -L-Fuc-(1,*O*)-CH<sub>3</sub>. **31** comprises L-Fuc linked to fragment 160 identified as competitive binder to the HBGA site in a NMR screening against Ast6139 VLPs (Rademacher *et al.*, 2011). Only partly depletion (~20%) of STD signals of fragment 160 by  $\alpha$ -L-Fuc-(1,*O*)-CH<sub>3</sub> suggested the presence of other binding sites for fragment 160 not targeted by HBGAs (Figure 4.21). The IC<sub>50</sub> for this partial depletion of 300  $\mu$ M in principle constitutes the upper limit of the K<sub>D</sub> of  $\alpha$ -L-Fuc-(1,*O*)-CH<sub>3</sub> for the respective binding site. An affinity in this range was obtained for L-Fuc binding to Vietnam026 P protein from direct STD titration (Hansman *et al.*, 2012). The nature of the different binding sites of fragment 160 should be addressed in studies with previously mentioned “knock-out” mutants of NoV VLPs.

## 5.9 Binding Mode and Affinity of HBGAs from SPR Measurements

Affinity measurements using surface plasmon resonance (SPR) can be accomplished with either the protein or the ligand immobilized to a sensor chip. Both approaches should in principle provide identical affinities. The sensitivity of the measurement is however much higher if the protein is in the mobile phase leading to a higher mass increase upon binding. Previous SPR studies with NoV VLPs in the mobile phase have been reported with immobilization of either monovalent carbohydrates (Shirato *et al.*, 2008) or carbohydrates coupled to bovine/human serum albumin (de Rougemont *et al.*, 2011) and polyacrylamide (PAA) (Choi *et al.*, 2008). Binding of Ast6139 VLPs to immobilized monovalent carbohydrates was not observed whereas immobilization of PAA sugar conjugates demonstrated strong binding of NoV VLPs and suggested affinities in the pM range (Rademacher, 2008). The complex binding due to multivalency effects as well as a high ‘background’ response from unspecific binding to the PAA backbone did not allow quantification of NoV-HBGA



interaction from this setup. Therefore the opposite assay format with immobilized VLPs was established in this work. Similar setups have been used to study antibody binding to immobilized intact adenoviruses (Abad *et al.*, 2002) or different animal and plant viruses (Dubs *et al.*, 1992) only on a qualitative level.

Ast6139 VLPs were immobilized on CM5 sensor chips covered with a carboxylated dextran matrix at coverage rates up to 10000 RU VLPs. C1 sensor chips with a plain gold surface that allowed coverage of only 1000 RU VLPs were not suitable to detect binding even of large polymeric ligands (cf. Figure 4.37). A strong pH and buffering dependence of HBGA binding was found with an apparent pH optimum around pH 6.0 (Figure 4.30) that was validated in the indirect assay format with immobilized BSA sugar conjugates (Figure 4.43). It also confirmed previous studies with immobilized PAA sugar conjugates (Rademacher, 2008). An optimum binding affinity of NoV around pH 6 is plausible considering that the gastrointestinal mucosa has been reported to have a pH in the same range (Lucas, 1983; McEwan *et al.*, 1990). The binding was relatively stable at acidic pH. This is in accordance with the reported stability of VLPs from pH 3 to 7 (Ausar *et al.*, 2006) that allows the safe passage of infective virions through the acidic gut. A drastic decrease of binding strength was observed at basic pH for which conformational changes of VLPs have been reported (Ausar *et al.*, 2006; Cuellar *et al.*, 2010). In a published work, binding of NoV VLPs to immobilized carbohydrates was studied using Tris-HCl pH 7.4 as running buffer (Shirato *et al.*, 2008). In SPR experiments with Ast6139 VLPs the interaction with HBGAs was considerably weakened under such condition. In fact, phosphate buffer pH 7.4 was used to efficiently remove bound analyte. The reason for this may lie in different VLP preparations, slightly different buffer conditions or yet other unknown assay conditions. For example, buffering strength was shown to be critical for VLP binding.

For several VLP covered sensor chips negative response differences were observed for injections of HBGA fragments. This was likely due to refractive index artifacts that can occur for very different flow cell composition. They may be reduced by immobilization of an appropriated reference protein at identical coverage as the VLPs. On one sensor chip positive responses were observed and provided affinity constants for a range of HBGAs (Table 4.10). For L-Fuc an affinity of 60 to 70 mM has been obtained which is at least one order of magnitude weaker than the affinity obtained from competitive and direct STD titrations (~1.7 mM). However it confirmed previous competitive SPR experiments on immobilized PAA-Fuc that provided an  $IC_{50}$  value for L-Fuc around 60 mM (Rademacher, 2008). Considering the much higher avidity of VLPs for PAA-Fuc on the chip, the  $IC_{50}$

from this assay is a close approximation of the  $K_D$  of L-Fuc. The maximal response in the direct SPR measurement suggested the presence of more than one ( $\sim 3$ ) binding sites per VP1 monomer with the apparent  $K_D$  being a weighted average of the affinities of all binding sites. In support of this, STD titration curves of  $\alpha$ -L-Fuc-(1,*O*)-CH<sub>3</sub> can be fitted in such a way, that the high affinity component ( $\sim 2$  mM) is complemented by a second lower affinity component (40 to 50 mM). The high affinity component may not be detectable in SPR due to sensitivity limitations. Another explanation would be the fundamental difference in the applied assay formats: a static assay allowing rebinding effects in case of STD titrations, and the dynamic formation and dissociation of interactions under continuous flow in case of SPR. The latter is likely closer to the conditions in biological systems. Affinities determined by STD titration would therefore constitute an overestimation of binding strength to NoV VLPs. The different buffering conditions applied for measurements with SPR (10 mM sodium acetate buffer pH 5.0) and STD (25 mM sodium phosphate buffer pH 7.0, both with 154 mM NaCl) would rather argue for a weaker binding in STD experiments and can therefore not explain the differences in measured affinities.

From SPR measurements with other HBGAs an affinity increase from monosaccharidic L-Fuc (60 – 70 mM) over H-disaccharide (40 – 60 mM) to H trisaccharide ( $\sim 10$  mM) was observed. This is likely due to an increased number of protein-ligand contacts. Crystal structures of NoV P proteins with HBGA fragments up to pentasaccharides predicted several such contacts. While the measurement of H-disaccharide suggested presence of six to 12 binding sites per VP1 monomer, the binding of H trisaccharide type 6 can be explained by a 1:1 Langmuir isotherm. It is supposed that H trisaccharide can only be accommodated in the known HBGA binding pocket while L-Fuc and H-disaccharide also bind to other sites on the capsid surface. In case of H-disaccharide a contribution of its hydrophobic spacer to the binding cannot be excluded. In favor of this, SPR experiments suggested eight binding sites per VP1 monomer for H disaccharide opposed to only three sites for L-Fuc.

Measurement of the difucosylated compound **30** exceeded the maximum response for a 1:1 binding by far (40 – 60). The measured affinity (9 to 14 mM) was therefore not trustworthy although it would be plausible considering an affinity increase from multivalency effects.

In conclusion, SPR measurements with immobilized VLPs could in principle provide affinity constants for small carbohydrates. However the high difficulties in reproducing experiments with positive response differences suggest that further studies for optimization of assay conditions especially concerning a possible reference protein are necessary.

### 5.10 Lead Compounds for Entry-Inhibitor Design

The strict conservation of the L-Fuc recognition site among NoV GII.4 isolates from three decades (Bok *et al.*, 2009a; Lindesmith *et al.*, 2008) encouraged attempts to target this site by entry-inhibitors. Considering the absence of medication or vaccination strategies against NoV, such inhibitors are highly desirable in order to combat future epidemic outbreaks, confine the economic losses for example for hospitals and to reduce the burden for high-risk patients. Prototype inhibitors obtained from two different screening approaches were tested for binding to and inhibition of Ast6139 VLPs with direct and competitive STD NMR and SPR measurements.

First hit compounds for entry-inhibitor design were obtained from NMR screening of the Maybridge fragment library (molecular weights < 300 Da) against Ast6139 VLPs using STD NMR and spin-lock filtered experiments (Rademacher, 2008; Rademacher *et al.*, 2011). A very high initial hit rate above 60% was reduced to 12% ‘specific’ hits by competition experiments with HBGA. One of these competitive hits, fragment 160, was chosen for the design and synthesis of inhibitors (Guiard *et al.*, 2011) tested in this work.

A high hit rate in NMR screening studies has been described previously (Huth *et al.*, 2005; Post, 2003) and is even increased by very efficient cross saturation of large VLPs. In a screening study based on inhibition of NoV VLP binding to saliva a much lower hit rate was found (Feng & Jiang, 2007). Interestingly the same study furnished inhibitors that were active against NoV from both genogroup II (VA387, MOH) and genogroup I (Norwalk). This raises hope that inhibitors directed against the HBGA binding pocket may provide protection against a broad range of NoV strains even from outside of the GII.4 genocluster. A reason for the apparently shared binding site geometries may be the strict dependency of NoV infections on HBGA binding. The only limited number of possible attachment factors therefore causes convergent evolution of binding pockets.

Another explanation for the high hit rate found in the NMR screening against Ast6139 is the large number of interaction sites, e.g. hydrophobic patches, provided by the VLPs. ‘Unspecific’ binding of fragment 160 to other sites than the HBGA pocket was suggested from competitive STD titration of the heterodivalent compound **31** (comprising L-Fuc and fragment 160) with  $\alpha$ -L-Fuc-(1,0)-CH<sub>3</sub>. Similar experiments suggested unspecific binding of the octyl spacer of A trisaccharide (see section 4.6.1). The K<sub>D</sub> obtained for **31** from SPR measurements is increased by factors 25, 16 and 4 compared to that obtained for L-Fuc, H-di- and H trisaccharide type 6. The length of the linker was too short to allow simultaneous

binding of Fuc and fragment 160 to adjacent HBGA sites of a P dimer (25 Å). But even in this case multivalency effects can occur due to a reduction of the effective  $k_{\text{off}}$  rate as it has been described for lectins binding to mucins (Dam *et al.*, 2009) and for inhibitors of glycosidases comprising only a single binding pocket (Decroocq *et al.*, 2011). Binding of fragment 160 to other sites is also likely to contribute to the increased affinity of **31**. Such ‘unspecific’ binding is not necessarily undesired as it may increase the overall avidity for VLPs while the attached Fuc still provides specificity.

In addition to the competitive fragment 160, four ‘adjacent site’ fragments from NMR screening showing ILOEs to  $\alpha$ -L-Fuc-(1,*O*)-CH<sub>3</sub> were used as functional groups in synthesis of multivalent inhibitors (Guiard *et al.*, 2011). Such inhibitors follow the classical route of fragment-based drug design. It aims to identify and link fragments that bind in close proximity in the targeted binding pocket to yield lead compounds with affinity increases up to the product of the  $K_D$  of the fragments (Campos-Olivas, 2011; Carr *et al.*, 2005).

The second approach for entry-inhibitor design employed *in silico* screening of a virtual library of fucosylated compounds against the HBGA binding site of NoV. The four compounds with the highest calculated free energy were synthesized by Julie Guiard (unpublished data). Beside this one compound had a very low solubility contradictory to *in silico* predictions. The same was true for many compounds of the Maybridge fragment library indicating that prediction of physical properties of drug-like molecules is a challenging task (Foloppe & Chen, 2009). Despite very similar affinity scores *in silico*, SPR measurements of the three remaining compounds displayed very different binding strengths and modes to immobilized VLPs emphasizing the reported large uncertainty of calculated free energies (DeMarco & Woods, 2008; Woods & Tessier, 2010). The binding isotherm of compound **42** unambiguously reflected a two-site binding behavior with a high affinity component in the  $\mu\text{M}$  range (170 – 280  $\mu\text{M}$ ) complemented by a low affinity binding in the higher mM range (Table 4.11 and Figure 5.7). Since the maximum response for the high affinity binding can be explained by a 1:1 binding model, it likely reflects binding to the HBGA site of VLPs. All three aromatic rings of **42** came into close contact to the protein surface in the docking model (Figure 5.7). In particular, a 90° kink at the sulfamide group allowed stacking interactions of the dimethyl pyrimidine ring with the aromatic ring of H297'. Simultaneous recognition of the L-Fuc and the aromatic groups may explain the affinity increase by at least two orders of magnitude compared to of L-Fuc alone. A close recognition of the aromatic rings is confirmed by observation of strong saturation transfer to these groups (Figure 4.18). STD NMR provides no information on

the protein site. Therefore saturation transfer could likewise originate from ‘unspecific’ binding to other sites. For fragment 160 STD experiments suggested that 80% of the observed saturation transfer results from binding to other sites than the HBGA site (Figure 4.21). But observation of only medium saturation transfer to functional groups for the other virtual screening hits is in good agreement with the observed lower affinities.

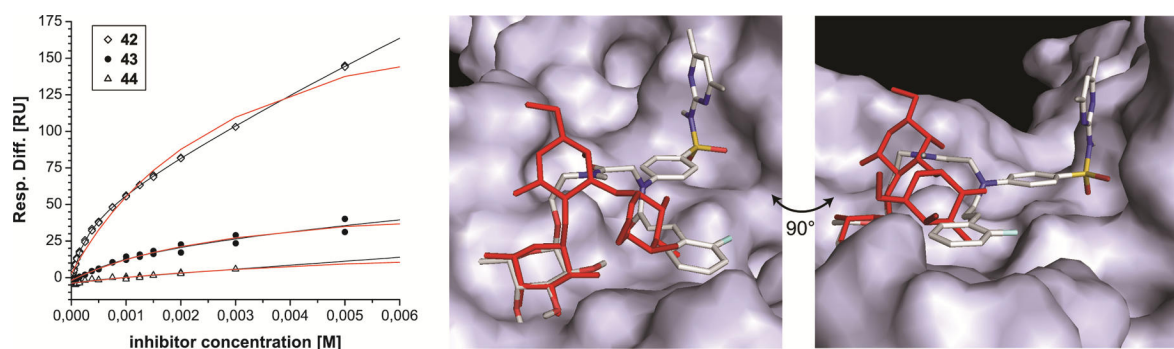


Figure 5.7. Basis of high affinity binding of virtual screening hit **42**. (Left) binding isotherms and curve fitting to a 1:1 binding model (red lines) and a two-site binding model (black lines); the curve form of **42** implicates a two-site binding behavior with a high affinity component of 170 to 280  $\mu\text{M}$ . (Right) docking model of **42** in the HBGA pocket of VA387.

### 5.11 Titration Experiments with Polymeric Inhibitors

Polymeric PAA-based inhibitors were obtained from hits of both NMR and virtual library screening (Guiard *et al.*, 2011). Competitive SPR experiments and hemagglutination assays with RBCs indicated that the PAA backbone mediates unspecific binding and caused precipitation of VLPs at nM concentrations in a process critically dependent on the incubation time. Precipitation of  $\mu\text{g}$  VLP amounts in presence of nM concentrations of polymer was visible in NMR samples. The absence of a response of the PAA backbone to immobilized VLPs particularly indicated a slow on-rate of this unspecific interaction. In contrast, inhibition by monosaccharidic L-Fuc was independent from preincubation time in accordance with very fast on- and off-rates.

Prototype inhibitors contained 20 to 30 monomeric repeating units with  $\alpha$ -L-Fuc and/or a screening hit. The resulting polymer architecture likely allowed simultaneous binding of functional groups to HBGA binding sites of a VP1 dimer (25 Å distance) or two neighboring dimers (75 Å distance). This resulted in increased avidities due to multivalency effects as it has been described for other systems (Horan *et al.*, 1999; Kitov *et al.*, 2008a; Kitov *et al.*, 2008b; Kitov *et al.*, 2011; Kitov *et al.*, 2000; Munoz *et al.*, 2009; Tran *et al.*, 2011).

For the polymer containing only Fuc (**35**), binding curves from direct SPR experiments showed only weak binding. Apparently the binding was too weak (in the mM range) to be detected with this assay format in the applied concentrations range (up to 750  $\mu$ M). In contrast, competitive SPR experiments demonstrated an increase in the inhibition efficiency by a factor of  $\sim 1000$  for this polymer (80  $\mu$ M) compared to monovalent L-Fuc (70 mM). The  $IC_{50}$  for the polymer is given per Fuc unit allowing a direct quantification of the observed multivalency effect.

In general,  $IC_{50}$  values from competition experiments with SPR and STD NMR were significantly lower than the  $K_D$  values obtained from direct SPR measurements (Table 5.1). Considering the Cheng-Prusoff equation the  $IC_{50}$  should be an upper limit for the  $K_D$  of the competing ligand. The critical time dependence of the inhibition mechanism led to strong increase of observed avidity in experiments allowing pre-incubation with VLPs. This again emphasizes the high impact of the used method on the observed effects.

*Table 5.1.  $K_D$  and  $IC_{50}$  values of polymers from different assay formats. Errors of measurements are omitted for clarity. Where results stem from multiple flow cells in SPR or different reporter protons in STD, a range for  $K_D$  or  $IC_{50}$  is given. The label 'ILOE' identifies polymers with 'adjacent site' fragments.*

Compound	Functionalities	$K_D$ (SPR) (cf. Table 4.13)	$IC_{50}$ (SPR) (cf. Table 4.14)	$IC_{50}$ (STD) (cf. Table 4.8)	titer (HA) (cf. Table 4.16)
<b>34</b>	PAA backbone	no binding	weak inhibition at nM conc.	n.d.	0.2 $\mu$ M (no full inhibition)
<b>L-Fuc</b>	monovalent Fuc	66 mM	60 mM	n.d.	n.d.
<b>35</b>	Fuc	> 1 mM	80 $\mu$ M	500 – 800 $\mu$ M	125 $\mu$ M
<b>36</b>	fragment 160	590 – 640 $\mu$ M	n.d.	n.d.	0.5 $\mu$ M
<b>37</b>	Fuc + fragment 160	n.d.	0.61 $\mu$ M	n.d.	3.9 $\mu$ M
<b>38</b> <sup>ILOE</sup>	Fuc + fragment 191	550 – 640 $\mu$ M	20 $\mu$ M	8 – 20 $\mu$ M	0.2 $\mu$ M
<b>39</b> <sup>ILOE</sup>	Fuc + fragment 473	170 – 190 $\mu$ M	5.7 $\mu$ M	5 – 8 $\mu$ M	2.0 $\mu$ M
<b>40</b> <sup>ILOE</sup>	Fuc + fragment 151	1.3 mM	40 $\mu$ M	180 – 230 $\mu$ M	1.0 $\mu$ M
<b>41</b> <sup>ILOE</sup>	Fuc + fragment 231	630 – 670 $\mu$ M	40 $\mu$ M	400 – 1000 $\mu$ M	0.2 $\mu$ M
<b>46</b>	<b>42</b>	130 – 160 $\mu$ M	n.d.	4 – 5 $\mu$ M	n.d.
<b>47</b>	<b>42</b>	200 – 230 $\mu$ M	n.d.	n.d.	n.d.

Qualitative comparison of the results obtained from SPR, NMR and hemagglutination assays reveals a similar ranking of the affinities and/or inhibition efficiencies of polymers (Table 5.1). For instance, the polymer with the highest affinity in the direct SPR assay (**46**) also displayed the best  $IC_{50}$  of all tested polymers in competitive STD experiments. Of the four polymers with 'adjacent site' ('ILOE') fragments polymer **39** with fragment 473 had

the highest activity in all assay types except the hemagglutination assay. The accuracy of this cell-based assay is considered to provide only a rough estimation of inhibitor efficiencies. It can for example identify the relatively large difference between the polymer with Fuc (**35**) and other polymers containing additional fragments from library screening. Combination of all results allows ranking of the polymeric inhibitors according to their efficiencies, i.e. lowest  $K_D$  and/or lowest  $IC_{50}$  value:

$$46 < 37 < 39^{ILOE} < 38^{ILOE} \sim 41^{ILOE} < 40^{ILOE} < 36^{160} < 35^{Fuc} \ll 34$$

The two best inhibitors contain a fucosylated compound from virtual screening (**46**) or L-Fuc and fragment 160 from the Maybridge library identified as competitive binder (**37**). In case of the polymers with Fuc and ‘adjacent site’ fragments (indicated by ‘ILOE’ in superscript), further experiments should be accomplished to evaluate if the observed ranking is correlated to the different affinities of the fragments or instead is a result of favorable or unfavorable orientation with respect to the Fuc. The latter factor has a high impact on the strength of the multivalency effect (Kitov & Bundle, 2003). It is significantly increased if simultaneous binding of both functional groups is allowed. In case of fragment 473, the preferred orientation has been indicated by ILOE experiments with  $\alpha$ -L-Fuc-(1,*O*)-CH<sub>3</sub> in presence of Ast6139 (data not shown). However the information has not yet been considered in the design of the linker. Optimization of the linker type and length is envisioned to provide further increase of inhibitor efficiency from improved multivalency effects (Kitov *et al.*, 2003).

Polymer **46** containing compound **42** from virtual screening displayed the strongest binding to immobilized VLPs and the highest efficiency in competitive STD titrations. Its superior activity is therefore confirmed in two very different assay formats. In contrast to polymers with ‘ILOE’ fragments from NMR screening, the individual functional groups providing affinity to the interaction are already in the correct orientation in case of **46**. In virtual screening, whole drug-like molecules instead of fragments are docked to the targeted binding site. Those molecules allowing optimal positioning of functional groups are identified by prediction of the free binding energy. The probability to find hits with ‘perfect fit’ increases with the size and diversity of the virtual compound library (Irwin, 2008; Koppen, 2009; Sun, 2008). Nevertheless, the results indicated that the true affinity of virtual screening hits can be very different despite similar affinity scores. This is likely due flexibility in the protein not correctly reproduced by *in silico* methods.

The results suggest that computational methods involving virtual screening of compound libraries can much faster and easier yield high efficiency inhibitors similar or even superior to that from more laborious fragment screening approaches. However, in case of polymers with 'ILOE' fragments optimization of the linker length may result in much higher affinities even exceeding that of polymer **46**.

In summary, the best inhibitors demonstrate a significant affinity increase by three orders of magnitude compared to the monovalent interaction of L-Fuc. Further experiments such as inactivation assays with infectious NoV particles should address the ability of these prototype inhibitors to prevent NoV infections in humans. Furthermore, experiments presented in this work should be repeated with VLPs from other NoV strains to evaluate the applicability to a broader range of NoV. In view of the highly conserved HBGA recognition site among GII.4 strains this will be likely observed. Encouragement also comes from studies that furnished inhibitors with 'cross reactivity' against both GII and GI NoV strains (Feng & Jiang, 2007).



## 6 Summary and Outlook

In a first part of this work, the binding of a GII.4 NoV to its attachment factors on host cells has been studied using NMR spectroscopy in combination with other biophysical methods. A large variety of synthetic HBGA fragments subjected to these experiments has furnished a detailed picture of the structural requirements for binding. L-fucose has been identified as the minimal binding motif, which can be extended via a secretor-type  $\alpha(1,2)$ -linkage present in ABH antigens, or via  $\alpha(1,3)$  or  $\alpha(1,4)$  linkages present in Lewis antigens. This contradicts previous findings from ELISA-based binding assays with saliva and synthetic oligosaccharides that showed a strict secretor-dependent binding of a closely related GII.4 strain. This has been addressed to the different detection sensitivity of ELISA assays opposed to STD NMR experiments. The use of VLPs instead of isolated viral capsid proteins has been very beneficial for STD NMR experiments and allowed detection of even weak binding interactions (Rademacher & Peters, 2008).

Group epitope mapping from STD NMR experiments delivered binding epitopes at atomic resolution that in some cases allowed to deduce the orientation of the oligosaccharide in the HBGA binding pocket of NoV. For example, distinct STD effects for the *N*-acetyl moieties of Le<sup>x</sup> and Le<sup>a</sup> antigens unambiguously reflected their orientation in the binding pocket. Structural data from co-crystallization of HBGA with NoV capsid proteins were in well agreement with the observations from STD NMR experiments.

As a highlight, the bioactive conformation of sLe<sup>x</sup> binding to NoV VLPs has been elucidated employing transferred NOESY experiments. A special concern in this respect was the flexible  $\alpha(2,3)$  linkage of sLe<sup>x</sup>. Comparison with results from MD simulations led to a reasonable model of sLe<sup>x</sup> binding to Ast6139 VLPs. Importantly, the models show that the conformational flexibility of the sialic acid residue is maintained in the bound state.

STD as well as SPR titration experiments provided affinity data for several HBGA fragments in the low millimolar range and suggested the presence of other low affinity binding sites on the VLP surface. Further systematic STD NMR studies with other NoV strains and VLPs carrying single site mutations may help to unravel the closely linked interplay of amino acid variation and HBGA binding patterns in the future.

This study shows that STD binding epitopes complement structural information from protein crystal structures of HBGA complexes with viral capsid proteins. As an advantage over protein crystallization, STD experiments are conducted under physiological conditions. For the future it will be interesting to compare STD binding epitopes of VLPs and

P protein dimers that have been used in the co-crystallization experiments. Such studies may resolve the question how binding of NoV to its attachment factors is modulated by the assembly of VLPs as compared to isolated capsid proteins.

In conjunction with molecular docking studies and MD simulations STD NMR can provide experimentally verified structural models of a large variety of strains and mutants that is not as easy and fast available by protein crystallography. Furthermore, STD NMR provides detailed binding information for caliciviruses for which no structural information is available as in the case of bovine NoV NB2 (Zakhour *et al.*, 2009) and in the case of rabbit calicivirus RHDV (Rademacher *et al.*, 2008).

The second part of this work has been concerned with the design of medication strategies directed against the step of host cell attachment. Information from the natural HBGA binding pattern as well as from two different screening approaches was combined to design and synthesize prototype inhibitors (synthesis work has been carried out by Pavel I. Kitov and Julie Giuard of the University of Alberta, Edmonton). Hit compounds originated from an NMR screening of a fragment library (Rademacher *et al.*, 2011) and from an *in silico* screening of a virtual compound library (P.I. Kitov, unpublished results). Heterobivalent and multivalent PAA-based inhibitors were then tested for their affinity and inhibitory efficiency towards NoV VLPs. All inhibitors contained L-Fuc, which furnished binding specificity, and a compound with binding affinity for NoV from NMR or virtual library screening. The two best polymeric inhibitors had a 500-fold increased affinity and a 1000-fold increased inhibitory efficiency as compared to the respective monovalent inhibitors. The affinities of the polymeric inhibitors were calculated per monomeric repeating unit to allow for a comparison with the monovalent interaction as determined from direct and competitive SPR titrations, respectively. This first generation of inhibitors has not yet been optimized for linker type, linker length or the type of the polymeric backbone. Optimization of these parameters is likely to yield inhibitors with higher efficiency in the future.

Beside STD NMR titrations, SPR has been instrumental to derive binding affinities. Several advantages but also difficulties with different SPR assay formats have been observed. Immobilization of VLPs allowed direct determination of affinities for HBGA and polyvalent prototype inhibitors. However the observed mass increase, and hence sensitivity, is very low for small HBGA fragments. Furthermore, negative response differences were frequently observed likely due to refractive index artifacts. Assay

optimization with special concern on immobilization of a preferentially “inert” protein on the reference flow cell will likely improve the reproducibility of measurements.

Competitive SPR assays with PAA sugars immobilized on the sensor surface allowed determination of  $IC_{50}$  values for multivalent inhibitors. However the high ‘background’ from unspecific VLP binding to the PAA backbone on the reference flow cell could potentially obscure weaker binding effects. In contrast, immobilization of BSA neoglycoconjugates furnished selective binding to conjugates with fucosylated carbohydrates. Binding to BSA on the reference flow cell was small. BSA neoglycoconjugates therefore represent an alternative to PAA sugars with a high background response and should be further evaluated for the determination of  $IC_{50}$  values.

As closest biological assay, the inhibitory efficiency of prototype inhibitors has been tested in hemagglutination assays. Although red blood cells are not relevant for the pathogenesis of NoV infection, they display the same HBGAs and resemble the mucosal epithelium in the gastrointestinal tract. The hemagglutination test is very sensitive to the assay preparation and only provides low precision. Nevertheless, the obtained titers of multivalent compounds for inhibition of hemagglutination by VLPs are in a range comparable with the results of competitive SPR and STD titrations.

SPR experiments demonstrated a strong pH dependency of HBGA binding to VLPs, with an optimum around pH 6.0. Similar experiments may also be necessary for a detailed inspection of the pH and temperature dependence of VLP inhibition by multivalent compounds.

Furthermore, experiments involving cell culture or animal models should evaluate the suitability of prototype inhibitors for the prevention of infection in the future. However, to date cell culture models are only available for murine NoV (Taube *et al.*, 2009; Wobus *et al.*, 2004). Cell culture and animal models also exist for the animal calicivirus RHDV.

An interesting perspective is the further development of multivalent inhibitors towards infection-preventing additives for ex-vivo applications. NoV display a high environmental stability and resistance towards many disinfectants (da Silva *et al.*, 2011; Duizer *et al.*, 2004a; Koopmans, 2009). An efficient inactivator of NoV may be applied to limit commencing epidemic outbreaks in crowded environments such as hospitals and nursing homes. Medical treatments for chronically infected immunocompromised patients are highly desirable but will require thorough testing of *in vivo* toxicity and efficacy of prototype inhibitors.



## 7 Appendix

### 7.1 List of Chemicals

Chemical	Description	Producer
D <sub>2</sub> O:	deuteriumoxid 100% (99,97% D)	Euriso-top
acetic acid:		Merck
acetic acid- <i>d</i> 3:	99% D	Aldrich
BisTris:	2,2-Bis-(hydroxyethyl)-iminotris-(hydroxymethyl)methane	Fluka
Bradford Reagent:		Bio-Rad
BSA:	Bovine Serum Albumin	Serva
BsaI:	restriction enzyme	Fermentas
Cellfectin Reagent:		Invitrogen
cesium chloride:		Sigma-Aldrich
Eco81I:	restriction enzyme	Takara
EDC:	1-ethyl-3-(3-dimethylaminopropyl) carbodiimide, Amine Coupling Kit	GE Healthcare
ethanolamine:	Amine Coupling Kit	GE Healthcare
Freon 113:	1,1,2-trichloro-1,2,2-trifluoroethane	Sigma-Aldrich
Glycine:		Sigma
HBS-P buffer pH 7.4:		GE Healthcare
hydrochloric acid:		Merck
Insect-Xpress:	protein free medium for insect cell culture	BioWhittaker
MES:	2-( <i>N</i> -morpholino)ethanesulfonic acid	Sigma
methanol- <i>d</i> 4:	99% D	Aldrich
NcoI:	restriction enzyme	New England Biolabs
Neutravidin:		Pierce
NHS:	<i>N</i> -hydroxysuccinimide, Amine Coupling Kit	GE Healthcare
sodium acetate:		Merck
sodium azide:		Merck
sodium chloride:		Roth
Na <sub>2</sub> HPO <sub>4</sub> :	disodium hydrogen phosphate anhydrate	Merck
NaH <sub>2</sub> PO <sub>4</sub> ·2H <sub>2</sub> O:	sodium dihydrogen phosphate dihydrate	Merck
sodium hydroxide:		Merck
Surfactant P-20:		GE Healthcare
Triton X-100:		Fluka
TSP- <i>d</i> 4:	<i>d</i> 4-trimethylsilyl-2,2,3,3-tetradeuteropropionic acid, 98% D	Cambridge Isotope Laboratories , Inc.
XhoI:	restriction enzyme	Fermentas

## 7.2 List of Equipment

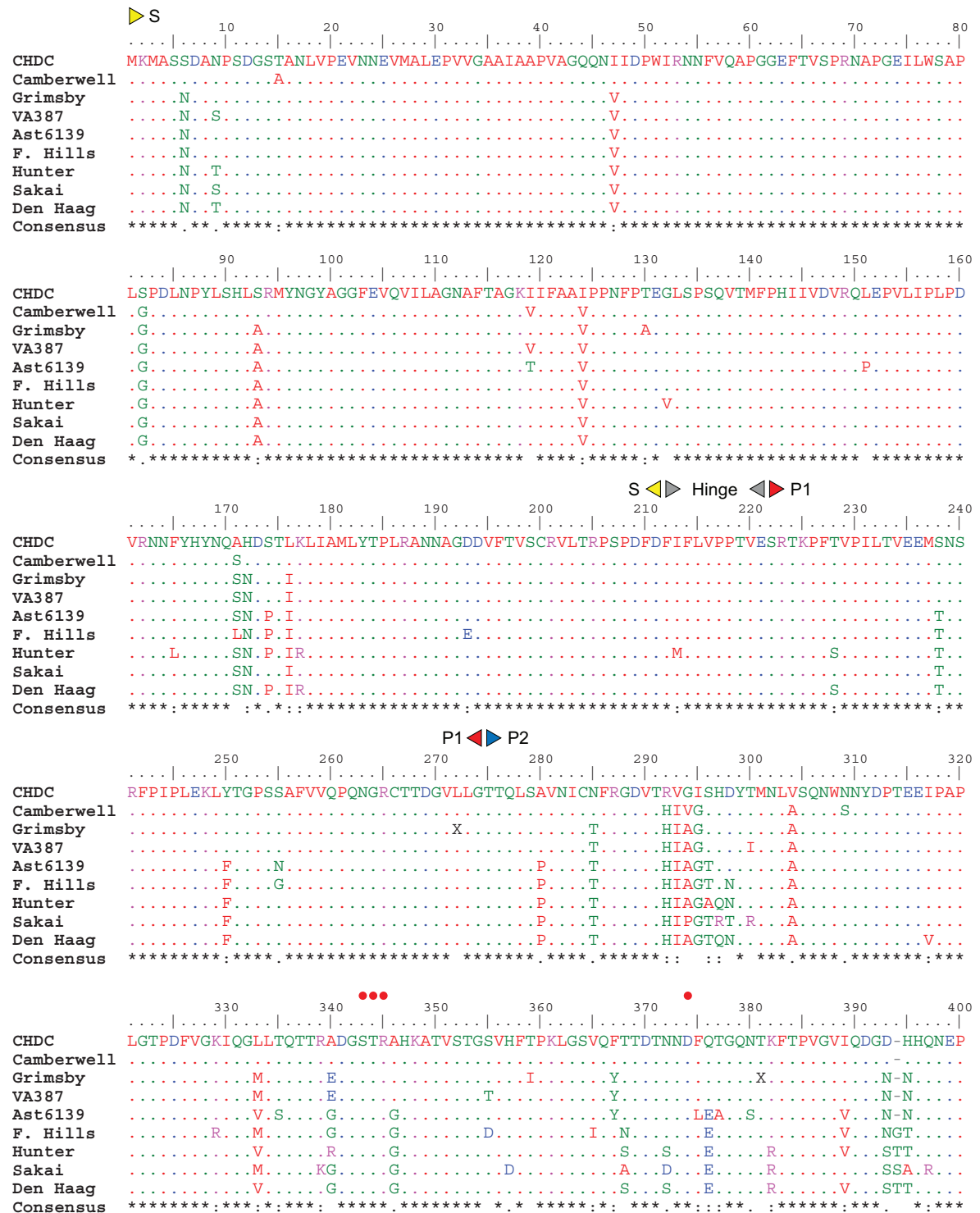
Instrument	Name	Manufacturer
Balances:	Micro Balance MC210S	Satorius
	MC1	Satorius
Centrifuges:	Centrifuge 5810	Eppendorf
	Centrifuge 5415 D	Eppendorf
	Allegra 64R centrifuge	Beckman Coulter
	Ultracentrifuge	Beckman Coulter
Lyophilisator:	BETA A	Christ
	ALPHA 1-2 LD plus	Christ
NMR spectrometer:	Bruker Avance DRX or AVIII 500 MHz with TCI cryogenic probe	Bruker
	3 mm NMR Tubes for Bruker MATCH holder	Hilgenberg
	5 mm NMR Tubes for Bruker MATCH holder	Hilgenberg
NMR sample changer:	SampleXpress	Bruker
pH meter:	pH 330	WTW
SPR spectrometer:	Biacore 3000	Biacore AB/ GE Healthcare
	CM5 sensor chips	GE Healthcare
	C1 sensor chips	GE Healthcare
UV spectrometer:	NanoDrop ND-1000 spectrophotometer	Peqlab

## 7.3 List of used Software

Software	Producer/ weblink
Biacore 3000 Control Software:	Biacore AB/ GE Healthcare
BIAevaluation Software:	Biacore AB/ GE Healthcare
ChemSketch v.12.00:	ACD/Labs, <a href="http://www.acdlabs.com/">http://www.acdlabs.com/</a>
ClustalW:	<a href="http://www.ebi.ac.uk/Tools/msa/clustalw2/">http://www.ebi.ac.uk/Tools/msa/clustalw2/</a>
GlyTorsion	<a href="http://www.glycosciences.de/tools/glytorsion/">http://www.glycosciences.de/tools/glytorsion/</a>
Instant JChem:	ChemAxon, <a href="http://www.chemaxon.com/jchem/">http://www.chemaxon.com/jchem/</a>
LigPlot v.4.5.3.:	available via <a href="http://www.ebi.ac.uk/pdbsum/">http://www.ebi.ac.uk/pdbsum/</a>
Origin 7.0:	Microcal
PyMOL version 0.98:	Schrödinger, <a href="http://www.pymol.org/">http://www.pymol.org/</a>
SWEET2 modeling software:	<a href="http://www.glycosciences.de/modeling/sweet2/">http://www.glycosciences.de/modeling/sweet2/</a>
Sybyl-X 1.2:	Tripos
TopSpin 2.1/ 3.0:	Bruker

## 7.4 Sequence Alignments of Norovirus Capsid Proteins

Multiple sequence alignment of VP1 sequences of NoV strains from genotype GII.4 over a period of 32 years (cf. section 1.3):



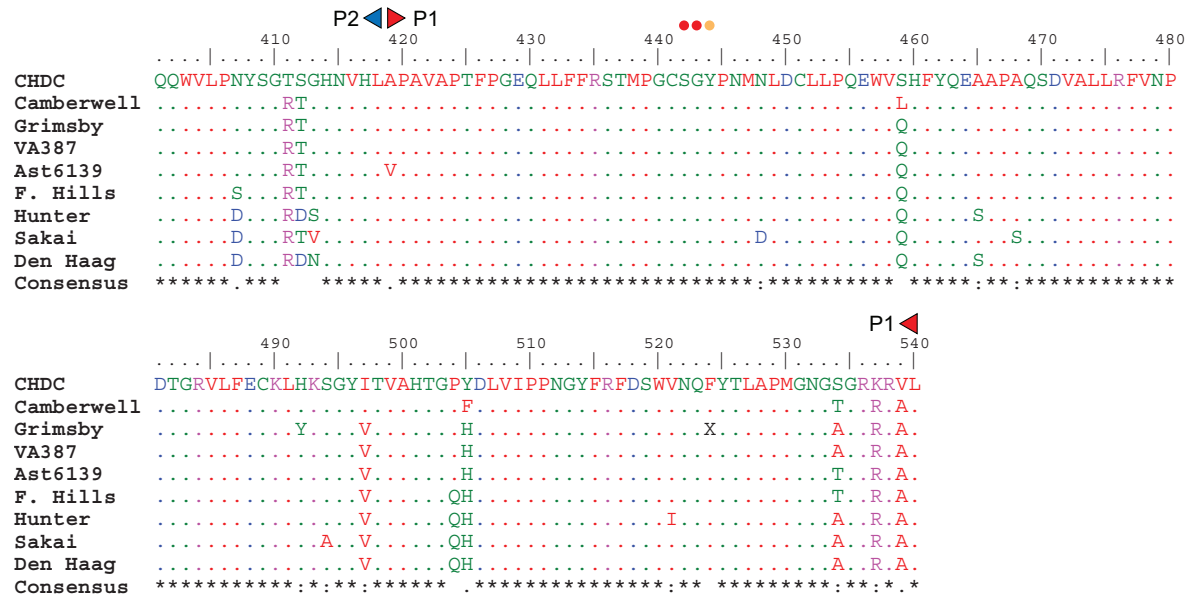


Figure 7.1. Sequence alignment of NoV GII.4 strains from 32 years. ClustalW alignment of VP1 from the strains CHDC (Hu/NoV/GII.4/CHDC2094/1974/US, GenBank entry FJ537135); Camberwell (Hu/NoV/GII.4/Camberwell/1994/AUS, AAD33961.1); Grimsby (Hu/NoV/GII.4/Grimsby/1995/UK, CAA06169.1); VA387 (NLV/VA98387/1998, AAK84679.2); Ast6139 (Ast6139/01/Sp, CAE47529.1); F. Hills (Hu/NoV/GII.4/Farmington Hills/2002/US, AAR97663.1); Hunter (Hu/NoV/GII.4/Hunter/2004/AUS, AAZ31376.2); Sakai (Hu/NoV/GII.4/Sakai/2005/JP, BAE98194.1); Den Haag (Hu/NoV/GII.4/DenHaag54/ 2006/NL, ABL74389.1). All strains represent identically named GII.4 clusters except strains VA387 (Grimsby cluster) and Ast6139 (Farmington Hills cluster). Domain borders are indicated by triangles. Red and orange circles indicate residues involved in hydrogen bonds and hydrophobic contacts, respectively, with Fuc as seen in the crystal structure of VA387 with A and B trisaccharides (Cao *et al.*, 2007).



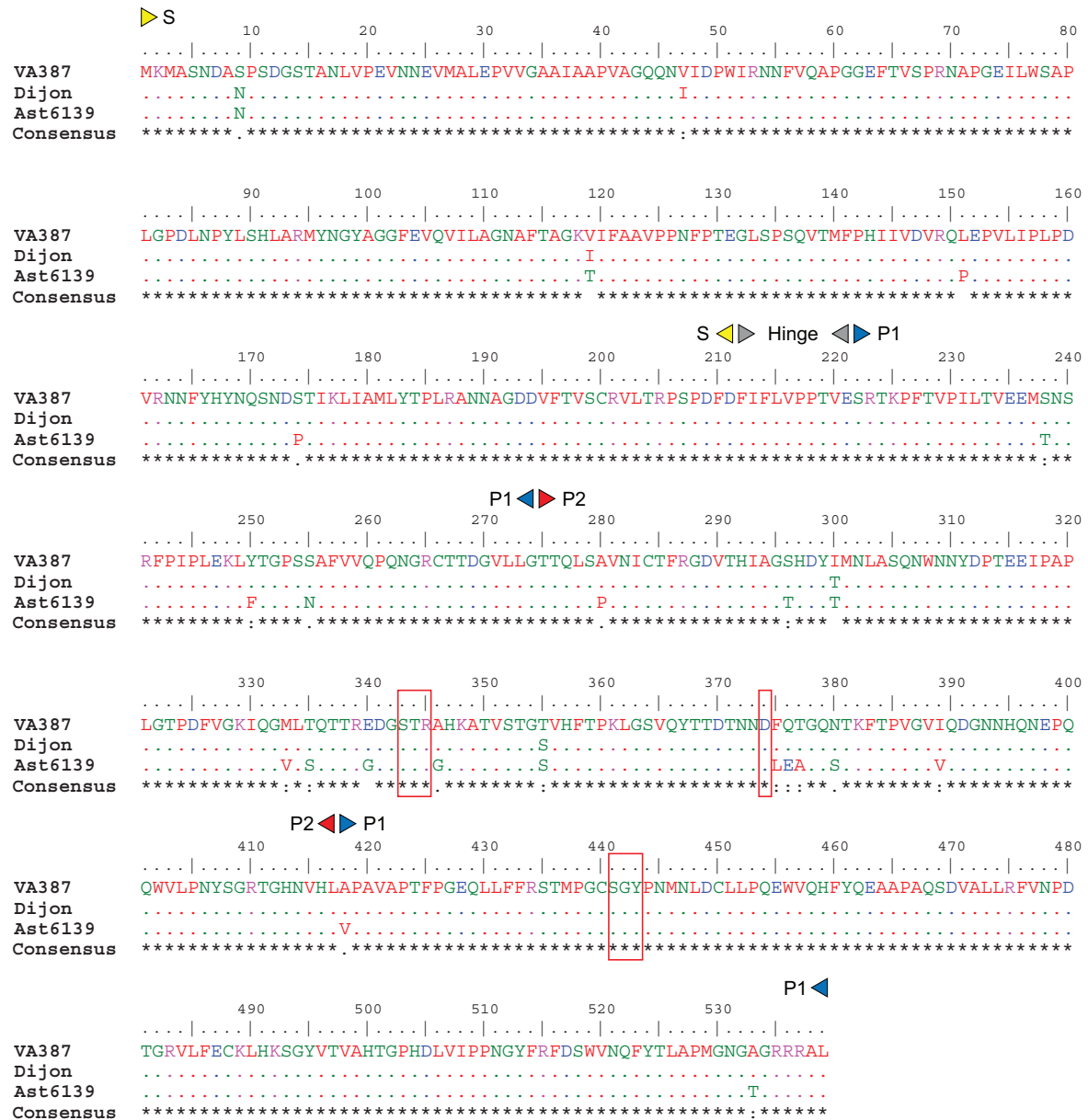


Figure 7.2. Sequence alignment of closely related NoV GII.4 strains. Alignment of the major capsid protein sequences of strains VA387, Dijon (NLV/DIJON171/96, GenBank entry AAL79839.1) and Ast6139. Domain borders are indicated by triangles. Red boxes mark residues interacting with Fuc as seen in the crystal structure of VA387 with A and B trisaccharides (Cao *et al.*, 2007).

## 7.5 LigPlot Analysis of Norovirus-HBGA Complexes

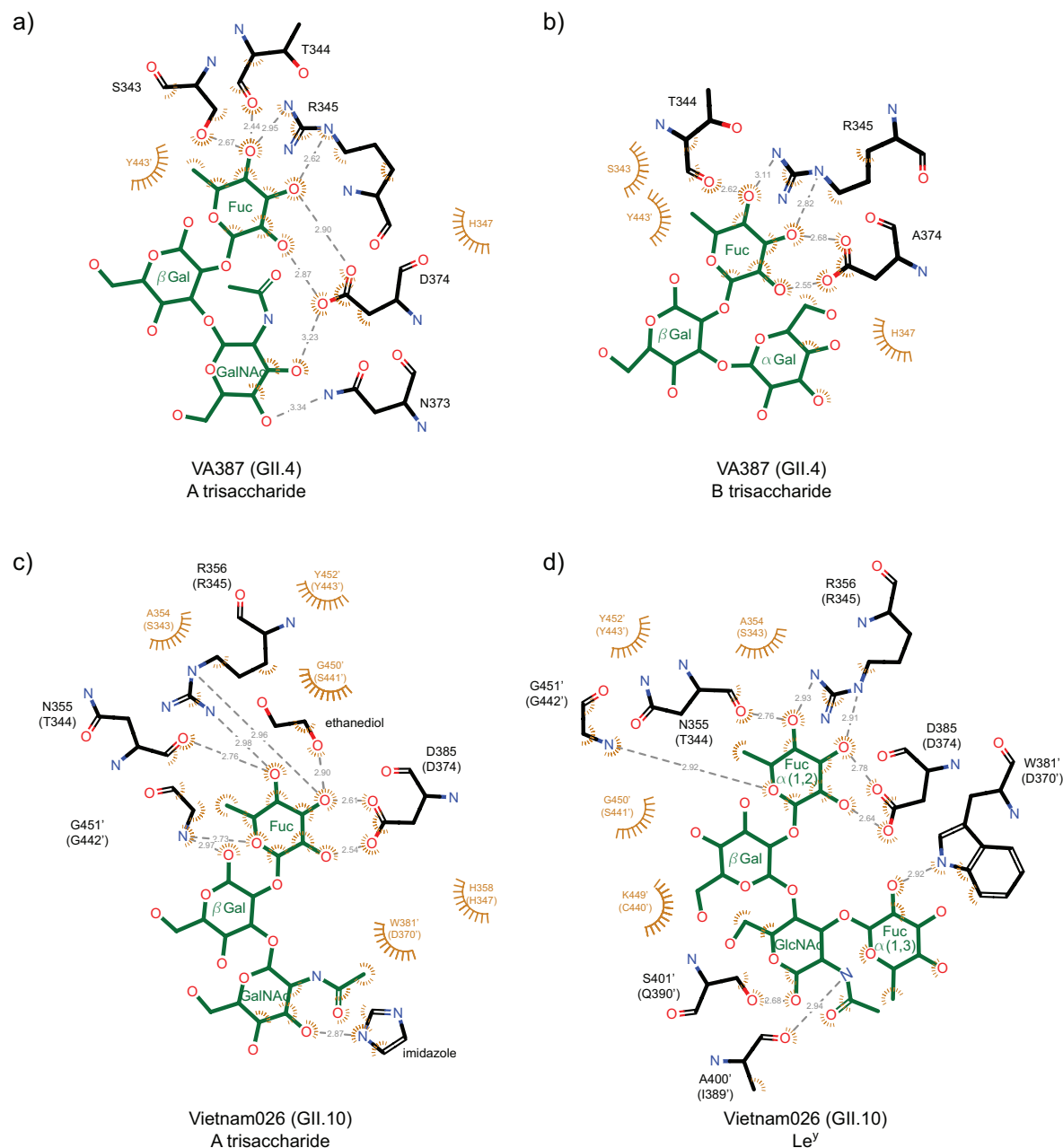


Figure 7.3. HBGA binding pocket of GII NoV from protein crystallization. a)-b) Binding pocket of GII.4 strain VA387 in complex with A trisaccharide (a) (pdb code: 2obs) and B trisaccharide (b) (pdb code: 2obt) (Cao *et al.*, 2007). c)-d) Binding pocket of the rare GII.10 strain Vietnam026 in complex with A trisaccharide (c) (pdb code: 3pa1) and Le<sup>y</sup> (d) (pdb code: 3pa2) (Hansman *et al.*, 2011); residues in brackets are corresponding residues in VA387 as identified by sequence alignment. Figures show hydrogen bonds and hydrophobic interactions predicted with LigPlot; in a) and b) hydrophobic interactions from Y443' were added manually as they were not predicted by LigPlot.

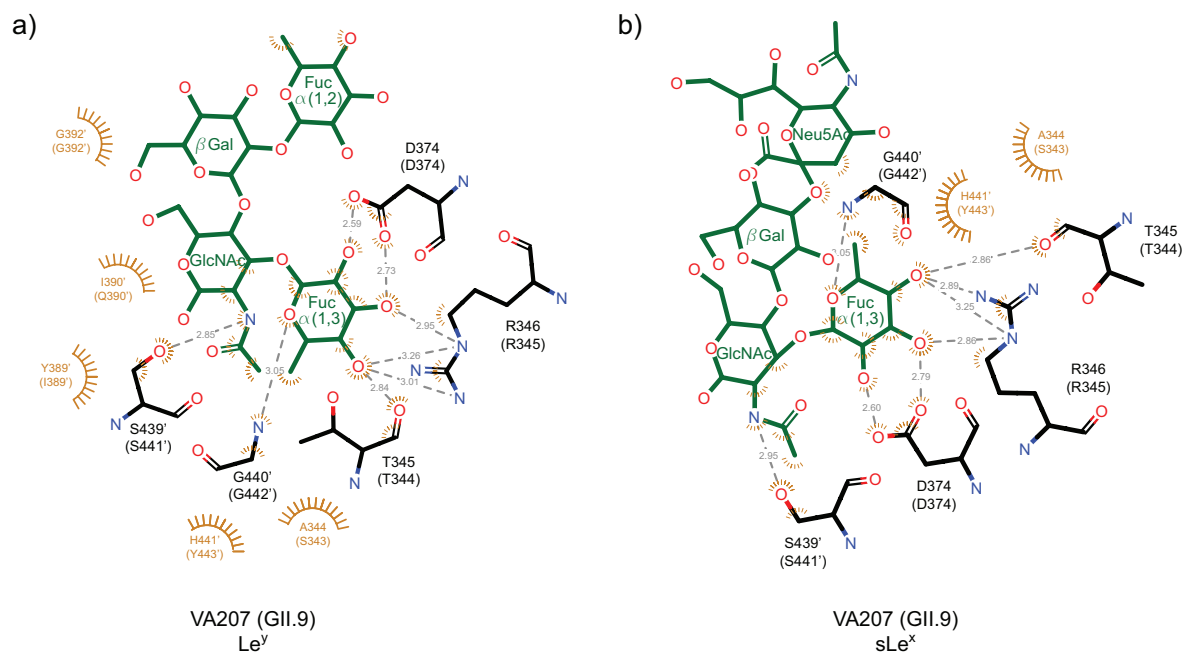


Figure 7.4. Interaction sites of Lewis antigens with a GII.9 NoV. Hydrogen bonds and hydrophobic interactions predicted by LigPlot (available via <http://www.ebi.ac.uk/pdbsum/>) for the crystal structures of the GII.9 strain VA207 in complex with Le<sup>y</sup> (a) (pdb code: 3pun) and sLe<sup>x</sup> (b) (pdb code: 3pvd) (Chen *et al.*, 2011); residues in brackets are corresponding residues of the GII.4 strains VA387 that are identical with Ast6139 except for V389'.

## 7.6 NMR Experiments

### 7.6.1 STD Titration of $\alpha$ -L-Fuc-(1,*O*)-CH<sub>3</sub>

$\alpha$ -L-Fuc-(1,*O*)-CH<sub>3</sub> (**2**) was subjected to STD titration (Christoph Rademacher, unpublished results). To a sample of 0.66 mg/mL or 61.3 nM Ast6139 VLPs (corresponding to 11  $\mu$ M binding sites assuming 180 binding sites per VLP) in 23 mM deuterated phosphate buffer pH 7.0 with 154 mM NaCl  $\alpha$ -L-Fuc-(1,*O*)-CH<sub>3</sub> was titrated from 19  $\mu$ M to 54 mM. The VLPs were diluted by 22% during the titration. STD spectra were performed on a Bruker Avance DRX or AV III 500 MHz NMR spectrometer equipped with a TCI cryogenic probe at a temperature of 298 K. The STD effects and STD amplification factors (equation 6) were determined and plotted against the ligand excess. The titration curves were fitted to a Langmuir binding isotherm of a one-site (equation 4) using the ligand excess as dependent variable *c*. The *K<sub>D</sub>* value was estimated from the ratio of ligand excess to ligand concentration from the titration. The curves were also fitted to a two-site Langmuir binding model:

$$\text{STD AF}(c) = \frac{\text{STD AF}_{\text{max1}} * c}{K_{D1} + c} + \frac{\text{STD AF}_{\text{max2}} * c}{K_{D2} + c} \quad (12)$$

with STD AF<sub>max1</sub> and STD AF<sub>max2</sub> being the maximal STD amplification factor at infinite ligand concentration for the high and the low affinity components, respectively, and *K<sub>D1</sub>* and *K<sub>D2</sub>* being the equilibrium dissociation constants of the high and the low affinity components, respectively. The results from curve fitting using Origin 7.0 (Microcal) are shown in Figure 7.5 and Table 7.1.

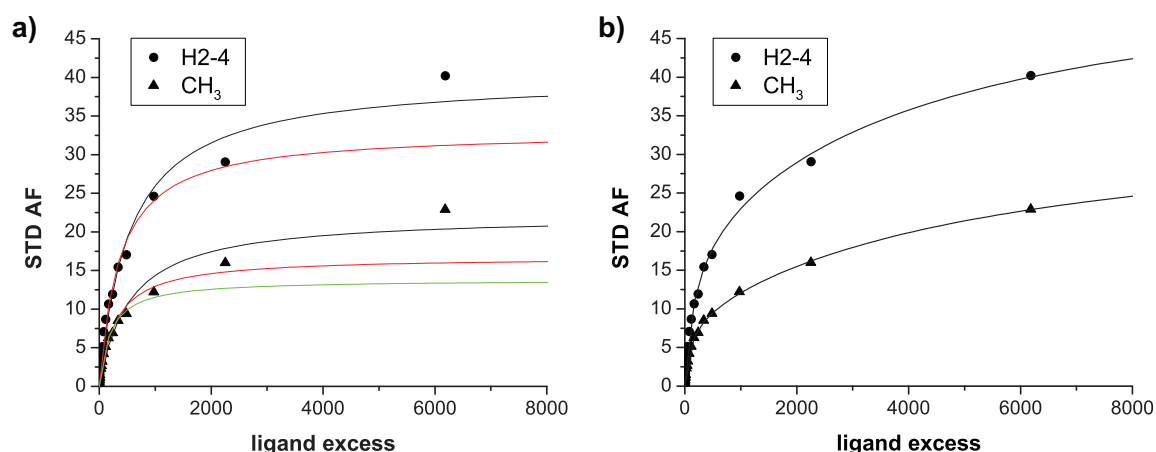


Figure 7.5. STD titration of  $\alpha$ -L-Fuc-(1,*O*)-CH<sub>3</sub> (**2**). a) Plots of STD amplification factors versus ligand excess (ca. 1/100 of ligand concentration in mM) and curve fittings to a 1:1 Langmuir binding model (equation 4) including all data points (black lines) and excluding the last (red lines) and the last two data points (green line); b) plots of STD AF versus ligand excess and curve fittings to a two-site binding model (equation 12) including all data points. The fitting results are compiled in Table 7.1.

Table 7.1. Results from curve fitting of  $\alpha$ -L-Fuc-(1,*O*)-CH<sub>3</sub> titration curves.

Proton	Range fitted	K <sub>D1</sub>	STD AF <sub>max1</sub>	K <sub>D2</sub>	STD AF <sub>max2</sub>	R <sup>2</sup> /χ <sup>2</sup>
<b>One-site binding model</b>						
H2-4	all data points	5.5 mM (± 0.6 mM)	40.1 (± 1.7)	–	–	0.9801/ 2.69
	0-2254 (21 mM)	3.7 mM (± 0.3 mM)	33.0 (± 1.2)	–	–	0.9906/ 0.76
CH <sub>3</sub>	all data points	5.4 mM (± 0.9 mM)	22.2 (± 1.3)	–	–	0.9608/ 1.58
	0-2254 (21 mM)	3.0 mM (± 0.4 mM)	16.7 (± 0.8)	–	–	0.9809/ 0.43
	0-976 (10 mM)	2.0 mM (± 0.2 mM)	13.8 (± 0.6)	–	–	0.9890/ 0.16
<b>Two-site binding model</b>						
H2-4	all data points	1.7 mM (± 0.4 mM)	18.7 (± 3.3)	40 mM (± 20 mM)	37.3 (± 4.3)	0.9969/ 0.47
CH <sub>3</sub>	all data points	1.0 mM (± 0.1 mM)	8.7 (± 0.5)	48 mM (± 9 mM)	26.9 (± 1.8)	0.9964/ 0.06

## 7.6.2 K<sub>D</sub> of HBGs from Competitive STD Titrations

Different HBGs at a concentration [L]=1 mM were titrated with  $\alpha$ -L-Fuc-(1,*O*)-CH<sub>3</sub> (**2**) in presence of Ast6139 VLPs. Fitting of the inhibition curves (absolute STD effect of reporter signals versus  $\alpha$ -L-Fuc-(1,*O*)-CH<sub>3</sub> concentration) to equation 5 yielded IC<sub>50</sub> values of  $\alpha$ -L-Fuc-(1,*O*)-CH<sub>3</sub> for depletion of HBGs (see Table 4.7). Both reporter ligand and VLP concentrations were kept constant. With the help of the Cheng-Prusoff equation

(equation 6) the affinities  $K_D$  of depleted HBGAs are calculated from  $[L]$ ,  $IC_{50}$  and  $K_I$  of the competing ligand  $\alpha$ -L-Fuc-(1,*O*)-CH<sub>3</sub> (Cheng & Prusoff, 1973):

$$K_I = \frac{IC_{50}}{1 + \frac{[L]}{K_D}}$$

For the  $K_I$  ( $=K_D$ ) of  $\alpha$ -L-Fuc-(1,*O*)-CH<sub>3</sub> the values determined by direct STD titration (Table 7.1) were taken: the high affinity components from fitting to a two-site binding model (1.7 and 1.0 mM for H2-4 and CH<sub>3</sub>, respectively) and the affinities from the fit to a one-site binding model (3.7 and 2.0 mM for H2-4 and CH<sub>3</sub>, respectively). The results are compiled in Table 7.2. Errors were calculated taking into account the errors of the  $IC_{50}$  values and of the  $K_D$  values of  $\alpha$ -L-Fuc-(1,*O*)-CH<sub>3</sub>.

Table 7.2. Calculation of  $K_D$  values of HBGAs from  $IC_{50}$  values. For  $K_I$  of  $\alpha$ -L-Fuc-(1,*O*)-CH<sub>3</sub> (**2**) ( $K_{I,Fuc}$ ) affinities from direct STD titration (cf. Table 7.1) were taken. Calculation of  $K_D$  is not possible if the  $IC_{50}$  is lower than the assumed  $K_I$  (indicated by 'n.d.').

Ligand displaced	Reporter signal	$IC_{50,Fuc}$ [mM]	$K_D$ (displaced ligand) [mM]			
			$K_{I,Fuc}=1$ mM ( $\pm 0.1$ mM)	$K_{I,Fuc}=1.7$ mM ( $\pm 0.4$ mM)	$K_{I,Fuc}=2.0$ mM ( $\pm 0.2$ mM)	$K_{I,Fuc}=3.7$ mM ( $\pm 0.3$ mM)
A trisaccharide octyl glycoside <b>4</b>	GalNAc H4	5.4 ( $\pm 0.8$ )	0.23 ( $\pm 0.06$ )	0.46 ( $\pm 0.22$ )	0.59 ( $\pm 0.34$ )	2.18 ( $\pm 1.45$ )
	NAc	5.4 ( $\pm 0.6$ )	0.23 ( $\pm 0.05$ )	0.46 ( $\pm 0.21$ )	0.59 ( $\pm 0.32$ )	2.18 ( $\pm 1.37$ )
	Fuc H1	5.2 ( $\pm 1.5$ )	0.24 ( $\pm 0.09$ )	0.49 ( $\pm 0.30$ )	0.63 ( $\pm 0.45$ )	2.47 ( $\pm 1.99$ )
B trisaccharide methyl glycoside <b>5b</b>	Gal H3	4.1 ( $\pm 0.9$ )	0.32 ( $\pm 0.10$ )	0.71 ( $\pm 0.39$ )	0.95 ( $\pm 0.62$ )	9.25 ( $\pm 6.81$ )
	Fuc H1	4.7 ( $\pm 1.0$ )	0.27 ( $\pm 0.08$ )	0.57 ( $\pm 0.31$ )	0.74 ( $\pm 0.48$ )	3.70 ( $\pm 2.70$ )
	Fuc CH <sub>3</sub>	4.2 ( $\pm 0.9$ )	0.31 ( $\pm 0.10$ )	0.68 ( $\pm 0.37$ )	0.91 ( $\pm 0.59$ )	7.40 ( $\pm 5.41$ )
sLe <sup>x</sup> <b>14</b>	NAc	3.9 ( $\pm 0.4$ )	0.34 ( $\pm 0.07$ )	0.77 ( $\pm 0.34$ )	1.05 ( $\pm 0.57$ )	18.5 ( $\pm 11.5$ )
<b>30</b> (difucosyl. compound)	Fuc CH <sub>3</sub>	2.0 ( $\pm 0.2$ )	1.00 ( $\pm 0.20$ )	5.67 ( $\pm 2.47$ )	n.d.	n.d.
	H1' <sub>a/b</sub>	1.8 ( $\pm 0.8$ )	1.25 ( $\pm 0.68$ )	17.0 ( $\pm 13.3$ )	n.d.	n.d.
<b>31</b> (160 + Fuc)	Fuc H4	5.7 ( $\pm 2.1$ )	0.21 ( $\pm 0.10$ )	0.43 ( $\pm 0.30$ )	0.54 ( $\pm 0.43$ )	1.85 ( $\pm 1.64$ )
	Fuc CH <sub>3</sub>	5.8 ( $\pm 1.5$ )	0.21 ( $\pm 0.07$ )	0.41 ( $\pm 0.25$ )	0.53 ( $\pm 0.37$ )	1.76 ( $\pm 1.37$ )

An assumed  $K_I$  of 3.7 mM for  $\alpha$ -L-Fuc-(1,*O*)-CH<sub>3</sub> results in  $K_D$  values for B trisaccharide and sLe<sup>x</sup> that are above that of  $\alpha$ -L-Fuc-(1,*O*)-CH<sub>3</sub>. Since the affinity of oligosaccharides is assumed to be higher than that of the monosaccharidic Fuc, the respective values are regarded to be invalid (forth column in grey).

*Calculation of  $K_D$  from mathematical conversion of the Cheng-Prusoff equation:*

Analogue to the titration of B trisaccharide **5b** with  $\alpha$ -L-Fuc-(1,*O*)-CH<sub>3</sub> **2**, a sample of 1 mM  $\alpha$ -L-Fuc-(1,*O*)-CH<sub>3</sub> was titrated with B trisaccharide **5b**. IC<sub>50</sub> values of 0.66 mM ( $\pm 0.16$  mM) and 1.45 mM ( $\pm 0.57$  mM) were obtained for reporter signals H5 and CH<sub>3</sub> resulting in an arithmetic mean of 1.1 mM ( $\pm 0.4$  mM). The arithmetic mean of the IC<sub>50</sub> value of  $\alpha$ -L-Fuc-(1,*O*)-CH<sub>3</sub> for titration of B trisaccharide is 4.3 mM ( $\pm 0.9$  mM).

A mathematical approach was applied to calculate  $K_D$  values of B trisaccharide and  $\alpha$ -L-Fuc-(1,*O*)-CH<sub>3</sub> from these two IC<sub>50</sub> values by conversion and substitution of the Cheng-Prusoff equation. Therefore the assumption  $K_I=K_D$  is made for the two ligands.

Cheng-Prusoff equation for titration of  $\alpha$ -L-Fuc-(1,*O*)-CH<sub>3</sub> with B trisaccharide **5b**:

$$K_I^{Btri} = \frac{IC_{50}^{Btri}}{1 + \frac{[Fuc]}{K_D^{Fuc}}} \quad (I)$$

Cheng-Prusoff equation for titration of B trisaccharide **5b** with  $\alpha$ -L-Fuc-(1,*O*)-CH<sub>3</sub>:

$$K_I^{Fuc} = \frac{IC_{50}^{Fuc}}{1 + \frac{[Btri]}{K_D^{Btri}}} \quad (II)$$

Solving equation II for  $K_D^{Btri}$ :

$$1 + \frac{[Btri]}{K_D^{Btri}} = \frac{IC_{50}^{Fuc}}{K_I^{Fuc}}$$

$$K_D^{Btri} = \frac{[Btri]}{\frac{IC_{50}^{Fuc}}{K_I^{Fuc}} - 1} \quad (III)$$

Assumptions:

$$K_I^{Btri} = K_D^{Btri} \quad \text{and} \quad K_I^{Fuc} = K_D^{Fuc}$$

Combination of I and III:

$$K_D^{Btri} = \frac{IC_{50}^{Btri}}{1 + \frac{[Fuc]}{K_D^{Fuc}}} = \frac{[Btri]}{\frac{IC_{50}^{Fuc}}{K_D^{Fuc}} - 1} \quad (IV)$$

Solving equation IV for  $K_D^{Fuc}$ :

$$\begin{aligned}
 IC_{50}^{Btri} * \left( \frac{IC_{50}^{Fuc}}{K_D^{Fuc}} - 1 \right) &= [Btri] * \left( 1 + \frac{[Fuc]}{K_D^{Fuc}} \right) \\
 \frac{IC_{50}^{Btri} * IC_{50}^{Fuc}}{K_D^{Fuc}} - IC_{50}^{Btri} &= [Btri] + \frac{[Btri] * [Fuc]}{K_D^{Fuc}} \\
 \frac{1}{K_D^{Fuc}} (IC_{50}^{Btri} * IC_{50}^{Fuc} - [Btri] * [Fuc]) &= [Btri] + IC_{50}^{Btri} \\
 K_D^{Fuc} &= \frac{IC_{50}^{Btri} * IC_{50}^{Fuc} - [Btri] * [Fuc]}{[Btri] + IC_{50}^{Btri}} \quad (V)
 \end{aligned}$$

Analogous, combination of II and III and solvation for  $K_D^{Btri}$  yields:

$$K_D^{Btri} = \frac{IC_{50}^{Fuc} * IC_{50}^{Btri} - [Fuc] * [Btri]}{[Fuc] + IC_{50}^{Fuc}} \quad (VI)$$

Known variables:

$$[Fuc] = [Btri] = 1 \text{ mM}$$

$$IC_{50}^{Btri} = 1.1 \text{ mM } (\pm 0.4 \text{ mM})$$

$$IC_{50}^{Fuc} = 4.3 \text{ mM } (\pm 0.9 \text{ mM})$$

Insertion of known variables into V:

$$K_D^{Fuc} = \frac{1.1 \text{ mM} * 4.3 \text{ mM} - 1 \text{ mM} * 1 \text{ mM}}{1 \text{ mM} + 1.1 \text{ mM}}$$

$$K_D^{Fuc} = 1.7 \text{ mM } (\pm 1.3 \text{ mM})$$

Analogous, insertion of known variables into VI:

$$K_D^{Btri} = \frac{4.3 \text{ mM} * 1.1 \text{ mM} - 1 \text{ mM} * 1 \text{ mM}}{1 \text{ mM} + 4.3 \text{ mM}}$$

$$K_D^{Btri} = 0.7 \text{ mM } (\pm 0.5 \text{ mM})$$

Due to error propagation the inaccuracy of  $K_D^{Btri}$  and  $K_D^{Fuc}$  determined from mathematical conversion of the Cheng-Prusoff equation is relatively high. But the calculated values are very close to the  $K_D$  estimated by direct STD titration of  $\alpha$ -L-Fuc-(1,*O*)-CH<sub>3</sub> (cf. Table 7.1) and the  $K_D$  of B trisaccharide **5b** calculated from its IC<sub>50</sub> (cf. Table 7.2).



### 7.6.3 TrREOSY Experiment of sLe<sup>x</sup>

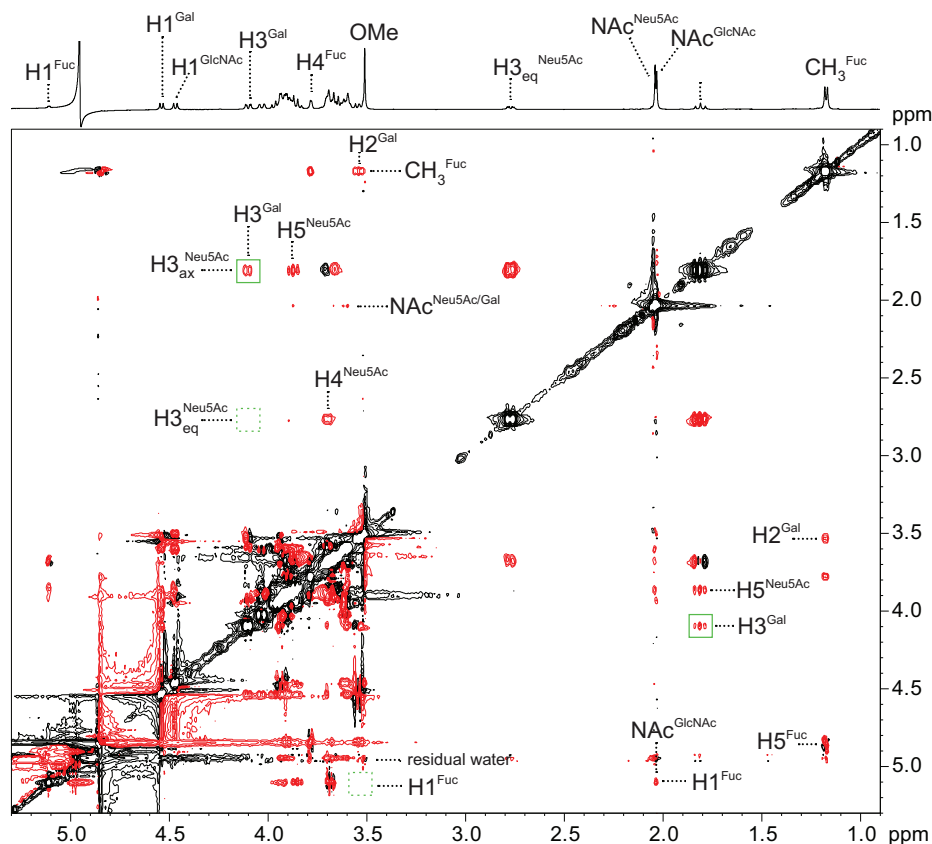


Figure 7.6. trROESY spectrum of sLe<sup>x</sup> in presence of VLPs. The spectrum of sLe<sup>x</sup> **14** was recorded at 500 MHz with a mixing time of 150 ms. The temperature was set to 298 K. Signals around  $\delta(^1\text{H})=4.7$  ppm are disturbed by the high amount of residual water despite a 3-9-19 WATERGATE solvent suppression sequence. The signal was partly removed by application of a qfil baseline procession scheme.

### 7.6.4 TrNOEs Simulated for Simple Two-Spin Systems

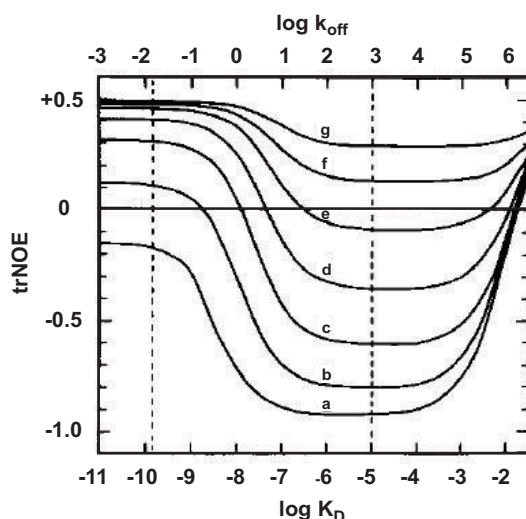


Figure 7.7. Dependence of trNOE intensity on  $K_D$  and  $k_{on}$ . Steady state trNOEs for a two-spin system IS were simulated as a function of the  $K_D$  and the  $k_{off}$  ( $k_{on}$  fixed at  $10^{-8} \text{ M}^{-1}\text{s}^{-1}$ ) for different ligand over protein ratios: a) 2; b) 4; c) 8; d) 16; e) 32; f) 64; g) 128. Crossing regions between slow, intermediate and fast exchange on the relaxation time scale are indicated by vertical lines. The figure was adapted from (Neuhaus & Williamson, 2000).

### 7.6.5 STD Titration of Virtual Screening Hit 42

Chemical shift changes of 1D  $^1\text{H}$  signals of **42** during titration in presence of ast6139 VLPs and compared to the chemical shift of a 2 mM sample of **42** in absence of VLPs; all experiments measured in 23 mM phosphate buffer pH 7.0, 154 mM NaCl:

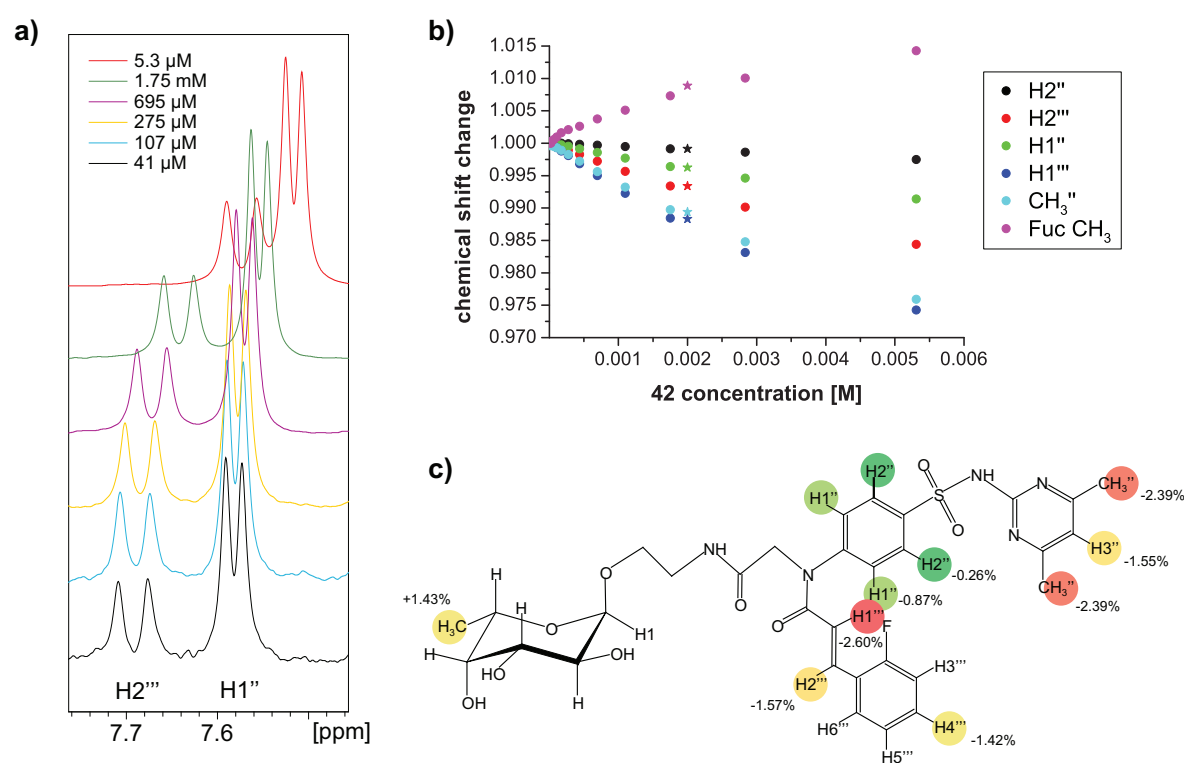


Figure 7.8. Chemical shift changes during titration of **42**. a) 1D  $^1\text{H}$  NMR spectra showing the signals  $\text{H2}'''$  and  $\text{H1}''$  at increasing concentrations of **42**; the scales of the spectra were adjusted to show signals at similar size; all spectra were referenced to TSP (0 ppm). b) Observed chemical shift changes during titration in presence of VLPs normalized to the chemical shifts of the 16.5  $\mu\text{M}$  sample (circles); the star symbols represent the chemical shifts of a 2 mM sample in absence of VLPs. c) Structural formula of **42** with colored circles indicating small (green) to large (red) absolute chemical shift changes (shown in %).

### 7.6.6 Assignment of HBGA Fragments

All spectra were assigned at a temperature of 282 K and referenced to TSP-*d*4. Carbohydrates **3a**, **5a**, **5b**, **6** and **7** were assigned by Dr. Christoph Rademacher and published in his PhD thesis (Rademacher, 2008). Assignments for **4**, **9**, **10**, **11**, **12** and **13** have also been published in my Master thesis (Langpap, 2008).

#### L-Fucose (1)

Residue	Proton	$\delta$ ( $^1\text{H}$ ) [ppm]	$\delta$ ( $^{13}\text{C}$ ) [ppm]
$\alpha$ -Fuc	H1	5.204	n.d.
	H2	3.763	n.d.
	H3	3.862	n.d.
	H4	3.82	n.d.
	H5	4.207	n.d.
	CH <sub>3</sub>	1.209	n.d.
$\beta$ -Fuc	H1	4.561	n.d.
	H2	3.446	n.d.
	H3	3.647	n.d.
	H4	3.750	n.d.
	H5	3.82	n.d.
	CH <sub>3</sub>	1.249	n.d.

#### $\alpha$ -Fuc-(1,O)-CH<sub>3</sub> (2)

Residue	Proton	$\delta$ ( $^1\text{H}$ ) [ppm]	$\delta$ ( $^{13}\text{C}$ ) [ppm]
$\alpha$ -Fuc	H1	4.781	n.d.
	H2	3.81	n.d.
	H3	3.81	n.d.
	H4	3.81	n.d.
	H5	4.058	n.d.
	CH <sub>3</sub>	1.233	n.d.
	OMe	3.402	n.d.

#### H disaccharide (**3a**), $\alpha$ -L-Fuc-(1,2)- $\beta$ -D-Gal-(1,O)- $^{13}\text{CH}_3$

Residue	Proton	$\delta$ ( $^1\text{H}$ ) [ppm]	$\delta$ ( $^{13}\text{C}$ ) [ppm]
$\alpha$ -Fuc	H1	5.15	102.99
	H2	3.80	71.60
	H3	3.89	72.62
	H4	3.83	74.92
	H5	4.28	70.03
	CH <sub>3</sub>	1.23	18.09
$\beta$ -Gal	H1	4.44	105.66
	H2	3.54	81.29
	H3	3.85	76.40
	H4	3.94	69.97
	H5	3.71	78.06
	H61/H62	3.81/ 3.79	63.94
	CH <sub>3</sub>	3.62/ 3.33	60.15

A trisaccharide (**4**),  $\alpha$ -D-GalNAc-(1,3)-[ $\alpha$ -L-Fuc-(1,2)]- $\beta$ -D-Gal-(1,*O*)-(CH<sub>2</sub>)<sub>7</sub>CH<sub>3</sub>

Residue	Proton	$\delta$ ( <sup>1</sup> H) [ppm]	$\delta$ ( <sup>13</sup> C) [ppm]
$\alpha$ -Fuc	H1	5.342	101.51
	H2	3.786	70.78
	H3	3.826	72.72
	H4	3.826	72.72
	H5	4.495	69.83
	CH <sub>3</sub>	1.239	18.34
$\beta$ -Gal	H1	4.547	104.46
	H2	3.822	75.01
	H3	3.969	78.86
	H4	4.224	65.95
	H5	3.651	77.93
	H61/H62	3.805/ 3.735	64.34
$\alpha$ -GalNAc	H1	5.179	94.09
	H2	4.240	52.60
	H3	3.912	70.81
	H4	3.996	71.48
	H5	4.234	74.05
	H6	3.770	64.34
	NAc	2.050	24.86
octyl	H1 <sub>a</sub> /H1 <sub>b</sub>	3.972/ 3.678	73.74
	H2	1.622	31.97
	H3-7	1.343 – 1.287	28.42 – 34.22
	H8	0.872	16.45

B trisaccharide (**5a**),  $\alpha$ -D-Gal-(1,3)-[ $\alpha$ -L-Fuc-(1,2)]- $\beta$ -D-Gal-(1,*O*)-(CH<sub>2</sub>)<sub>7</sub>CH<sub>3</sub>

Residue	Proton	$\delta$ ( <sup>1</sup> H) [ppm]	$\delta$ ( <sup>13</sup> C) [ppm]
$\alpha$ -Fuc	H1	5.23	101.87
	H2	3.73	70.93
	H3	3.73	72.96
	H4	3.73	75.18
	H5	4.41	70.09
	CH <sub>3</sub>	1.14	18.73
$\beta$ -Gal	H1	4.48	104.74
	H2	3.77	75.39
	H3	3.89	79.47
	H4	4.21	66.53
	H5	3.60	77.94
	H61/H62	3.73/ 3.68	64.24
$\alpha$ -Gal	H1	5.16	96.03
	H2	3.80	71.33
	H3	3.79	72.63
	H4	3.88	72.52
	H5	4.16	74.35
	H6	3.66	64.56
octyl	H1 <sub>a</sub> /H1 <sub>b</sub>	3.89/ 3.59	74.05
	H2	1.54	32.17
	H3-7	1.20-1.25	25.28-34.41
	H8	0.79	25.28

B trisaccharide (**5b**),  $\alpha$ -D-Gal-(1,3)-[ $\alpha$ -L-Fuc-(1,2)]- $\beta$ -D-Gal-(1,*O*)-CH<sub>3</sub>

Residue	Proton	$\delta$ ( <sup>1</sup> H) [ppm]	$\delta$ ( <sup>13</sup> C) [ppm]
$\alpha$ -Fuc	H1	5.22	101.84
	H2	3.78	70.44
	H3	3.82	72.37
	H4	3.82	74.62
	H5	4.35	69.63
	CH <sub>3</sub>	1.20	17.80
$\beta$ -Gal	H1	4.48	105.29
	H2	3.78	76.41
	H3	3.96	78.41
	H4	4.28	65.87
	H5	3.69	77.19
	H61/H62	3.82/ 3.77	63.67
$\alpha$ -Gal	H1	5.24	95.54
	H2	3.87	70.78
	H3	3.93	72.02
	H4	3.96	71.98
	H5	4.28	73.70
	H6	3.74	64.02
	OMe	3.89	59.74

B trisaccharide (**5c**),  $\alpha$ -D-Gal-(1,3)-[ $\alpha$ -L-Fuc-(1,2)]- $\beta$ -D-Gal-(1,*O*)-(CH<sub>2</sub>)<sub>8</sub>COOC<sub>2</sub>H<sub>5</sub>  
<sup>13</sup>C chemical shifts were referenced to  $\alpha$ -Fuc C1 of B trisaccharide **5a** instead of TSP.

Residue	Proton	$\delta$ ( <sup>1</sup> H) [ppm]	$\delta$ ( <sup>13</sup> C) [ppm]
$\alpha$ -Fuc	H1	5.312	101.87*
	H2	3.792	71.00
	H3	3.810	73.15
	H4	3.809	75.22
	H5	4.489	70.04
	CH <sub>3</sub>	1.221	18.75
$\beta$ -Gal	H1	4.557	104.70
	H2	3.850	75.57
	H3	3.979	79.72
	H4	4.286	66.71
	H5	3.687	77.97
	H61/H62	3.811/ 3.757	64.34
$\alpha$ -Gal	H1	5.248	96.24
	H2	3.885	71.39
	H3	3.885	72.82
	H4	3.974	72.75
	H5	4.235	74.50
	H6	3.739	64.81
ethylnonanoate	H1 <sub>a</sub> /H1 <sub>b</sub>	3.965/ 3.675	74.17
	H2/H7	1.615/ 1.621	27.77/ 32.31
	H3-6	1.31 – 1.36	28.7 – 32.0
	H8	2.382	37.24
	H1'	4.156	64.83
	H2'	1.258	16.57

H trisaccharide type 1 (**6**),  $\alpha$ -L-Fuc-(1,2)- $\beta$ -D-Gal-(1,3)- $\beta$ -D-GlcNAc-(1,*O*)-(CH<sub>2</sub>)<sub>7</sub>CH<sub>3</sub>

Residue	Proton	$\delta$ ( <sup>1</sup> H) [ppm]	$\delta$ ( <sup>13</sup> C) [ppm]
$\alpha$ -Fuc	H1	5.19	n.d.
	H2	3.76	n.d.
	H3	3.69	n.d.
	H4	3.76	n.d.
	H5	4.31	n.d.
	CH <sub>3</sub>	1.23	n.d.
$\beta$ -Gal	H1	4.67	n.d.
	H2	3.58	n.d.
	H3	3.85	n.d.
	H4	3.89	n.d.
	H5	3.68	n.d.
	H61/H62	3.84/ 3.85	n.d.
$\beta$ -GlcNAc	H1	4.42	n.d.
	H2	3.79	n.d.
	H3	3.98	n.d.
	H4	n.d.	n.d.
	H5	3.50	n.d.
	H61/H62	3.94/ 3.78	n.d.
	NAc	2.07	n.d.
octyl	H1 <sub>a</sub> /H1 <sub>b</sub>	3.88/ 3.54	n.d.
	H2	1.53	n.d.
	H3-7	1.28 – 1.30	n.d.
	H8	0.87	n.d.

H trisaccharide type 2 (**7**),  $\alpha$ -L-Fuc-(1,2)- $\beta$ -D-Gal-(1,4)- $\beta$ -D-GlcNAc-(1,*O*)-(CH<sub>2</sub>)<sub>8</sub>COOCH<sub>3</sub>

Residue	Proton	$\delta$ ( <sup>1</sup> H) [ppm]	$\delta$ ( <sup>13</sup> C) [ppm]
$\alpha$ -Fuc	H1	5.34	102.67
	H2	3.82	71.48
	H3	3.83	72.89
	H4	3.86	74.99
	H5	4.28	70.29
	CH <sub>3</sub>	1.27	18.69
$\beta$ -Gal	H1	4.59	103.41
	H2	3.70	79.67
	H3	3.91	76.85
	H4	3.91	72.48
	H5	3.73	78.64
	H61/H62	3.81/ n.d.	64.65
$\beta$ -GlcNAc	H1	4.52	104.51
	H2	3.79	58.67
	H3	3.68	75.86
	H4	3.83	79.15
	H5	3.49	78.71
	H6	4.02	63.50
	NAc	2.07	25.59
Lemieux	H2	2.43	37.09
	H3	1.64	27.64
	H4-7	1.33	28.40-31.68
	H8	1.58	31.97
	H9 <sub>a</sub> /H9 <sub>b</sub>	3.95/ 3.61	74.03
	CH <sub>3</sub>	3.71	55.52

H trisaccharide type 6 (**8**),  $\alpha$ -L-Fuc-(1,2)- $\beta$ -D-Gal-(1,4)-D-Glc

Residue	Proton	$\delta$ ( $^1\text{H}$ ) [ppm]	$\delta$ ( $^{13}\text{C}$ ) [ppm]
$\alpha$ -Fuc	H1	5.320	102.16
	H2	3.797	71.01
	H3	3.797	72.50
	H4	3.822	74.53
	H5	4.279/ 4.248	69.80
	CH <sub>3</sub>	1.237	18.06
$\beta$ -Gal	H1	4.542	103.04
	H2	3.672	79.10
	H3	3.880	76.45
	H4	3.889	72.01
	H5	3.771	72.40
	H6	3.964	62.94
$\alpha/\beta$ -Glc	H1	5.234/ 4.648	94.70/ 98.79
	H2	3.594/ 3.300	74.15/ 76.73
	H3	n.d./ 3.592	n.d./ 77.16
	H4	3.696/ 3.737	78.14/ 78.50
	H5	n.d./ 3.490	n.d./ 78.21
	H6	3.906/ 3.803	62.85/ 64.03
	H6'	3.789/ 3.736	62.85/ 64.03

 $\alpha$ -L-Fuc-(1,3)- $\beta$ -D-GlcNAc-(1,*O*)-CH<sub>3</sub> (**9**)

Residue	Proton	$\delta$ ( $^1\text{H}$ ) [ppm]	$\delta$ ( $^{13}\text{C}$ ) [ppm]
$\alpha$ -Fuc	H1	4.985	102.97
	H2	3.689	70.81
	H3	3.835	72.41
	H4	3.804	74.68
	H5	4.340	69.77
	CH <sub>3</sub>	1.161	18.11
$\beta$ -GlcNAc	H1	4.448	104.68
	H2	3.839	58.03
	H3	3.629	83.30
	H4	3.534	71.47
	H5	3.498	78.76
	H6	3.956/ 3.763	63.58
	NAc	2.026	25.03
	OMe	3.514	60.03

Lewis<sup>x</sup> (**10**),  $\beta$ -D-Gal-(1,4)-[ $\alpha$ -L-Fuc-(1,3)]- $\beta$ -D-GlcNAc-(1,*O*)-CH<sub>3</sub>

Residue	Proton	$\delta$ ( <sup>1</sup> H) [ppm]	$\delta$ ( <sup>13</sup> C) [ppm]
$\alpha$ -Fuc	H1	5.115	101.73
	H2	3.689	70.63
	H3	3.914	72.13
	H4	3.800	74.84
	H5	4.870	69.71
	CH <sub>3</sub>	1.183	18.26
$\beta$ -Gal	H1	4.462	104.76
	H2	3.510	73.98
	H3	3.666	75.34
	H4	3.900	71.29
	H5	3.606	78.08
	H6	3.727	64.53
$\beta$ -GlcNAc	H1	4.471	104.76
	H2	3.925	58.61
	H3	3.855	77.95
	H4	3.937	76.29
	H5	3.606	78.08
	H6	4.024/ 3.879	62.64
	NAc	2.033	25.39
	OMe	3.511	60.11

Lewis<sup>a</sup> (**11**),  $\beta$ -D-Gal-(1,3)-[ $\alpha$ -L-Fuc-(1,4)]- $\beta$ -D-GlcNAc-(1,*O*)-CH<sub>3</sub>

Residue	Proton	$\delta$ ( <sup>1</sup> H) [ppm]	$\delta$ ( <sup>13</sup> C) [ppm]
$\alpha$ -Fuc	H1	5.031	100.95
	H2	3.809	70.45
	H3	3.896	71.87
	H4	3.896	71.87
	H5	4.903	69.74
	CH <sub>3</sub>	1.186	18.18
$\beta$ -Gal	H1	4.495	105.85
	H2	3.490	73.21
	H3	3.634	75.02
	H4	3.882	71.18
	H5	3.579	77.65
	H6	3.735	64.53
$\beta$ -GlcNAc	H1	4.450	104.71
	H2	3.907	58.37
	H3	4.062	78.92
	H4	3.737	75.19
	H5	3.562	78.24
	H6	4.001/ 3.876	62.36
	NAc	2.042	25.04
	OMe	3.512	60.00



Lewis<sup>y</sup> (**12**),  $\alpha$ -L-Fuc-(1,2)- $\beta$ -D-Gal-(1,4)-[ $\alpha$ -L-Fuc-(1,3)]- $\beta$ -D-GlcNAc-(1,*O*)-CH<sub>3</sub>

Residue	Proton	$\delta$ ( <sup>1</sup> H) [ppm]	$\delta$ ( <sup>13</sup> C) [ppm]
$\alpha$ -Fuc (1,2)	H1	5.293	102.28
	H2	3.798	71.09
	H3	3.833	74.54
	H4	3.798	72.56
	H5	4.275	69.83
	CH <sub>3</sub>	1.282	18.32
$\alpha$ -Fuc (1,3)	H1	5.101	101.61
	H2	3.693	70.48
	H3	3.923	72.01
	H4	3.815	74.70
	H5	4.904	69.83
	CH <sub>3</sub>	1.246	18.32
$\beta$ -Gal	H1	4.515	103.12
	H2	3.664	79.13
	H3	3.862	76.39
	H4	3.862	71.60
	H5	3.599	77.76
	H6	3.720	64.36
$\beta$ -GlcNAc	H1	4.450	104.75
	H2	3.916	58.65
	H3	3.829	77.95
	H4	3.934	76.23
	H5	3.475	78.44
	H6	4.051/ 3.850	62.79
	NAc	2.035	25.08
	OMe	3.506	60.12

Lewis<sup>b</sup> (**13**),  $\alpha$ -L-Fuc-(1,2)- $\beta$ -D-Gal-(1,3)-[ $\alpha$ -L-Fuc-(1,4)]- $\beta$ -D-GlcNAc-(1,*O*)-CH<sub>3</sub>

Residue	Proton	$\delta$ ( <sup>1</sup> H) [ppm]	$\delta$ ( <sup>13</sup> C) [ppm]
$\alpha$ -Fuc (1,2)	H1	5.157	102.45
	H2	3.738	71.12
	H3	3.723	72.18
	H4	3.759	74.75
	H5	4.344	69.12
	CH <sub>3</sub>	1.266	18.16
$\alpha$ -Fuc (1,4)	H1	5.029	100.73
	H2	3.809	70.61
	H3	3.853	71.57
	H4	3.832	74.77
	H5	4.871	70.03
	CH <sub>3</sub>	1.266	18.16
$\beta$ -Gal	H1	4.655	103.50
	H2	3.615	79.30
	H3	3.814	76.43
	H4	3.937	71.92
	H5	3.580	77.66
	H6	3.746	64.47
$\beta$ -GlcNAc	H1	4.327	105.60
	H2	3.814	58.44
	H3	4.131	77.47
	H4	3.713	74.94

H5	3.542	78.17
H6	3.990/ 3.875	62.25
NAc	2.067	25.00
OMe	3.483	60.11

sialyl-Le<sup>x</sup> (**14**),  $\alpha$ -D-Neu5Ac-(2,3)- $\beta$ -D-Gal-(1,4)-[ $\alpha$ -L-Fuc-(1,3)]- $\beta$ -D-GlcNAc-(1,*O*)-CH<sub>3</sub>

Residue	Proton	$\delta$ ( <sup>1</sup> H) [ppm]	$\delta$ ( <sup>13</sup> C) [ppm]
Neu5Ac	H3 <sub>eq</sub> / H3 <sub>ax</sub>	2.773/ 1.810	42.60
	H4	3.684	71.27
	H5	3.874	54.52
	H6	3.655	75.73
	H7	3.606	70.90
	H8	3.920	74.74
	H9	3.890/ 3.648	65.35
	NAc	2.038	24.90
$\alpha$ -Fuc	H1	5.106	101.60
	H2	3.677	70.50
	H3	3.905	72.02
	H4	3.782	74.74
	H5	4.850	69.57
	CH <sub>3</sub>	1.174	18.14
$\beta$ -Gal	H1	4.539	104.43
	H2	3.540	72.11
	H3	4.102	78.42
	H4	3.938	70.13
	H5	3.601	77.95
	H6	3.697	64.43
$\beta$ -GlcNAc	H1	4.464	104.66
	H2	3.927	58.45
	H3	3.846	77.77
	H4	3.964	76.10
	H5	3.601	77.95
	H6	4.032/ 3.900	62.40
	NAc	2.029	25.00
	OMe	3.508	60.03

sialyl-Le<sup>a</sup> (**15**),  $\alpha$ -D-Neu5Ac-(2,3)- $\beta$ -D-Gal-(1,3)-[ $\alpha$ -L-Fuc-(1,4)]- $\beta$ -D-GlcNAc-(1,*O*)-(CH<sub>2</sub>)<sub>3</sub>NHCOOCH<sub>2</sub>C<sub>6</sub>H<sub>5</sub> (numbering of the spacer starts at the glycosidic oxygen)

Residue	Proton	$\delta$ ( <sup>1</sup> H) [ppm]	$\delta$ ( <sup>13</sup> C) [ppm]
Neu5Ac	H3 <sub>eq</sub> / H3 <sub>ax</sub>	2.778/ 1.775	42.86
	H4	3.665	71.37
	H5	3.865	54.49
	H6	3.619	75.53
	H7	3.622	70.74
	H8	3.862	74.78
	H9	3.814/ 3.646	65.06
	NAc	2.036	18.16
$\alpha$ -Fuc	H1	5.012	100.96
	H2	3.794	70.56
	H3	3.884	71.90
	H4	3.783	74.76
	H5	4.902	69.73
	CH <sub>3</sub>	1.178	18.17
$\beta$ -Gal	H1	4.536	105.71
	H2	3.515	71.54
	H3	4.063	78.30
	H4	3.910	69.69
	H5	3.540	77.67
	H6	3.700	64.60
$\beta$ -GlcNAc	H1	4.481	103.87
	H2	3.890	58.46
	H3	4.046	78.90
	H4	3.723	75.15
	H5	3.525	78.26
	H6	3.963/ 3.846	62.42
	NAc	2.029	18.16
carbamoyl	H1-4	7.453-7.434	21.55/ 20.49
	H5	5.121	69.66
	H9	3.171	40.05
	H10	1.745	31.62
	H11	3.925/ 3.600	70.52

Xenoantigen (**29**),  $\alpha$ -D-Gal-(1,3)- $\alpha$ -D-Gal-(1,*O*)-CH<sub>3</sub>

Residue	Proton	$\delta$ ( <sup>1</sup> H) [ppm]	$\delta$ ( <sup>13</sup> C) [ppm]
$\alpha$ -Gal (1,3)	H1	5.158	97.74
	H2	3.859	71.09
	H3	3.965	72.07
	H4	4.013	71.97
	H5	4.179	73.70
	H6	3.743	63.86
$\alpha$ -Gal-OMe	H1	4.887	102.18
	H2	3.984	69.43
	H3	3.947	76.81
	H4	4.242	68.13
	H5	3.914	73.47
	H6	3.771	64.10
	OMe	3.431	57.81

Compound **30** (two  $\alpha$ -L-Fuc moieties linked via triazole/glycerol linker)

Residue	Proton	$\delta$ ( $^1\text{H}$ ) [ppm]	$\delta$ ( $^{13}\text{C}$ ) [ppm]
$\alpha$ -Fuc	H1	5.010	101.64
	H2	3.770	71.14
	H3	3.849	72.19
	H4	3.787	74.88
	H5	4.012	70.14
	CH <sub>3</sub>	1.128	18.27
linker	H1' <sub>a/b</sub>	4.777	63.51
	H <sub>ar</sub>	8.101	129.0
	H1''/H3''	4.74/ 4.52	55.93
	H2''	4.563	71.28

Compound **31** ( $\alpha$ -L-Fuc linked to fragment 160 via triazole/glycerol linker)

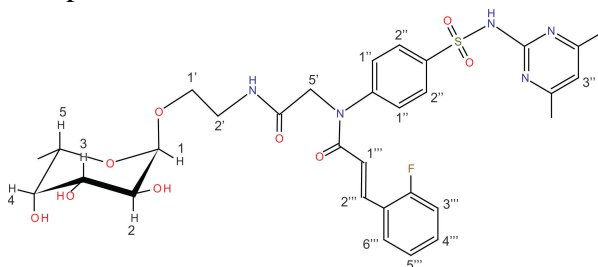
Sample for assignment: 0.5 mM in D<sub>2</sub>O; second set of peaks (oligomerized **31**) in brackets.

Residue	Proton	$\delta$ ( $^1\text{H}$ ) [ppm]	$\delta$ ( $^{13}\text{C}$ ) [ppm]
$\alpha$ -Fuc	H1	4.975	101.36
	H2	3.777	70.82
	H3	3.800	72.39
	H4	3.752	74.66
	H5	3.956	69.81
	CH <sub>3</sub>	1.111	18.13
fragment 160	H1 <sub>a</sub> /H1 <sub>b</sub>	5.288 (5.312)	64.48
	H3'	7.108 (7.056)	131.98 (132.17)
	H4'	7.276 (7.232)	126.92
	H5''	7.447 (7.433)	116.01
	CH3''	2.687	20.71
linker	H1' <sub>a/b</sub>	4.703	63.47
	H <sub>ar1</sub>	7.879 (7.814)	128.57
	H <sub>ar2</sub>	7.879 (7.794)	127.46
	H1''/H3''	4.04 – 4.58	55.69
	H2''	4.463 (4.340)	71.16
	H1''' <sub>a/b</sub>	4.412/ 4.380	38.62/ 38.95

Compound **32**

Residue	Proton	$\delta$ ( $^1\text{H}$ ) [ppm]	$\delta$ ( $^{13}\text{C}$ ) [ppm]
$\alpha$ -Fuc	H1		
	H2	3.770	
	H3	3.850	
	H4	3.787	
	H5	4.006	
	CH <sub>3</sub>	1.125	
linker	H1' <sub>a/b</sub>	4.790	
	H <sub>ar</sub>	8.095	
	H1''	4.580	
	H2''	4.007	

### Compound 42

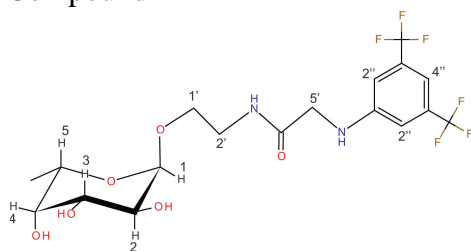


Residue	Proton	$\delta$ ( $^1\text{H}$ ) [ppm]	$\delta$ ( $^{13}\text{C}$ ) [ppm]
$\alpha$ -Fuc	H1	4.829	100.82
	H2	3.745	70.71
	H3	3.745	72.12
	H4	3.656	74.43
	H5	3.859	69.18
	$\text{CH}_3$	1.045	17.94
linker	$\text{H1}'_{\text{a}}/\text{H1}'_{\text{b}}$	3.725/ 3.502	69.14
	$\text{H2}'_{\text{a}}/\text{H2}'_{\text{b}}$	3.539/ 3.434	42.11
	$\text{H5}'$	4.587	55.47
benzene	$\text{H1}''$	7.553	130.35
	$\text{H2}''$	8.067	131.82
dimethylpyrimidine	$\text{H3}''$	6.677	114.24
	$\text{CH}_3''$	2.272	24.02
ethenylfluorobenzene	$\text{H1}'''$	6.402	123.04
	$\text{H2}'''$	7.643	138.88
	$\text{H3}'''/\text{H5}'''$	7.056	127.2/ 118.45
	$\text{H4}'''$	7.382	134.78
	$\text{H6}'''$	7.231	131.79

The chemical structure shows a nucleoside derivative. The sugar moiety is a five-membered ring with carbons labeled 1' through 5'. The base is a pyridine ring with carbons labeled 1'' through 4''. The sugar and base are connected via a sulfonamide group (-SO<sub>2</sub>-NH-). The sugar has hydroxyl groups at positions 1', 2', and 3'. The base has a methyl group at position 4''.

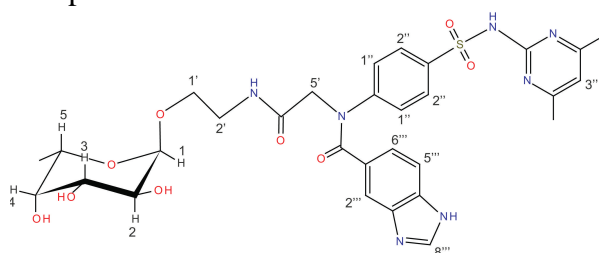
Residue	Proton	$\delta$ ( $^1\text{H}$ ) [ppm]	$\delta$ ( $^{13}\text{C}$ ) [ppm]
$\alpha$ -Fuc	H1	4.769	100.89
	H2	3.673	70.43
	H3	3.519	72.10
	H4	3.521	74.40
	H5	3.528	69.15
	$\text{CH}_3$	17.636	17.58
linker	$\text{H1}'_{\text{a}}/\text{H1}'_{\text{b}}$	3.670/ 3.468	69.10
	$\text{H2}'_{\text{a}}/\text{H2}'_{\text{b}}$	3.484	41.61
	$\text{H5}'$	3.911	49.22
benzene	$\text{H1}''$	6.717	114.26
	$\text{H2}''$	7.806	131.85
dimethylpyrimidine	$\text{H3}''$	6.733	114.13
	$\text{CH}_3''$	2.368	24.03

## Compound 44



Residue	Proton	$\delta$ ( $^1\text{H}$ ) [ppm]	$\delta$ ( $^{13}\text{C}$ ) [ppm]
$\alpha$ -Fuc	H1	4.783	101.38
	H2	3.677	70.45
	H3	3.534	72.10
	H4	3.510	74.42
	H5	3.587	69.21
	CH <sub>3</sub>	1.079	17.93
linker	H1' <sub>a</sub> /H1' <sub>b</sub>	3.695/3.510	69.15
	H2' <sub>a</sub> /H2' <sub>b</sub>	3.491	41.64
	H5'	3.970	49.24
1,3-di(trifluoro-methyl)benzene	H2''	7.136	114.85
	H4''	7.440	113.73

## Compound 45



Residue	Proton	$\delta$ ( $^1\text{H}$ ) [ppm]	$\delta$ ( $^{13}\text{C}$ ) [ppm]
$\alpha$ -Fuc	H1	4.823	100.82
	H2	3.706	70.68
	H3	3.674	72.09
	H4	3.511	74.42
	H5	3.757	69.18
	CH <sub>3</sub>	1.035	17.89
linker	H1' <sub>a</sub> /H1' <sub>b</sub>	3.720/3.511	69.18
	H2' <sub>a</sub> /H2' <sub>b</sub>	3.584/3.455	42.02
	H5'	4.728	54.76
benzene	H1''	7.832	131.86
	H2''	7.397	130.08
dimethylpyrimidine	H3'''	6.443	114.27
	CH <sub>3</sub> '''	1.971	24.03
benzimidazole	H2'''	7.497	134.75
	H5'''	7.444	n.d.
	H6'''	7.322	126.03
	H8'''	8.210	146.51

## 7.6.7 Used Pulse Programs and Parameters

### *STD NMR Experiments*

STD experiment with 3-9-19 WATERGATE (written by Dr. Andrew Benie):

```
;std19.ab
;avance-version 21.12.2004
;Dr. A.J.Benie
;1D STD/REF experiment with watergate- 2 channel SER file version
;uses NBL to obtain REF and STD interleaved 2D data file
;process using splitser and fidadd with dc=1

#include <Avance.incl>
#include <Grad.incl>

;NS DS NBL bug fix code
"ds=ds/2"
"ns=ns+ds"
"d12=20u"

1 ze
  10u st0
  10u st
2 d12 p10:f1
  d1 fql:f2
  10u st
3 p13:sp14:f2
  d28
  lo to 3 times l6
  d12 p11:f1
  p1 ph1
  50u UNBLKGRAD
  p16:gpl
  d16 p118:f1
  p27*0.231 ph3
  d19*2
  p27*0.692 ph3
  d19*2
  p27*1.462 ph3
  d19*2
  p27*1.462 ph4
  d19*2
  p27*0.692 ph4
  d19*2
  p0*0.231 ph4
  46u
  p16:gpl
  d16
  4u BLKGRAD
  go=2 ph31
  30m wr #0 if #0
exit

ph1=0 0 2 2
ph2=1 1 3 3
ph3=0 0 0 0 1 1 1 1 2 2 2 2 3 3 3 3
ph4=2 2 2 2 3 3 3 3 0 0 0 0 1 1 1 1
ph31=0 2 2 0 2 0 0 2

;p10 : f1 channel - power level during saturation [120dB]
;p11 : f1 channel - power level for pulse (default)
;p12 : f2 channel - [120 dB]
;p118: f1 channel - power level for 3-9-19 (watergate)
;sp14: f2 channel - 90 degree shaped pulse [50 dB]
```

```

;p0 : f1 channel - 90 degree pulse at p118
;          use for fine adjustment
;p1 : f1 channel - 90 degree high power pulse
;p13: f2 channel - 90 degree shaped pulse [49 msec]
;p16: homospoil/gradient pulse
;p27: f1 channel - 90 degree pulse at p118
;d1 : relaxation delay; 1-5 * T1 - saturation time (see 16)
;d12: delay for power switching [20 usec]
;d16: delay for homospoil/gradient recovery
;d19: delay for binomial water suppression
;      d19 = (1/(2*d)), d = distance of next null (in Hz)
;d28: delay between shaped pulses [1 msec]
;l6: loop for STD/REF saturation. Time = 16*(p13+d28) [10-80]
;
;NS: 16 * n
;DS: 32
;
;use gradient ratio:      gp 1
;                          20
;for z-only gradients:
;gpz1: 20%
;use gradient file:
;gpnaml: SINE.100
;
;
;NBL: 2 (number of irradiation frequencies)
;td1: 2 (NBL)
;
;this pulse program produces a ser-file (PARMOD = 2D)

```

### STD experiment with 3-9-19 WATERGATE (Bruker pulse sequence):

```

;stdiffgpl9.3
;avance-version (06/12/11)
;pseudo 2D sequence
;  for saturation transfer difference
;with shaped pulse train for saturation on f2 channel
;alternating between on and off resonance
;  to be defined by fq2list
;with spoil sequence to destroy unwanted magnetization
;water suppression using 3-9-19 pulse sequence with gradients
;with spinlock to suppress protein signals
;(use parameterset STDDIFFGP19.3)
;
;M. Mayer & B. Meyer, Angew. Chem. Int. Ed. 38, 1784-1788 (1999)
;M. Mayer & B. Meyer, Angew. Chem. 111, 1902-1906 (1999)
;M. Piotto, V. Saudek & V. Sklenar, J. Biomol. NMR 2, 661 - 666 (1992)
;V. Sklenar, M. Piotto, R. Leppik & V. Saudek, J. Magn. Reson.,
;  Series A 102, 241 -245 (1993)
;
;$CLASS=HighRes
;$DIM=2D
;$TYPE=
;$SUBTYPE=
;$COMMENT=

#include <Avance.incl>
#include <Grad.incl>
#include <Delay.incl>

"d11=30m"
"p29=d29"
"l5=d20/p13+0.5"
"d31=p13*15"

```



```

"DELTA1=d1-d31"

1 ze
  3m fq2:f2 st0
2 3m
3 3m
4 d11
  6m

5 50u UNBLKGRAD
  4u pl10:f1
  (p17 ph2)
  (p17*2 ph3)
  4u
  p30:gp1
  10m pl1:f1
  4u BLKGRAD

  DELTA1

6 (p13:sp13 ph4):f2
  4u
  lo to 6 times l5

  p1 ph1
  4u pl29:f1
  (p29 ph5)

  50u UNBLKGRAD
  p16:gp2
  d16 pl18:f1
  p27*0.231 ph6
  d19*2
  p27*0.692 ph6
  d19*2
  p27*1.462 ph6
  d19*2
  p27*1.462 ph7
  d19*2
  p27*0.692 ph7
  d19*2
  p0*0.231 ph7
  46u
  p16:gp2
  d16
  4u BLKGRAD

  goscnp ph31

  3m fq2:f2 st
  lo to 3 times nbl
  3m ipp1 ipp5 ipp6 ipp7 ipp31
  lo to 4 times ns
  d11 wr #0
  3m rpp1 rpp5 rpp6 rpp7 rpp31
  3m zd
  lo to 5 times l4
exit

ph1=0 2
ph2=0
ph3=1
ph4=0
ph5=1 1 1 1 1 1 1 3 3 3 3 3 3 3 3
ph6=0 0 1 1 2 2 3 3
ph7=2 2 3 3 0 0 1 1
ph31=0 2 2 0

```

```

;p11 : f1 channel - power level for pulse (default)
;p12 : f2 channel - power level for pulse (default)          [120 dB]
;p110: f1 channel - power level for TOCSY-spinlock
;p118: f1 channel - power level for 3-9-19-pulse (watergate)
;p129: f1 channel - power level for trim pulse
;sp13: f2 channel - shaped pulse for saturation              [40 - 60 dB]
;p0 : f1 channel - 90 degree pulse at p118
;      use for fine adjustment
;p1 : f1 channel - 90 degree high power pulse
;p13: f2 channel - shaped pulse for saturation                [50 msec]
;p16: homospoil/gradient pulse
;p17: f1 channel - trim pulse                                [2.5 msec]
;p27: f1 channel - 90 degree pulse at p118
;p29: f1 channel - trim pulse
;p30: gradient pulse                                         [3 msec]
;d1 : relaxation delay; 1-5 * T1
;d11: delay for disk I/O                                     [30 msec]
;d16: delay for homospoil/gradient recovery
;d19: delay for binomial water suppression
;      d19 = (1/(2*d)), d = distance of next null (in Hz)
;d20: saturation time
;d29: spinlock time                                          [10 - 50 msec]
;d31: saturation time as executed
;l4: 14 = number of averages = (total number of scans) / NS
;l5: loop for saturation: p13 * l5 = saturation time
;NS: 8 * n
;DS: 4
;td1: number of experiments
;NBL: NBL = number of irradiation frequencies

;define FQ2LIST (irradiation frequencies)
;      (list has to be stored in "/u/exp/stan/nmr/lists/fl")
;use gradient ratio:      gp 1 : gp 2
;                        40 : 30
;for z-only gradients:
;gpz1: 40%
;gpz2: 30%

;use gradient files:
;gpnaml: SINE.100
;gpnam2: SINE.100

;this pulse program produces a ser-file (PARMOD = 2D)

;The STD experiment is protected by international patents owned by:
;Alepharma Licensing, Raamfeld 67, 22397 Hamburg, Germany.
;For commercial use (direct or indirect) please contact the company for
;licensing information at:
;E-mail: info@alepharma-licensing.com,
;Fax: +49 4060847812,
;Tel: +49 1701685158 or +49 1712788867.

;$Id: stddiffgpl9.3,v 1.2.4.3 2006/12/11 09:59:57 ber Exp $

```

Table 7.3. Sample composition and experimental parameters for STD NMR.

Pulse program	Ligand <sup>[a]</sup>	VLPs <sup>[b]</sup>	Ligand excess <sup>[c]</sup>	Parameters <sup>[d]</sup>	Saturation time
				T=282 K on=-4 ppm off=300 ppm relaxation delay=25 s <sup>[e]</sup> TD=32k	
std19.ab	<b>4, 5b</b>	0.89 mg/mL NoV	30:1	ns=128 - 3600	0.35 – 4 s
	<b>31</b>	0.22 mg/mL NoV	140:1	ns=1024 – 4096 relaxation delay=5s	0.35 – 4 s
	fragment <b>160</b> (1.7 mM)	0.33 mg/mL NoV	90:1	ns=128	0.5 – 8 s
	<b>5a, 9, 10, 11, 12, 13, 14, 15, 30</b>	0.22 mg/mL NoV	140:1	ns=1024 – 7616	0.5 s
	<b>32</b>	0.22 mg/mL NoV	140:1	ns=2048	2 s
	<b>16, 17, 18, 19, 20, 21, 22, 23, 24, 25, 26, 27, 28, 29</b>	0.22 mg/mL NoV	140:1	ns= 4096 – 8192 relaxation delay=1.5 s	2 s
	<b>29</b>	0.24 mg/mL NB2	120:1	ns=128 – 1024	0.5 – 4 s
	<b>5a, 10, 16, 23, 24</b>	0.24 mg/mL NB2	120:1	ns=816 – 1024	2 s
stddiffgp19.3	<b>5c</b>	0.22 mg/mL NoV	140:1	ns=112 - 512	0.5 – 2 s
	<b>42, 43, 44, 45</b>	0.22 mg/mL NoV	140:1	ns=128 – 2560	0.35 – 4 s
	<b>1, 2, 3a, 6, 7, 8</b>	0.22 mg/mL NoV	140:1	ns=864 – 960	0.5 s
	<b>2</b> (1 mM)	0.23 mg/mL D391A	260:1	ns=896	0.5 s
	<b>5b</b> (1 mM)	0.23 mg/mL D391A	260:1	ns=64 – 1088	0.25 – 4 s
	<b>2</b>	0.12 mg/mL H395A	260:1	ns=1088	0.5 s
	<b>5b</b>	0.12 mg/mL H395A	260:1	ns=256 – 1280	0.35 – 2 s

[a] ligand concentration was 0.5 mM except stated otherwise

[b] NoV: human NoV strain Ast6139; D391A, H395A: Ast6139 mutants; NB2: bovine NoV Newbury2

[c] ligand excess is calculated with respect to the binding site concentration assuming 180 b.s. per VLP

[d] T: temperature; on, off: on- and off-resonance frequencies; relaxation delay: d1 in stddiffgp19.3, d1 plus d20 (saturation time) in std19.ab; TD: number of data points in the direct dimension; ns: number of accumulated experiments (scans)

[e] relaxation delay was 25 s if not stated otherwise

### NOESY and ROESY Experiments

NOESY: with W5 WATERGATE (Bruker pulse sequence noesygp-phw5), with 3-9-19 WATERGATE (Bruker pulse sequence noesygp-ph19) or without water suppression (Bruker pulse sequence noesygp-ph)

ROESY: with 3-9-19 WATERGATE (Bruker pulse sequence roesygp-ph19.2)

Table 7.4. Sample composition and parameters for NOESY and ROESY NMR.

Pulse program	Ligand	VLPs <sup>[a]</sup>	Ligand excess <sup>[b]</sup>	Parameters <sup>[c]</sup>	Mixing time (d8)
noesygp-phw5	<b>14</b> (250 $\mu$ M)	1.2 mg/mL	12.5:1	T=298 K; ns=16; d1=2 s; TD=4096/ 512	25 ms – 5 s
	<b>14</b> (1 mM)	–	–	T=298 K; ns=8; d1=2 s; TD=4096/ 512	100 – 1000 ms
noesygp-ph19	<b>14</b> (250 $\mu$ M)	1.2 mg/mL	12.5:1	T=298 K; ns=32; d1=2 s; TD=8192/ 512	250 ms
noesygp-ph	<b>14</b> (1 mM)	–	–	T=310 K; ns=8; d1=1.5 s; TD=4096/ 512	100 ms – 5 s
roesygp-ph19.2	<b>14</b> (0.8 mM)	1.2 mg/mL	40:1	T=298 K; ns=64; d1=2 s; TD=2048/ 512	150 ms

[a] human NoV strain Ast6139 (wildtype)

[b] ligand excess is calculated with respect to the binding site concentration assuming 180 b.s. per VLP

[c] T: temperature; ns: number of accumulated experiments (scans); d1: relaxation delay; TD: data points in the direct and indirect dimension, respectively

### Assignment Experiments

HSQC: phase sensitive with <sup>13</sup>C decoupling during acquisition (Bruker pulse sequence hsqcetgp)

COSY: phase sensitive and multiple quantum filter (Bruker pulse sequence cosygp-phfph)

TOCSY: with W5 WATERGATE (Bruker pulse sequence mlevgp-phw5)

HMBC: gradient selective with quantum filter (Bruker pulse sequence hmbcgp-l2ndqf)

1D cssf TOCSY: gradient enhanced 1D chemical shift selective filter TOCSY experiment (written by Philip Robinson (Robinson *et al.*, 2004)):

```
# 1 "/opt/topspin/exp/stan/nmr/lists/pp/1d_cssf_tocsy.pr"
;ld_cssf_tocsy.pr
;written by philip robinson 110202
;Modified on 14/02/04 by Dusan Uhrin to
;include optional water suppression
;and purging of the antiphase components
```

```
;Dummy scans treated properly

# 1 "/opt/topspin/exp/stan/nmr/lists/pp/Avance.incl" 1
;Avance.incl
;
;avance-version (07/01/22)
;
;$CLASS=HighRes Incl
;$COMMENT=

;$Id: Avance1.incl,v 1.10.6.2 2007/01/22 13:54:46 ber Exp $
# 8 "/opt/topspin/exp/stan/nmr/lists/pp/1d_cssf_tocsy.pr" 2

# 1 "/opt/topspin/exp/stan/nmr/lists/pp/Grad.incl" 1
;Grad.incl - include file for Gradient Spectroscopy
;
;avance-version (02/05/31)
;
;$CLASS=HighRes Incl
;$COMMENT=

define list<gradient> EA=<EA>

;$Id: Grad1.incl,v 1.7.10.1 2005/11/10 13:18:56 ber Exp $
# 9 "/opt/topspin/exp/stan/nmr/lists/pp/1d_cssf_tocsy.pr" 2

# 1 "/opt/topspin/exp/stan/nmr/lists/pp/Delay.incl" 1
;Delay.incl - include file for commonly used delays
;
;version 00/02/07
;
;$CLASS=HighRes Incl
;$COMMENT=

;general delays

define delay DELTA
define delay DELTA1
define delay DELTA2
define delay DELTA3
define delay DELTA4
define delay DELTA5
define delay DELTA6
define delay DELTA7
define delay DELTA8

define delay TAU
define delay TAU1
define delay TAU2
define delay TAU3
define delay TAU4
define delay TAU5

;delays for centering pulses

define delay CEN_HN1
define delay CEN_HN2
define delay CEN_HN3
define delay CEN_HC1
define delay CEN_HC2
define delay CEN_HC3
define delay CEN_HC4
define delay CEN_HP1
define delay CEN_HP2
define delay CEN_CN1
```

```

define delay CEN_CN2
define delay CEN_CN3
define delay CEN_CN4
define delay CEN_CP1
define delay CEN_CP2

;loop counters

define loopcounter COUNTER
define loopcounter SCALEF
define loopcounter FACTOR1
define loopcounter FACTOR2
define loopcounter FACTOR3

;$Id: Delay.incl,v 1.11.10.1 2005/11/10 13:18:56 ber Exp $
# 10 "/opt/topspin/exp/stan/nmr/lists/pp/ld_cssf_tocsy.pr" 2

"p2=p1*2"
"FACTOR1=(d9/(p6*115.112))/2+0.5"
"l1=FACTOR1*2"
"d12=20u"
"d13=3u"
"p13=50000"
"p18=p13-200u"
"d20=20u"

# 1 "mc_line 22 file /opt/topspin/exp/stan/nmr/lists/pp/ld_cssf_tocsy.pr
expanding definition part of mc command before ze"
define delay MCWRK
define delay MCREST
"MCWRK = 0.333333*30m"
"MCREST = 30m - 30m"
# 22 "/opt/topspin/exp/stan/nmr/lists/pp/ld_cssf_tocsy.pr"
1 ze
# 1 "mc_line 22 file /opt/topspin/exp/stan/nmr/lists/pp/ld_cssf_tocsy.pr
expanding definition of mc command after ze"
# 23 "/opt/topspin/exp/stan/nmr/lists/pp/ld_cssf_tocsy.pr"
# 1 "mc_line 23 file /opt/topspin/exp/stan/nmr/lists/pp/ld_cssf_tocsy.pr
expanding start label for mc command"
2 MCWRK * 3
LBLF0, MCREST
# 24 "/opt/topspin/exp/stan/nmr/lists/pp/ld_cssf_tocsy.pr"
3 50u setnmr2^0 setnmr0^34^32^33

d12 fq=cnst1(bf ppm):f1
d12 p19:f1
d1 cw:f1 ph29
d13 do:f1
d12 p11:f1
d12 fq=cnst2(bf ppm):f1
50u setnmr2|0 setnmr0|34|32|33

p1 ph1 ; this is the start of cssf
d23*0.5
p16:gp1
d16 p10:f1
(p11:sp1 ph2:r):f1
d13
d12 p11:f1
p2 ph3
p16:gp1*-1
d16
d23*0.5

p1 ph4 ; back to z axis
4u

```

```

p16:gp2
d16 p110:f1

4 p6*3.556 ph23
p6*4.556 ph25
p6*3.222 ph23
p6*3.167 ph25
p6*0.333 ph23
p6*2.722 ph25
p6*4.167 ph23
p6*2.944 ph25
p6*4.111 ph23

p6*3.556 ph25
p6*4.556 ph23
p6*3.222 ph25
p6*3.167 ph23
p6*0.333 ph25
p6*2.722 ph23
p6*4.167 ph25
p6*2.944 ph23
p6*4.111 ph25

p6*3.556 ph25
p6*4.556 ph23
p6*3.222 ph25
p6*3.167 ph23
p6*0.333 ph25
p6*2.722 ph23
p6*4.167 ph25
p6*2.944 ph23
p6*4.111 ph25

p6*3.556 ph23
p6*4.556 ph25
p6*3.222 ph23
p6*3.167 ph25
p6*0.333 ph23
p6*2.722 ph25
p6*4.167 ph23
p6*2.944 ph25
p6*4.111 ph23
lo to 4 times l1

# 105 "/opt/topspin/exp/stan/nmr/lists/pp/ld_cssf_tocsy.pr"

d16 p11:f1
p16:gp4
d16

d20 p11:f1
4u setnmr2^0 setnmr0^34^32^33
p1 ph5
go=2 ph31
# 1 "mc_line 115 file /opt/topspin/exp/stan/nmr/lists/pp/ld_cssf_tocsy.pr
expanding mc command in line"
MCWRK wr #0
MCWRK id23 MCWRK zd
lo to LBLF0 times td0

# 116 "/opt/topspin/exp/stan/nmr/lists/pp/ld_cssf_tocsy.pr"

50u rd23
lo to 2 times l3
wr #0
30m setnmr2^0 setnmr0^34^32^33
exit

```

```

ph1=0
ph2=0 1
ph3=0
ph4=0
ph5=0
ph23=3
ph25=1
ph29=0
ph30=0
ph31=0 2

;p10 : 120dB
;p11 : f1 channel - power level for pulse (default)
;p19 : f1 channel - power level for water presaturation
;p110: f1 channel - power level for TOCSY-spinlock
;sp1 : f1 channel - shaped pulse 180 degree
;p1 : f1 channel - 90 degree high power pulse
;p2 : f1 channel - 180 degree high power pulse
;p6: 90 degree pulse for tocsy spinlock
;p11: f1 channel - 180 degree shaped pulse
;p13: 50ms Crp40.1000
;p18: 50ms-200us gradient pulse
;sp2: 180 deg adiab. Crp40.1000
;SPNAM2: Crp40.1000
;p16: homospoil/gradient pulse
;d1 : relaxation delay; 1-5 * T1
;d9 : TOCSY mixing time
;cnst1: HOD
;cnst2: = olp
;d12: delay for power switching
;d16: delay for homospoil/gradient recovery
;d23: CSSF delay
;id23: increment of CSSF
;l2: id23*l2 is the length of cssf
;NS: 2 * TD0 * l3
;DS: 4

;for z-only gradients:
;gpz1: 20%
;gpz2: 6%
;gpz3: 4%
;gpz4: 30%

;use gradient files:
;gpnam1: SINE.100
;gpnam2: SINE.100
;gpnam3: SINE.1000
;gpnam4: SINE.100

```

---

### 1D cssf NOESY (written by Philip Robinson (Robinson *et al.*, 2004)):

```

# 1 "/opt/topspin/exp/stan/nmr/lists/pp/1d_cssf_noesy.pr"
;1d_cssf_noesy with water presat

;written by philip robinson 110202
;Modified on 14/02/04 by Dusan Uhrin to
;include optional water suppression
;and purging of the antiphase components
;Proper treatment of dummy scans

# 1 "/opt/topspin/exp/stan/nmr/lists/pp/Avance.incl" 1
;Avance.incl
;avance-version (07/01/22)

```



```
;
;$CLASS=HighRes Incl
;$COMMENT=

;$Id: Avancel.incl,v 1.10.6.2 2007/01/22 13:54:46 ber Exp $
# 9 "/opt/topspin/exp/stan/nmr/lists/pp/ld_cssf_noesy.pr" 2

# 1 "/opt/topspin/exp/stan/nmr/lists/pp/Grad.incl" 1
;Grad.incl - include file for Gradient Spectroscopy
;
;avance-version (02/05/31)
;
;$CLASS=HighRes Incl
;$COMMENT=

define list<gradient> EA=<EA>

;$Id: Gradl.incl,v 1.7.10.1 2005/11/10 13:18:56 ber Exp $
# 10 "/opt/topspin/exp/stan/nmr/lists/pp/ld_cssf_noesy.pr" 2

# 1 "/opt/topspin/exp/stan/nmr/lists/pp/Delay.incl" 1
;Delay.incl - include file for commonly used delays
;
;version 00/02/07
;
;$CLASS=HighRes Incl
;$COMMENT=

;general delays

define delay DELTA
define delay DELTA1
define delay DELTA2
define delay DELTA3
define delay DELTA4
define delay DELTA5
define delay DELTA6
define delay DELTA7
define delay DELTA8

define delay TAU
define delay TAU1
define delay TAU2
define delay TAU3
define delay TAU4
define delay TAU5

;delays for centering pulses

define delay CEN_HN1
define delay CEN_HN2
define delay CEN_HN3
define delay CEN_HC1
define delay CEN_HC2
define delay CEN_HC3
define delay CEN_HC4
define delay CEN_HP1
define delay CEN_HP2
define delay CEN_CN1
define delay CEN_CN2
define delay CEN_CN3
define delay CEN_CN4
define delay CEN_CP1
define delay CEN_CP2
```

```

;loop counters

define loopcounter COUNTER
define loopcounter SCALEF
define loopcounter FACTOR1
define loopcounter FACTOR2
define loopcounter FACTOR3

;$Id: Delay.incl,v 1.11.10.1 2005/11/10 13:18:56 ber Exp $
# 11 "/opt/topspin/exp/stan/nmr/lists/pp/ld_cssf_noesy.pr" 2

"p2=p1*2"
"d21=d8*cnst3-p16-d16"
"d22=d8*(0.5-cnst3)-p16-d16"
"d12=20u"
"d13=3u"
"p13=50000"
"p18=p13-200u"

# 1 "mc_line 22 file /opt/topspin/exp/stan/nmr/lists/pp/ld_cssf_noesy.pr
expanding definition part of mc command before ze"
define delay MCWRK
define delay MCREST
"MCWRK = 0.333333*30m"
"MCREST = 30m - 30m"
# 22 "/opt/topspin/exp/stan/nmr/lists/pp/ld_cssf_noesy.pr"
1 ze
# 1 "mc_line 22 file /opt/topspin/exp/stan/nmr/lists/pp/ld_cssf_noesy.pr
expanding definition of mc command after ze"
# 23 "/opt/topspin/exp/stan/nmr/lists/pp/ld_cssf_noesy.pr"
# 1 "mc_line 23 file /opt/topspin/exp/stan/nmr/lists/pp/ld_cssf_noesy.pr
expanding start label for mc command"
2 MCWRK * 3
LBLF0, MCREST
# 24 "/opt/topspin/exp/stan/nmr/lists/pp/ld_cssf_noesy.pr"
3 50u setnmr2^0 setnmr0^34^32^33

d12 fq=cnst1(bf ppm):f1
d12 p19:f1
d1 cw:f1 ph29
d13 do:f1
d12 p11:f1
d12 fq=cnst2(bf ppm):f1
d12 setnmr2|0 setnmr0|34|32|33

p1 ph1 ;cssf starts here
d23*0.5
p16:gp1
d16 p10:f1
(p11:sp1 ph2:r):f1
d13
d12 p11:f1
p2 ph3
p16:gp1*-1
d16
d23*0.5

p1 ph4 ;noesy mixing
d21
p16:gp2
d16
3u
(p2 ph5):f1
3u
p16:gp3
d16

```

```
d22

d21
p16:gp4
d16
3u
(p2 ph6):f1
3u
p16:gp5
d16
d22

# 79 "/opt/topspin/exp/stan/nmr/lists/pp/ld_cssf_noesy.pr"

4u setnmr2^0 setnmr0^34^32^33

p1 ph7
go=2 ph31
# 1 "mc_line 84 file /opt/topspin/exp/stan/nmr/lists/pp/ld_cssf_noesy.pr
expanding mc command in line"
MCWRK wr #0
MCWRK id23 MCWRK zd
lo to LBLF0 times td0

# 85 "/opt/topspin/exp/stan/nmr/lists/pp/ld_cssf_noesy.pr"

50u rd23
lo to 3 times l3
wr #0
exit

ph1=0
ph2=0 1
ph3=0
ph4=0
ph5=0
ph6=0
ph7=0
ph29=0
ph30=0
ph31=2 0

;p10 : 120dB
;p11 : f1 channel - power level for pulse (default)
;p11 : f1 channel - power level for water presaturation
;sp1 : f1 channel - shaped pulse 180 degree
;p1 : f1 channel - 90 degree high power pulse
;p2 : f1 channel - 180 degree high power pulse
;p11: f1 channel - 180 degree shaped pulse
;p16: homospoil/gradient pulse
;d1 : relaxation delay; 1-5 * T1
;d8 : mixing time
;p13: 50ms Crp40.1000
;p18: 50ms-200us gradient pulse
;sp2: 180 deg adiab. Crp40.1000
;d12: delay for power switching
;d16: delay for homospoil/gradient recovery
;d21: d8*cnst3-p16-d16
;d22: d8*(0.5-cnst3)-p16-d16
;cnst1: HOD
;cnst2: = olp
;cnst3: typically 0.2-0.4
;d23: CSSF delay
;id23: increment of CSSF
;l2: l2*id23 is the length of cssf
;l3: loop for long term accumulation
;NS: 2 * TD0 * l3
;DS: 4
```

```

;for z-only gradients:
;gpz1: 20%
;gpz2: 33%
;gpz3:-13%
;gpz4:25%
;gpz5:-15%
;gpz6:4%
;gpz7:30%

;use gradient files:
;gpnam1: SINE.100
;gpnam2: SINE.100
;gpnam3: SINE.100
;gpnam4: SINE.100
;gpnam5: SINE.100
;gpnam6: SINE.1000
;gpnam7: SINE.100

```

Table 7.5. Experimental parameters for assignment experiments.

Pulse program	Ligand <sup>[a]</sup>	Parameters <sup>[b]</sup>
		T=282 K
hsqcetgp		ns=8 – 32; d1=1.5 – 2s; TD=2048/ 256
cosygpmfph		ns=2 – 32; d1=1.5 – 2 s; TD=2048 – 4096/ 256 – 512
mlevgpphw5	<b>8, 31</b>	ns=2 – 4; d1=1.5 – 2 s; TD=4096/ 1024; d9=80 ms
hmbcgpl2ndqf	<b>31</b> (5 mM in methanol- <i>d</i> 4)	ns=64; d1=1.2 s; TD=2048/ 256
1d_cssf_tocsy	<b>8, 9, 10, 11, 14, 15, 31</b>	ns=2 – 8; d1=; TD=32k; d9=60 – 100 ms; TD0=1 – 25
1d_cssf_noesy	<b>31</b>	ns=8; d1=1.5 s; TD=32k; d8=750 ms; TD0=1 – 21

[a] only given if the experiment was not applied to nearly all ligands

[b] T: temperature; ns: number of accumulated experiments (scans); d1: relaxation delay; TD: data points in the direct and indirect dimension, respectively; d9: TOCSY mixing time; d8: NOESY mixing time; TD0: loop count in 1D-cssf experiments (measure for the selectivity of the irradiation pulse)

## 7.7 Sensorgrams from SPR Experiments

### 7.7.1 Measurements with HBGAs

Measurement of L-Fuc (**1**):

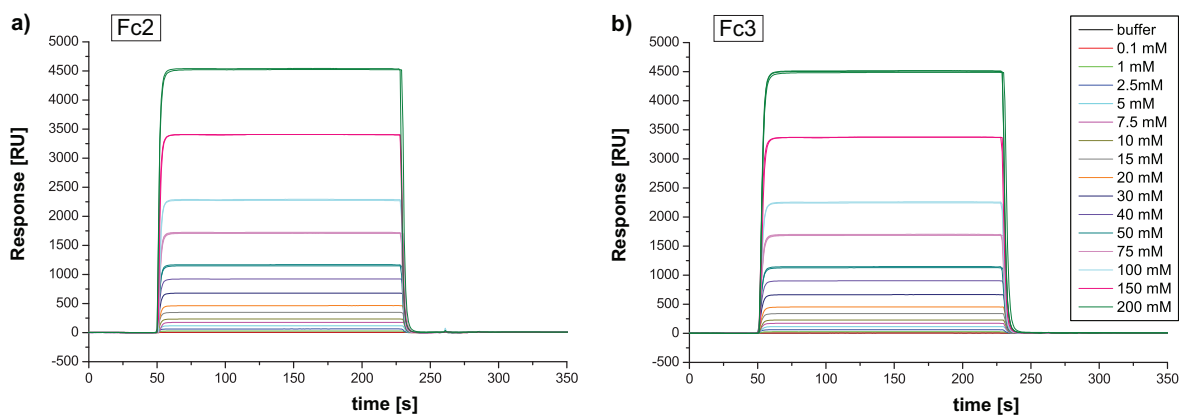


Figure 7.9. Sensorgrams of L-Fuc (**1**) injections on sensor chip C. a) Fc2 with 5260 RU VLPs; b) Fc3, only activated and deactivated (reference) (cf. Figure 4.27). 50–230 s: injection of 30  $\mu$ L of L-Fuc dilutions at a flow rate of 10  $\mu$ L/min. Regeneration was not necessary as the baseline was recovered after injection stop instantaneously.

Measurement of H antigen type 6 (**8a**):

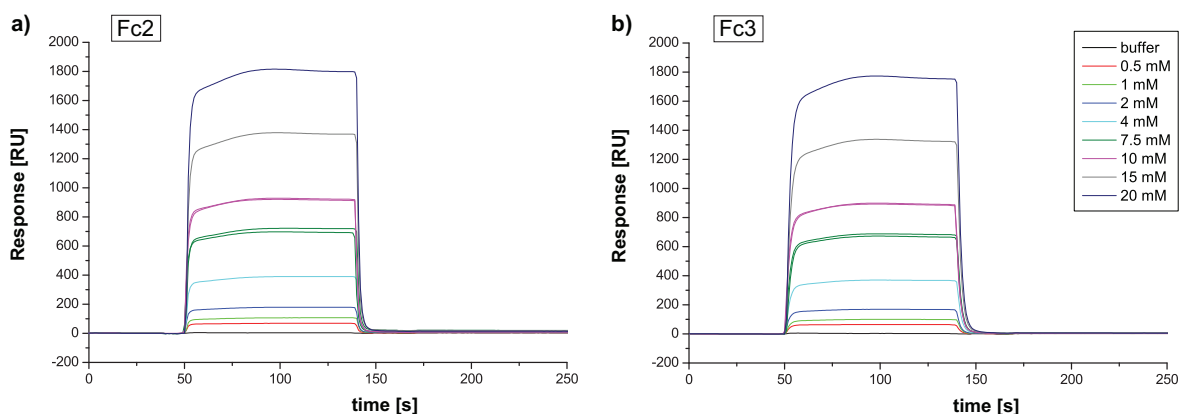


Figure 7.10. Sensorgrams of H type 6 (**8a**) injections on sensor chip C. a) Fc2 with 5260 RU VLPs; b) Fc3, only activated and deactivated (reference) (cf. Figure 4.28). 50–140 s: injection of 15  $\mu$ L of H type 6 at a flow rate of 10  $\mu$ L/min. Regeneration was not necessary as the baseline was recovered after injection stop instantaneously.

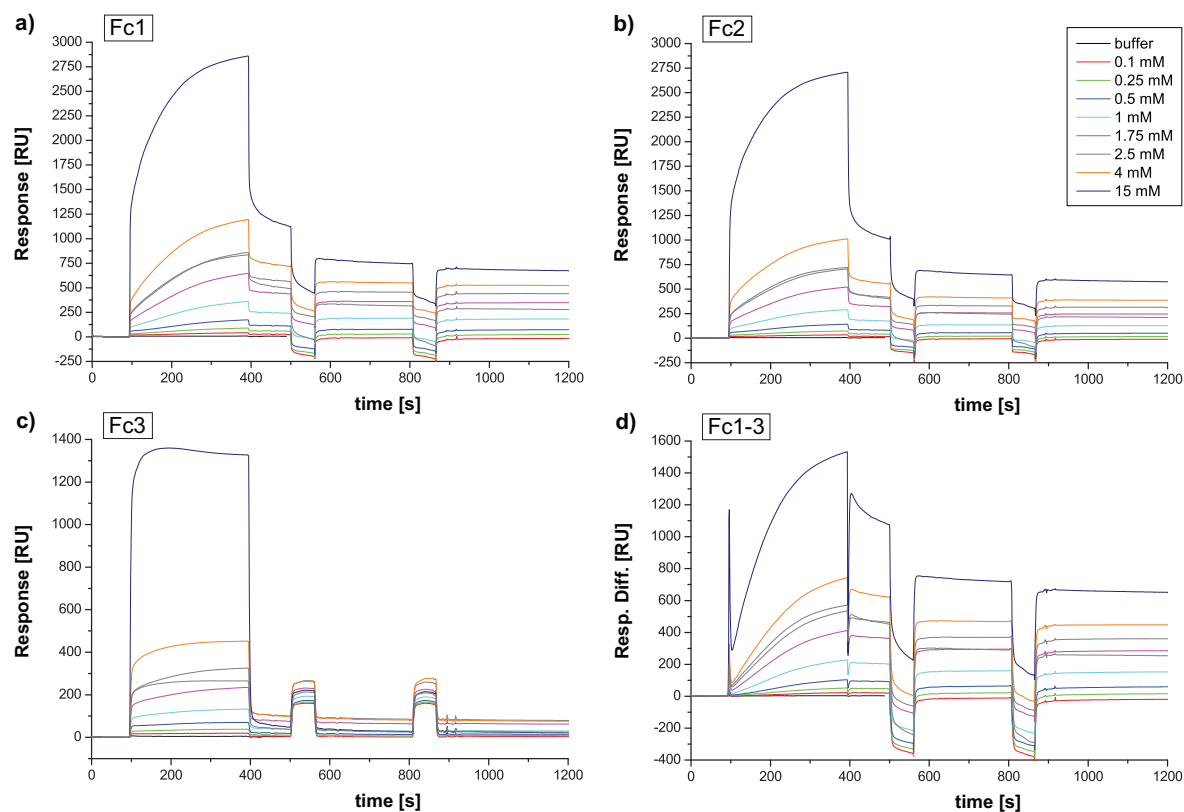
Measurement of compound **30**:

Figure 7.11. Sensorgrams of compound **30** injections on sensor chip C. a) Fc1 with 7050 RU immobilized Ast6139 VLPs; b) Fc2 with 5260 RU VLPs; c) Fc3, only activated and deactivated (reference); d) difference curves for Fc1 after reference curve subtraction (cf. Figure 4.28). 100–400 s: injection of 50  $\mu$ L of compound **30** at a flow rate of 10  $\mu$ L/min; 450 and 800 s: regeneration with each 10  $\mu$ L of phosphate buffer pH 7.4.

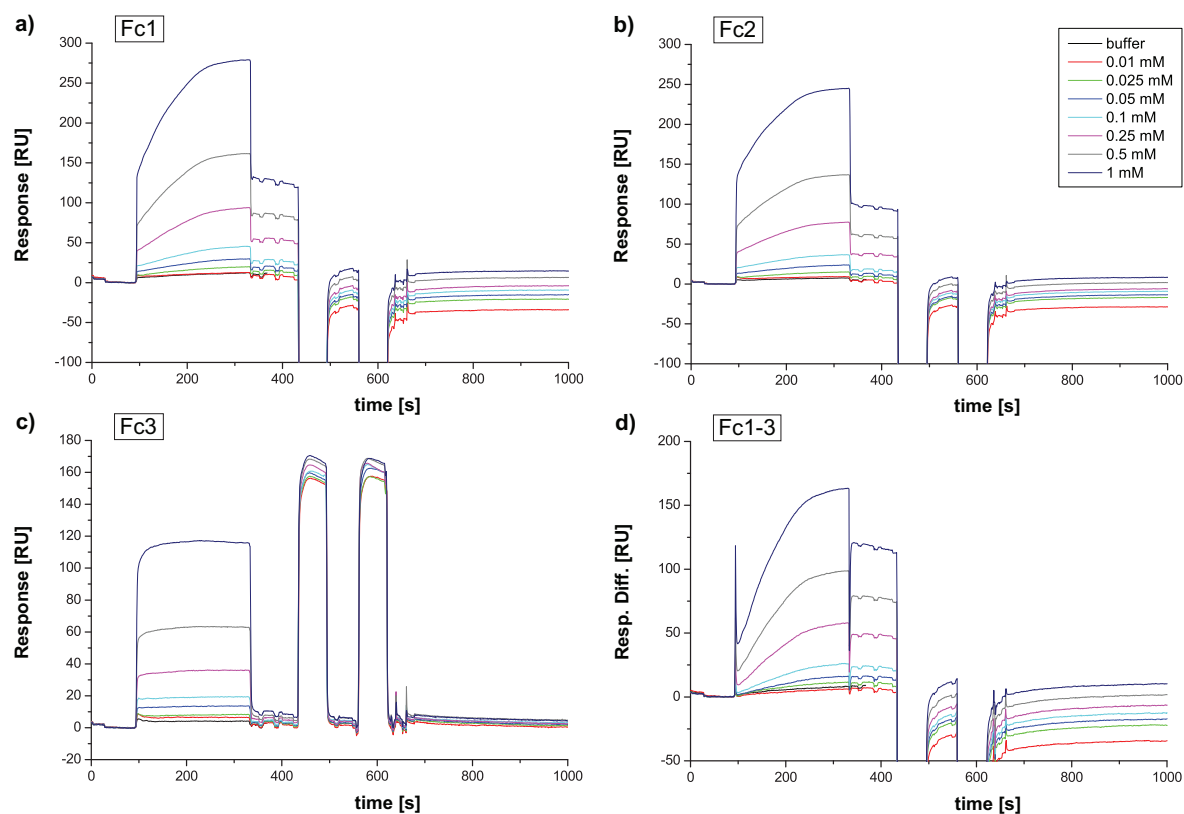
Measurement of compound **31**:

Figure 7.12. Sensorgrams of compound **31** injections on sensor chip C. a) Fc1 with 7050 RU immobilized Ast6139 VLPs; b) Fc2 with 5260 RU VLPs; c) Fc3, only activated and deactivated (reference); d) difference curves for Fc1 after subtraction of the reference curves (cf. Figure 4.28). 100–340 s: injection of 80  $\mu$ L of compound **31** at a flow rate of 20  $\mu$ L/min; 430 and 560 s: regeneration with each 20  $\mu$ L of phosphate buffer pH 7.4.

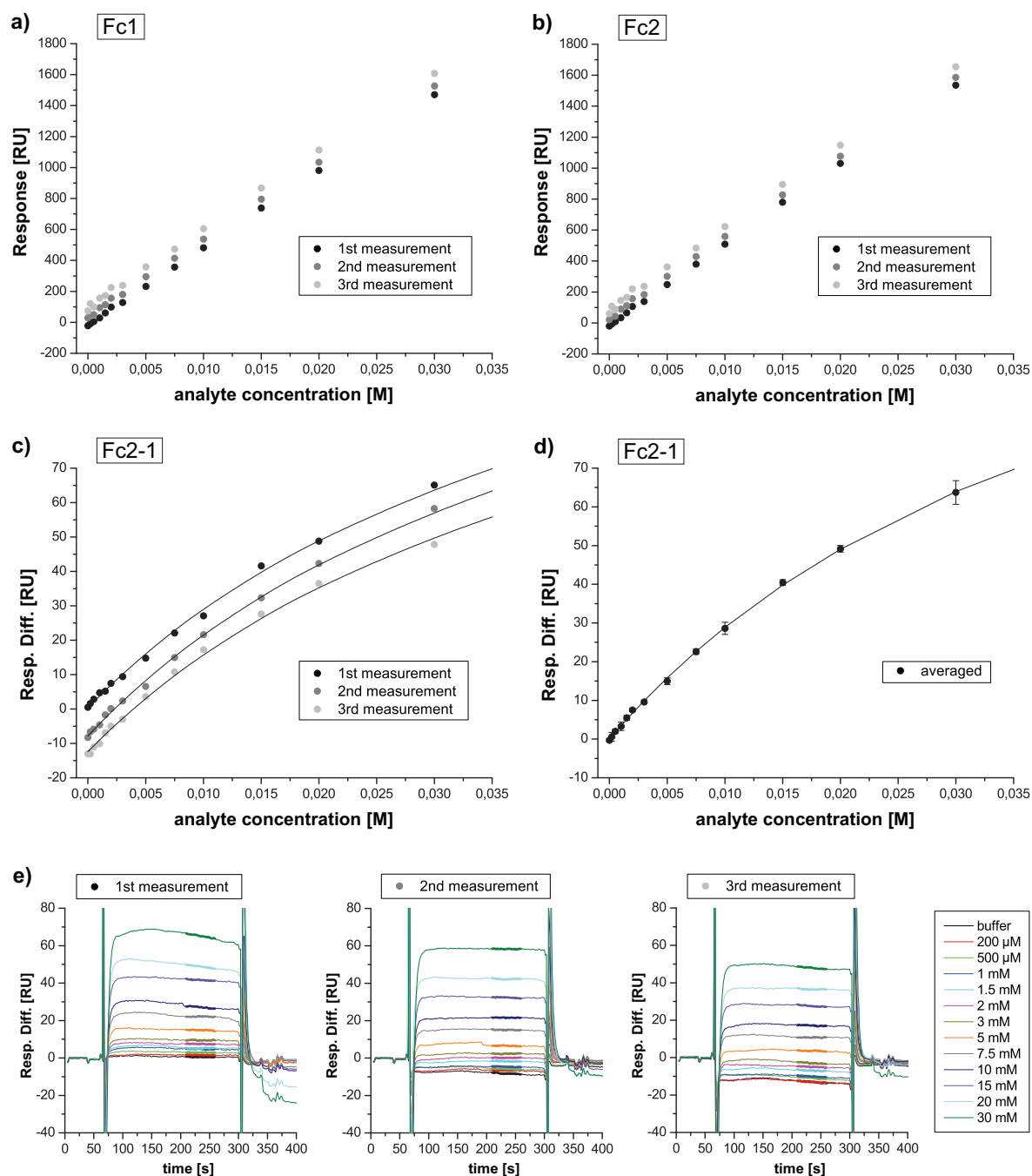
Measurement of H-disaccharide (**3b**):

Figure 7.13. Measurement of H-disaccharide **3b** on sensor chip A in triplicate. a),b) Absolute responses for three titration series on Fc1 (reference) (a) and Fc2 with 3500 RU VLPs (b). c),d) Response differences for Fc2 after reference subtraction and fitting curves to a 1:1 binding model (black lines, equation 9) before (c) and after y-shift correction (d); curves in c) were fitted globally to one  $K_D$  but allowing different  $RU_{max}$  values and y-shifts; in d) the isotherms were corrected for the fitted y-shifts from c), averaged and refitted; e) difference curves for Fc2 after reference subtraction.



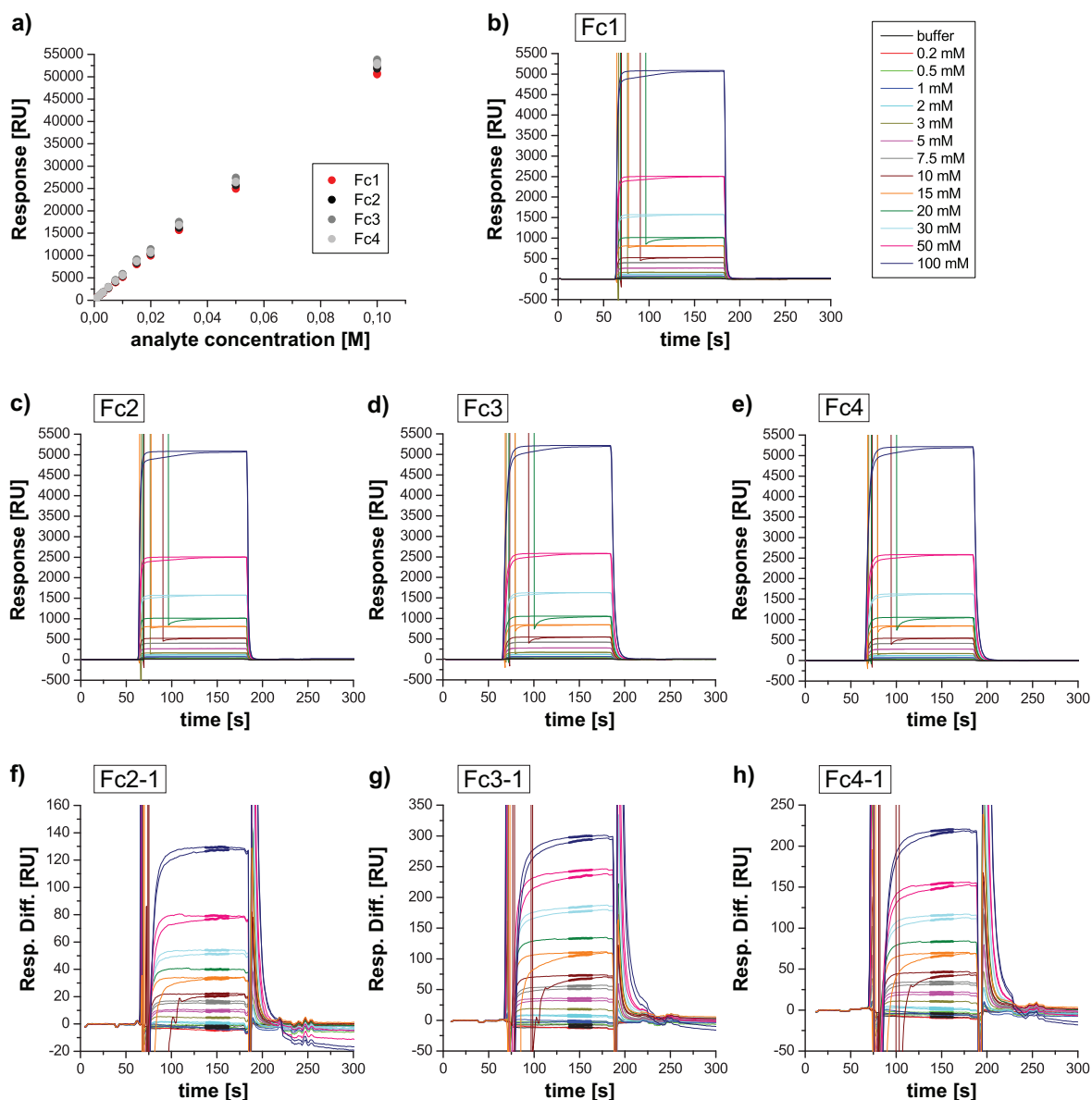


Figure 7.14. Measurement of H-disaccharide **3b** on sensor chip A in duplicate. a) Absolute responses for Fc1 (reference), Fc2 (3500 RU VLPs), Fc3 (7300 RU VLPs) and Fc4 (5200 RU VLPs). b-e) Sensorgrams for H-disaccharide injections. f-h) Difference curves for after subtraction of reference curves. In three measurements (concentrations 10, 15 and 20 mM) air was injected in the beginning. The 10 and 15 mM measurements were included in the curve fitting since equilibrium level of the other measurement was reached. In contrast, curves for 20 mM were excluded from the curve fitting and are left out in f) to h).

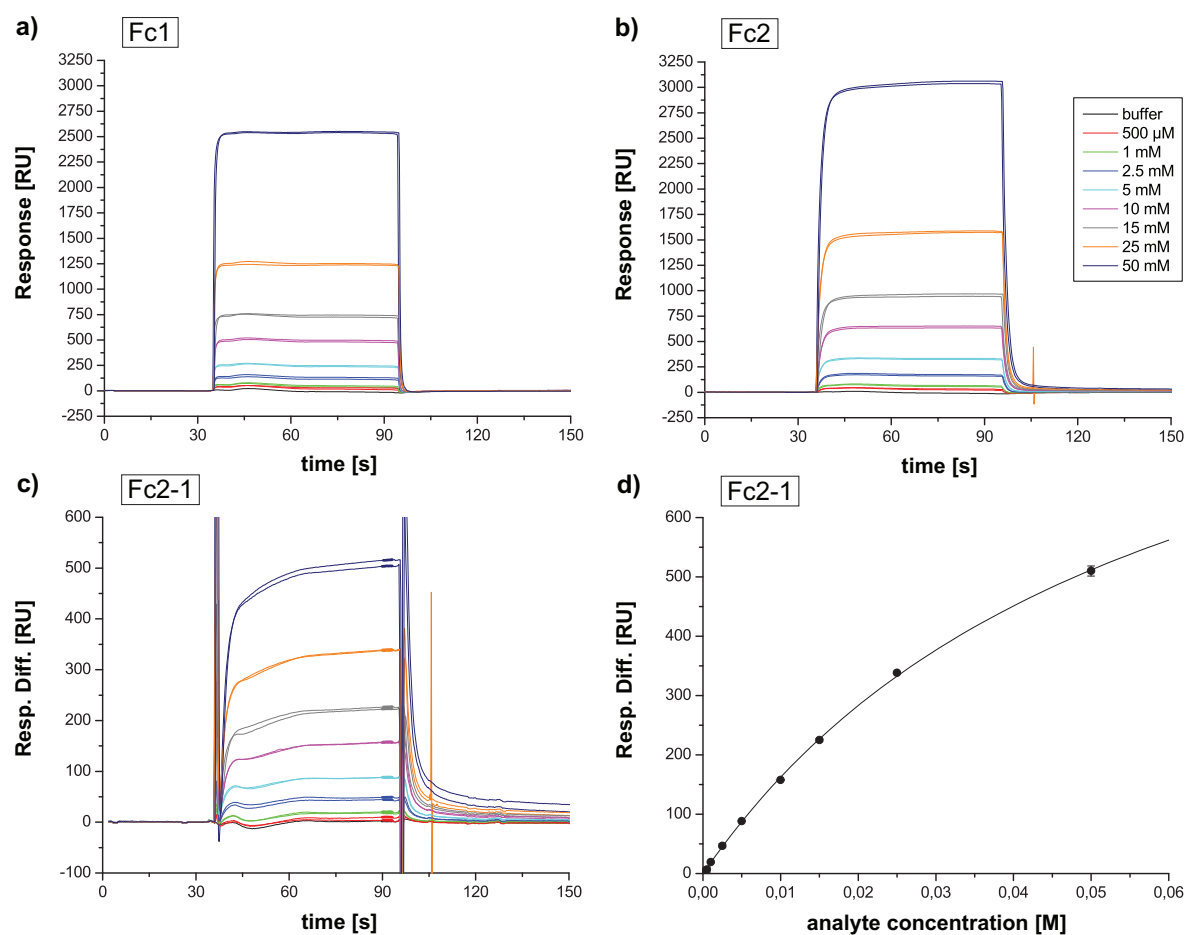


Figure 7.15. Measurement of H-disaccharide **3b** on sensor chip B in duplicate. a),b) Sensorgrams for Fc1 (reference) and Fc2 (12000 RU VLPs). c) Difference curves for Fc2 after subtraction of reference curves. d) Binding isotherm for Fc2-1 and fitting curve to a 1:1 binding model (black line, equation 9).

### 7.7.2 Measurements with Hits from Virtual Library Screening

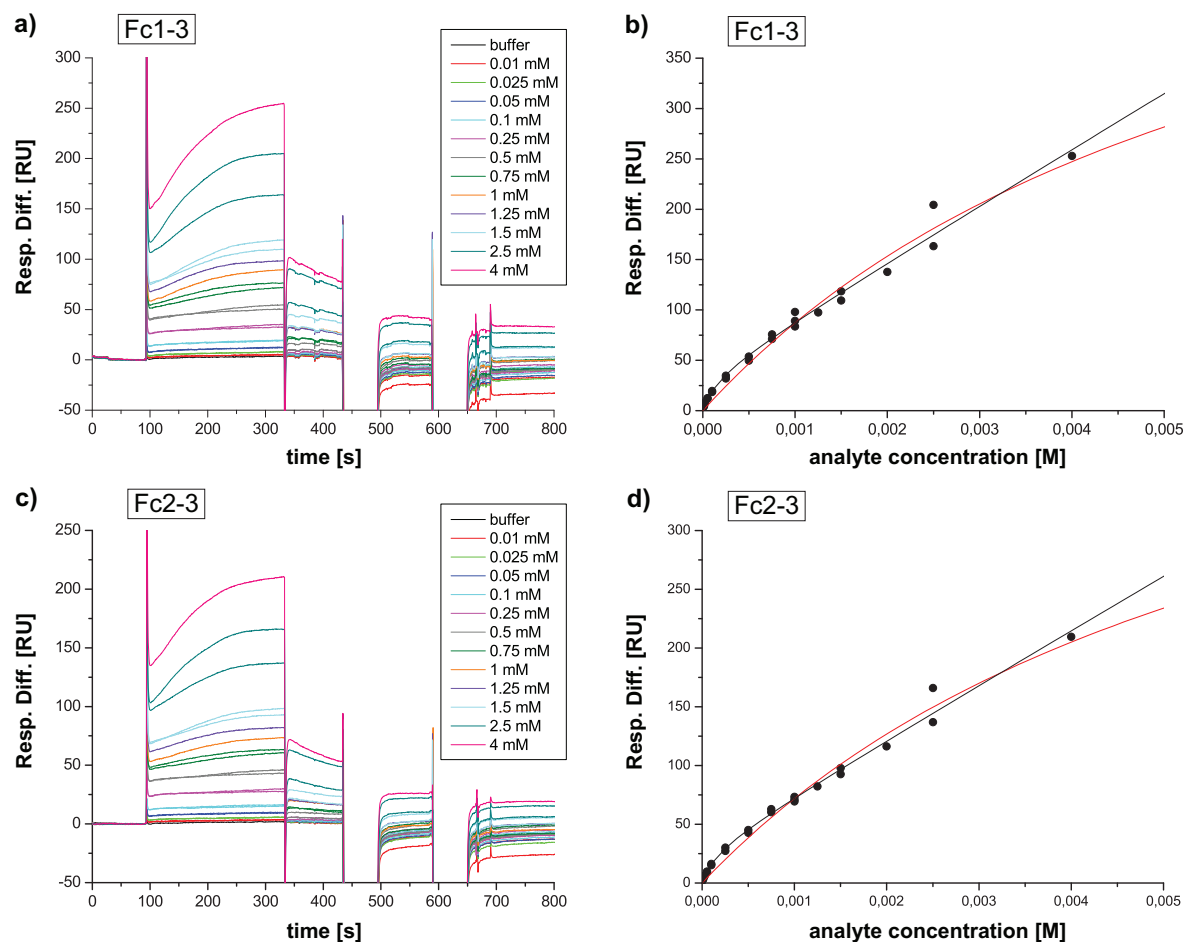


Figure 7.16. Measurement of virtual screening hit **42** on sensor chip C. a),c) Difference curves for Fc1 (7050 RU VLPs) and Fc2 (5260 RU VLPs) after reference curve subtraction; 100–340 s: injection of 80  $\mu$ L of **42** at a flow rate of 20  $\mu$ L/min; 430 and 590 s: regeneration with 1 minute injections of phosphate buffer pH 7.4. b),d) Binding isotherms for **42** on Fc1 (b) and Fc2 (d) and fitting curves to a 1:1 binding model (red lines, equation 9) and a two-site binding model (black lines, equation 10) (cf. Table 4.11).

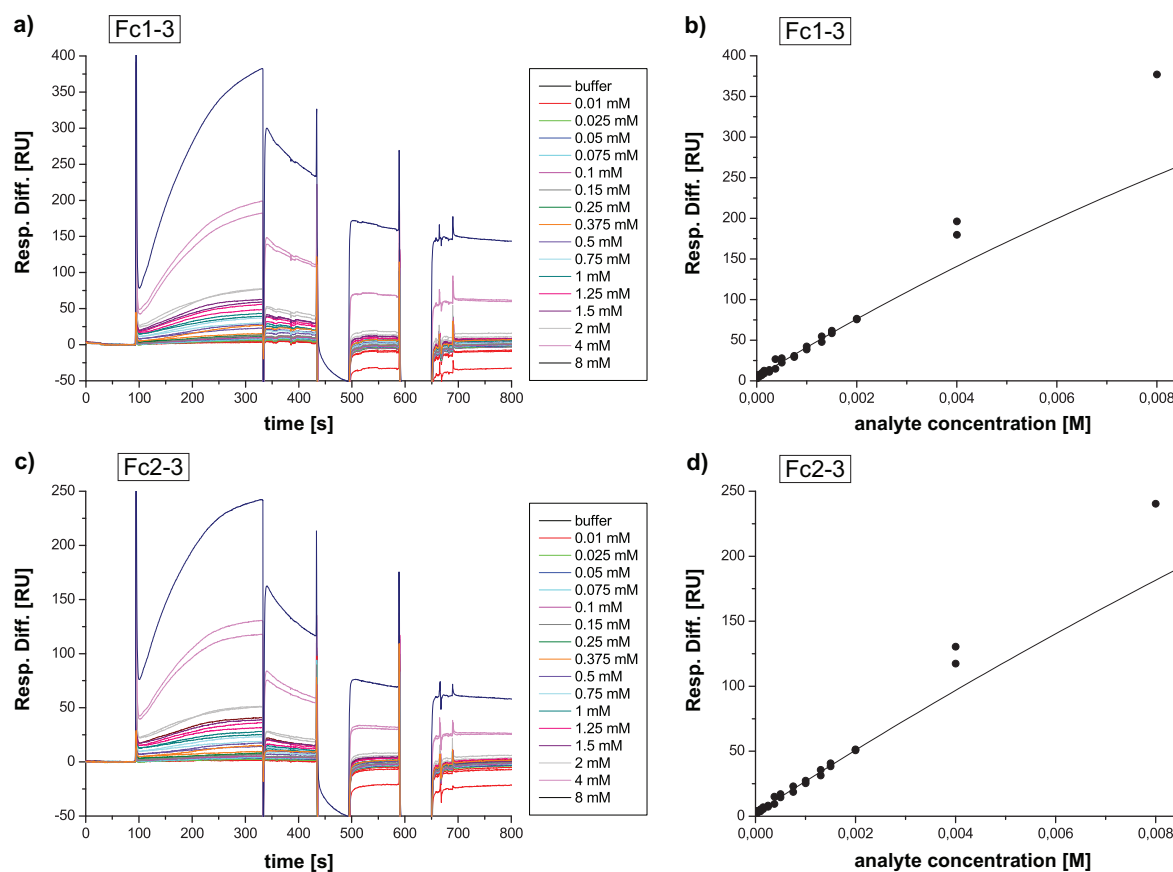


Figure 7.17. Measurement of virtual screening compound **43** on sensor chip C. a),c) Difference curves for Fc1 (7050 RU VLPs) and Fc2 (5260 RU VLPs) after reference curve subtraction; 100–340 s: injection of 80  $\mu$ L of **43** at a flow rate of 20  $\mu$ L/min; 430 and 590 s: regeneration with 1 minute injections of phosphate buffer pH 7.4. b),d) Binding curves for Fc1 (b) and Fc2 (d) and fitting curves to a 1:1 binding model (black lines, equation 9) (cf. Table 7.6); data points for 4 mM and 8 mM are regarded as outliers and were not excluded from fitting.

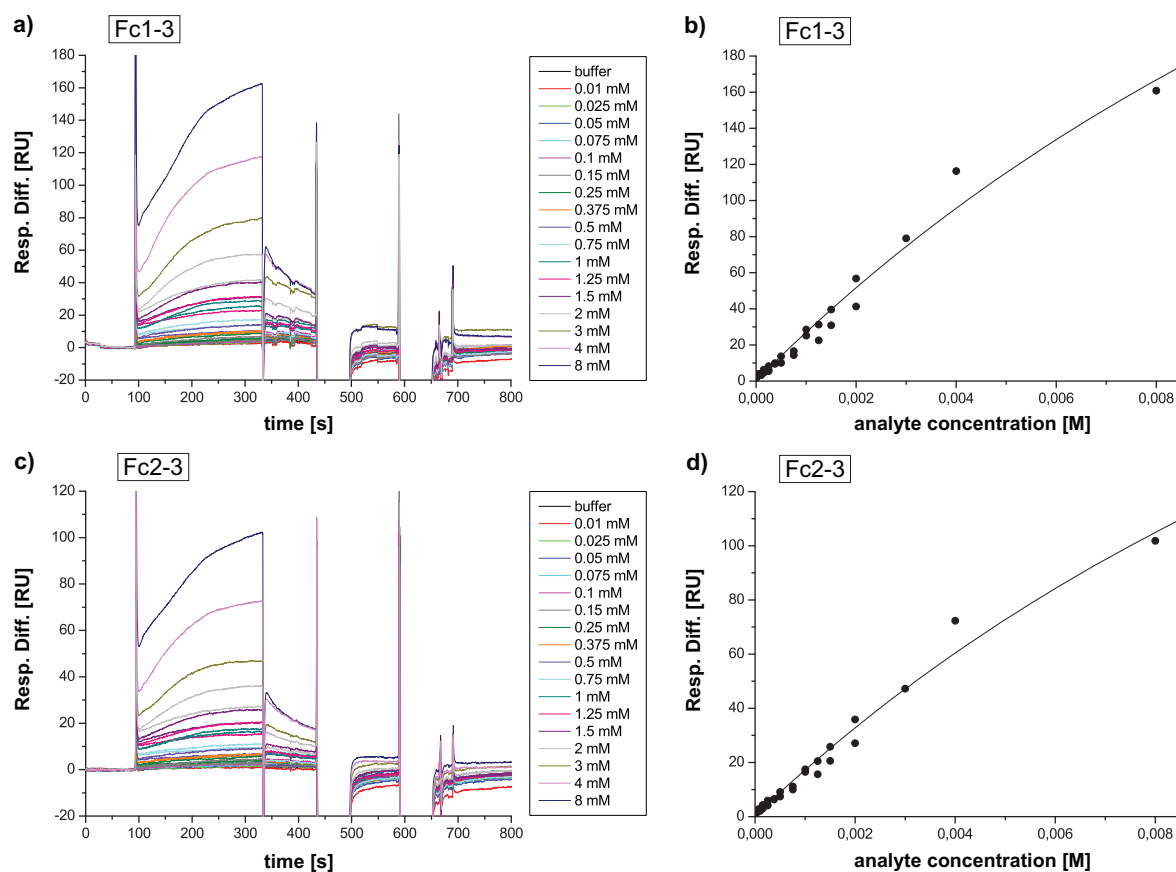


Figure 7.18. Measurement of virtual screening hit **44** on sensor chip C. a),c) Difference curves for Fc1 (7050 RU VLPs) and Fc2 (5260 RU VLPs) after reference curve subtraction; 100–340 s: injection of 80  $\mu$ L of **44** at a flow rate of 20  $\mu$ L/min; 430 and 590 s: regeneration with 1 minute injections of phosphate buffer pH 7.4. b),d) Binding curves for Fc1 (b) and Fc2 (d) and fitting curves to a 1:1 binding model (black lines, equation 9) (Table 7.6).

Table 7.6. Results from SPR measurements of **43** and **44** on sensor chip C.

Compound	$K_D$ [mM]	$RU_{max}$ [RU]	$R^2/\chi^2$	Flow cell	Coverage [RU]	Theor. $RU_{max}$
<b>43</b>	<b>37.3</b> ( $\pm 54.6$ )	1410 ( $\pm 1960$ )	0.9884/ 5.9	Fc1	7050	61.8
	<b>69.5</b> ( $\pm 152.7$ )	1740 ( $\pm 3710$ )	0.9920/ 1.8	Fc2	5260	46.1
<b>44</b>	<b>23.3</b> ( $\pm 7.5$ )	651 ( $\pm 167$ )	0.9761/ 29.8	Fc1	7050	56.0
	<b>23.0</b> ( $\pm 6.3$ )	405 ( $\pm 88$ )	0.9822/ 8.7	Fc2	5260	41.8

### 7.7.3 Measurements with Polymeric Inhibitors

Polymers **36**, **38**, **39**, **40**, **41**, **46** and **47** were measured on sensor chip F covered with wildtype Ast6139 VLPs with the following coverage: Fc1: reference (only activated/deactivated), Fc2: 1600 RU VLPs; Fc3: 5100 RU VLPs, Fc4: 3700 RU VLPs.

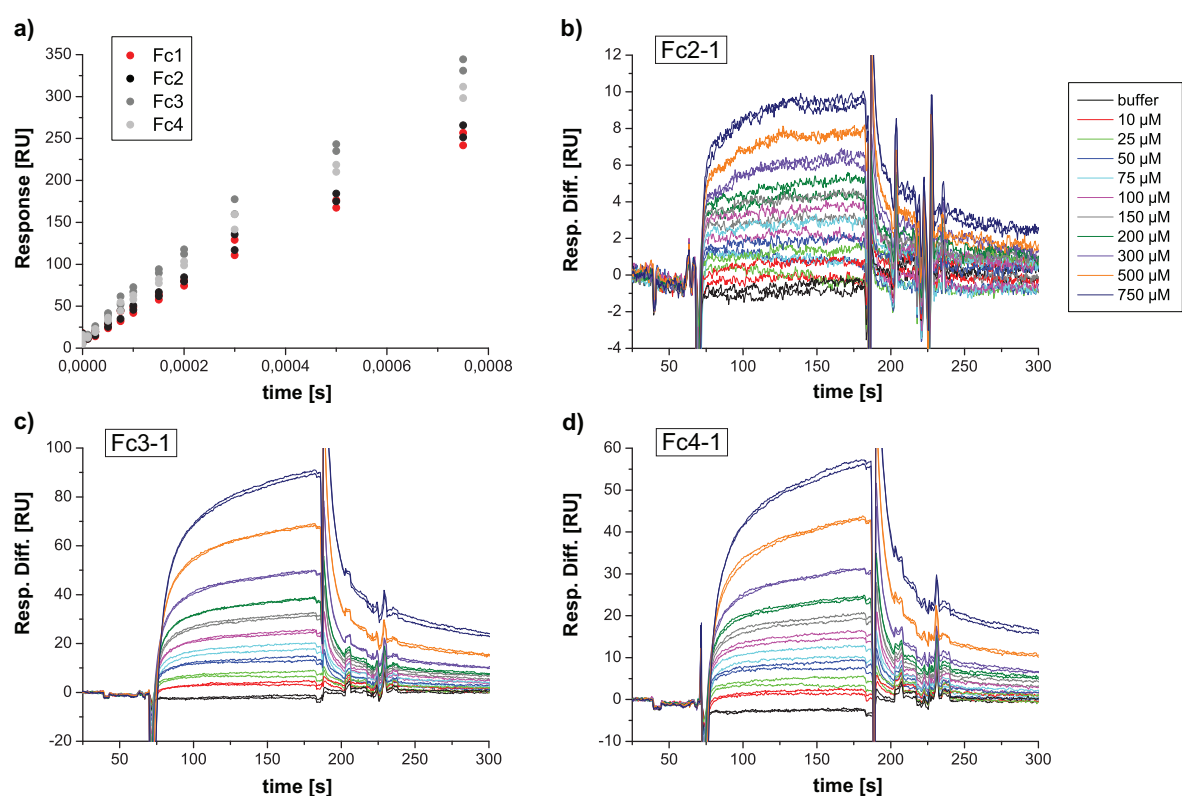


Figure 7.19. Measurement of polymeric compound **36**.

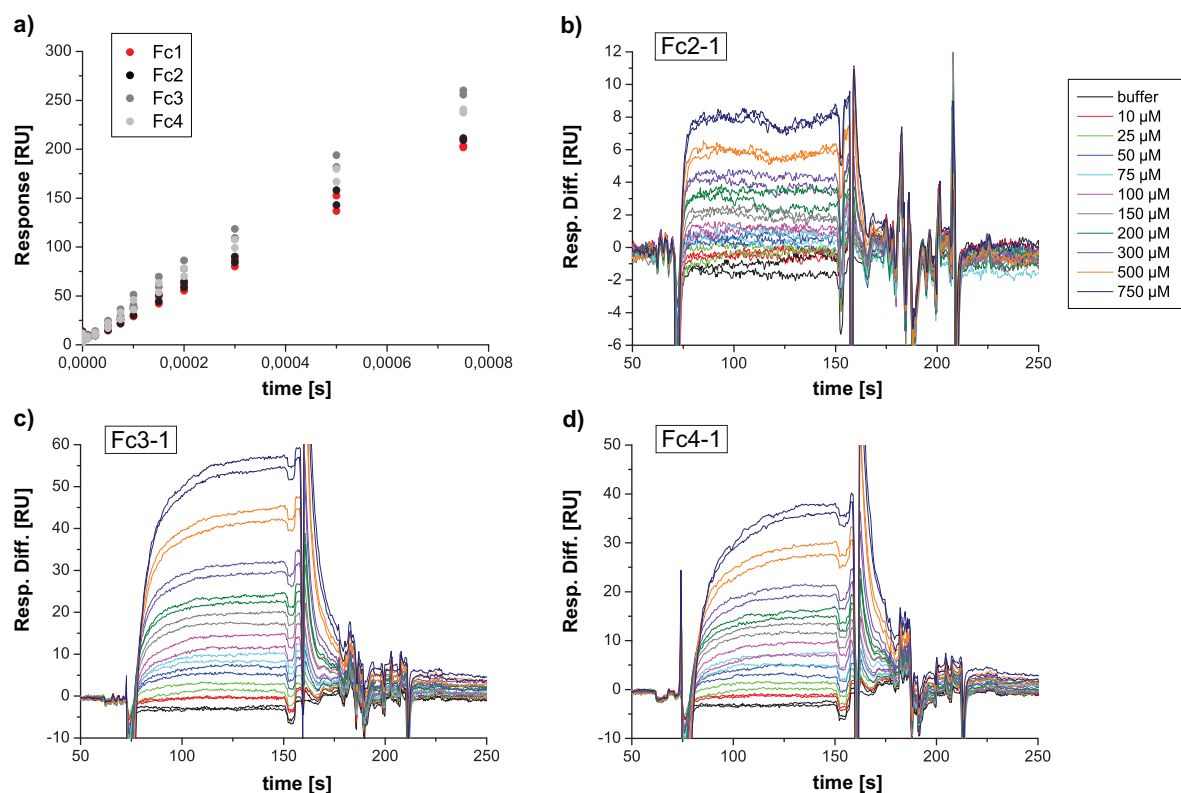


Figure 7.20. Measurement of polymeric compound 38.

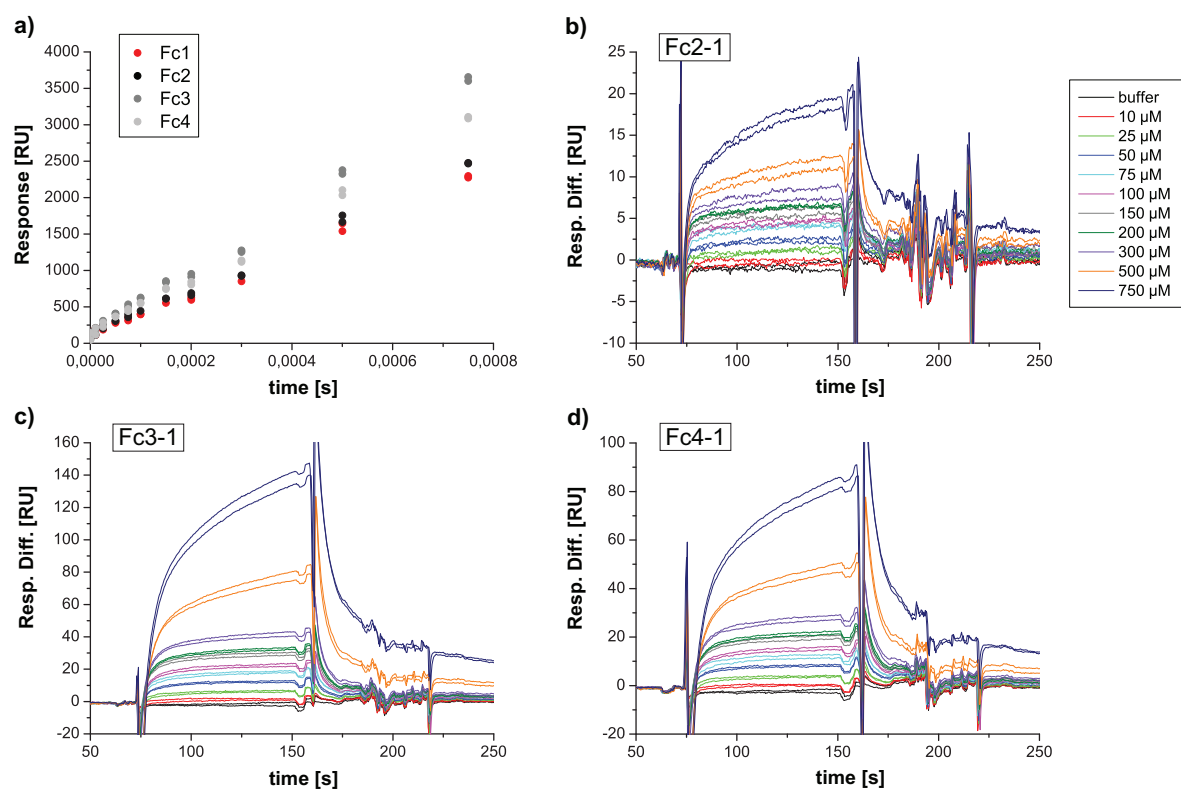


Figure 7.21. Measurement of polymeric compound 39.

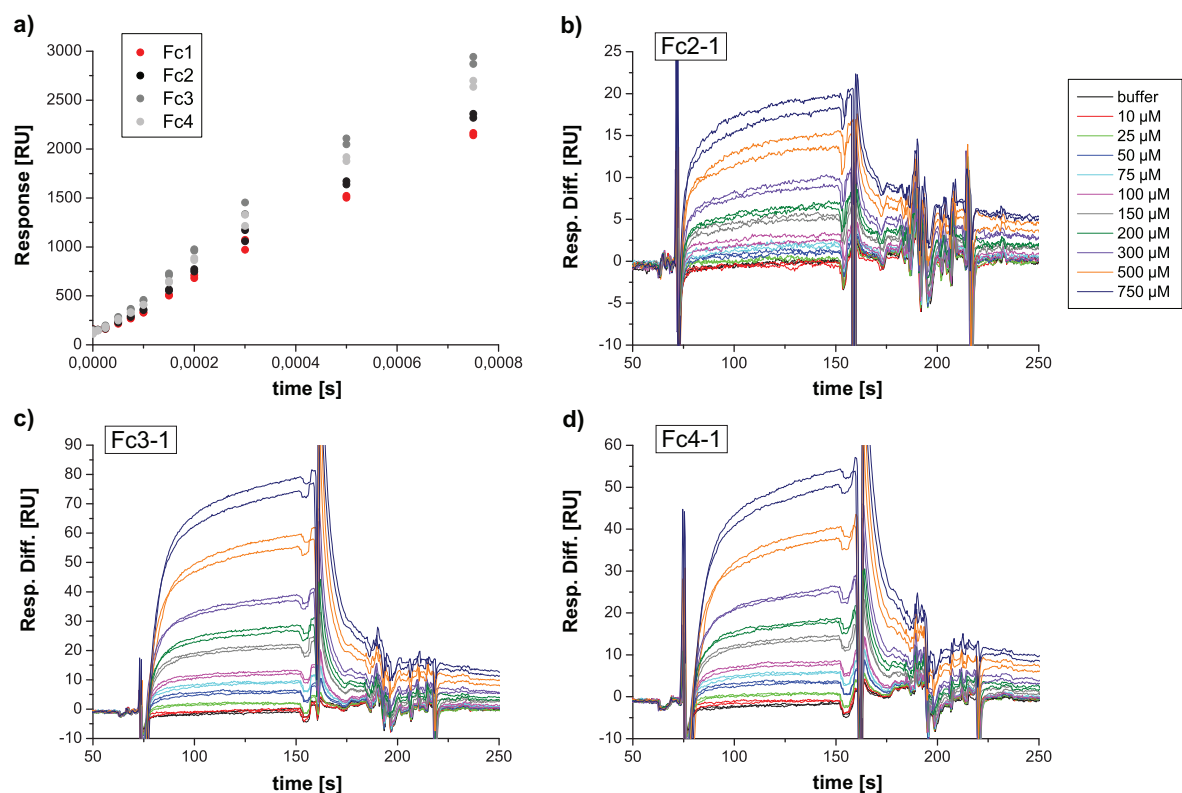


Figure 7.22. Measurement of polymeric compound 40.

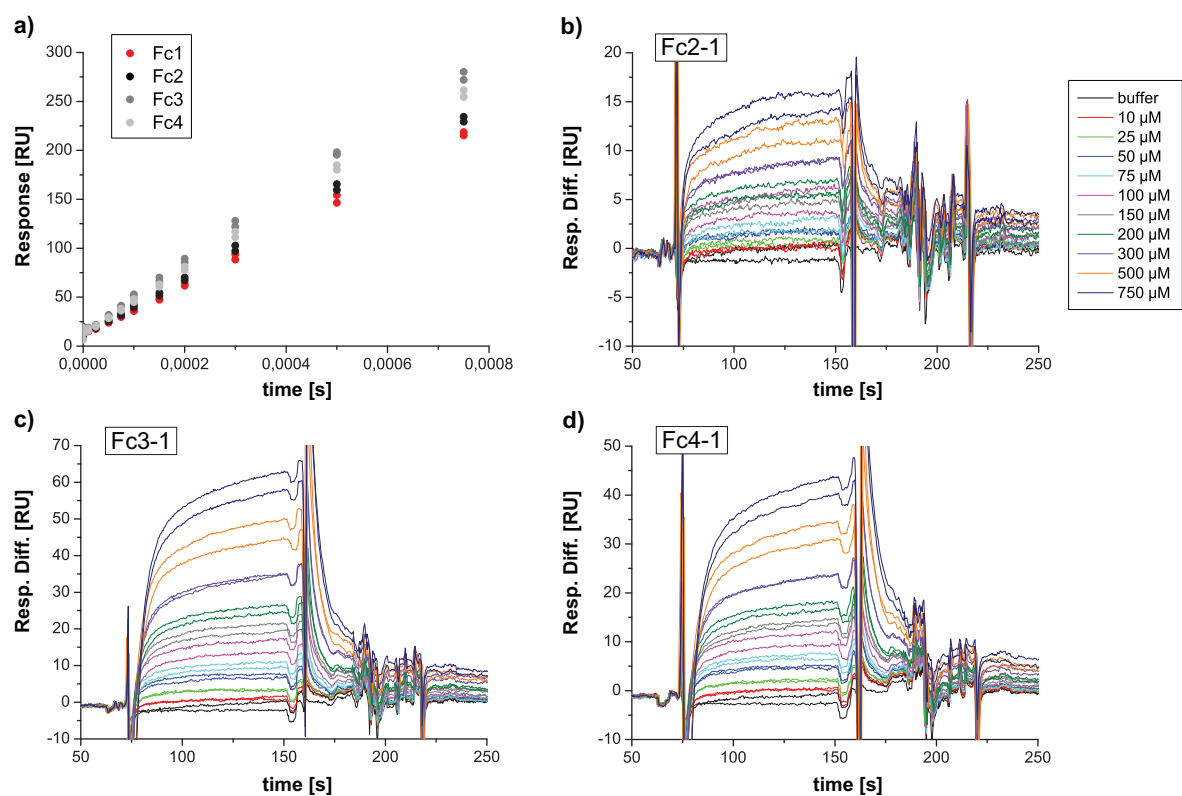


Figure 7.23. Measurement of polymeric compound 41.



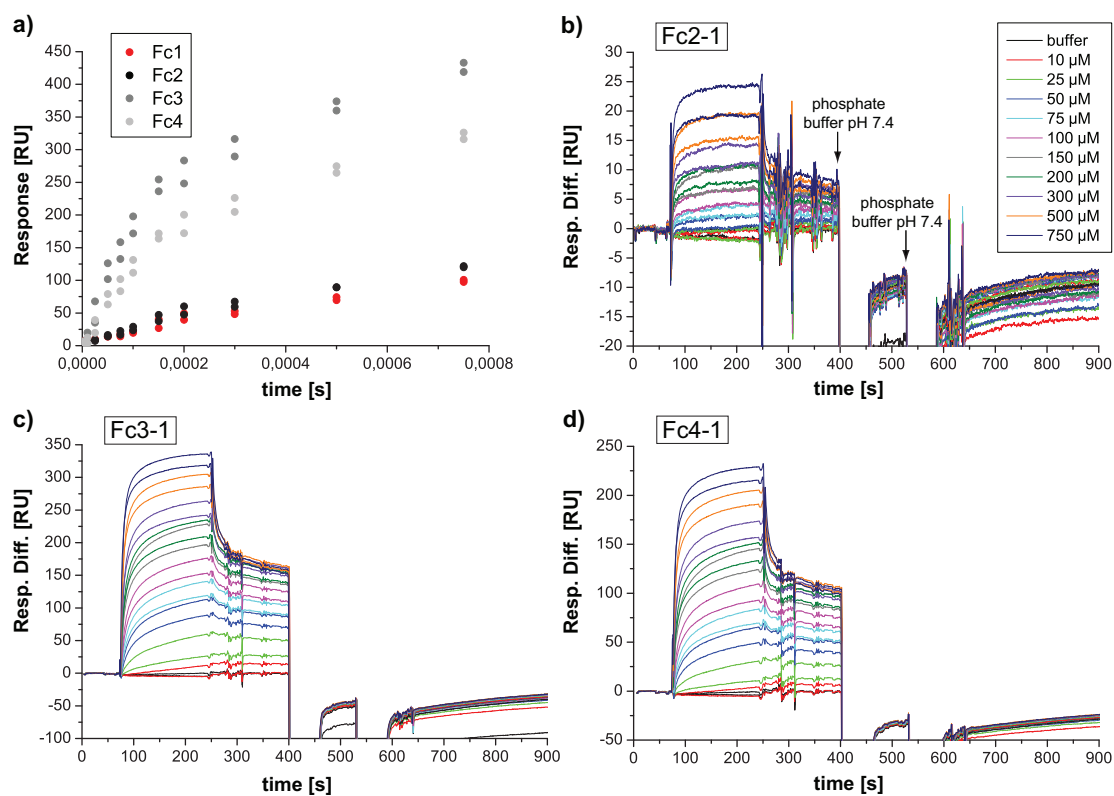


Figure 7.24. Measurement of polymeric compound 46.

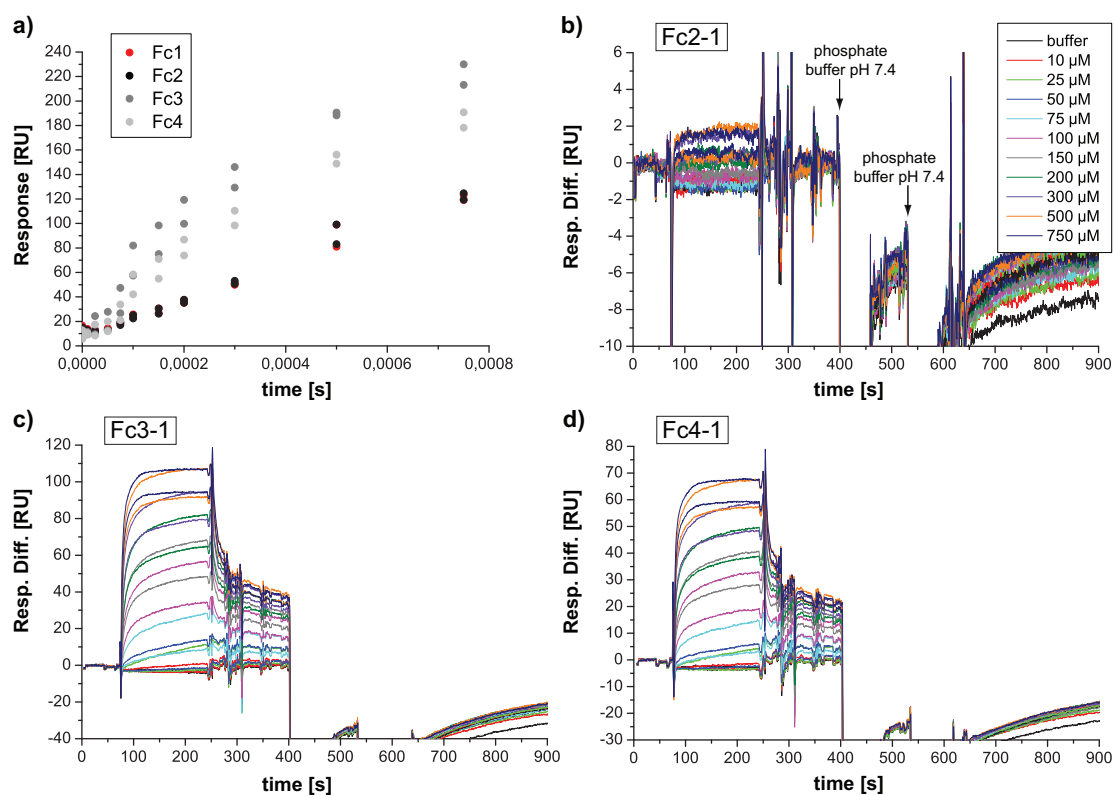


Figure 7.25. Measurement of polymeric compound 47.

### 7.7.4 SPR Assays with Immobilized PAA Sugar Conjugates

The dependence of VLP binding to immobilized PAA sugars on the flow rate (Figure 7.26) and on the injected VLP concentration (Figure 7.27) was tested on a C1 sensor chip with the following coverage: Fc1: 230 RU PAA-biotin (reference); Fc2: 210 RU PAA-Fuc and 110 RU PAA-biotin; Fc3: 220 RU PAA-H-disaccharide and 140 RU PAA-biotin; Fc4: 210 RU PAA-B trisaccharide and 130 RU PAA-biotin (cf. section 4.8.1).

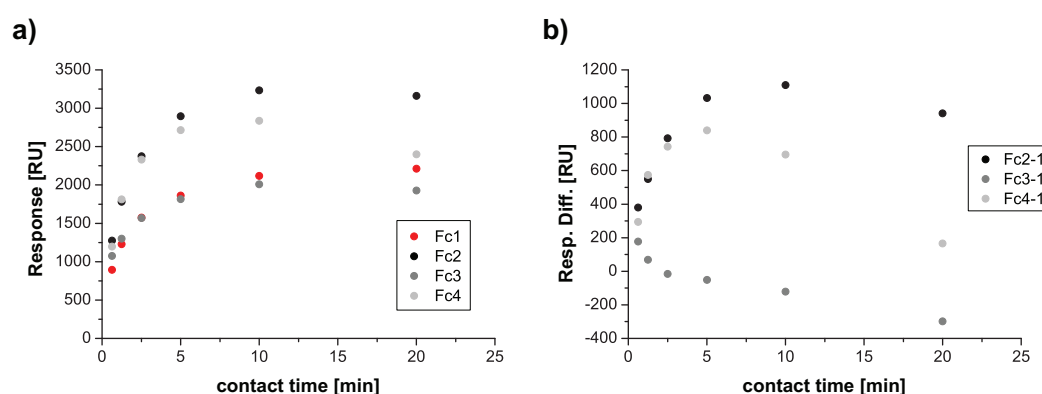


Figure 7.26. Dependence of VLP binding to PAA sugars on the flow rate. Absolute responses (a) and response differences (b) for injection of 20  $\mu\text{L}$  at flow rates of 32, 16, 8, 4, 2 and 1  $\mu\text{L}/\text{min}$  corresponding to contact times of 0.625, 1.25, 2.5, 5, 10 and 20 min, respectively.

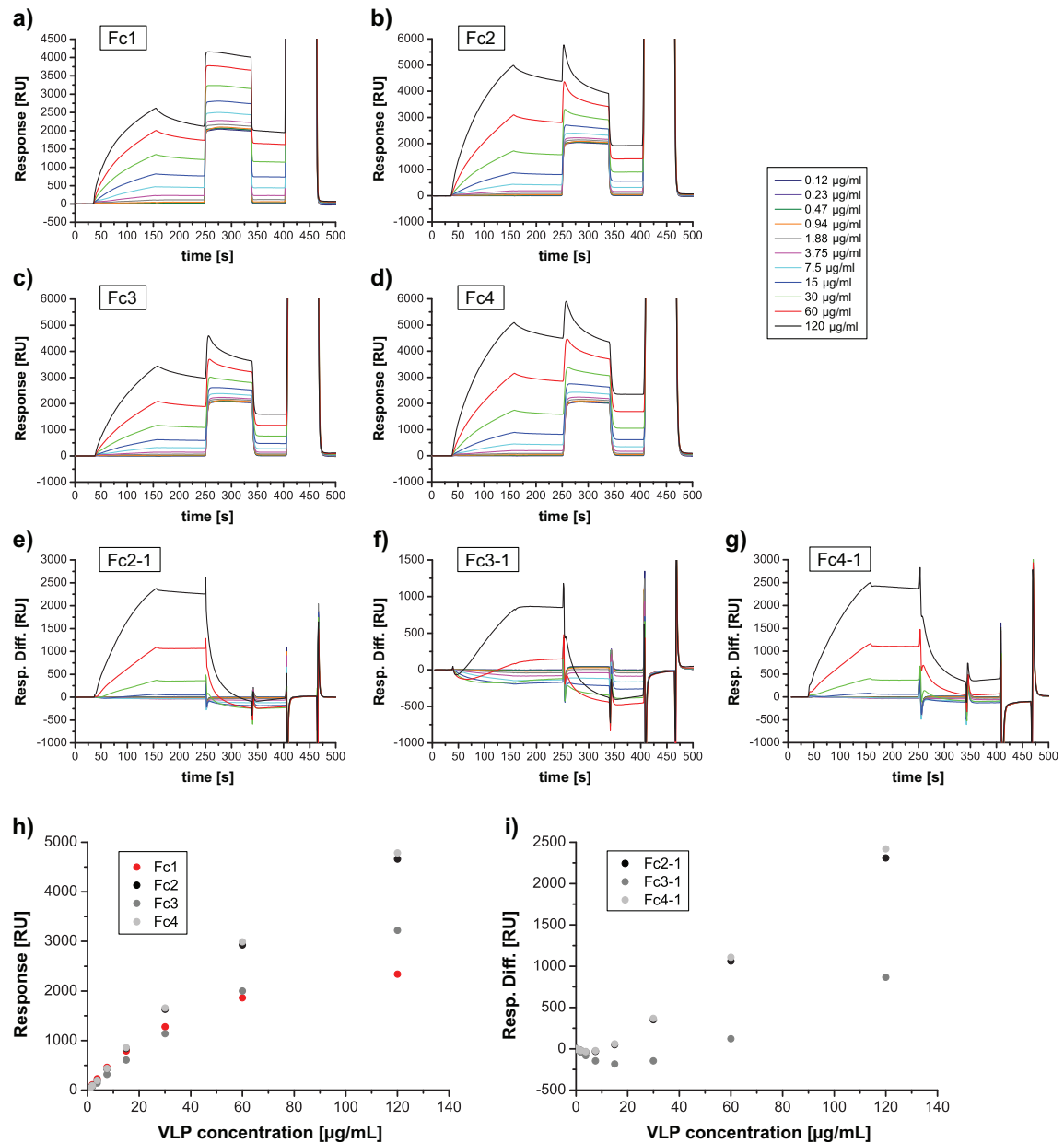


Figure 7.27. Concentration dependent binding of VLPs to PAA sugars. a)-d) Sensorgrams and e)-g) difference curves for injection of 20  $\mu\text{L}$  VLPs with increasing concentration at a flow rate of 10  $\mu\text{L/min}$ ; 250-340s: injection of 15  $\mu\text{L}$  100 mM L-Fuc; at 410s: regeneration with 10  $\mu\text{L}$  phosphate buffer pH 7.4. h) Absolute responses and i) response differences as a function of VLP concentration.

## Competitive measurement of polymeric compounds:

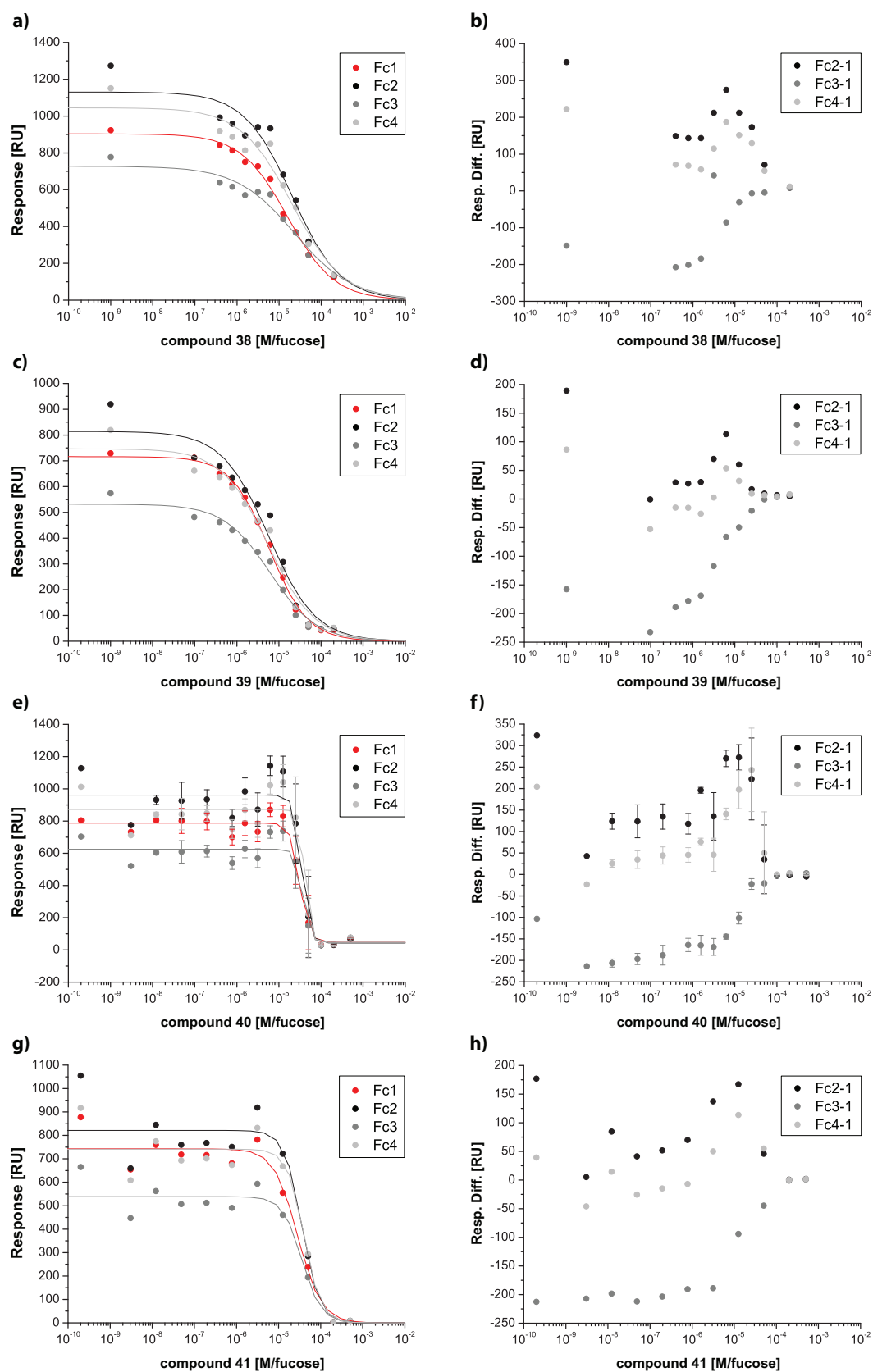


Figure 7.28. Inhibition curves for polymeric compounds on different PAA sugars. Fc1: reference; Fc2: PAA-Fuc; Fc3: PAA-H disaccharide; Fc4: PAA-B trisaccharide.

Table 7.7. Competitive measurements with polymeric compounds on PAA sugars. Polymers **35** and **37** were measured on a C1 sensor chip covered with 151 RU PAA on Fc1 (reference) and 90 RU PAA-Fuc on Fc2. All other polymers were measured on a C1 sensor chip covered with: Fc1: 230 RU PAA (reference); Fc2: 210 RU PAA-Fuc; Fc3: 220 RU PAA-H-disaccharide; Fc4: 210 RU PAA-B trisaccharide.

No.	Functionality	IC <sub>50</sub> [μM]	RU <sub>max</sub> [RU]	RU <sub>min</sub> [RU]	Hill slope	R <sup>2</sup> /χ <sup>2</sup>	Fc
<b>34</b>	PAA backbone	no inhibition curve					
<b>35</b>	fucose	<b>60</b> (± 20)	371 (± 5)	166 (± 42)	1.51 (± 0.54)	0.9372/ 262	1
		<b>80</b> (± 30)	494 (± 6)	202 (± 67)	1.41 (± 0.44)	0.9532/ 320	2
<b>37</b>	fucose + fragment 160	<b>0.51</b> (± 0.03)	403 (± 3)	108 (± 6)	1.49 (± 0.11)	0.9974/ 48.6	1
		<b>0.61</b> (± 0.03)	527 (± 3)	106 (± 7)	1.46 (± 0.09)	0.9983/ 64.1	2
<b>38</b>	fucose + fragment 191	<b>20</b> (± 1.7)	903 (± 21)	0 (± 0)	0.79 (± 0.06)	0.9923/ 736	1
		<b>20</b> (± 6.5)	1131 (± 76)	0 (± 0)	0.76 (± 0.18)	0.9378/ 9578	2
		<b>20</b> (± 6.2)	728 (± 37)	0 (± 0)	0.63 (± 0.10)	0.9608/ 1950	3
		<b>20</b> (± 6.2)	1045 (± 66)	0 (± 0)	0.71 (± 0.15)	0.9455/ 6696	4
<b>39</b>	fucose + fragment 473	<b>5.9</b> (± 0.5)	716 (± 13)	0 (± 0)	0.95 (± 0.06)	0.9961/ 354	1
		<b>5.7</b> (± 1.6)	814 (± 49)	0 (± 0)	0.79 (± 0.13)	0.9617/ 4191	2
		<b>6.1</b> (± 1.2)	532 (± 22)	0 (± 0)	0.79 (± 0.09)	0.9806/ 853	3
		<b>5.6</b> (± 1.3)	746 (± 37)	0 (± 0)	0.79 (± 0.11)	0.9743/ 2304	4
<b>40</b>	fucose + fragment 151	<b>30</b> (± 2.6)	787 (± 16)	0 (± 0)	3.94 (± 0.99)	0.9815/ 2489	1
		<b>40</b> (± 5.5)	961 (± 38)	0 (± 0)	4.64 (± 2.00)	0.9358/ 13908	2
		<b>40</b> (± 5.5)	625 (± 22)	0 (± 0)	5.19 (± 2.22)	0.9419/ 4977	3
		<b>40</b> (± 6.9)	872 (± 34)	0 (± 0)	6.10 (± 4.09)	0.9359/ 11174	4
<b>41</b>	fucose + fragment 231	<b>30</b> (± 6.5)	743 (± 27)	0 (± 0)	1.56 (± 0.45)	0.9621/ 4643	1
		<b>40</b> (± 10)	821 (± 44)	0 (± 0)	2.09 (± 1.19)	0.9177/ 13033	2
		<b>40</b> (± 9.6)	539 (± 25)	0 (± 0)	1.92 (± 0.87)	0.9371/ 4142	3
		<b>40</b> (± 10)	741 (± 35)	0 (± 0)	2.16 (± 1.28)	0.9321/ 8465	4

## 8 Literature

Abad LW, Neumann M, Tobias L, Obenauer-Kutner L, Jacobs S, Cullen C (2002) Development of a biosensor-based method for detection and isotyping of antibody responses to adenoviral-based gene therapy vectors. *Anal Biochem* **310**: 107-13

Abente EJ, Sosnovtsev SV, Bok K, Green KY (2010) Visualization of feline calicivirus replication in real-time with recombinant viruses engineered to express fluorescent reporter proteins. *Virology* **400**: 18-31

Angulo J, Enriquez-Navas PM, Nieto PM (2010) Ligand-receptor binding affinities from saturation transfer difference (STD) NMR spectroscopy: the binding isotherm of STD initial growth rates. *Chemistry* **16**: 7803-12

Asanaka M, Atmar RL, Ruvolo V, Crawford SE, Neill FH, Estes MK (2005) Replication and packaging of Norwalk virus RNA in cultured mammalian cells. *Proc Natl Acad Sci U S A* **102**: 10327-32

Atmar RL, Bernstein DI, Harro CD, Al-Ibrahim MS, Chen WH, Ferreira J, Estes MK, Graham DY, Opekun AR, Richardson C, Mendelman PM (2011) Norovirus vaccine against experimental human Norwalk Virus illness. *N Engl J Med* **365**: 2178-87

Atmar RL, Estes MK (2006) The epidemiologic and clinical importance of norovirus infection. *Gastroenterol Clin North Am* **35**: 275-90, viii

Ausar SF, Foubert TR, Hudson MH, Vedvick TS, Middaugh CR (2006) Conformational stability and disassembly of Norwalk virus-like particles. Effect of pH and temperature. *J Biol Chem* **281**: 19478-88

Bailey D, Thackray LB, Goodfellow IG (2008) A single amino acid substitution in the murine norovirus capsid protein is sufficient for attenuation in vivo. *J Virol* **82**: 7725-8

Baker M, Prasad BV (2010) Rotavirus cell entry. *Curr Top Microbiol Immunol* **343**: 121-48

Bank-Wolf BR, Konig M, Thiel HJ (2010) Zoonotic aspects of infections with noroviruses and sapoviruses. *Vet Microbiol* **140**: 204-12

Barcena J, Morales M, Vazquez B, Boga JA, Parra F, Lucientes J, Pages-Mante A, Sanchez-Vizcaino JM, Blasco R, Torres JM (2000) Horizontal transmissible protection against myxomatosis and rabbit hemorrhagic disease by using a recombinant myxoma virus. *J Virol* **74**: 1114-23

Barcena J, Verdaguer N, Roca R, Morales M, Angulo I, Risco C, Carrascosa JL, Torres JM, Caston JR (2004) The coat protein of Rabbit hemorrhagic disease virus contains a molecular switch at the N-terminal region facing the inner surface of the capsid. *Virology* **322**: 118-34

Beersma MF, Schutten M, Vennema H, Hartwig NG, Mes TH, Osterhaus AD, van Doornum GJ, Koopmans M (2009) Norovirus in a Dutch tertiary care hospital (2002-

2007): frequent nosocomial transmission and dominance of GIIb strains in young children. *J Hosp Infect* **71**: 199-205

Benie AJ, Moser R, Bauml E, Blaas D, Peters T (2003) Virus-ligand interactions: identification and characterization of ligand binding by NMR spectroscopy. *J Am Chem Soc* **125**: 14-5

Bereszczak JZ, Barbu IM, Tan M, Xia M, Jiang X, van Duijn E, Heck AJ (2012) Structure, stability and dynamics of norovirus P domain derived protein complexes studied by native mass spectrometry. *J Struct Biol* **177**: 273-82

Berger S, Braun S (2004) *200 and More NMR Experiments: A Practical Course*, 1st edn: Wiley-VCH

Bertolotti-Ciarlet A, Crawford SE, Hutson AM, Estes MK (2003) The 3' end of Norwalk virus mRNA contains determinants that regulate the expression and stability of the viral capsid protein VP1: a novel function for the VP2 protein. *J Virol* **77**: 11603-15

Best MD (2009) Click chemistry and bioorthogonal reactions: unprecedented selectivity in the labeling of biological molecules. *Biochemistry* **48**: 6571-84

Bhella D, Gatherer D, Chaudhry Y, Pink R, Goodfellow IG (2008) Structural insights into calicivirus attachment and uncoating. *J Virol* **82**: 8051-8

Blazevic V, Lappalainen S, Nurminen K, Huhti L, Vesikari T (2011) Norovirus VLPs and rotavirus VP6 protein as combined vaccine for childhood gastroenteritis. *Vaccine* **29**: 8126-33

Boga JA, Martin Alonso JM, Casais R, Parra F (1997) A single dose immunization with rabbit haemorrhagic disease virus major capsid protein produced in *Saccharomyces cerevisiae* induces protection. *J Gen Virol* **78** ( Pt 9): 2315-8

Bok K, Abente EJ, Realpe-Quintero M, Mitra T, Sosnovtsev SV, Kapikian AZ, Green KY (2009a) Evolutionary Dynamics of GII.4 Noroviruses over a 34-Year Period. *J Virol* **83**: 11890-901

Bok K, Prikhodko VG, Green KY, Sosnovtsev SV (2009b) Apoptosis in murine norovirus-infected RAW264.7 cells is associated with downregulation of survivin. *J Virol* **83**: 3647-56

Brown KE, Cohen BJ (1992) Haemagglutination by parvovirus B19. *J Gen Virol* **73** ( Pt 8): 2147-9

Bu W, Mamedova A, Tan M, Xia M, Jiang X, Hegde RS (2008) Structural basis for the receptor binding specificity of Norwalk virus. *J Virol* **82**: 5340-7

Bull RA, Eden JS, Rawlinson WD, White PA (2010) Rapid evolution of pandemic noroviruses of the GII.4 lineage. *PLoS Pathog* **6**: e1000831

Campos-Olivas R (2011) NMR screening and hit validation in fragment based drug discovery. *Curr Top Med Chem* **11**: 43-67

Cao S, Lou Z, Tan M, Chen Y, Liu Y, Zhang Z, Zhang XC, Jiang X, Li X, Rao Z (2007) Structural basis for the recognition of blood group trisaccharides by norovirus. *J Virol* **81**: 5949-57

Carlsson B, Kindberg E, Buesa J, Rydell GE, Lidon MF, Montava R, Abu Mallouh R, Grahn A, Rodriguez-Diaz J, Bellido J, Arnedo A, Larson G, Svensson L (2009) The G428A nonsense mutation in FUT2 provides strong but not absolute protection against symptomatic GII.4 Norovirus infection. *PLoS ONE* **4**: e5593

Carr RA, Congreve M, Murray CW, Rees DC (2005) Fragment-based lead discovery: leads by design. *Drug Discov Today* **10**: 987-92

Casset F, Imberty A, Perez S, Etzler ME, Paulsen H, Peters T (1997) Transferred nuclear Overhauser enhancement (NOE) and rotating-frame NOE experiments reflect the size of the bound segment of the Forssman pentasaccharide in the binding site of Dolichos biflorus lectin. *Eur J Biochem* **244**: 242-50

Chabre YM, Roy R (2010) Design and creativity in synthesis of multivalent neoglycoconjugates. *Adv Carbohydr Chem Biochem* **63**: 165-393

Changotra H, Jia Y, Moore TN, Liu G, Kahan SM, Sosnovtsev SV, Karst SM (2009) Type I and type II interferons inhibit the translation of murine norovirus proteins. *J Virol* **83**: 5683-92

Cheetham S, Souza M, Meulia T, Grimes S, Han MG, Saif LJ (2006) Pathogenesis of a genogroup II human norovirus in gnotobiotic pigs. *J Virol* **80**: 10372-81

Chen R, Neill JD, Estes MK, Prasad BV (2006) X-ray structure of a native calicivirus: structural insights into antigenic diversity and host specificity. *Proc Natl Acad Sci U S A* **103**: 8048-53

Chen Y, Tan M, Xia M, Hao N, Zhang XC, Huang P, Jiang X, Li X, Rao Z (2011) Crystallography of a lewis-binding norovirus, elucidation of strain-specificity to the polymorphic human histo-blood group antigens. *PLoS Pathog* **7**: e1002152

Cheng Y, Prusoff WH (1973) Relationship between the inhibition constant (K<sub>1</sub>) and the concentration of inhibitor which causes 50 per cent inhibition (I<sub>50</sub>) of an enzymatic reaction. *Biochem Pharmacol* **22**: 3099-108

Choi JM, Hutson AM, Estes MK, Prasad BV (2008) Atomic resolution structural characterization of recognition of histo-blood group antigens by Norwalk virus. *Proc Natl Acad Sci U S A* **105**: 9175-80

Claasen B, Axmann M, Meinecke R, Meyer B (2005) Direct observation of ligand binding to membrane proteins in living cells by a saturation transfer double difference (STDD) NMR spectroscopy method shows a significantly higher affinity of integrin alpha(IIb)beta3 in native platelets than in liposomes. *J Am Chem Soc* **127**: 916-9



Claridge T (2000) *High-Resolution NMR Techniques in Organic Chemistry*, 1st edn: Pergamon

Clore GM, Gronenborn AM (1982) Theory and applications of the transferred nuclear overhauser effect to the study of the conformations of small ligands bound to proteins *J Magn Reson* **48**: 402-417

Cuellar JL, Meinhoevel F, Hoehne M, Donath E (2010) Size and mechanical stability of norovirus capsids depend on pH: a nanoindentation study. *J Gen Virol* **91**: 2449-56

D'Souza DH, Sair A, Williams K, Papafragkou E, Jean J, Moore C, Jaykus L (2006) Persistence of caliciviruses on environmental surfaces and their transfer to food. *Int J Food Microbiol* **108**: 84-91

da Silva AK, Kavanagh OV, Estes MK, Elimelech M (2011) Adsorption and aggregation properties of norovirus GI and GII virus-like particles demonstrate differing responses to solution chemistry. *Environ Sci Technol* **45**: 520-6

Dalvit C (2008) Theoretical Analysis of the Competition Ligand-Based NMR Experiments and Selected Applications to Fragment Screening and Binding Constant Measurements. *Concepts in Magnetic Resonance Part A* **32A**: 341-372

Dalvit C (2009) NMR methods in fragment screening: theory and a comparison with other biophysical techniques. *Drug Discov Today* **14**: 1051-7

Dam TK, Brewer CF (2007) Fundamentals of Lectin-Carbohydrate Interactions. In *Comprehensive Glycoscience - From Chemistry to Systems Biology*, Kamerling J, Boons GJ, Lee Y, Suzuki A, Taniguchi N, Voragen AGJ (eds), pp 397-452. Elsevier

Dam TK, Brewer CF (2009) Lectins as Pattern Recognition Molecules: The Effects of Epitope Density in Innate Immunity#. *Glycobiology*

Dam TK, Gerken TA, Brewer CF (2009) Thermodynamics of multivalent carbohydrate-lectin cross-linking interactions: importance of entropy in the bind and jump mechanism. *Biochemistry* **48**: 3822-7

Day YS, Baird CL, Rich RL, Myszka DG (2002) Direct comparison of binding equilibrium, thermodynamic, and rate constants determined by surface- and solution-based biophysical methods. *Protein Sci* **11**: 1017-25

de Haro L, Ferracci G, Opi S, Iborra C, Quetglas S, Miquelis R, Leveque C, Seagar M (2004) Ca<sup>2+</sup>/calmodulin transfers the membrane-proximal lipid-binding domain of the v-SNARE synaptobrevin from cis to trans bilayers. *Proc Natl Acad Sci U S A* **101**: 1578-83

de Rougemont A, Ruvoen-Clouet N, Simon B, Estienney M, Elie-Caille C, Aho S, Pothier P, Le Pendu J, Boireau W, Belliot G (2011) Qualitative and Quantitative Analysis of the Binding of GII.4 Norovirus Variants onto Human Blood Group Antigens. *J Virol* **85**: 4057-70

- Decroocq C, Rodriguez-Lucena D, Russo V, Mena Barragan T, Ortiz Mellet C, Compain P (2011) The multivalent effect in glycosidase inhibition: probing the influence of architectural parameters with cyclodextrin-based iminosugar click clusters. *Chemistry* **17**: 13825-31
- DeMarco ML, Woods RJ (2008) Structural glycobiology: a game of snakes and ladders. *Glycobiology* **18**: 426-40
- Donaldson EF, Lindesmith LC, Lobue AD, Baric RS (2008) Norovirus pathogenesis: mechanisms of persistence and immune evasion in human populations. *Immunol Rev* **225**: 190-211
- Donaldson EF, Lindesmith LC, Lobue AD, Baric RS (2010) Viral shape-shifting: norovirus evasion of the human immune system. *Nat Rev Microbiol* **8**: 231-41
- Dou D, He G, Mandadapu SR, Aravapalli S, Kim Y, Chang KO, Groutas WC (2012a) Inhibition of noroviruses by piperazine derivatives. *Bioorg Med Chem Lett* **22**: 377-9
- Dou D, Mandadapu SR, Alliston KR, Kim Y, Chang KO, Groutas WC (2012b) Cyclosulfamide-based derivatives as inhibitors of noroviruses. *Eur J Med Chem* **47**: 59-64
- Dou D, Tiew KC, Mandadapu SR, Gunnam MR, Alliston KR, Kim Y, Chang KO, Groutas WC (2012c) Potent norovirus inhibitors based on the acyclic sulfamide scaffold. *Bioorg Med Chem*
- Dubs MC, Altschuh D, Van Regenmortel MH (1992) Interaction between viruses and monoclonal antibodies studied by surface plasmon resonance. *Immunol Lett* **31**: 59-64
- Duffy S, Shackelton LA, Holmes EC (2008) Rates of evolutionary change in viruses: patterns and determinants. *Nat Rev Genet* **9**: 267-76
- Duizer E, Bijkerk P, Rockx B, De Groot A, Twisk F, Koopmans M (2004a) Inactivation of caliciviruses. *Appl Environ Microbiol* **70**: 4538-43
- Duizer E, Schwab KJ, Neill FH, Atmar RL, Koopmans MP, Estes MK (2004b) Laboratory efforts to cultivate noroviruses. *J Gen Virol* **85**: 79-87
- Earp RL, Dessy RE (1998) Surface Plasmon Resonance. In *Commercial Biosensors: Application to Clinical, Bioprocess, and Environmental Samples*, Ramsay G (ed). New York: John Wiley & Sons, Inc.
- Estes MK, Ball JM, Guerrero RA, Opekun AR, Gilger MA, Pacheco SS, Graham DY (2000) Norwalk virus vaccines: challenges and progress. *J Infect Dis* **181 Suppl 2**: S367-73
- Fankhauser RL, Monroe SS, Noel JS, Humphrey CD, Bresee JS, Parashar UD, Ando T, Glass RI (2002) Epidemiologic and molecular trends of "Norwalk-like viruses" associated with outbreaks of gastroenteritis in the United States. *J Infect Dis* **186**: 1-7

Farkas T, Cross RW, Hargitt E, 3rd, Lerche NW, Morrow AL, Sestak K (2010) Genetic diversity and histo-blood group antigen interactions of rhesus enteric caliciviruses. *J Virol* **84**: 8617-25

Farkas T, Sestak K, Wei C, Jiang X (2008) Characterization of a rhesus monkey calicivirus representing a new genus of Caliciviridae. *J Virol* **82**: 5408-16

Feng K, Divers E, Ma Y, Li J (2011) Inactivation of a human norovirus surrogate, human norovirus virus-like particles, and vesicular stomatitis virus by gamma irradiation. *Appl Environ Microbiol* **77**: 3507-17

Feng X, Jiang X (2007) Library screen for inhibitors targeting norovirus binding to histo-blood group antigen receptors. *Antimicrob Agents Chemother* **51**: 324-31

Fersht A (ed) (1999) *Structure and mechanism in protein science: a guide to enzyme catalysis and protein folding*. W.H. Freeman: New York

Fiege B, Rademacher C, Cartmell J, Kitov PI, Parra F, Peters T (2012) Molecular Details of the Recognition of Blood Group Antigens by a Human Norovirus as Determined by STD NMR Spectroscopy. *Angew Chem Int Ed Engl* **51**: 928-32

Fielding L (2007) NMR methods for the determination of protein–ligand dissociation constants. *Progress in Nuclear Magnetic Resonance Spectroscopy* **51**: 219-242

Foloppe N, Chen IJ (2009) Conformational sampling and energetics of drug-like molecules. *Curr Med Chem* **16**: 3381-413

Gagneux P, Varki A (1999) Evolutionary considerations in relating oligosaccharide diversity to biological function. *Glycobiology* **9**: 747-55

Gamblin SJ, Skehel JJ (2010) Influenza haemagglutinin and neuraminidase membrane glycoproteins. *J Biol Chem*

Geissler K, Schneider K, Platzer G, Truyen B, Kaaden OR, Truyen U (1997) Genetic and antigenic heterogeneity among feline calicivirus isolates from distinct disease manifestations. *Virus Res* **48**: 193-206

Graham BS, Crowe J, Jr. (2007) Immunization against viral diseases, p. 487-538. In *Fields Virology*, Knipe DM, Howley PM, Griffin DE (eds), 5th edn. Philadelphia, PA: Lippincott Williams & Wilkins

Green KY, Chanock RM, Kapikian AZ (2001) Human caliciviruses, p. 841-874. In *Fields Virology*, Knipe DM, Howley PM, Griffin DE (eds), 4th edn. Philadelphia, PA: Lippincott Williams & Wilkins

Green KY, Lew JF, Jiang X, Kapikian AZ, Estes MK (1993) Comparison of the reactivities of baculovirus-expressed recombinant Norwalk virus capsid antigen with those of the native Norwalk virus antigen in serologic assays and some epidemiologic observations. *J Clin Microbiol* **31**: 2185-91

Greer AL, Drews SJ, Fisman DN (2009) Why "winter" vomiting disease? Seasonality, hydrology, and Norovirus epidemiology in Toronto, Canada. *Ecohealth* **6**: 192-9

Guiard J, Fiege B, Kitov PI, Peters T, Bundle DR (2011) "Double-click" protocol for synthesis of heterobifunctional multivalent ligands: toward a focused library of specific norovirus inhibitors. *Chemistry* **17**: 7438-41

Guillon P, Ruvoen-Clouet N, Le Moullac-Vaidye B, Marchandeu S, Le Pendu J (2009) Association between expression of the H histo-blood group antigen, alpha1,2fucosyltransferases polymorphism of wild rabbits, and sensitivity to rabbit hemorrhagic disease virus. *Glycobiology* **19**: 21-8

Guo M, Evermann JF, Saif LJ (2001) Detection and molecular characterization of cultivable caliciviruses from clinically normal mink and enteric caliciviruses associated with diarrhea in mink. *Arch Virol* **146**: 479-93

Hajduk PJ, Greer J (2007) A decade of fragment-based drug design: strategic advances and lessons learned. *Nat Rev Drug Discov* **6**: 211-9

Hakomori S (1981) Blood group ABH and Ii antigens of human erythrocytes: chemistry, polymorphism, and their developmental change. *Semin Hematol* **18**: 39-62

Hale AD, Crawford SE, Ciarlet M, Green J, Gallimore C, Brown DW, Jiang X, Estes MK (1999) Expression and self-assembly of Grimsby virus: antigenic distinction from Norwalk and Mexico viruses. *Clin Diagn Lab Immunol* **6**: 142-5

Hale AD, Lewis DC, Jiang X, Brown DW (1998) Homotypic and heterotypic IgG and IgM antibody responses in adults infected with small round structured viruses. *J Med Virol* **54**: 305-12

Hansman GS, Biertumpfel C, Georgiev I, McLellan JS, Chen L, Zhou T, Katayama K, Kwong PD (2011) Crystal Structures of GII.10 and GII.12 Norovirus Protruding Domains in Complex with Histo-Blood Group Antigens Reveal Details for a Potential Site of Vulnerability. *J Virol*

Hansman GS, Shahzad-UI-Hussan S, McLellan JS, Chuang GY, Georgiev I, Shimoike T, Katayama K, Bewley CA, Kwong PD (2012) Structural basis for norovirus inhibition and fucose mimicry by citrate. *J Virol* **86**: 284-92

Harrington PR, Lindesmith L, Yount B, Moe CL, Baric RS (2002) Binding of Norwalk virus-like particles to ABH histo-blood group antigens is blocked by antisera from infected human volunteers or experimentally vaccinated mice. *J Virol* **76**: 12335-43

Harris R, Kiddle GR, Field RA, Milton MJ, Ernst B, Magnani JL, Homans SW (1999) Stable-isotope-assisted NMR studies on C-13-enriched sialyl Lewis(x) in solution and bound to E-selectin. *Journal of the American Chemical Society* **121**: 2546-2551

Haselhorst T, Fiebig T, Dyason JC, Fleming FE, Blanchard H, Coulson BS, von Itzstein M (2011) Recognition of the GM3 ganglioside glycan by Rhesus rotavirus particles. *Angew Chem Int Ed Engl* **50**: 1055-8

- Haselhorst T, Garcia JM, Islam T, Lai JC, Rose FJ, Nicholls JM, Peiris JS, von Itzstein M (2008) Avian influenza H5-containing virus-like particles (VLPs): host-cell receptor specificity by STD NMR spectroscopy. *Angew Chem Int Ed Engl* **47**: 1910-2
- Haselhorst T, Weimar T, Peters T (2001) Molecular recognition of sialyl Lewis(x) and related saccharides by two lectins. *J Am Chem Soc* **123**: 10705-14
- Heimburg-Molinaro J, Lum M, Vijay G, Jain M, Almogren A, Rittenhouse-Olson K (2011) Cancer vaccines and carbohydrate epitopes. *Vaccine* **29**: 8802-26
- Hein CD, Liu XM, Wang D (2008) Click chemistry, a powerful tool for pharmaceutical sciences. *Pharm Res* **25**: 2216-30
- Herbst-Kralovetz M, Mason HS, Chen Q (2010) Norwalk virus-like particles as vaccines. *Expert Rev Vaccines* **9**: 299-307
- Ho JG, Kitov PI, Paszkiewicz E, Sadowska J, Bundle DR, Ng KK (2005) Ligand-assisted aggregation of proteins. Dimerization of serum amyloid P component by bivalent ligands. *J Biol Chem* **280**: 31999-2008
- Horan N, Yan L, Isobe H, Whitesides GM, Kahne D (1999) Nonstatistical binding of a protein to clustered carbohydrates. *Proc Natl Acad Sci U S A* **96**: 11782-6
- Horm KM, D'Souza DH (2011) Survival of human norovirus surrogates in milk, orange, and pomegranate juice, and juice blends at refrigeration (4 degrees C). *Food Microbiol* **28**: 1054-61
- Huang P, Farkas T, Zhong W, Tan M, Thornton S, Morrow AL, Jiang X (2005) Norovirus and histo-blood group antigens: demonstration of a wide spectrum of strain specificities and classification of two major binding groups among multiple binding patterns. *J Virol* **79**: 6714-22
- Huth JR, Sun C, Sauer DR, Hajduk PJ (2005) Utilization of NMR-derived fragment leads in drug design. *Methods Enzymol* **394**: 549-71
- Hutson AM, Airaud F, LePendou J, Estes MK, Atmar RL (2005) Norwalk virus infection associates with secretor status genotyped from sera. *J Med Virol* **77**: 116-20
- Hutson AM, Atmar RL, Estes MK (2004) Norovirus disease: changing epidemiology and host susceptibility factors. *Trends Microbiol* **12**: 279-87
- Hutson AM, Atmar RL, Graham DY, Estes MK (2002) Norwalk virus infection and disease is associated with ABO histo-blood group type. *J Infect Dis* **185**: 1335-7
- Hutson AM, Atmar RL, Marcus DM, Estes MK (2003) Norwalk virus-like particle hemagglutination by binding to h histo-blood group antigens. *J Virol* **77**: 405-15
- Imberty A, Mikros E, Koca J, Mollicone R, Oriol R, Perez S (1995) Computer simulation of histo-blood group oligosaccharides: energy maps of all constituting disaccharides and

potential energy surfaces of 14 ABH and Lewis carbohydrate antigens. *Glycoconj J* **12**: 331-49

Irwin JJ (2008) Community benchmarks for virtual screening. *J Comput Aided Mol Des* **22**: 193-9

Jason-Moller L, Murphy M, Bruno J (2006) Overview of Biacore systems and their applications. *Curr Protoc Protein Sci* **Chapter 19**: Unit 19 13

Jayalakshmi V, Krishna NR (2002) Complete relaxation and conformational exchange matrix (CORCEMA) analysis of intermolecular saturation transfer effects in reversibly forming ligand-receptor complexes. *J Magn Reson* **155**: 106-18

Jiang V, Jiang B, Tate J, Parashar UD, Patel MM (2010) Performance of rotavirus vaccines in developed and developing countries. *Hum Vaccin* **6**: 532-42

Jiang X, Huang P, Zhong W, Tan M, Farkas T, Morrow AL, Newburg DS, Ruiz-Palacios GM, Pickering LK (2004) Human milk contains elements that block binding of noroviruses to human histo-blood group antigens in saliva. *J Infect Dis* **190**: 1850-9

Jiang X, Wang M, Graham DY, Estes MK (1992) Expression, self-assembly, and antigenicity of the Norwalk virus capsid protein. *J Virol* **66**: 6527-32

Jiang X, Zhong WM, Farkas T, Huang PW, Wilton N, Barrett E, Fulton D, Morrow R, Matson DO (2002) Baculovirus expression and antigenic characterization of the capsid proteins of three Norwalk-like viruses. *Arch Virol* **147**: 119-30

Johnston CP, Qiu H, Ticehurst JR, Dickson C, Rosenbaum P, Lawson P, Stokes AB, Lowenstein CJ, Kaminsky M, Cosgrove SE, Green KY, Perl TM (2007) Outbreak management and implications of a nosocomial norovirus outbreak. *Clin Infect Dis* **45**: 534-40

Kahn JA (2009) HPV vaccination for the prevention of cervical intraepithelial neoplasia. *N Engl J Med* **361**: 271-8

Kapikian AZ, Wyatt RG, Dolin R, Thornhill TS, Kalica AR, Chanock RM (1972) Visualization by immune electron microscopy of a 27-nm particle associated with acute infectious nonbacterial gastroenteritis. *J Virol* **10**: 1075-81

Katpally U, Voss NR, Cavazza T, Taube S, Rubin JR, Young VL, Stuckey J, Ward VK, Virgin HWt, Wobus CE, Smith TJ (2010) High-resolution cryo-electron microscopy structures of murine norovirus 1 and rabbit hemorrhagic disease virus reveal marked flexibility in the receptor binding domains. *J Virol* **84**: 5836-41

Katsamba PS, Park S, Laird-Offringa IA (2002) Kinetic studies of RNA-protein interactions using surface plasmon resonance. *Methods* **26**: 95-104

Keeler J (2005) *Understanding NMR Spectroscopy*, 1st edn: John Wiley & Sons

Kerr PJ, Kitchen A, Holmes EC (2009) The Origin and Phylodynamics of Rabbit Hemorrhagic Disease virus. *J Virol*

Kindberg E, Akerlind B, Johnsen C, Knudsen JD, Heltberg O, Larson G, Bottiger B, Svensson L (2007) Host genetic resistance to symptomatic norovirus (GGII.4) infections in Denmark. *J Clin Microbiol* **45**: 2720-2

Kitov PI, Bundle DR (2003) On the nature of the multivalency effect: a thermodynamic model. *J Am Chem Soc* **125**: 16271-84

Kitov PI, Lipinski T, Paszkiewicz E, Solomon D, Sadowska JM, Grant GA, Mulvey GL, Kitova EN, Klassen JS, Armstrong GD, Bundle DR (2008a) An entropically efficient supramolecular inhibition strategy for Shiga toxins. *Angew Chem Int Ed Engl* **47**: 672-6

Kitov PI, Mulvey GL, Griener TP, Lipinski T, Solomon D, Paszkiewicz E, Jacobson JM, Sadowska JM, Suzuki M, Yamamura K, Armstrong GD, Bundle DR (2008b) In vivo supramolecular templating enhances the activity of multivalent ligands: a potential therapeutic against the Escherichia coli O157 AB5 toxins. *Proc Natl Acad Sci U S A* **105**: 16837-42

Kitov PI, Paszkiewicz E, Sadowska JM, Deng Z, Ahmed M, Narain R, Griener TP, Mulvey GL, Armstrong GD, Bundle DR (2011) Impact of the nature and size of the polymeric backbone on the ability of heterobifunctional ligands to mediate shiga toxin and serum amyloid p component ternary complex formation. *Toxins (Basel)* **3**: 1065-88

Kitov PI, Sadowska JM, Mulvey G, Armstrong GD, Ling H, Pannu NS, Read RJ, Bundle DR (2000) Shiga-like toxins are neutralized by tailored multivalent carbohydrate ligands. *Nature* **403**: 669-72

Kitov PI, Shimizu H, Homans SW, Bundle DR (2003) Optimization of tether length in nonglycosidically linked bivalent ligands that target sites 2 and 1 of a Shiga-like toxin. *J Am Chem Soc* **125**: 3284-94

Koopmans M (2008) Progress in understanding norovirus epidemiology. *Curr Opin Infect Dis* **21**: 544-52

Koopmans M (2009) Noroviruses in healthcare settings: a challenging problem. *J Hosp Infect* **73**: 331-7

Koppen H (2009) Virtual screening - what does it give us? *Curr Opin Drug Discov Devel* **12**: 397-407

Koppisetty CA, Nasir W, Strino F, Rydell GE, Larson G, Nyholm PG (2010) Computational studies on the interaction of ABO-active saccharides with the norovirus VA387 capsid protein can explain experimental binding data. *J Comput Aided Mol Des* **24**: 423-31

Kroneman A, Vennema H, Deforche K, v d Avoort H, Penaranda S, Oberste MS, Vinje J, Koopmans M (2011) An automated genotyping tool for enteroviruses and noroviruses. *J Clin Virol* **51**: 121-5

Kroneman A, Verhoef L, Harris J, Vennema H, Duizer E, van Duynhoven Y, Gray J, Iturriza M, Bottiger B, Falkenhorst G, Johnsen C, von Bonsdorff CH, Maunula L, Kuusi M, Pothier P, Gallay A, Schreier E, Hohne M, Koch J, Szucs G, Reuter G, Krisztalovics K, Lynch M, McKeown P, Foley B, Coughlan S, Ruggeri FM, Di Bartolo I, Vainio K, Isakbaeva E, Poljsak-Prijatelj M, Grom AH, Mijovski JZ, Bosch A, Buesa J, Fauquier AS, Hernandez-Pezzi G, Hedlund KO, Koopmans M (2008) Analysis of integrated virological and epidemiological reports of norovirus outbreaks collected within the foodborne viruses in Europe Network from 1 July 2001 to 30 June 2006. *J Clin Microbiol* **46**: 2959-65

Langpap B. Investigation of Norovirus Receptor Recognition Patterns with STD NMR Spectroscopy. M. Sc., University of Lübeck, Lübeck, 2008

Larkin MA, Blackshields G, Brown NP, Chenna R, McGettigan PA, McWilliam H, Valentin F, Wallace IM, Wilm A, Lopez R, Thompson JD, Gibson TJ, Higgins DG (2007) Clustal W and Clustal X version 2.0. *Bioinformatics* **23**: 2947-8

Larsson MM, Rydell GE, Grahm A, Rodriguez-Diaz J, Akerlind B, Hutson AM, Estes MK, Larson G, Svensson L (2006) Antibody prevalence and titer to norovirus (genogroup II) correlate with secretor (FUT2) but not with ABO phenotype or Lewis (FUT3) genotype. *J Infect Dis* **194**: 1422-7

Lay MK, Atmar RL, Guix S, Bharadwaj U, He H, Neill FH, Sastry KJ, Yao Q, Estes MK (2010) Norwalk virus does not replicate in human macrophages or dendritic cells derived from the peripheral blood of susceptible humans. *Virology* **406**: 1-11

Le Guyader F, Loisy F, Atmar RL, Hutson AM, Estes MK, Ruvoen-Clouet N, Pommepuy M, Le Pendu J (2006) Norwalk virus-specific binding to oyster digestive tissues. *Emerg Infect Dis* **12**: 931-6

Le Pendu J (2004) Histo-blood group antigen and human milk oligosaccharides: genetic polymorphism and risk of infectious diseases. *Adv Exp Med Biol* **554**: 135-43

Le Pendu J, Ruvoen-Clouet N, Kindberg E, Svensson L (2006) Mendelian resistance to human norovirus infections. *Semin Immunol* **18**: 375-86

Lemieux RU, Bock K, Delbaere LTJ, Koto S, Rao VS (1980) The conformations of oligosaccharides related to the ABH and Lewis human blood group determinants. *Can J Chem* **58**: 631-653

Lew JF, Kapikian AZ, Jiang X, Estes MK, Green KY (1994) Molecular characterization and expression of the capsid protein of a Norwalk-like virus recovered from a Desert Shield troop with gastroenteritis. *Virology* **200**: 319-25

Lieberg B, Nylander C, Lundström I (1983) Surface plasmon resonance for gas detection and biosensing. *Sensors Actuators* **4**: 299-304

Lindesmith L, Moe C, Lependu J, Frelinger JA, Treanor J, Baric RS (2005) Cellular and humoral immunity following Snow Mountain virus challenge. *J Virol* **79**: 2900-9



- Lindesmith L, Moe C, Marionneau S, Ruvoen N, Jiang X, Lindblad L, Stewart P, LePendou J, Baric R (2003) Human susceptibility and resistance to Norwalk virus infection. *Nat Med* **9**: 548-53
- Lindesmith LC, Debbink K, Swanstrom J, Vinje J, Costantini V, Baric RS, Donaldson EF (2012) Monoclonal antibody-based antigenic mapping of norovirus GII.4-2002. *J Virol* **86**: 873-83
- Lindesmith LC, Donaldson EF, Baric RS (2011) Norovirus GII.4 strain antigenic variation. *J Virol* **85**: 231-42
- Lindesmith LC, Donaldson EF, Lobue AD, Cannon JL, Zheng DP, Vinje J, Baric RS (2008) Mechanisms of GII.4 norovirus persistence in human populations. *PLoS Med* **5**: e31
- Liu SJ, Xue HP, Pu BQ, Quian NH (1984) A new viral disease in rabbits. *Anim Husb Vet Med* **16**: 253-255
- Lobue AD, Thompson JM, Lindesmith L, Johnston RE, Baric RS (2009) Alphavirus-adjuvanted Norovirus VLP Vaccines: Heterologous, Humoral, and Mucosal Immune Responses Protect from Murine Norovirus Challenge. *J Virol*
- London RE (1999) Theoretical analysis of the inter-ligand overhauser effect: a new approach for mapping structural relationships of macromolecular ligands. *J Magn Reson* **141**: 301-11
- Lopez PH, Schnaar RL (2006) Determination of glycolipid-protein interaction specificity. *Methods Enzymol* **417**: 205-20
- Lopman B, Vennema H, Kohli E, Pothier P, Sanchez A, Negredo A, Buesa J, Schreier E, Reacher M, Brown D, Gray J, Iturriza M, Gallimore C, Bottiger B, Hedlund KO, Torven M, von Bonsdorff CH, Maunula L, Poljsak-Prijatelj M, Zimsek J, Reuter G, Szucs G, Melegh B, Svennson L, van Duynhoven Y, Koopmans M (2004) Increase in viral gastroenteritis outbreaks in Europe and epidemic spread of new norovirus variant. *Lancet* **363**: 682-8
- Lopman B, Zambon M, Brown DW (2008) The evolution of norovirus, the "gastric flu". *PLoS Med* **5**: e42
- Lucas M (1983) Determination of acid surface pH in vivo in rat proximal jejunum. *Gut* **24**: 734-9
- Maalouf H, Zakhour M, Le Pendu J, Le Saux JC, Atmar RL, Le Guyader FS (2010) Distribution in tissue and seasonal variation of norovirus genogroup I and II ligands in oysters. *Appl Environ Microbiol* **76**: 5621-30
- Macher BA, Galili U (2008) The Galalpha1,3Galbeta1,4GlcNAc-R (alpha-Gal) epitope: a carbohydrate of unique evolution and clinical relevance. *Biochim Biophys Acta* **1780**: 75-88

- Makino A, Shimojima M, Miyazawa T, Kato K, Tohya Y, Akashi H (2006) Junctional adhesion molecule 1 is a functional receptor for feline calicivirus. *J Virol* **80**: 4482-90
- Marin MS, Martin Alonso JM, Perez Ordoyo Garcia LI, Boga JA, Arguello-Villares JL, Casais R, Venugopal K, Jiang W, Gould EA, Parra F (1995) Immunogenic properties of rabbit haemorrhagic disease virus structural protein VP60 expressed by a recombinant baculovirus: an efficient vaccine. *Virus Res* **39**: 119-28
- Marionneau S, Airaud F, Bovin NV, Le Pendu J, Ruvoen-Clouet N (2005) Influence of the combined ABO, FUT2, and FUT3 polymorphism on susceptibility to Norwalk virus attachment. *J Infect Dis* **192**: 1071-7
- Marionneau S, Cailleau-Thomas A, Rocher J, Le Moullac-Vaidye B, Ruvoen N, Clement M, Le Pendu J (2001) ABH and Lewis histo-blood group antigens, a model for the meaning of oligosaccharide diversity in the face of a changing world. *Biochimie* **83**: 565-73
- Marionneau S, Ruvoen N, Le Moullac-Vaidye B, Clement M, Cailleau-Thomas A, Ruiz-Palacois G, Huang P, Jiang X, Le Pendu J (2002) Norwalk virus binds to histo-blood group antigens present on gastroduodenal epithelial cells of secretor individuals. *Gastroenterology* **122**: 1967-77
- Matthews JE, Dickey BW, Miller RD, Felzer JR, Dawson BP, Lee AS, Rocks JJ, Kiel J, Montes JS, Moe CL, Eisenberg JN, Leon JS (2012) The epidemiology of published norovirus outbreaks: a review of risk factors associated with attack rate and genogroup. *Epidemiol Infect*: Epub ahead of print
- Mayer M, James TL (2004) NMR-based characterization of phenothiazines as a RNA binding scaffold. *J Am Chem Soc* **126**: 4453-60
- Mayer M, Meyer B (1999) Characterization of Ligand Binding by Saturation Transfer Difference NMR Spectroscopy. *Angew Chem Int Ed Engl* **38**: 1784-1788
- Mayer M, Meyer B (2001) Group epitope mapping by saturation transfer difference NMR to identify segments of a ligand in direct contact with a protein receptor. *J Am Chem Soc* **123**: 6108-17
- McEwan GT, Schousboe B, Skadhauge E (1990) Direct measurement of mucosal surface pH of pig jejunum in vivo. *Zentralbl Veterinarmed A* **37**: 439-44
- McFadden N, Bailey D, Carrara G, Benson A, Chaudhry Y, Shortland A, Heeney J, Yarovinsky F, Simmonds P, Macdonald A, Goodfellow I (2011) Norovirus regulation of the innate immune response and apoptosis occurs via the product of the alternative open reading frame 4. *PLoS Pathog* **7**: e1002413
- Meloncelli PJ, Lowary TL (2009) Synthesis of ABO Histo-Blood Group Type V and VI Antigens. *Aust J Chem* **62**: 558-574
- Meyer B, Peters T (2003) NMR Spectroscopy Techniques for Screening and Identifying Ligand Binding to Protein Receptors. *Angew Chem Int Ed Engl* **42**: 864-890

Milland J, Sandrin MS (2006) ABO blood group and related antigens, natural antibodies and transplantation. *Tissue Antigens* **68**: 459-66

Mollicone R, Cailleau A, Imberty A, Gane P, Perez S, Oriol R (1996) Recognition of the blood group H type 2 trisaccharide epitope by 28 monoclonal antibodies and three lectins. *Glycoconj J* **13**: 263-71

Mollicone R, Cailleau A, Oriol R (1995) Molecular genetics of H, Se, Lewis and other fucosyltransferase genes. *Transfus Clin Biol* **2**: 235-42

Morrow AL, Ruiz-Palacios GM, Jiang X, Newburg DS (2005) Human-milk glycans that inhibit pathogen binding protect breast-feeding infants against infectious diarrhea. *J Nutr* **135**: 1304-7

Moss SR, Turner SL, Trout RC, White PJ, Hudson PJ, Desai A, Armesto M, Forrester NL, Gould EA (2002) Molecular epidemiology of Rabbit haemorrhagic disease virus. *J Gen Virol* **83**: 2461-7

Motomura K, Yokoyama M, Ode H, Nakamura H, Mori H, Kanda T, Oka T, Katayama K, Noda M, Tanaka T, Takeda N, Sato H (2010) Divergent evolution of norovirus GII/4 by genome recombination from May 2006 to February 2009 in Japan. *J Virol* **84**: 8085-97

Mounts AW, Ando T, Koopmans M, Bresee JS, Noel J, Glass RI (2000) Cold weather seasonality of gastroenteritis associated with Norwalk-like viruses. *J Infect Dis* **181 Suppl 2**: S284-7

Mumphrey SM, Changotra H, Moore TN, Heimann-Nichols ER, Wobus CE, Reilly MJ, Moghadamfalahi M, Shukla D, Karst SM (2007) Murine norovirus 1 infection is associated with histopathological changes in immunocompetent hosts, but clinical disease is prevented by STAT1-dependent interferon responses. *J Virol* **81**: 3251-63

Munoz EM, Correa J, Fernandez-Megia E, Riguera R (2009) Probing the relevance of lectin clustering for the reliable evaluation of multivalent carbohydrate recognition. *J Am Chem Soc* **131**: 17765-7

Munoz FJ, Rumero A, Sinisterra JV, Santos JJ, Andre S, Gabius HJ, Jimenez-Barbero J, Hernaiz MJ (2008) Versatile strategy for the synthesis of biotin-labelled glycans, their immobilization to establish a bioactive surface and interaction studies with a lectin on a biochip. *Glycoconj J* **25**: 633-46

Myszka DG (2000) Kinetic, equilibrium, and thermodynamic analysis of macromolecular interactions with BIACORE. *Methods Enzymol* **323**: 325-40

Nam HJ, Gurda-Whitaker B, Gan WY, Ilaria S, McKenna R, Mehta P, Alvarez RA, Agbandje-McKenna M (2006) Identification of the sialic acid structures recognized by minute virus of mice and the role of binding affinity in virulence adaptation. *J Biol Chem* **281**: 25670-7

- Neill JD, Meyer RF, Seal BS (1995) Genetic relatedness of the caliciviruses: San Miguel sea lion and vesicular exanthema of swine viruses constitute a single genotype within the Caliciviridae. *J Virol* **69**: 4484-8
- Neill JD, Meyer RF, Seal BS (1998) The capsid protein of vesicular exanthema of swine virus serotype A48: relationship to the capsid protein of other animal caliciviruses. *Virus Res* **54**: 39-50
- Neu U, Stehle T, Atwood WJ (2009) The Polyomaviridae: Contributions of virus structure to our understanding of virus receptors and infectious entry. *Virology* **384**: 389-99
- Neuhaus D, Williamson MP (2000) *The Nuclear Overhauser Effect in Structural and Conformational Analysis*, 2nd edn: John Wiley & Sons, Inc.
- Ng KK, Pendas-Franco N, Rojo J, Boga JA, Machin A, Alonso JM, Parra F (2004) Crystal structure of norwalk virus polymerase reveals the carboxyl terminus in the active site cleft. *J Biol Chem* **279**: 16638-45
- Nilsson M, Hedlund KO, Thorhagen M, Larson G, Johansen K, Ekspong A, Svensson L (2003) Evolution of human calicivirus RNA in vivo: accumulation of mutations in the protruding P2 domain of the capsid leads to structural changes and possibly a new phenotype. *J Virol* **77**: 13117-24
- Nordgren J, Kindberg E, Lindgren PE, Matussek A, Svensson L (2010) Norovirus gastroenteritis outbreak with a secretor-independent susceptibility pattern, Sweden. *Emerg Infect Dis* **16**: 81-7
- Oliver SL, Asobayire E, Dastjerdi AM, Bridger JC (2006) Genomic characterization of the unclassified bovine enteric virus Newbury agent-1 (Newbury1) endorses a new genus in the family Caliciviridae. *Virology* **350**: 240-50
- Oliver SL, Dastjerdi AM, Wong S, El-Attar L, Gallimore C, Brown DW, Green J, Bridger JC (2003) Molecular characterization of bovine enteric caliciviruses: a distinct third genogroup of noroviruses (Norwalk-like viruses) unlikely to be of risk to humans. *J Virol* **77**: 2789-98
- Olofsson S, Bergstrom T (2005) Glycoconjugate glycans as viral receptors. *Ann Med* **37**: 154-72
- Oriol R, Le Pendu J, Mollicone R (1986) Genetics of ABO, H, Lewis, X and related antigens. *Vox Sang* **51**: 161-71
- Otter A, Lemieux RU, Ball RG, Venot AP, Hindsgaul O, Bundle DR (1999) Crystal state and solution conformation of the B blood group trisaccharide alpha-L-Fucp-(1-->2)-[alpha-D-Galp]-(1-->3)]-beta-D-Galp-OCH<sub>3</sub>. *Eur J Biochem* **259**: 295-303
- Otto PH, Clarke IN, Lambden PR, Salim O, Reetz J, Liebler-Tenorio EM (2011) Infection of calves with bovine norovirus GIII.1 strain Jena virus: an experimental model to study the pathogenesis of norovirus infection. *J Virol* **85**: 12013-21

- Parra F, Prieto M (1990) Purification and characterization of a calicivirus as the causative agent of a lethal hemorrhagic disease in rabbits. *J Virol* **64**: 4013-5
- Parrino TA, Schreiber DS, Trier JS, Kapikian AZ, Blacklow NR (1977) Clinical immunity in acute gastroenteritis caused by Norwalk agent. *N Engl J Med* **297**: 86-9
- Patel MM, Widdowson MA, Glass RI, Akazawa K, Vinje J, Parashar UD (2008) Systematic literature review of role of noroviruses in sporadic gastroenteritis. *Emerg Infect Dis* **14**: 1224-31
- Patenaude SI, Seto NO, Borisova SN, Szpacenko A, Marcus SL, Palcic MM, Evans SV (2002) The structural basis for specificity in human ABO(H) blood group biosynthesis. *Nat Struct Biol* **9**: 685-90
- Pellecchia M, Becattini B, Crowell KJ, Fattorusso R, Forino M, Fragai M, Jung D, Mustelin T, Tautz L (2004) NMR-based techniques in the hit identification and optimisation processes. *Expert Opin Ther Targets* **8**: 597-611
- Pengelley SC, Chapman DC, Mark Abbott W, Lin HH, Huang W, Dalton K, Jones IM (2006) A suite of parallel vectors for baculovirus expression. *Protein Expr Purif* **48**: 173-81
- Perspicace S, Banner D, Benz J, Muller F, Schlatter D, Huber W (2009) Fragment-based screening using surface plasmon resonance technology. *J Biomol Screen* **14**: 337-49
- Peters T (2007) The Use of NMR Spectroscopy in Carbohydrate-Protein Molecular Interactions. In *Comprehensive Glycoscience - From Chemistry to Systems Biology*, Kamerling J, Boons GJ, Lee Y, Suzuki A, Taniguchi N, Voragen AGJ (eds) Vol. 3, pp 805-819. Elsevier
- Peters T, Meyer B, Stuike-Prill R, Somorjai R, Brisson JR (1993) A Monte Carlo method for conformational analysis of saccharides. *Carbohydr Res* **238**: 49-73
- Piliarik M, Vaisocherova H, Homola J (2009) Surface plasmon resonance biosensing. *Methods Mol Biol* **503**: 65-88
- Plath C, Weimar T, Peters H, Peters T (2006) Assaying sialyltransferase activity with surface plasmon resonance. *Chembiochem* **7**: 1226-30
- Poppe L, Brown GS, Philo JS, Nikrad PV, Shah BH (1997) Conformation of sLex Tetrasaccharide, Free in Solution and Bound to E-, P-, and L-Selectin. *J Am Chem Soc* **119**: 1727-1736
- Post CB (2003) Exchange-transferred NOE spectroscopy and bound ligand structure determination. *Curr Opin Struct Biol* **13**: 581-8
- Prasad BV, Hardy ME, Dokland T, Bella J, Rossmann MG, Estes MK (1999) X-ray crystallographic structure of the Norwalk virus capsid. *Science* **286**: 287-90

- Prasad BV, Matson DO, Smith AW (1994) Three-dimensional structure of calicivirus. *J Mol Biol* **240**: 256-64
- Rademacher C. Investigations into Viral Entry Mechanisms. PhD, University of Lübeck, Lübeck, 2008
- Rademacher C, Guiard J, Kitov PI, Fiege B, Dalton KP, Parra F, Bundle DR, Peters T (2011) Targeting norovirus infection-multivalent entry inhibitor design based on NMR experiments. *Chemistry* **17**: 7442-53
- Rademacher C, Krishna NR, Palcic M, Parra F, Peters T (2008) NMR experiments reveal the molecular basis of receptor recognition by a calicivirus. *J Am Chem Soc* **130**: 3669-75
- Rademacher C, Peters T (2008) Molecular Recognition of Ligands by Native Viruses and Virus-like Particles as Studied by NMR Experiments. *Top Curr Chem* **273**: 183-202
- Radford AD, Gaskell RM, Hart CA (2004) Human norovirus infection and the lessons from animal caliciviruses. *Curr Opin Infect Dis* **17**: 471-8
- Reitsma S, Slaaf DW, Vink H, van Zandvoort MA, oude Egbrink MG (2007) The endothelial glycocalyx: composition, functions, and visualization. *Pflugers Arch* **454**: 345-59
- Rester U (2008) From virtuality to reality - Virtual screening in lead discovery and lead optimization: a medicinal chemistry perspective. *Curr Opin Drug Discov Devel* **11**: 559-68
- Reuter G, Zimsek-Mijovski J, Poljsak-Prijatelj M, Di Bartolo I, Ruggeri FM, Kantala T, Maunula L, Kiss I, Kecskemeti S, Halaihel N, Buesa J, Johnsen C, Hjulsager CK, Larsen LE, Koopmans M, Bottiger B (2010) Incidence, diversity, and molecular epidemiology of sapoviruses in swine across Europe. *J Clin Microbiol* **48**: 363-8
- Robinson PT, Pham TN, Uhrin D (2004) In phase selective excitation of overlapping multiplets by gradient-enhanced chemical shift selective filters. *J Magn Reson* **170**: 97-103
- Rogers GN, Paulson JC (1983) Receptor determinants of human and animal influenza virus isolates: differences in receptor specificity of the H3 hemagglutinin based on species of origin. *Virology* **127**: 361-73
- Rohayem J, Munch J, Rethwilm A (2005) Evidence of recombination in the norovirus capsid gene. *J Virol* **79**: 4977-90
- Ruvoen-Clouet N, Ganiere JP, Andre-Fontaine G, Blanchard D, Le Pendu J (2000) Binding of rabbit hemorrhagic disease virus to antigens of the ABH histo-blood group family. *J Virol* **74**: 11950-4
- Ruvoen-Clouet N, Mas E, Marionneau S, Guillon P, Lombardo D, Le Pendu J (2006) Bile-salt-stimulated lipase and mucins from milk of 'secretor' mothers inhibit the binding of Norwalk virus capsids to their carbohydrate ligands. *Biochem J* **393**: 627-34

- Rydell GE, Kindberg E, Larson G, Svensson L (2011) Susceptibility to winter vomiting disease: a sweet matter. *Rev Med Virol* **21**: 370-82
- Rydell GE, Nilsson J, Rodriguez-Diaz J, Ruvoen-Clouet N, Svensson L, Le Pendu J, Larson G (2009) Human noroviruses recognize sialyl Lewis x neoglycoprotein. *Glycobiology* **19**: 309-20
- Saif MA, Bonney DK, Bigger B, Forsythe L, Williams N, Page J, Babiker ZO, Guiver M, Turner AJ, Hughes S, Wynn RF (2011) Chronic norovirus infection in pediatric hematopoietic stem cell transplant recipients: a cause of prolonged intestinal failure requiring intensive nutritional support. *Pediatr Transplant* **15**: 505-9
- Schauer R (2009) Sialic acids as regulators of molecular and cellular interactions. *Curr Opin Struct Biol* **19**: 507-14
- Scheffler K, Brisson JR, Weisemann R, Magnani JL, Wong WT, Ernst B, Peters T (1997) Application of homonuclear 3D NMR experiments and 1D analogs to study the conformation of sialyl Lewis(x) bound to E-selectin. *J Biomol NMR* **9**: 423-36
- Scheffler K, Ernst B, Katopodis A, Magnani JL, Wang WT, Weisemann R, Peters T (1995) Determination of the Bioactive Conformation of the Carbohydrate Ligand in the E-Selectin/Sialyl Lewis x Complex. *Angew Chem Int Ed Engl* **34**: 1841-1844
- Scipioni A, Mauroy A, Vinje J, Thiry E (2008) Animal noroviruses. *Vet J* **178**: 32-45
- Seet BT, McCaughan CA, Handel TM, Mercer A, Brunetti C, McFadden G, Fleming SB (2003) Analysis of an orf virus chemokine-binding protein: Shifting ligand specificities among a family of poxvirus viroceptors. *Proc Natl Acad Sci U S A* **100**: 15137-42
- Seto NO, Compston CA, Szpacenko A, Palcic MM (2000) Enzymatic synthesis of blood group A and B trisaccharide analogues. *Carbohydr Res* **324**: 161-9
- Shanker S, Choi JM, Sankaran B, Atmar RL, Estes MK, Prasad BV (2011) Structural Analysis of Histo-Blood Group Antigen Binding Specificity in a Norovirus GII.4 Epidemic Variant: Implications for Epochal Evolution. *J Virol* **85**: 8635-45
- Shirato H, Ogawa S, Ito H, Sato T, Kameyama A, Narimatsu H, Xiaofan Z, Miyamura T, Wakita T, Ishii K, Takeda N (2008) Noroviruses distinguish between type 1 and type 2 histo-blood group antigens for binding. *J Virol* **82**: 10756-67
- Siebenga JJ, Beersma MF, Vennema H, van Biezen P, Hartwig NJ, Koopmans M (2008) High prevalence of prolonged norovirus shedding and illness among hospitalized patients: a model for in vivo molecular evolution. *J Infect Dis* **198**: 994-1001
- Siebenga JJ, Lemey P, Kosakovsky Pond SL, Rambaut A, Vennema H, Koopmans M (2010) Phylodynamic reconstruction reveals norovirus GII.4 epidemic expansions and their molecular determinants. *PLoS Pathog* **6**: e1000884

Siebenga JJ, Vennema H, Renckens B, de Bruin E, van der Veer B, Siezen RJ, Koopmans M (2007) Epochal evolution of GGII.4 norovirus capsid proteins from 1995 to 2006. *J Virol* **81**: 9932-41

Siebenga JJ, Vennema H, Zheng DP, Vinje J, Lee BE, Pang XL, Ho EC, Lim W, Choudekar A, Broor S, Halperin T, Rasool NB, Hewitt J, Greening GE, Jin M, Duan ZJ, Lucero Y, O'Ryan M, Hoehne M, Schreier E, Ratcliff RM, White PA, Iritani N, Reuter G, Koopmans M (2009) Norovirus illness is a global problem: emergence and spread of norovirus GII.4 variants, 2001-2007. *J Infect Dis* **200**: 802-12

Smith AW, Skilling DE, Cherry N, Mead JH, Matson DO (1998) Calicivirus emergence from ocean reservoirs: zoonotic and interspecies movements. *Emerg Infect Dis* **4**: 13-20

Souza M, Azevedo MS, Jung K, Cheetham S, Saif LJ (2008) Pathogenesis and immune responses in gnotobiotic calves after infection with the genogroup II.4-HS66 strain of human norovirus. *J Virol* **82**: 1777-86

Stanley P, Cummings RD (2009) Structures Common to Different Glycans. In *Essentials of Glycobiology*, Varki A, Cummings RD, Esko JD, Freeze HH, Stanley P, Bertozzi CR, Hart GW, Etzler ME (eds), 2nd edn. Cold Spring Harbor (NY): Cold Spring Harbor Laboratory Press

Straub TM, Bartholomew RA, Valdez CO, Valentine NB, Dohnalkova A, Ozanich RM, Bruckner-Lea CJ, Call DR (2011) Human norovirus infection of caco-2 cells grown as a three-dimensional tissue structure. *J Water Health* **9**: 225-40

Straub TM, Honer zu Bentrup K, Orosz-Coghlan P, Dohnalkova A, Mayer BK, Bartholomew RA, Valdez CO, Bruckner-Lea CJ, Gerba CP, Abbaszadegan M, Nickerson CA (2007) In vitro cell culture infectivity assay for human noroviruses. *Emerg Infect Dis* **13**: 396-403

Strong DW, Thackray LB, Smith TJ, Virgin HW (2012) Protruding domain of capsid protein is necessary and sufficient to determine murine norovirus replication and pathogenesis in vivo. *J Virol* **86**: 2950-8

Stuart AD, Brown TD (2007) Alpha2,6-linked sialic acid acts as a receptor for Feline calicivirus. *J Gen Virol* **88**: 177-86

Stuike-Prill R, Meyer B (1990) A new force-field program for the calculation of glycopeptides and its application to a heptacosapeptide-decasaccharide of immunoglobulin G1. Importance of 1-6-glycosidic linkages in carbohydrate-peptide interactions. *Eur J Biochem* **194**: 903-19

Sukhrie FH, Siebenga JJ, Beersma MF, Koopmans M (2010) Chronic shedders as reservoir for nosocomial transmission of norovirus. *J Clin Microbiol*

Sun H (2008) Pharmacophore-based virtual screening. *Curr Med Chem* **15**: 1018-24



- Swann SL, Brown SP, Muchmore SW, Patel H, Merta P, Locklear J, Hajduk PJ (2011) A unified, probabilistic framework for structure- and ligand-based virtual screening. *J Med Chem* **54**: 1223-32
- Tamminen K, Huhti L, Koho T, Lappalainen S, Hytonen VP, Vesikari T, Blazevec V (2012) A comparison of immunogenicity of norovirus GII-4 virus-like particles and P-particles. *Immunology* **135**: 89-99
- Tan M, Fang P, Chachiyo T, Xia M, Huang P, Fang Z, Jiang W, Jiang X (2008a) Noroviral P particle: structure, function and applications in virus-host interaction. *Virology* **382**: 115-23
- Tan M, Hegde RS, Jiang X (2004a) The P domain of norovirus capsid protein forms dimer and binds to histo-blood group antigen receptors. *J Virol* **78**: 6233-42
- Tan M, Jiang X (2005a) Norovirus and its histo-blood group antigen receptors: an answer to a historical puzzle. *Trends Microbiol* **13**: 285-93
- Tan M, Jiang X (2005b) The p domain of norovirus capsid protein forms a subviral particle that binds to histo-blood group antigen receptors. *J Virol* **79**: 14017-30
- Tan M, Xia M, Cao S, Huang P, Farkas T, Meller J, Hegde RS, Li X, Rao Z, Jiang X (2008b) Elucidation of strain-specific interaction of a GII-4 norovirus with HBGA receptors by site-directed mutagenesis study. *Virology* **379**: 324-34
- Tan M, Xia M, Chen Y, Bu W, Hegde RS, Meller J, Li X, Jiang X (2009) Conservation of carbohydrate binding interfaces: evidence of human HBGA selection in norovirus evolution. *PLoS ONE* **4**: e5058
- Tan M, Zhong W, Song D, Thornton S, Jiang X (2004b) E. coli-expressed recombinant norovirus capsid proteins maintain authentic antigenicity and receptor binding capability. *J Med Virol* **74**: 641-9
- Tan MM, J.; Jiang, X. (2006) C-Terminal Arginine Cluster Is Essential for Receptor Binding of Norovirus Capsid Protein. *J Virol* **80**: 7322-7331
- Taube S, Perry JW, Yetming K, Patel SP, Auble H, Shu L, Nawar HF, Lee CH, Connell TD, Shayman JA, Wobus CE (2009) Ganglioside-linked terminal sialic acid moieties on murine macrophages function as attachment receptors for murine noroviruses. *J Virol* **83**: 4092-101
- Teunis PF, Moe CL, Liu P, Miller SE, Lindesmith L, Baric RS, Le Pendu J, Calderon RL (2008) Norwalk virus: how infectious is it? *J Med Virol* **80**: 1468-76
- Thiel HJ, Konig M (1999) Caliciviruses: an overview. *Vet Microbiol* **69**: 55-62
- Thorven M, Grahn A, Hedlund KO, Johansson H, Wahlfrid C, Larson G, Svensson L (2005) A homozygous nonsense mutation (428G-->A) in the human secretor (FUT2) gene provides resistance to symptomatic norovirus (GGII) infections. *J Virol* **79**: 15351-5

- Thouvenin E, Laurent S, Madelaine MF, Rasschaert D, Vautherot JF, Hewat EA (1997) Bivalent binding of a neutralising antibody to a calicivirus involves the torsional flexibility of the antibody hinge. *J Mol Biol* **270**: 238-46
- Tran HA, Kitov PI, Paszkiewicz E, Sadowska JM, Bundle DR (2011) Multifunctional multivalency: a focused library of polymeric cholera toxin antagonists. *Org Biomol Chem* **9**: 3658-71
- Trott O, Olson AJ (2010) AutoDock Vina: improving the speed and accuracy of docking with a new scoring function, efficient optimization, and multithreading. *J Comput Chem* **31**: 455-61
- Tu ET, Bull RA, Kim MJ, McIver CJ, Heron L, Rawlinson WD, White PA (2008) Norovirus excretion in an aged-care setting. *J Clin Microbiol* **46**: 2119-21
- Varki A, Schauer R (2009) Sialic Acids. In *Essentials of Glycobiology*, Varki A, Cumming RD, Esko JD, Freeze HH, Stanley P, Bertozzi CR, Hart GW, Etzler ME (eds), 2nd edn. Cold Spring Harbor (NY): Cold Spring Harbor Laboratory Press
- Wang S, Shan X, Patel U, Huang X, Lu J, Li J, Tao N (2010) Label-free imaging, detection, and mass measurement of single viruses by surface plasmon resonance. *Proc Natl Acad Sci U S A*
- Wang YS, Liu D, Wyss DF (2004) Competition STD NMR for the detection of high-affinity ligands and NMR-based screening. *Magn Reson Chem* **42**: 485-9
- Widdowson MA, Rockx B, Schepp R, van der Poel WH, Vinje J, van Duynhoven YT, Koopmans MP (2005) Detection of serum antibodies to bovine norovirus in veterinarians and the general population in the Netherlands. *J Med Virol* **76**: 119-28
- Wingfield T, Gallimore CI, Xerry J, Gray JJ, Klapper P, Guiver M, Blanchard TJ (2010) Chronic norovirus infection in an HIV-positive patient with persistent diarrhoea: A novel cause. *J Clin Virol* **49**: 219-22
- Wobus CE, Karst SM, Thackray LB, Chang KO, Sosnovtsev SV, Belliot G, Krug A, Mackenzie JM, Green KY, Virgin HW (2004) Replication of Norovirus in cell culture reveals a tropism for dendritic cells and macrophages. *PLoS Biol* **2**: e432
- Wobus CE, Thackray LB, Virgin HWt (2006) Murine norovirus: a model system to study norovirus biology and pathogenesis. *J Virol* **80**: 5104-12
- Woode GN, Bridger JC (1978) Isolation of small viruses resembling astroviruses and caliciviruses from acute enteritis of calves. *J Med Microbiol* **11**: 441-52
- Woods RJ, Tessier MB (2010) Computational glycoscience: characterizing the spatial and temporal properties of glycans and glycan-protein complexes. *Curr Opin Struct Biol*
- Xi JN, Graham DY, Wang KN, Estes MK (1990) Norwalk virus genome cloning and characterization. *Science* **250**: 1580-3

Xia M, Tan M, Wei C, Zhong W, Wang L, McNeal M, Jiang X (2011) A candidate dual vaccine against influenza and noroviruses. *Vaccine* **29**: 7670-7

Yan J, Kline AD, Mo H, Shapiro MJ, Zartler ER (2003) The effect of relaxation on the epitope mapping by saturation transfer difference NMR. *J Magn Reson* **163**: 270-6

Yuriev E, Farrugia W, Scott AM, Ramsland PA (2005) Three-dimensional structures of carbohydrate determinants of Lewis system antigens: implications for effective antibody targeting of cancer. *Immunol Cell Biol* **83**: 709-17

Zakhour M, Ruvoen-Clouet N, Charpilienne A, Langpap B, Poncet D, Peters T, Bovin N, Le Pendu J (2009) The alphaGal epitope of the histo-blood group antigen family is a ligand for bovine norovirus Newbury2 expected to prevent cross-species transmission. *PLoS Pathog* **5**: e1000504

Zhang XF, Dai YC, Zhong W, Tan M, Lv ZP, Zhou YC, Jiang X (2012) Tannic acid inhibited norovirus binding to HBGA receptors, a study of 50 Chinese medicinal herbs. *Bioorg Med Chem* **20**: 1616-23

Zhao Y, Chapman DA, Jones IM (2003) Improving baculovirus recombination. *Nucleic Acids Res* **31**: E6-6

Zheng DP, Ando T, Fankhauser RL, Beard RS, Glass RI, Monroe SS (2006) Norovirus classification and proposed strain nomenclature. *Virology* **346**: 312-23



## Acknowledgment

My deepest gratitude goes to Professor Thomas Peters for the possibility to work on a fascinating project in a very enjoyable scientific environment, for offering continuous support, advice and encouragement in all stages of this thesis including revision of the manuscript. I would also like to thank for the possibility to attend a number of very stimulating conferences and symposia during my PhD.

This thesis would not have been possible without the generous supply with VLPs by Professor Francisco Parra (University of Oviedo, Spain) and his group members Dr. Kevin P. Dalton and Inés Nicieza. I am also very grateful for the possibility of two research stays in Francisco group to learn methods for recombinant baculovirus expression in insect cells. Especially Kevin assisted and promoted me in cloning and expression of mutant VLPs.

For the supply with bovine norovirus VLPs and the opportunity for a joint work I like to thank Didier Poncet (CNRS Gif-sur-Yvette, France) and Jaques LePendue (University of Nantes, France).

I very much thank Dr. Pavel I. Kitov, Dr. Julie Guiard and Eugenia Paszkiewicz from the University of Alberta, Edmonton for the design and synthesis of prototype inhibitors against NoV. Their efforts contributed to a large part of this work.

For the supply with precious carbohydrate samples I like to thank Monica Palcic and Ole Hindsgaul from the Carlsberg Laboratory in Copenhagen, Todd L. Lowary and David R. Bundle from the University of Alberta, Edmonton, Beat Ernst from the University of Basel, and finally Wilfried Hellebrandt from the University of Lübeck.

Many members of the Institute of Chemistry at the University of Lübeck deserve my heartfelt thanks for contributing to this work in many ways. Dr. Hanne Peters spent advice and support concerning all aspects of the lab work. Hanne and Dr. Rosa Puls helped and guided the supervision of students in lab courses that brought me valuable experience in teaching. I thank Dr. Christoph Rademacher for the passionate introduction into the project and for offering helpful discussions throughout this thesis. With Dr. Bärbel Blaum who was assigned to the norovirus project during her postdoc time I share memories on many fruitful discussions and experimental progress. Many thanks go to Dr. Karsten Seeger and Dr. Thorsten Biet for enthusiastic efforts explaining concepts and peculiarities of NMR. I owe sincere thanks to Dr. Thomas Weimar and Thies Köhli for helpful support with the

operation of the Biacore instrument and discussion of results. I would also like to thank all other members of the institute for providing an enjoyable environment for research and for helpful discussions and encouragement. I especially thank Dr. Nora Sindhuwinata, Dr. Karsten Seeger and Dr. Christoph Rademacher for their invaluable support with revision of the manuscript.

I am in debt to the Deutsche Forschungsgemeinschaft for financial support of my PhD thesis on the human norovirus project.

Finally, I owe my deepest gratitude and heartfelt thanks to my family and to my beloved husband Thomas for being a constant source of encouragement and support without that it would not have been possible to finish this thesis.